JOURNAL OF CARDIOVASCULAR MAGNETIC RESONANCE®
Vol. 6, No. 1, pp. 359–456, 2004

Poster Abstracts: New Methods

475. Improved Visualization and Control for Scan Plane Navigation in Real-Time Cardiac MRI

Graham A. Wright, Ph.D., Jeff A. Stainsby, M.Sc., Nick Hu, M.Sc., Dingrong Yi, Ph.D., Perry Radau, Ph.D.
Imaging Research, Sunnybrook and Women's College Health Science Centre, University of Toronto, Toronto, ON, Canada.

Introduction: For interactive real-time MR, it is important to efficiently prescribe scan planes and obtain visual feedback on the prescription. This is necessary for applications such as basic 3D navigation (e.g. for coronary artery localization) and guidance of interventions. Existing methods such as 2D images and 3D mice provide some of the required prescription flexibility but suffer from non-intuitive representations of the input and output data. In addition, existing 3D mice can not visually represent a static scan plane position.

Purpose: Our goal is to improve the visualization and control interface for scan plane positioning in 3-space both through providing a visual reference in a previously acquired 3D data set and with a physical model of the scan plane in 3-space.

Methods: Interactive real-time scanning was implemented on a 1.5T scanner (GE CV/i) with 2 mm in-plane resolution for 120 ms acquisitions displayed at 15 frames-per-second using a sliding window reconstruction (Kerr et al., 1997). A 3D visualization tool was written using VTK (Schroeder et al., 1998) which displays the current low-resolution real-time image in addition to the following image data from a pre-acquired high-resolution 3D data set: 3 orthogonal cut planes, an interactive volume of intersecting cut planes or volume rendered data, and the oblique cut plane corresponding to the location of the current real-time image plane (Figure 1). A 6 degree-of-freedom (6DOF), statically balanced, robotic arm was also developed which is capable of automatically moving a representative scan plane and normal vector to the current real-time scan plane position (Figure 2). In addition the robotic arm can be used as a scan plane prescription device via sensors on each of the 6 joints. To coordinate the interactive real-time scanning, 3D visualization tool, and 6DOF robotic arm that may be running on different computers, a socket-based server was written. This server provides the current scan plane position and image from the real-time scan when requested by the other two applications.

Results: An initial implementation of the combined scanning and visualization system was completed and

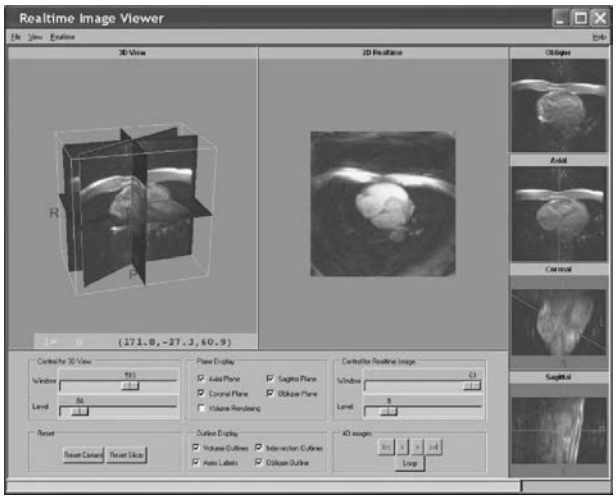

Figure 1. 3D visualization tool showing prior 3D data with oblique cut plane (left), current real-time image (centre), and various cut planes (right). (*View this art in color at www.dekker.com.*)

DOI: 10.1081/JCMR-120028320
Copyright © 2004 by Marcel Dekker, Inc.
1097-6647 (Print); 1532-429X (Online)
www.dekker.com

ORDER REPRINTS

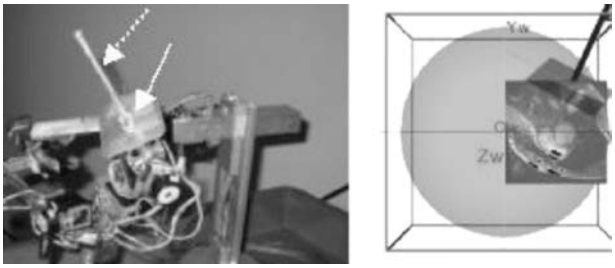

Figure 2. 6DOF robotic arm (left) showing representative scan plane (solid line) and normal vector (dotted line) and a graphical display of the arm position (right). (*View this art in color at www.dekker.com.*)

tested for imaging healthy subjects. A volumetric FIESTA data set was first acquired and loaded as the reference in the 3D visualization tool. Interactive real-time scanning was initiated and an oblique plane representing the current scan plane was continually updated on the 3D visualization tool and robotic arm. Currently the interactive real-time interface operates on the local scanner computer and the 3D visualization tool and robot driver software runs on a separate computer running a Real-Time Linux operating system. In the future all 3 applications will be fully integrated on the same system. In addition, we will incorporate a 4D data set as the prior data so that the reference image is from the same spatial location and cardiac phase as the current real-time scan plane. Finally, future developments will allow the 6DOF robotic arm and oblique cut plane on the 3D visualization tool to be used to drive the position of the scan plane itself.

Conclusions: Visualization tools—both physical and software—were integrated with interactive real-time MRI scanning to enhance the efficiency and intuitiveness of scan plane localization. This system could be applied wherever fast intuitive localization or tracking in 3D is required.

REFERENCES

Kerr, et al. (1997). *Magn. Reson. Med.* 38:355–367.
Schroeder, W. J., et al. (1998). *The VTK User's Guide*. Kitware: New York.

476. Anatomic Guidance with Three-Dimensional MRI for Stereotactic, Real-Time Radiofrequency Ablation in the Heart

Timm Dickfeld, Hugh Calkins, Menekhem Zviman, Glen Meininger, Ariel Roguin, Krystl Frank, Ron Berger, Hugh Calkins, Henry Halperin. *Cardiology, Johns Hopkins University, Baltimore, MD, USA*.

Introduction: Targets for radiofrequency ablation (RFA) of atrial fibrillation, atrial flutter, and non-idiopathic ventricular tachycardia (VT) are increasingly being selected based on anatomic considerations. Because fluoroscopy provides only limited information about the relationship between catheter positions and cardiac structures, and is associated with radiation risk, other approaches to mapping may be beneficial.

Purpose: This study sought to determine if a novel concept of stereotactic, anatomic MR guidance could safely and accurately guide catheter navigation and ablation.

Methods: To evaluate true anatomical catheter guidance, three dimensional (3D) Magnetic Resonance (MR) images were superimposed on an electromagnetic catheter positioning system using fiducial markers. This allowed the dynamic display of the catheter position on previously acquired MRI in real time. Position error during catheter navigation was determined in a phantom model and during left and right heart catheterization of domestic swine ($n = 7$). To assess the accuracy of RFA single ablation lesions were performed at the fossa ovalis that was identified on the MR image ($n = 5$). Reproducibility of RFA was evaluated with repeated ablations at the identical anatomic site in the RA ($n = 8$). Straight three point lines were created in the RV and LV to assess the ability to facilitate complex ablation procedures ($n = 6$).

Results: Display of the catheter position in real-time on the MRI allowed targeted catheter navigation without the use of fluoroscopy. In vitro-accuracy and precision were (mean ± SEM) 1.1 ± 0.1 mm and 0.3 ± 0.1 mm and in vivo-accuracy and precision were 2.7 ± 0.5 mm and 2.0 ± 0.4 mm, respectively. After the targeted ablations to the fossa ovalis (accuracy) all ablation sites were located within the fossa ovalis as demonstrated on the pathological specimen with an average distance of 3.9 ± 2.1 mm from its center. In two of the experiments the ablation catheter was passed into the left atrium and anatomically targeted ablation performed in the lateral wall of the left atrial appendage. Average distance of the triple, repeated RA ablations (precision) was 3.9 ± 0.5 mm. The ventricular three point lesions deviated 1.7 ± 0.2 mm from a straight line and point distance differed by 2.3 ± 0.6 mm from the pathological specimen.

Conclusion: Real-time display of the catheter position on 3D-MRI allows accurate and precise RFA

Copyright © Marcel Dekker, Inc. All rights reserved.

ORDER REPRINTS

guided by the true anatomy in all four cardiac chambers. This may facilitate anatomically based ablation procedures in e.g. atrial fibrillation or non-idiopathic VT and decrease radiation times.

477. Use of Magnetic Resonance Imaging to Evaluate the Depth and Transmurality of Radiofrequency Ablation Lesions

Timm Dickfeld, Ritsushi Kato, Menkhem Zviman, Glen Meininger, Ariel Roguin, Krystl Frank, Ron Berger, Hugh Calkins, Henry Halperin. *Cardiology, Johns Hopkins University, Baltimore, MD, USA*.

Introduction: The transmural extent of radiofrequency ablation (RFA) is highly predictive of the procedural success for either focal ablation or creation of isolation lines in e.g. idiopathic ventricular tachycardia, atrial flutter and atrial fibrillation. However, current imaging technologies like fluoroscopy or echocardiography are unable to accurately assess the thickness of the created lesion.

Purpose: Therefore, we tried to determine the transmural extent of RFA using magnetic resonance imaging (MRI).

Methods: RFA were created on the epicardial surface of the right ventricle in 18 mongrel dogs using a power-controlled, water-cooled 7-French catheter system (10 to 50 W for 30 s). The ablation lesions were imaged with non-contrast enhanced T1-weighted (SPGR: spoiled gradient recalled acquisition) and T2-weighted (FSE: fast spin echo) protocols, or after intravenous injection of 0.225 mmol/kg gadolinium using a T1-weighted fast gradient echo (FGRE) sequence. Ablation lesions and intramural extent were analyzed in the MR images and compared to the gross anatomy and histopathology.

Results: 59 RF lesions were created extending 2.2 mm to 8.3 mm into the ventricular wall and resulting in 17 transmural ablations. Lesions were accurately detected with all three imaging protocols. Non-contrast enhanced T2-weigthed images had a sensitivity of 100% and a specificity of 93.4% to detect transmural extent but slightly overestimated lesion thickness by 0.81 mm. For T1-weighted imaging protocols the sensitivity and specificity were 71.4% and 100% without contrast and 85.7% and 94.4% after gadolinium injection. Transmural extent of the lesion as assessed with the T1-weighted protocols was underestimated by 0.15 mm without and overestimated by 1.22 mm with contrast. The correlation with the histopathological specimen was excellent with all three imaging protocols ($r = 0.89$, $r = 0.89$, and $r = 0.93$, respectively).

Conclusion: Successful transmural RFA can be accurately assessed using MRI with and without contrast enhancement. Therefore, MRI might provide a useful tool to determine the procedural success for complex ablation procedures and guide further therapeutic strategies.

478. Comprehensive Coronary Imaging in an Integrated Real-Time Cardiac MRI Environment

Ajit Shankaranarayanan,[1] Andres Carrillo,[1] Phil Yang,[2] Bob Hu,[3] Jane Johnson,[1] Jean Brittain,[1] Michael McConnell.[2] [1]*ASL West, GE Medical Systems, Menlo Park, CA, USA*, [2]*Stanford University, Palo Alto, CA, USA*, [3]*Palo Alto Medical Foundation, Palo Alto, CA, USA*.

Introduction: MRI can non-invasively image coronary arteries using several techniques, including real-time, gated, contrast-enhanced, and black-blood approaches. However, the traditional user interface requires separate sequences for each of these techniques and provides minimal flexibility for rapidly changing scan locations and parameters. To provide the user with a comprehensive approach to coronary MRI, we have developed a real-time interactive imaging environment that can rapidly switch to a gated high-resolution spiral bright-blood, IR-prepped, or black-blood acquisition. Real-time coronary imaging can localize the desired scan plane and the user can then interactively select the inversion pulse parameters to provide non-con-

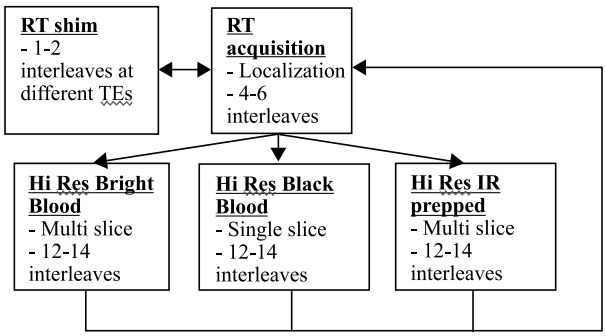

Figure 1. Workflow of the comprehensive coronary artery imaging tool. (*View this art in color at www.dekker.com.*)

Copyright © Marcel Dekker, Inc. All rights reserved.

ORDER REPRINTS

trast or contrast-enhanced angiography or coronary wall imaging.

Method: The new real-time coronary artery imaging tool was implemented on a GE 1.5 T Signa Twinspeed system (GE Medical Systems, Milwaukee, WI) with a high performance gradient system achieving a maximum gradient strength of 40 mT/m and maximum slew rate of 150 mT/m/msec. The configuration included EXCITE technology with vector array processors running optimized sliding-window, gridding reconstruction software (Shankaranarayanan et al., 2003) and a Linux host for high display rates.

Figure 1 shows the workflow of the coronary imaging tool. The tool has five modes of operation: an interactive real-time mode used to navigate to the slice of interest, a real-time shimming tool (Carrillo et al., 2003) used to optimize the center frequency and shim for the localized volume of interest, a multi slice high-resolution gated acquisition mode for bright blood imaging, a single slice high-resolution gated black-blood acquisition for coronary wall imaging and a multi slice high-resolution gated IR prepped acquisition for first pass contrast enhanced coronary angiography.

The inversion time (TI) for the black-blood imaging mode is set according to the heart rate and blood T1. The method utilizes two inversion recovery pulses (a non-selective 180° inversion immediately followed by a slice-selective 180° adiabatic inversion pulse) to null the blood (Edelman et al., 1991). The high-resolution IR prepped mode consists of only the non-selective inversion pulse. The user interface additionally provides a slider to change the TI of the acquisition in real time. The remaining default parameters for all acquisitions include 5 mm slice thickness, 20 cm FOV and 30° flip angle. All the modes use a 13 ms spectral-spatial excitation pulse. Contextual information including slice location and orientation and ''prescan'' parameters is automatically shared.

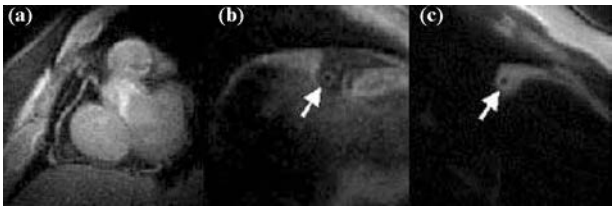

Figure 2. Coronary artery images acquired using the integrated real-time environment: (a) bright-blood RCA image, (b) black-blood cross-sectional image of the RCA coronary wall, (c) fat-selective black-blood image at the same location as image (b) illustrating the epicardial fat surrounding the RCA. (*View this art in color at www.dekker.com.*)

Results: Figure 2 illustrates an image of the right coronary artery (RCA) and the coronary wall of a healthy volunteer acquired using the coronary imaging tool. Good visualization of the artery and the wall was achieved in a single exam utilizing the real-time tool. The total time taken to localize and obtain all three images was less than 8 min.

Discussion and Conclusion: The clinical standard of x-ray coronary angiography is typically performed by initial localization of the imaging plane by fluoroscopy immediately followed by high-resolution angiography. We have developed a technique that closely follows this workflow and have expanded the available contrast mechanisms by integrating black-blood and IR-prepped imaging. The result is a more dynamic, efficient and comprehensive imaging tool.

REFERENCES

Shankaranarayanan, A., et al. (2003). *ISMRM*. 1072.
Carrillo, A., et al. (2003). *SCMR*. 417.
Edelman, R. R., et al. (1991). *Radiology*. 655–660.

479. Three-Dimensional Myocardial Strain Analysis with High Temporal Resolution, Using HARP

Sandra R. R. Tecelao, M.Sc.,[1] Jaco J. M. Zwanenburg, M.Sc.,[2] Joost P. A. Kuijer, Ph.D.,[2] J. T. Marcus, Ph.D.[2]
[1]*Institute of Biophysics and Biomedical Engineering, University of Lisbon, Lisbon, Portugal*, [2]*Department of Physics and Medical Technology, VU University Medical Centre, Amsterdam, Netherlands.*

Introduction: HARP tracking has shown to be a fast automatic tool to obtain myocardial strain maps for the early detection of ischaemia. Currently HARP tracking is performed in 2D, which does not take into account the full 3D motion. Approaches to 3D HARP were presented by Ryf et al. (2002) and Pan et al. (2003). As yet, it is either not possible to obtain a high temporal resolution (Ryf et al., 2002) or to obtain the complete 3D strain tensor, including the radial strain (Pan et al., 2003).

Purpose: To determine the complete 3D myocardial strain tensor with high temporal resolution, based on HARP motion tracking in short-axis (SA) and long-axis (LA) image planes.

Methods: Acquisition—MR imaging with CSPAMM tagging was performed using SSFP cine

Copyright © Marcel Dekker, Inc. All rights reserved.

ORDER REPRINTS

imaging (Zwanenburg et al., 2003), which was applied with a multiple breath-hold scheme to obtain a high temporal resolution of 14 ms. Using 39 time frames, 550 ms of the cardiac cycle was covered. These tagging cines were acquired in five SA and three LA image planes in a healthy volunteer. In the LA planes, the tagging lines were adjusted orthogonal to the long axis direction. HARP tracking—In order to track the motion in the SA image planes, the 2D HARP tracking method developed by Osman et al. (1999) was used. In contrast to his implementation, a high-pass filter in k-space was used (Zwanenburg et al., 2003). The displacement obtained was filtered using a moving average filter (kernel size of 5 pixels). Motion tracking in the long-axis images was performed using a 1D HARP tracking method. 3D strain—The LA motion information was used to describe the LA displacement field throughout the myocardium. For the calculation of 3D motion of myocardial points, the motion trajectories on the SA image planes were combined with the motion in the long-axis direction. From the resulting 3D motion trajectories of myocardial points, the 3D strain tensor was calculated (Kuijer et al., 2000).

Results: The plots represent 3D strain curves versus time, calculated from 682 tracked myocardial points in the LV wall. The presented 3D strain parameters are: regional torsion (α_{cl}), longitudinal strain (ε_l), circumferential strain (ε_c) and radial strain (ε_r). These strain parameters are available for each temporal frame of 14 ms. The 50% recovery times of diastolic strain are for α_{cl} 364 ms, for ε_l 420 ms, for ε_c 434 ms and for ε_r 420 ms.

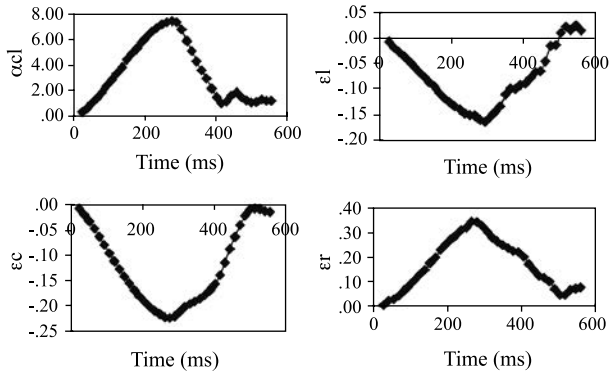

Figure 1.

In this 3D strain analysis approach, the spatial resolution in the SA HARP strain maps is optimally conserved. Interpolation and fitting are only used in the longitudinal direction. The early recovery of $_{cl}$ means that diastolic untwisting is faster than longitudinal, circumferential, and radial relaxation, as reported earlier (Rademakers et al., 1992) (Fig. 1).

Conclusions: The presented method yields a complete 3D myocardial strain analysis with high temporal resolution. Because it is based on HARP tracking, no user interaction is required during the tracking process and thus the method offers prospects for clinical applications with high temporal resolution. These applications include the detection of ischaemia, asynchronous contraction and diastolic dysfunction.

Acknowledgment: Supported by the Portuguese Foundation for Science and Technology, grant SFRH/BD/3005/2000.

REFERENCES

Kuijer, J. P. A., et al. (2000). *Magn. Reson. Imaging* 18:553–564.
Osman, et al. (1999). *Magn. Reson. Med.* 42:1048–1060.
Pan, L., et al. (2003). *ISMRM Proceedings*. Paper 950.
Rademakers, et al. (1992). *CIRC* 85:1572–1581.
Ryf, S., et al. (2002). *J. Magn. Reson. Imaging* 16(3):320–325.
Zwanenburg, J. J. M., Kuijer, J. P. A., et al. (2003). *Magn. Reson. Med.* 49:722–730.

480. The Use of a Highly Spatially Selective Cylindrical Radio Frequency Pulse for Coronary Vessel Wall Imaging

Matthias Stuber, Ph.D.,[1] Christoph Barmet,[2] Henning Steen, M.D.,[3] Harikrishna Tandri, M.D.,[3] Milind Deasi, M.D.,[1] Peter Boesiger, Ph.D.,[2] Warren J. Manning, M.D.[4] [1]*Radiology, Johns Hopkins University, Baltimore, MD, USA*, [2]*Biomedical Engineering, ETH Zurich, Zurich, Switzerland*, [3]*Cardiology, Johns Hopkins University, Baltimore, MD, USA*, [4]*Cardiology, Beth Israel Deaconess Medical Center and Harvard Medical School, Boston, MA, USA*.

Introduction: Free-breathing 'local-inversion' coronary vessel wall imaging has recently been introduced (Botnar et al., 2001) and positive coronary arterial remodeling has been characterized using this technique (Kim et al., 2002). 'Local inversion' is an extension of the dual-inversion concept in which a non selective inversion pre-pulse is followed by a 2D selective cylindrical re-inversion of the magnetization at the anatomical level of interest. After a time delay TI that

Copyright © Marcel Dekker, Inc. All rights reserved.

ORDER REPRINTS

allows for signal-nulling of the in-flowing blood into the coronary arteries, imaging is performed. As a result, the coronary lumen blood-pool appears signal suppressed and the adjacent coronary vessel wall is signal-enhanced. To optimize the signal-to-noise ratio (SNR) with this concept, a maximized efficiency of the re-inversion of the magnetization in the region of interest has to be ensured, and re-inversion of the blood flowing into the coronary arteries has to be avoided to maximize the contrast-to-noise ratio (CNR).

Purpose: To maximize SNR and CNR in 'local-inversion' coronary vessel wall imaging through the design of highly spatially selective cylindrical RF pulses.

Methods: For the design of 2D selective RF pulses, a numerical simulation of the Bloch-equations was implemented on a PC. Using this tool, we interactively designed RF and gradient waveforms that lead to a high spatial selectivity and re-inversion efficiency of 2D selective pulses. These software-prescribed RF and gradient waveforms were subsequently implemented on a commercial MR system (Philips 1.5T Intera) and combined with a preceding non-selective inversion pre-pulse, navigator technology for free-breathing data acquisition, and fat-suppressed 3D spiral imaging (Figure 1).

The cylindrical pulse diameter and spatial orientation can be defined on the user-interface of the scanner, and in-vivo, the central axis of the 2D pulse was localized concentric with the right coronary artery (RCA). Imaging parameters included 2 ramped (45−>90 Deg) RF excitations/RR interval (TR=30 ms, TE=2.3 ms, acquisition window=60 ms, 512 matrix, 400 mm FOV, $0.78 \times 0.78 \times 2$ mm voxel size, 10 slices), imaging was performed every other RR interval, and the heart-rate-dependent TI was 500–700 ms.

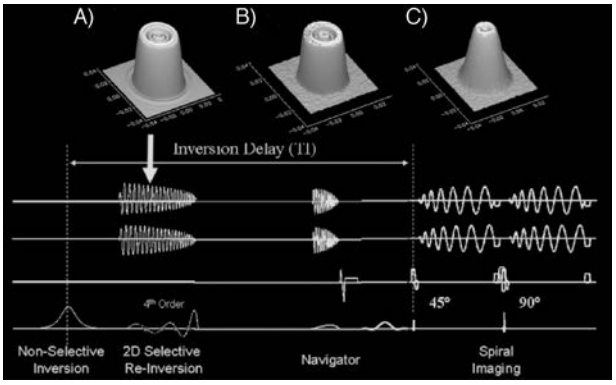

Figure 1. Imaging sequence for free-breathing 3D spiral coronary vessel wall imaging. A non-selective inversion pre-pulse is followed by a highly selective cylindrical re-inversion of the magnetization, the navigator for respiratory motion suppression, fat saturation and a dual-interleave spiral imaging sequence with ramped flip-angles. TI=inversion delay. In A) and B), the numerically simulated 2D pulse and the phantom experiment show an excellent agreement and a high selectivity of the pulse. In C), the previous pulse with lower selectivity (shallower slopes) and re-inversion efficiency (narrower tip) is shown. (*View this art in color at www.dekker.com.*)

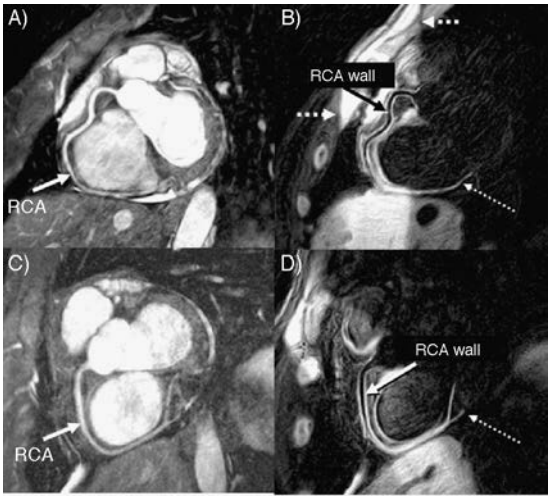

Figure 2. SSFP coronary MRA (A & C) used as a scout scan. In B) and D), the corresponding vessel wall images acquired with the highly selective cylindrical RF pulse (hatched arrows, B) in conjunction with a 3D spiral imaging sequence are displayed. In B) & D), note the high SNR on the vessel wall, the high CNR between wall and lumen, and the signal-enhanced distal portions of the RCA (dotted arrows). All images were acquired during free-breathing using navigator technology.

Results: 2D selective pulse—Using the simulation software, it was found that a spiral trajectory covering 4 side-lobes of the Fourier transform of a cylinder (in k-space during the excitation) leads to both an efficient re-inversion of the magnetization and a high spatial selectivity, while a reasonably short pulse duration (~10 ms) is obtained. In Figure 1A, the numerical simulation of the Mz magnetization is displayed adjacent to that of a scanner experiment in a phantom using the same pulse (Figure 1B). In Figure 1C, the Mz magnetization of the older 2D selective pulse covering (only) the central lobe of the Fourier transform of a cylinder is displayed for comparison. The tip of that pulse is narrower, suggesting a sub-optimal re-inversion-efficiency (and thus a potential penalty in SNR, since maximum re-inversion and SNR is only obtained at the tip of the pulse) when compared to the result of the new pulse. In parallel, the slopes of the newer pulse

Copyright © Marcel Dekker, Inc. All rights reserved.

ORDER REPRINTS

are much steeper, suggesting improved spatial selectivity. In-vivo experiments—In Figure 2, two example in-vivo coronary vessel wall images (B & D) obtained using the new cylindrical pulse are displayed adjacent to the SSFP coronary MRA from the same subjects. On the vessel wall images, a high signal intensity of the coronary wall and a signal suppressed coronary lumen over a long contiguous segment leads to a high CNR and an excellent vessel wall delineation.

Conclusions: Using a highly spatially selective cylindrical RF pulse with improved re-inversion efficiency, high-quality coronary vessel wall images can be obtained. The simulation software enables a very accurate and effective design of these complex cylindrical pulses.

REFERENCES

Botnar, et al. (2001). *Magn. Reson. Med.* 46(5).
Kim, et al. (2002). *Circulation* 106(3).

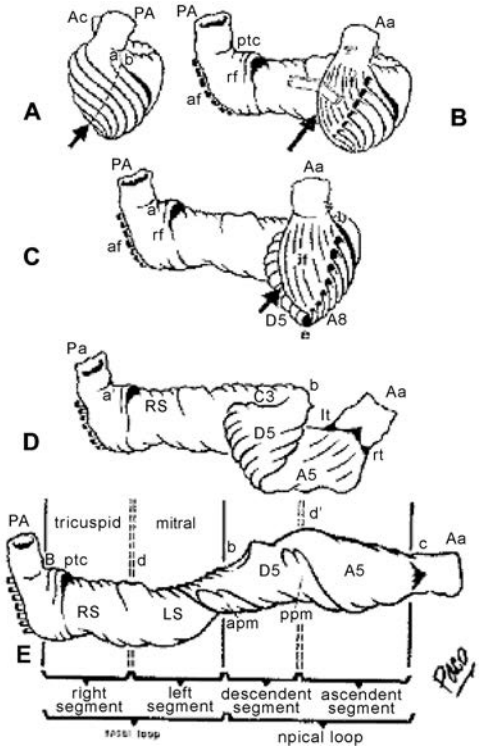

Figure 1. Schematic representation of the Torrent-Guasp concept for the myocardial band.

481. Interpreting Myocardial Morphology and Function from DENSE MRI Data Based on Fluid Mechanics Concepts

Nikoo R. Saber, Ph.D.,[1] Morteza Gharib, Ph.D.,[1] Han Wen, Ph.D.,[2] Gerald D. Buckberg, M.D.,[3] Brian D. Ross, M.D.[4] [1]*Aeronautics and Bioengineering, California Institute of Technology, Pasadena, CA, USA*, [2]*Laboratory of Cardiac Energetics, NIH/NHLBI, Bethesda, MD, USA*, [3]*Division of Cardiothoracic Surgery, UCLA School of Medicine, Los Angeles, CA, USA*, [4]*Magnetic Resonance Spectroscopy, Huntington Medical Research Institutes, Pasadena, CA, USA*.

Introduction: The concept of the helical heart was first introduced by Torrent-Guasp et al. (2001). It is hypothesized that ventricular cavities are defined by a single rope-like muscle band forming a double helix structure (Figure 1). However, this model of cardiac anatomy and fiber orientation has not been verified experimentally in vivo and its consequences for cardiac function have not been tested.

Displacement Encoding Stimulated Echo (DENSE) is a phase contrast method for measuring the Lagrangian displacement fields of the myocardial wall in vivo (Aletras et al., 1999). It provides a high spatial density of displacement measurements in the myocardium via stimulated echoes, while the image is always acquired at the same time point in the cardiac cycle.

Streamlines are defined in fluid mechanics as traces tangent to the flow velocity vectors at any given point in time and show the flow stream direction. We propose to apply this stream function concept to determine wall point trajectories from DENSE MRI data, where the traces now start from the initial position of each point and are tangent to the respective displacement vectors any instant. The resultant curves show the displacement pattern of points within the cardiac wall and can potentially identify myocardial fiber orientations or preferential contraction pathways.

Purpose:

1. Identifying myocardial fiber orientations and wall dynamics in vivo based on the Torrent-Guasp hypothesis of the helical heart.
2. Using DENSE and other MRI techniques as a means to accomplish the first goal.
3. Determining wall point trajectories from in vivo DENSE data via the application of the stream function concept adapted to the myocardial displacement field.

Methods: DENSE MRI data has been acquired for a human subject and two canine hearts at 1.0 mm

Copyright © Marcel Dekker, Inc. All rights reserved.

ORDER REPRINTS

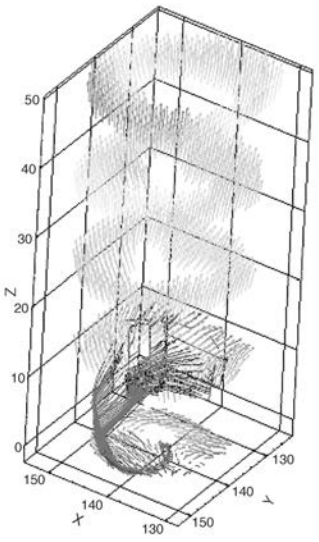

Figure 2. The onset of a helical structure from the stream functions (red curves) plotted for the 3D displacement vector field acquired using the DENSE method from a human subject. Note that the vertical axis is expanded. (*View this art in color at www.dekker.com.*)

spatial and 100 frames/second temporal resolutions. Trajectories of points on the heart walls are then derived from their displacement vectors in space, by applying the general stream function concept described above. This is done both longitudinally in 3D for the series of contiguous short axis slices, and in 2D for individual slices.

Results: The DENSE data presented in Figure 2 show a single phase 3D set from a human subject averaged at one time point during the cardiac cycle, i.e. end systole. In other words, the vectors illustrate the total displacement of each pixel between the QRS complex (start of systole) and the end-systolic phase. Point displacement trajectories described above are plotted on this 3D displacement field, where the onset of a helical pattern from the apex and following on to the planes above is evident. The 2D curves on Figure 3 are representative of the in-place stream traces on one sample apical short axis slice of the left ventricle. These trajectories identify the circumferential torsion occurring in the myocardium over the systolic period as well as the fiber orientation.

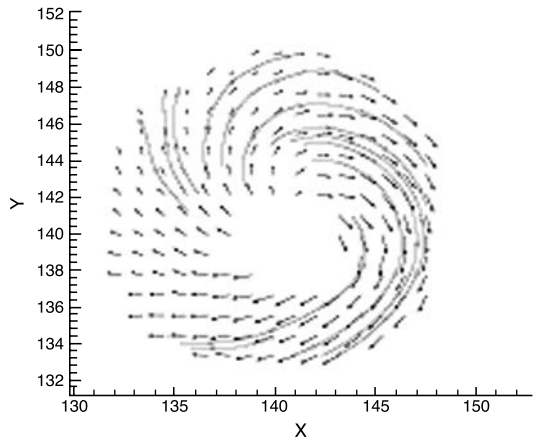

Figure 3. In-plane streamlines plotted for apical short-axis slice of DENSE data for a human left ventricle. (*View this art in color at www.dekker.com.*)

Conclusions: Our work in progress demonstrates the possibility of inferring myocardial fiber orientation and morphology from DENSE MRI data. The spatial and temporal resolution of the data acquired using this technique is superior to any other imaging modality involving myocardial tagging and tracking. The initiation of a 3D helical structure has been demonstrated, as well as varying contraction patterns across the ventricle wall. The results provide implications for cardiac function, such as preferential contraction pathways, and will have an impact on clinical diagnosis and treatment in the future.

REFERENCES

Aletras, A. H., Ding, S., Balaban, R. S., Wen, H. (1999). DENSE: displacement encoding with stimulated echoes in cardiac functional MRI. *J. Magn. Reson.* 137:247–252.

Torrent-Guasp, F., et al. (2001). Spatial orientation of the ventricular muscle band: physiologic contribution and surgical implications. *J. Thorac. Cardiovasc. Surg.* 122.2:389–392.

482. In vivo Measurement of the Elasticity and Internal Viscous Damping Constant of the Myocardium in Diastole

Han Wen, Ph.D., Eric Bennett. *Nhlbi, National Institutes of Health, Bethesda, MD, USA.*

Introduction: Compliance of the heart muscle in the relaxed diastole is a factor in the regulation of cardiac output by the Frank-Starling law, and in abnormalities of diastolic filling. In mechanical terms, compliance is measured by the elastic modulus and the internal viscous damping constant (IVDC) of the muscle. Although they have been measured in skinned and

Copyright © Marcel Dekker, Inc. All rights reserved.

ORDER REPRINTS

intact isolated cells (Roos and Brady, 1986), there are few non-invasive ways to measure these parameters in vivo. This paper describes a method to measure muscle compliance using MRI.

Purpose: The purpose is to quantify the elasticity and internal viscous damping constant of the muscle in the different areas of the heart non-invasively.

Methods: Beagles (n = 13) were anaesthetized and ventilated at 25 breaths/min. Right atrial pacing was realized with a MR compatible catheter via the femoral vein. Pacing and ventilation were synchronized to remove respiratory motion artifacts.

Scans were performed with a 1.5T clinical scanner (Sonata, Siemens). In a long-axis slice containing the lateral papillary column, myocardial wall motion during the diastolic period was mapped with DENSE tissue tracking (Aletras et al., 1999). The imaging parameters were: matrix size = 128×96, FOV = 190^2 mm^2, true temporal resolution $6.2 \sim 10$ ms. Phase-contrast blood flow velocity maps of the same slice were acquired at the same spatial and temporal resolution.

During diastolic filling, transient longitudinal pressure gradients exist in both ventricles, and are reflected by the accelaration and deccelaration of blood. The pressure gradients were quantified from the flow velocity maps (Navier–Stokes relation). In response to the pressure gradients, the myocardial wall develops longitudinal gradients of strains within the muscle. The amplitude and timing of this response is determined by the elastic modulus and the IVDC of the muscle. Assuming a simple cylindrical geometry and taking into account the inertial force from the acceleration of the muscle mass, the elasticity and the IVDC were calculated.

The compliance parameters were measured in the lateral wall, the septum, the papillary muscle, and the right ventricular wall.

Results: Figure 1 shows one frame of a multiphase tissue tracking data set.

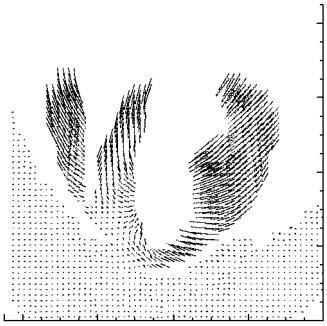

Figure 1.

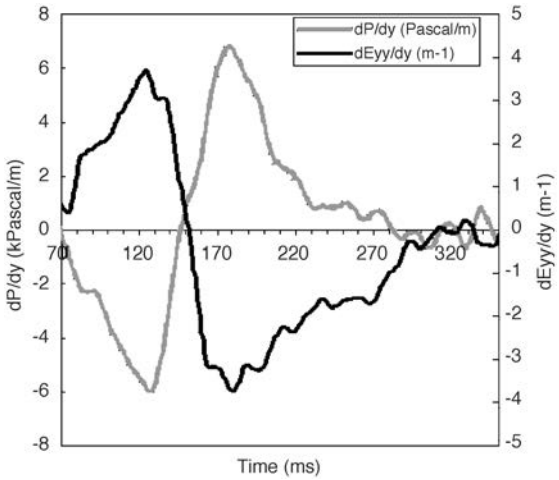

Figure 2.

Figure 2 shows the time traces of the pressure gradient dP/dy in the LV, and the longitudinal gradient of the longitudinal strain in the septum (dE_{yy}/dy), in a dog heart during diastole.

Table 1 summarizes the elastic modulus, the IVDC and the characteristic response times (IVDC/elastic modulus) of four regions of the heart. The results in the RV and the Papillary muscle had higher uncertainty. This is caused by the lower number of image pixels in these regions, and correspondingly higher noise levels in the derivative calculations.

Conclusions: The elastic modulus values are one twentieth of those obtained in skinned isolated cells. The current results will predict a LV dastolic suction of negative 1 to 2 mmHg, consistent with in vivo diastolic suction measurements (Bell et al., 1996). Thus the intact muscle is much more compliant than skinned cells. The characteristic response times are approximately one tenth of the isolated cells, suggesting that the living myocardium has much less internal friction than isolated cells.

Regional variability of the elastic constants suggests that they may be anisotropic and dependent on

Table 1.

Mean ± stdev (n = 13)	Elastic modulus (N/m2)	IVDC (sec*N/m2)	Characteristic response time (ms)
LV lateral	1610 ± 440	12 ± 12	2.1 ± 2.9
Septum	701 ± 230	19 ± 10	7.2 ± 6.3
Papillary muscle	1100 ± 640	22 ± 17	4.5 ± 6.0
RV	500 ± 330	12 ± 6	12 ± 13

Copyright © Marcel Dekker, Inc. All rights reserved.

ORDER REPRINTS

the fiber orientation. Because the measurements came from long-axis slices, they contained different mixtures of the cross-fiber and along-fiber components in different areas. The lowest elastic modulus was seen in the RV, where the measurement was predominantly cross-fiber.

REFERENCES

Aletras, A. H., Ding, S. J., Balaban, R. S., Wen, H. (1999). *J. Magn. Reson.* 137:247–252.

Bell, S. P., et al. (1996). *Am. J. Physiol.* 39(3):H1015–H1020.

Roos, K. P., Brady, A. J. (1986). *Am. J. Physiol.* 256(2):H539–H551.

483. MR-Coronary Angiography Using a Contrast-Enhanced Breath-Hold 3D-FIESTA-Sequence: Initial Experiences

Anja Zagrosek, M.D.,[1] Hassan Abdel-Aty, M.D.,[1] Ralph Noeske, Ph.D.,[2] Rainer Dietz, M.D.,[1] Matthias G. Friedrich, M.D.[1] [1]*Franz-Volhardt-Clinic, Humboldt–University, Berlin, Germany*, [2]*GE Medical Systems Deutschland, Berlin, Germany*.

Introduction: Contrast-enhanced SSFP pulse sequences are well established for magnetic resonance angiography (MRA) of peripheral vessels. Recent developments enabled contrast-enhanced breath-hold 3D-SSFP techniques for MR coronary angiography (MRCA).

Purpose: The goal of this study was a feasibility and reliability evaluation of this new technique. We sought to assess its ability to visualize the proximal and middle parts of the coronary arteries and furthermore we investigated the influence of contrast agent application on signal to noise and contrast to noise ratio (SNR and CNR) for each vessel.

Methods: 21 individuals (7 volunteers, mean age 41 years and 14 patients mean age 65 years with angiographically confirmed coronary artery disease underwent MRCA on a 1.5 T-scanner (GE Signa CV/*i*) using a contrast-enhanced breath-hold 3D-fat-sat SSFP sequence. Each exam was targeted at 2–3 of the coronary arteries (7 to 10 segments). A blinded reader rated the image quality for each coronary artery on a scale from 1 (unreadable) to 4 (excellent), based on a 10-segment model covering the whole coronary artery tree. SNR and CNR before and after application of contrast agent (GD-DTPA) were measured.

Results: Mean scan duration was 40 min. (range 25–55 min.), mean image quality scores were 3.6±0.5 in volunteers and 3.0±1.0 in patients. In 2 of 14 patients image quality was insufficient for analysis. In volunteers a total number of 52 out of 67 segments (78%) were visible whereas in patients only 75 of 111 segments (68%) could be depicted. Results for visible length are shown in Table 1. In the RCA, the application of Gd-DTPA increased SNR from 9.5±3.9 to 13.3±5.1 ($p=0.005$) and CNR from 7.5±3.7 to 10.1±4.5 ($p=0.01$), whereas there were no significant changes in the left coronary artery.

Conclusion: This 3D-SSFP-based technique allows depiction of extensive parts of the coronary arteries. When assessing the right coronary artery, application of contrast agent significantly improves CNR, which is not the case for the left coronary artery. Studies in larger patient populations however are warranted to determine the diagnostic performance of this technique in a clinical setting.

Table 1.

	Visible vessel length	
	Volunteers	Patients
LMCA	12.0±3.0 mm (7.3–15.0 mm)	12.0±1.0 mm (9.0–13.0 mm)
LAD	75.0±6.0 mm (68.0–82.0 mm)	51.0±20.0 mm (29.0–90.0 mm)
LCX	23.0±7.0 mm (15.0–32.0 mm)	34.0±12.0 mm (14.0–52.0 mm)
RCA	102.0±17.0 mm (79.0–135.0 mm)	84.0±37.0 mm (12.0–134.0 mm)

484. A New MRI Method for Atherosclerotic Plaque Detection Using a Novel MR Contrast Agent in vivo

Marc Sirol, M.D.,[1] Vitalii V. Itskovich, Ph.D.,[1] Venkatesh Mani, Ph.D.,[1] Juan Gilberto S. Aguinaldo, M.D.,[1] Hanns-Joachim Weinmann, Ph.D.,[2] Jean-François Toussaint, M.D., Ph.D.,[3] Valentin Fuster, M.D., Ph.D.,[1] Zahi A. Fayad, Ph.D.[1] [1]*Cardiovascular Institute, Mount Sinai School of Medicine, New York, NY, USA*, [2]*Schering, Berlin, Germany*, [3]*Service de Physiologie et Radioisotopes, Hopital Europeen Georges Pompidou, Paris, France*.

Introduction: Magnetic resonance (MR) molecular imaging using specific targets for atherosclerotic

Copyright © Marcel Dekker, Inc. All rights reserved.

ORDER REPRINTS

plaque detection may provide plaque activity and its potential to rupture.

Purpose: The aims of our study were: 1) to evaluate the use on plaques detection of a new class of contrast agents, gadofluorines (Gd-M (Schering AG)), that forms micelles in aqueous solutions; 2) to optimize MR plaque imaging methods using Gd-M.

Methods: Aortic plaques were induced in 12 rabbits. Six ''normal'' rabbits were used as control. MRI was performed before (PRE), and after (POST) injection (iv) of 50 μmol/kg of Gd-M, immediately, and at 1 and 24 hours. Two T1-weighted gradient echo MRI methods were optimized for: 1) blood flow suppression (dark blood; DB); and 2) plaque enhancement POST injection. DB imaging was performed using a) an inversion recovery (IR) prepulse (PP) or b) a diffusion (DIFF) based flow suppression prepulse. DIFF PP consisted of 3 rectangular radio frequency pulses separated by DIFF gradients. To enhance vessel wall delineation POST, the surrounding tissue was suppressed by using either IR PP or the combination of IR plus DIFF PP (DIFF-IR).

Results: The DIFF-IR sequence showed significant EN POST vs. PRE (1 hr: 164%; 24 hr: 207%). Using IR sequence, 24 hr POST EN was 37%; in 1 hr POST the vessel wall was not delineated due to poor flow suppression (very short blood T1). At 1 hr, and 24 hr POST, the contrast to noise ratio (CNR) was higher using DIFF-IR vs. IR ($p<0.05$). There was no POST EN in control.

Conclusion: The DIFF-IR method and Gd-M demonstrated EN with excellent CNR in atherosclerotic rabbits as early as 1 hr POST. Imaging of atherosclerotic plaque by molecular MR may provide understanding of the disease and play a role in detection before clinical events.

485. The Role of Still-Frame Parametric Imaging in Magnetic Resonance Assessment of Left Ventricular Wall Motion by Non-Cardiologists

Eran Toledo, Ph.D.,[1] Enrico G. Caiani, Ph.D.,[2] Peter MacEneaney, M.D.,[1] Keith A. Collins, M.S.,[1] Roberto M. Lang, M.D.,[1] Victor Mor-Avi, Ph.D.[1] [1]*Medicine/Cardiology, University of Chicago, Chicago, IL, USA*, [2]*Biomedical Engineering, Politecnico di Milano, Milan, Italy*.

Background: The assessment of left ventricular (LV) wall motion from cardiac magnetic resonance (CMR) images is based on subjective visual interpretation of dynamic loops, often performed by non-cardiologists who do not have the specialized training and experience in the evaluation of regional LV function. We tested the hypothesis that adding computer-generated still-frame parametric images of LV wall motion to the dynamic loops could improve the accuracy and reduce the inter-observer variability of the CMR assessment of LV wall motion.

Methods: Dynamic images were obtained using a 1.5T scanner (GE) using an EKG-gated steady state free precession (FIESTA) pulse sequence in 6 to 10 short axis slices in 18 consecutive cardiac patients (10 with regional wall motion abnormalities, 2 with global hypokinesis and 6 with normal wall motion). Each image loop was then used to automatically generate a still-frame parametric image of wall motion, wherein each pixel is assigned a value equal to the sum of the amplitude of the first two harmonics in Fourier decomposition of local intensity over time series. In these images, pixels that changed between blood (high MR signal) and myocardial tissue (low MR signal) during the cardiac cycle were brighter than those that remained blood or tissue throughout the cardiac cycle. Thus, the thickness of the bright band surrounding the LV cavity in these images reflects the extent of regional endocardial motion (Figure 1). The dynamic images were initially reviewed by an expert cardiologist who graded regional LV wall motion in each segment in each slice as normal or abnormal. These grades were subsequently used as the ''gold standard'' for comparisons. The same dynamic images were then independently reviewed and graded by four general radiologists with different levels of experience in the interpretation of regional cardiac function. In a separate session, these non-expert readers reviewed the same images in random order in combination with a still

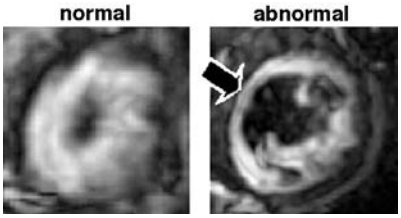

Figure 1.

Copyright © Marcel Dekker, Inc. All rights reserved.

ORDER REPRINTS

Table 1.

	Sensitivity	Specificity	Accuracy	Inter-observer variability
Dynamic images only	80%	76%	77%	52%
Dynamic + parametric images	83%*	80%*	81%*	33%*

*$p<0.05$.

frame parametric image generated from each dynamic loop, and graded LV wall motion once again based on the information in both types of images. Grades assigned to each segment by each non-expert in the two sessions were compared with the ''gold standard'' grades. Sensitivity, specificity and overall accuracy were calculated for each non-expert reader and averaged. In addition, inter-reader variability was assessed by calculating the percent of discordant grades, defined as percent of segments that were not graded identically by all four non-experts.

Results: The expert reader detected abnormal wall motion in 227/768 segments. The creation of parametric images was fully automated and required <5 sec on a 2 GHz Pentium 4 personal computer. The addition of still-frame parametric images resulted in improvement in sensitivity, specificity and accuracy of the non-expert interpretation (Table 1). Moreover, the availability of this additional information dramatically reduced the inter-observer variability (Table 1).

Conclusions. Still-frame parametric images of regional LV wall motion can be obtained quickly and automatically. Our results showed that these images provide additional information that improves the accuracy and reduces the inter-observer variability of the detection of regional wall motion abnormalities by non-cardiologists who are required to interpret cardiac images.

486. Enhanced Identification of Endocardial to Epicardial Flow Differences by M-Mode Display of Magnetic Resonance First-Pass Perfusion Studies

Daniel C. Lee, M.D.,[1] Edwin Wu, M.D.,[1] Thomas A. Holly, M.D.,[1] Orlando P. Simonetti, Ph.D.,[2] Kathleen R. Harris, B.A.,[1] Robert O. Bonow, M.D.,[1] Francis J. Klocke, M.D.[1] [1]*Feinberg Cardiovascular Research Institute, Northwestern University Medical School, Chicago, IL, USA*, [2]*Siemens Medical Solutions, Chicago, IL, USA*.

Introduction: During vasodilation, myocardium supplied by a stenotic artery demonstrates progressive reduction in flow from epi- to endocardium. The enhanced spatial resolution afforded by magnetic resonance first-pass perfusion imaging (MRFP) enables visualization of these transmural flow differences. Freehand drawing of multiple regions of interest (ROI) across the narrow span of the myocardial wall is imprecise and subject to user influence.

Purpose: We tested the hypothesis that analysis of flow using a novel ''M-Mode'' display of MRFP studies 1) allows quantification of the magnitude of transmural flow gradients in stenotic myocardium and 2) is more precise than traditional freehand drawing of ROI's.

Methods: Image Acqusition—Graded regional differences in coronary flow were produced during global coronary vasodilation in chronically instrumented dogs by partially occluding the left circumflex artery. 42 MRFP studies were performed on a 1.5 T scanner (Sonata, Siemens Medical Systems) using a single-shot inversion recovery true-FISP technique. Typical parameters were TR 500–600 msec, TI 270–280 msec, field of view 150×300 mm, matrix 77×256, voxel size $1.9\times1.2\times8$ mm. Fluorescent microspheres were injected into the left atrium immediately after each MR measurement for quantification of myocardial blood flow. Image Analysis—M-mode—Using NIH Image and a self-designed macro, voxel-by-voxel signal intensities across the myocardial wall were serially measured in the stenotic region throughout the first passage of contrast (top pane of

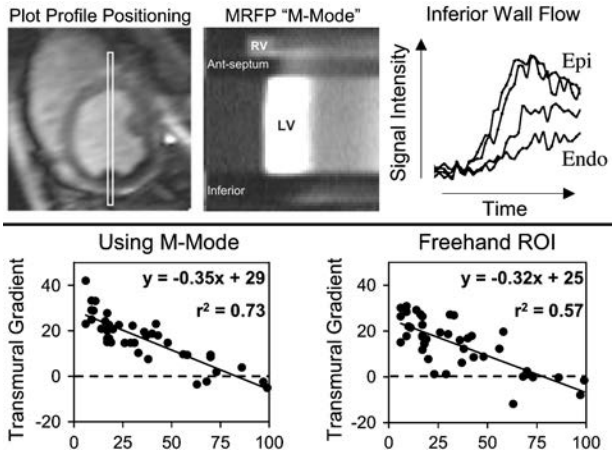

Figure 1. Relative regional flow by microspheres.

Copyright © Marcel Dekker, Inc. All rights reserved.

ORDER REPRINTS

Figure 1). Using a format similar to M-mode echocardiography, plot profiles were displayed as a function of time to facilitate subdivision of the myocardial wall in two-voxel steps. Signal–intensity curves were then generated for each subdivision. 3–6 curves could be obtained in the area of the inferior myocardium which included the posterior papillary muscle (6–12 voxels). The initial area under each curve was normalized to the highest value in that wall and taken to represent relative flow. Relative flow was plotted against layer number and the slope of the regression line measured to quantify the transmural flow gradient. Image Analysis—Freehand ROI—ROI's were manually drawn in the inner and outer thirds (endo- and epicardium) of the stenotic region in order to generate signal intensity curves. Transmural gradient was calculated in a similar manner as above.

Results: The delayed and diminished appearance of contrast in the endocardium relative to the epicardium was visually apparent in the M-Mode display. Transmural MRFP gradients derived both from M-Mode displays and freehand ROI's increased linearly with increasing severity of stenosis (bottom pane of Figure 1). Although the relationship between severity of stenosis and transmural gradient was demonstrated by both methods, the correlation was stronger for the M-mode as compared to the freehand technique ($y = -0.35x + 29$, $r^2 = 0.73$ versus $y = -0.32x + 25$, $r^2 = 0.57$).

The ability to visualize regional signal intensity changes over time in a single frame (rather than a 30–40 frame cine loop) also provided improved recognition of artifacts from motion and signal contamination originating outside the myocardium.

Conclusions: MRFP can identify endocardial to epicardial flow differences in areas of reduced perfusion reserve. Quantification of transmural flow gradients using an M-Mode display of MRFP demonstrates a closer relationship to severity of stenosis than measurement by freehand drawing of ROI's.

487. Coil Setup Optimization for 2D SENSE in Whole-Heart Coronary MRA

Martin Bührer, Michael E. Huber, Dr., Sebastian Kozerke, Dr., Peter Boesiger, Prof. Dr. *Insitute for Biomedical Engineering, ETH Zürich, Zürich, Switzerland.*

Introduction: Recently, a ''whole-heart'' imaging protocol for coronary MRA has been suggested (Weber et al., 2003), which covers the entire heart with a large non-angulated 3D measurement volume. Scan time is reduced using SENSE (Pruessmann et al., 1999) along one phase-encode direction (Weber et al., 2003).

In this work, accelerated ''whole-heart'' coronary imaging with sensitivity encoding in both phase encoding directions (2D-SENSE) (Weiger et al., 2002) was investigated.

To reduce the spatially dependent noise amplification in SENSE, an optimal coil setup was derived. In-vivo feasibility of 2D-SENSE for ''whole-heart'' imaging is demonstrated on healthy subjects.

Purpose: To present an optimized coil setup for accelerated ''whole-heart'' coronary MRA using 2D-SENSE.

Methods: In SENSE images, the SNR depends on a spatially varying function g(r) (g-factor), given by:

$$\mathrm{SNR}(r)^{\mathrm{SENSE}} = \mathrm{SNR}^{\mathrm{full}}/(g(r) * R^{1/2})$$

(r = position vector, R = reduction factor, $\mathrm{SNR}^{\mathrm{full}}$ = SNR without SENSE) (Weiger et al., 2002). Therefore, for an optimized coil setup, the g-factor on the heart should be as small as possible.

For coil setup optimization, an array of 6 rectangular coil elements (R1) was arranged in 12 different geometric configurations. For comparison, a commercial cardiac-synergy coil was used. The measurements were performed on an elliptical phantom simulating the thorax. A low resolution 3D SENSE reference scan (FOV = 370×370 mm^2, 20 slices,

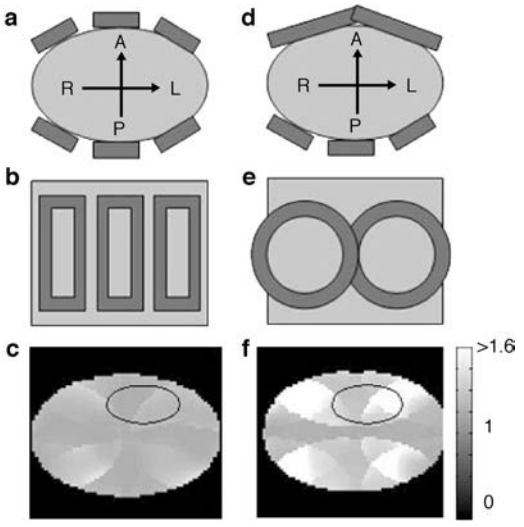

Figure 1. The g-maps of two different coil setups (left = 6 R1 coils, right = cardiac-synergy-coil, R = 4). The ellipse in the g-map indicates the position of the heart. (*View this art in color at www.dekker.com.*)

Copyright © Marcel Dekker, Inc. All rights reserved.

ORDER REPRINTS

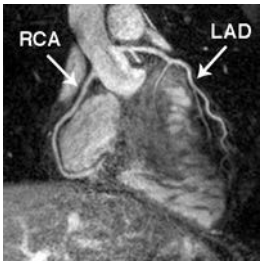

Figure 2. Simultaneous visualization of the right coronary artery (RCA) and the LAD. The image was acquired with the coil setup shown in Figure 1a,b and 2D-SENSE (R = 2.25).

voxel-size: $7.7 \times 7.7 \times 8$ mm^3) was acquired for each coil setup (TR = 8 ms; TE = 1.6 ms; flip angle = 5°). For evaluation of the phantom data, an ellipsoid of the size of the heart was positioned in the phantom images at locations similar to the in-vivo situation, and the mean g-factors inside were calculated (Figure 1c,f). This was used as a measure for the decrease of SNR expected on the heart in-vivo. The orientation of the measurement volume was varied as well as the reduction factor (R = 2.25, 3, 4) for 2D-SENSE.

The coil setup of the phantom measurement with the lowest g-factors was tested on three healthy subjects. A steady-state-free-precession sequence (TR = 5.2 ms, TE = 2.6 ms, flip angle = 90°, 17 RF excitations/cardiac cycle) with real-time respiratory motion correction was used. A 3D volume with 90 coronal slices (slice thickness = 1.5 mm, reconstructed to 0.75 mm, FOV = 240×240 mm^2, resolution = 1×1 mm^2) was acquired. All measurements were performed on a 1.5T Philips Intera (Philips Medical Systems, Best, The Netherlands).

Results: The calculations of the g-maps revealed that the standard cardiac-synergy coil (Figure 1d,e,f) does not provide adequate image quality at higher SENSE factors. Instead, a symmetric array of 3 R1 coils on the front- and the backside with the two phase encoding directions along the right–left (RL) and anterior–posterior (AP) directions performed best (Figure 1a,b,c). Using the optimized coil setup, the g-factor was 5–120% lower when compared to the cardiac-synergy coil, depending on the reduction factor.

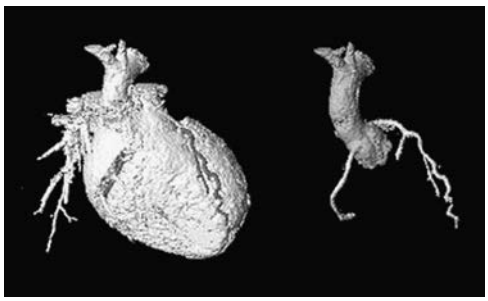

Figure 3. 3D surface rendering of the heart showing the coronary arteries reconstructed from a ''whole-heart'' scan with 2D SENSE (R = 2.25).

An in-vivo measurement using this optimized coil setup is shown in Figure 2. In particular, the left anterior descending coronary artery (LAD) can be displayed over a long segment. Although a reduction factor of 2.25 was used the noise in the image is relatively small.

Conclusions: Using an optimized coil setup, lower g factors are achieved when compared to the standard cardiac coil array, facilitating ''whole-heart'' coronary MRA with 2D-SENSE at acceleration factors greater than two (Figure 3).

REFERENCES

Pruessmann, K. P., et al. (1999). *MRM* 42:952–962.
Weber, O. M., et al. (2003). *JCMR* 5:23–24.
Weiger, M., et al. (2002). *MAGMA* 14:10–19.

488. Quantification of Coronary Atherosclerotic Plaque with MRI and Biomechanics: Initial Experience

Zheng Jie,[1] Faith E. Rowold, B.S.,[1] Jeffrey E. Saffitz, M.D.,[2] Pamela K. Woodard, M.D.,[1] Dalin Tang, Ph.D.[3]
[1]*Radiology, Washington University Medical School, St. Louis, MO, USA*, [2]*Pathology, Washington University Medical School, St. Louis, MO, USA*, [3]*Mathematics, Worcester Polytechnic Institute, Worcester, MA, USA*.

Introduction: Coronary atherosclerotic plaques may rupture without warning and cause acute syndromes such as myocardial infarction. The risk of atherosclerotic plaque disruption was thought to be closely related to plaque compositions and rupture triggers such as external mechanical and hemodynamic forces.

Purpose: The purpose of this study was to develop techniques to evaluate the MRI contrast and biomechanical stress and strain distributions in the plaques, based on MR images of coronary artery plaque specimens ex vivo.

Materials and Methods: Specimens—Seven coronary artery segments (LAD and/or LCx) were selectively collected from 6 autopsy patients (4M). There were three patients died of coronary artery disease

Copyright © Marcel Dekker, Inc. All rights reserved.

ORDER REPRINTS

Table 1. MRI and biomechanical properties of atherosclerotic plaques of coronary artery specimens.

Patients	Stenosis	T2 (LRNC)(ms)	T2 (FT)(ms)	Stress (dyn/cm^2)	Strain
CAD	86±6 (%)	35.4±4.8	62.4±15.5	2.32±0.55 ($\times 10^6$)*	0.17±0.02*
Non-CAD	79±12 (%)	35.2±6.6	69.0±20.4	1.33±0.42 ($\times 10^6$)	0.10±0.03

*P<0.002 between CAD and non-CAD.

(CAD; age = 55±16 years old) and three were died of other causes (non-CAD; age = 69±10 years old). MR Imaging—All imaging procedures were performed on a 3 T Siemens Allegra clinical system with the use of a single-loop coil. Multi-slice T1 and T2-weighted spin echo images were acquired along the cross sections with a resolution of 100×100 μm^2. T2-maps were reconstructed from multi-contrast images. Histograms were obtained after MR studies. Classification of plaque components (lipid-rich necrotic core or LRNC, calcification, fibrous tissue or FT) was based on histological findings and T2-weigthed contrast. T2 values of LRNC and FT were obtained by drawing ROI on these components. Biomechanical Analysis—Mesh was generated automatically for each component chosen. A finite element software package (ADINA) was used to perform stress/strain analysis. Maximum principal stress and all the other stress and strain components (total: 6) were obtained for analysis.

Results: There were no ruptured plaques in all patients. Total 14 slices of MR images were selected for analysis (CAD: n = 4; non-CAD: n = 10). Following Table 1 summarizes the findings from MR contrast and biomechanical properties. T2 of LRNC was substantially lower than that of fibrous tissue, including thickened intima. No statistically significant difference was observed between CAD and Non-CAD specimens in terms of T2 and stenosis degree(area narrowing). However, maximal values of maximal principal stress were 74% higher in plaques with CAD patients than non-CAD patients, whereas strain was also 70% higher in CAD patients. Figure 1 shows one plaque from a non-CAD patient.

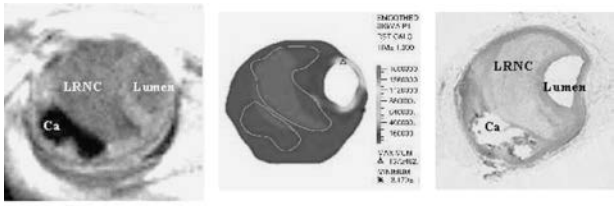

Figure 1. Large lipid filled necrotic core (LRNC) and calcification (Ca) presented in this plaque (a). Although there is a 93% stenosis, pathology analysis (c) suggested a mildly unstable condition. Maximal stress distribution map (b) demonstrates a maximal value 1.67×10^6 dyn/cm^2 (indicated by the triangle), which is slightly higher than the average value of non-CAD plaques (1.33×10^6 dyn/cm^2), indicating a less stable condition. (*View this art in color at www.dekker.com.*)

Conclusion: Non-invasive quantification of the MR contrast and mechanical properties of plaque may provide a useful biomarker for the assessment of vulnerability of atherosclerotic plaques.

489. Improved Saturation RF Pulse Design for Myocardial First Pass Perfusion at 3T

Niels Oesingmann, Ph.D.,[1] Qiang Zhang, Ph.D.,[2] Orlando Simonetti.[2] [1]*Siemens Medical Solutions, Erlangen, Germany*, [2]*Siemens Medical Solutions, Chicago, IL, USA*.

Introduction: Low spatial and temporal resolutions are two major limiting factors in the clinical application of MRI myocardial first pass perfusion techniques. Fast imaging techniques, e.g. partially parallel imaging and partial Fourier imaging (PFI) (Kellman et al., 2003; Zhang et al., 2003), are recently explored to improve the spatial and temporal resolutions at the expense of signal-to-noise ratio (SNR). The introduction of 3T MR scanners makes it possible for MRI first pass perfusion to achieve both high spatial/temporal resolution and a reasonable SNR. However, higher magnetic field (3T) introduces more B1 inhomogeneity, which is undesirable in saturation recovery methods used in MRI first pass perfusion.

Purpose: The purpose of this work was to overcome the non-uniform myocardial saturation on 3T MR scanners due to the B1 inhomogeneity. A new RF saturation pulse was designed for this purpose.

Methods: The new RF saturation pulse consists of three phase cycled 90° non-selective RF pulses with different time intervals for gradient spoilers (Figure 1A). This pulse design was implemented into a Turbo FLASH sequence, which allows both GRAP-

Copyright © Marcel Dekker, Inc. All rights reserved.

ORDER REPRINTS

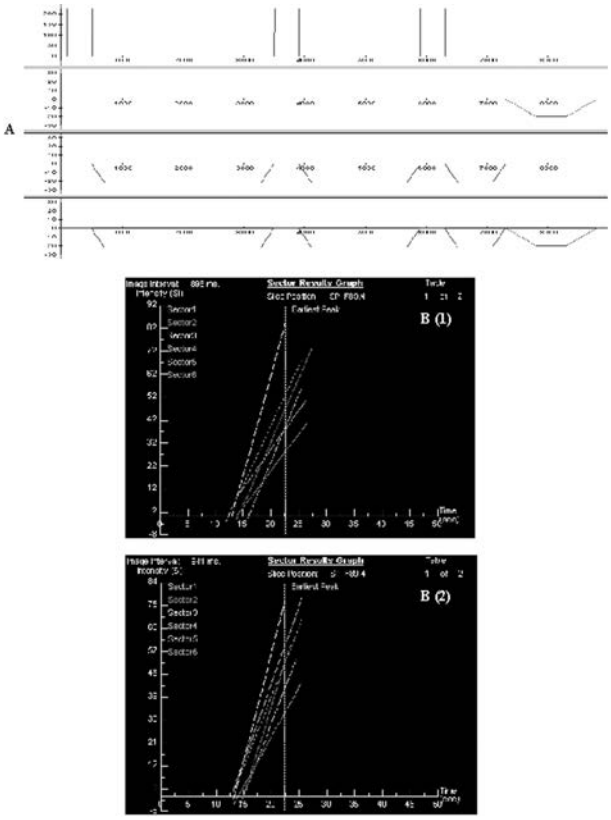

Figure 1. A. Three 90° hard pulses with variable spoiler gradients and an example upslope plot for B. (1) 1RF saturation pulse and C. (2) 3RF saturation pulse. (*View this art in color at www.dekker.com.*)

PA (Griswold et al., 2002) and PFI (Xu et al., 2001) acceleration techniques. Experiments were performed on a 3T Magnetom Trio system (gradient max amplitude 40 mT/m and max slew rate 200 mT/m/msec. Siemens Medical Solutions, Erlangen, Germany) equipped with eight independent receiver channels. An 8-element cardiac array coil was used. The sequence was tested in three healthy volunteers using IRB approved protocols. The imaging parameters were: bandwidth 770 Hz/pixel, FOV (220∼270)*(330∼360) mm^2, matrix 120*192, flip angle 15°, TR/TE 2.4/1.04 ms, slice thickness 8 mm, Partial Fourier factor 6/8, iPAT acceleration factor 2, 24 continuous k-space central lines were acquired as reference scans for GRAPPA and used to extract the phase-map for POCS. Data acquisition time was 130 ms/slice and total measurement time was 200 ms/slice including a 70 ms delay between the saturation pulse and 1st k-space line. Gd-DTPA was administered intravenously (4 ml/sec, 0.067 mmol/kg) followed by a saline flush. Two injections of Gd-DTPA were administed on each volunteer with a 20 minutes interval for two MR perfusion image acquisitions: one used the new saturation pulse (3RF) and the other used conventional one 90° non-selective saturation pulse (1RF). The order of the two image acquisition techniques was randomized.

The myocardial first-pass perfusion images were analyzed using Siemens Argus software. Signal uniformity within the myocardium was assessed by comparing the %STDEV (standard deviation / mean) of upslope between the 3RF design and the 1RF design. The myocardium was segmented into 6 equally-spaced sectors. %STDEV was first calculated for six sectors of each slice and it was then averaged over all 7 slices from three volunteers.

Results: The %STDEV of upslope for 1RF and 3RF designs were 28.74% and 14.63%, respectively. Smaller upslope %STDEV value of 3RF perfusion data indicates the new saturation pulse design provided better signal uniformity within the myocardium. Figure 1B displays two example upslope plots from one slice data acquired with 1RF and 3RF designs.

Conclusions: This new multiple saturation pulse design with phase cycling improves the spatial homogeneity of the magnetization preparation due to repeated RF saturation and gradient spoiling. Additionally, the measured signal changes should become less susceptible to inflow effects compared to the conventional single pulse preparation. This will allow a more accurate semi-quantitative analysis of MRI myocardial first pass images.

REFERENCES

Griswold, M., et al. (2002). *MRM* 47:1202–1210.
Kellman, P., et al. (2003). *ISMRM* 1658.
Xu, Y., et al. (2001). *JMRI* 14:628–635.
Zhang, Q., et al. (2003). *ISMRM* 1655.

490. Quantitative Wall Motion Imaging by Cine DENSE in Acute Myocardial Infarction: Initial Experience Using an SSFP-based Sequence

Frederick H. Epstein, Ph.D.,[1] Szilard Voros, M.D.,[2] Wesley D. Gilson, M.S.,[1] Christopher M. Kramer, M.D.[3] [1]*Radiology and Biomedical Engineering, University of Virginia, Charlottesville, VA, USA*, [2]*Cardiology, University of Virginia, Charlottesville, VA, USA*, [3]*Radiology and Cardiology, University of Virginia, Charlottesville, VA, USA*.

Copyright © Marcel Dekker, Inc. All rights reserved.

ORDER REPRINTS

Introduction: Displacement-encoding with stimulated echoes (DENSE) is a quantitative method for imaging intramyocardial strain with high spatial resolution and without performing tag detection. Original implementations of DENSE used single-phase imaging timed to measure systolic function (Aletras et al., 1999). We recently developed a breathhold cine DENSE sequence based on fast gradient echo/echo-planar imaging (FGRE-EPI) and validated it for strain quantification in healthy volunteers (Kim et al., 2003).

Purpose: The purposes of this study were 1) to increase the signal-to-noise ratio (SNR) in cine DENSE using steady-state free precession (SSFP) for data acquisition, and 2) to evaluate SSFP cine DENSE for detecting wall motion abnormalities in patients with myocardial infarction.

Methods: An ECG-gated SSFP sequence was modified for DENSE imaging as follows. As in SSFP myocardial tagging, upon R-wave detection an alpha/2 storing pulse was used to interrupt the steady state (Herzka et al., 2003). After applying displacement-encoding pulses in the frequency-encoding direction, a second alpha/2 pulse was used to approximately restore the steady state. During data acquisition, modified frequency-encoding gradients centered the displacement-encoded echo and nulled the gradient area over the repetition time. For time-independent suppression of T1-relaxation artifacts, complementary DENSE data sets were acquired (Kim et al., 2003). A third data set measured phase accumulation due to other sources. For each displacement-encoding direction, the three data sets were acquired in a single 15-second breathhold. Two-dimensional displacement-encoding was performed in two breathholds, with the frequency- and phase-encoding directions swapped in the second scan.

Image reconstruction and strain analysis were performed as previously described (Kim et al., 2003). Briefly, for each encoding direction, raw data from complementary acquisitions were subtracted. Subsequently, phase-reconstructed images were computed and corrected using the phase reference data. After segmentation of the myocardium and automatic phase unwrapping, relative 1D displacement was computed. One-dimensional data from orthogonal directions were combined to generate 2D displacement maps, and the 2D strain tensor, E, was computed by isoparametric formulation using quadrilateral elements.

Four healthy volunteers and 4 patients with inferior myocardial infarction were imaged on a 1.5T scanner within 1 week of the infarct after providing informed consent. The protocol included SSFP cine DENSE and conventional cine SSFP. For patients, inversion-recovery imaging for infarct detection following Gd-DTPA infusion was also performed (Simonetti et al., 2001). Parameters for DENSE included TR = 3.0 ms, flip angle = 25°, FOV = 360 mm, matrix = 128 × 108, slice thickness = 8 mm, and effective temporal resolution = 60 ms.

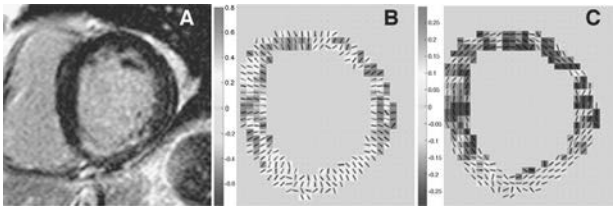

Figure 1. Gd-enhanced image depicting subendocardial infarction in the inferior wall (A). First (B) and second (C) principal strain maps from SSFP DENSE quantifying the corresponding wall motion defect demonstrate dysfunction in and beyond the Gd-enhanced zone. (*View this art in color at www.dekker.com.*)

Results: The SNR for SSFP cine DENSE was 16.8 ± 2.6 at end systole in volunteers. After correcting for differences in bandwidth and scan time, SSFP increased the normalized SNR by 30% compared to data acquired previously using FGRE-EPI. In patients, the SSFP cine DENSE SNR was 11.6 ± 5.0. This decrease was likely due to the larger body habitus of patients. Breathholding was well tolerated and good image registration between orthogonal data sets was obtained for all studies after correction for 2D translation. In Figure 1, an example Gd-enhanced image (A) and corresponding DENSE first and second principal strain maps (B and C, respectively) are shown, where the strain defect location agrees well with, but extends beyond the Gd-enhanced infarcted area. Areas of reduced strain agreed with Gd-enhanced regions in all patients.

Conclusions: SSFP improves SNR by approximately 30% in cine DENSE imaging compared to FGRE-EPI at 1.5T. Quantitative wall motion imaging with high spatial and temporal resolution and without tag detection is feasible in patients with myocardial infarction. Cine DENSE appears promising for the routine quantification of regional intramyocardial strain in patients.

REFERENCES

Aletras, et al. (1999). *JMR* 137:247–252.
Herzka, et al. (2003). *MRM* 49:329–340.

Copyright © Marcel Dekker, Inc. All rights reserved.

ORDER REPRINTS

Kim, et al. (2003). *Radiology in press.*
Simonetti, et al. (2001). *Radiology* 218(1):215–223.

491. Intracoronary Contrast Enhanced Myocardial Perfusion: Kinetics of Multiple Injections

Walter J. Rogers, Ph.D.,[1] C. Joon Choi, M.D., Ph.D.,[2] Frederick H. Epstein, Ph.D.,[1] Tom Sierocuk,[3] Mark Inderbitzen,[4] Christopher M. Kramer, M.D.[1] [1]*Radiology, University of Virginia, Charlottesville, VA, USA*, [2]*Cardiology, University of Virginia, Charlottesville, VA, USA*, [3]*Cordis Corporation, Miami Lakes, FL, USA*, [4]*Cordis Corporation, Miami Lakes, FL, USA*.

Introduction: Intra-venous injections ofGd-DTPA are useful for assessment of myocardial perfusion. However they cannot define the territory of myocardium perfused by each coronary artery or the extent of collateralization. Further, quantification of time–intensity curves must account for the contrast input function taken from the ventricular cavity which is distorted by passage through the venous system and non-linearity at high concentrations.

Purpose: The purpose of the study was to evaluate myocardial contrast distribution and kinetics of multiple intracoronary (IC) injections of dilute Gd-DTPA, which could then be applied during interventional CMR procedures for the assessment of myocardial perfusion in an individual arterial bed.

Methods: Four normal adult Yorkshire swine were studied using a Siemens Sonata with the animals supine using a phased array coil over the chest. An investigational MR compatible 8 French guide catheter (Cordis, Warren NJ) was positioned in the left main coronary ostia, 10 ml of 10% Gd-DTPA (Magnevist, Berlex Labs) was rapidly injected during acquisition of 4-slice/cardiac cycle short axis, ECG gated, GRE-EPI perfusion images. Image parameters included a TE of 1.28 msec, TR of 6.1 msec, flip angle of 25 degrees, slice thickness of 8 mm, 128^2 image matrix, and 250 mm FOV over 30–40 cardiac cycles. A second injection and image acquisition was performed 3–4 minutes later.

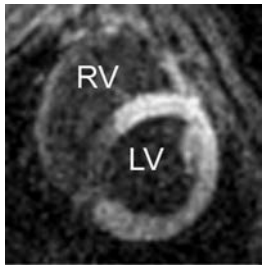

Figure 1.

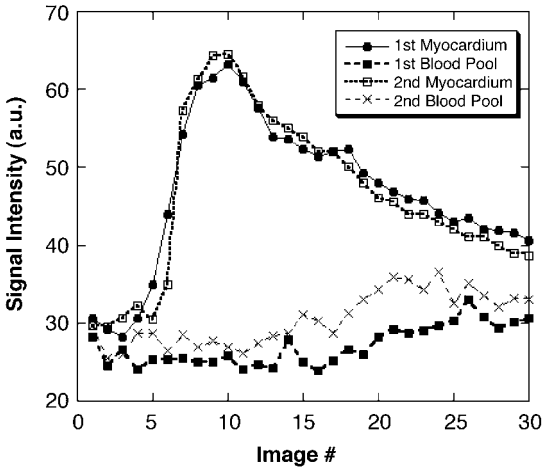

Figure 2.

Time–intensity (T–I) curves were generated from regions—of interest within the LV cavity and enhanced myocardium. Maximum upslope was generated from a linear fit of the first 2–3 myocardial points. The contrast-to-noise ratio (CNR) was computed as:$(\mathrm{ABS}(\mathrm{Signal}_{\text{enhanced myo}} - \mathrm{Signal}_{\text{non-enhanced myo}}))/\mathrm{SD}_{\text{non-enhanced myo}}$.

Results: Figure 1 displays a basal short axis image during contrast administration into the left main coronary artery. Uniform enhancement can be seen from 10–7 o'clock and a sharp transition to the non-enhanced right coronary distribution can be appreciated.

Figure 2 displays T–I curves from sequential IC injections. Both myocardial and LV cavity signal return to baseline by the second injection.

Mean upslope was not different between first and second injection (2.88 ± 0.68 and 2.79 ± 0.91, $P = \mathrm{NS}$). Mean time for myocardial signal to return to baseline was 2.35 ± 0.37 minutes. CNR for the 2 sequential injections was 8.67 ± 3.61 and 7.23 ± 1.97, $P = \mathrm{NS}$).

Conclusions: Selective IC administration of Gd-DTPA permits assessment of myocardial perfusion in specific coronary beds without alteration of the contrast input function through the venous system or concentration related signal non-linearity in the ventricular blood pool. Lack of significant contrast recirculation may permit multiple quantitative assessments of myocardial perfusion during MR-based coronary interventions.

Copyright © Marcel Dekker, Inc. All rights reserved.

ORDER REPRINTS

492. T2-Weighted Dark Blood and Vascular Wall MR Imaging Using the Combination of PSIF Techniques and Asymmetric Echo Acquisitions

Hung-Yu Lin, Shaoxiong Zhang, M.D., Ph.D., Jonathan S. Lewin, M.D., Jeffrey L. Duerk, Ph.D. *Biomedical Engineering/Radiology, Case Western Reserve University/University Hospitals of Cleveland, Cleveland, OH, USA*.

Introduction: High-resolution dark-blood magnetic resonance angiography (MRA) has proven to be a reliable technique for both visualization of the carotid artery wall and detection (or exclusion) of stenosis. The delay time necessary to achieve blood signal suppression often results in unacceptably long scan times with the traditional approach of Double Inversion Recovery Turbo Spin Echo (DIRTSE).To overcome this limitation, a new pulse sequence design is proposed that acquires dark blood T2-weighted images with 36% reduction in scan time, comparable image quality and identical flow suppression when compared to DIRTSE.

Purpose: To investigate a method that combines PSIF (a time-reversed version of the FISP sequence that uses the steady-state free precession (SSFP) spin echo) and asymmetric echo sampling to obtain dark blood and T_2-weighted images of the vascular wall in order to identify carotid artery atherosclerosis in significantly reduced scan time when compared to traditional TSE sequences.

Methods: All experiments were performed on a 1.5 Tesla MRI scanner (Sonata, Siemens Medical Solutions, Erlangen, Germany). The PSIF sequence structure collects the 2D Fourier encoded spin echo in the SSFP signal. Gradient refocusing is performed along only the phase encoding direction over each TR. Moreover, asymmetric sampling is applied to reduce the original echo time, thereby increasing the normally weak signal and reducing the sequence's typically high motion sensitivity. This reduction of TR and TE gives rise to stronger imaging signal and reduced susceptibility artifacts when compared to typical implementations of PSIF. Phantom and volunteer studies were performed to achieve fast T_2-weighted dark blood images with sufficient spatial resolution for clinical applications. The scan parameters (FOV/Matrix/TR/TE/Flip Angle/Bandwidth) were as following: 130×130 mm/256×256/14 ms/7 ms/53°/200 KHz and typical acquisition time was 32 sec for a single slice. A limited patient study was conducted to acquire carotid vessel wall images from both PSIF and clinically used TSE sequences.

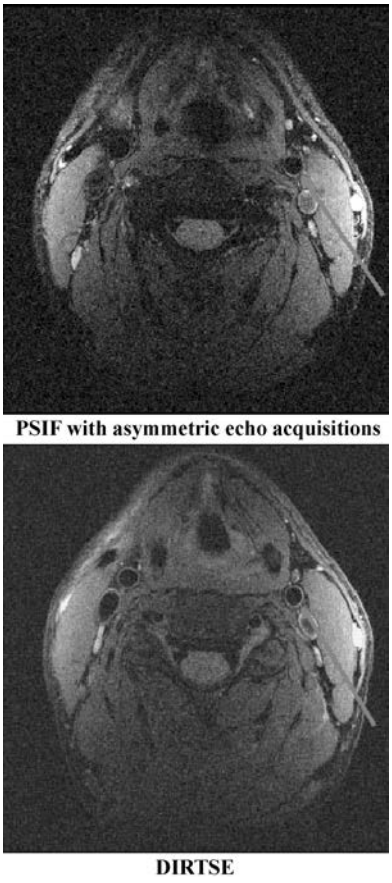

Figure 1. In-vivo T2-weighted dark blood and vascular wall MR imaging result comparison. (*View this art in color at www.dekker.com.*)

Results: In-plane spatial resolution of 0.51×0.51 $mm^2 \times 1$ mm slice thickness was achieved in both phantom studies and in four volunteers. The acquisition time was 32 sec for one 2D PSIF vessel wall image for in-vivo volunteer studies. This corresponds to a total scan time reduction of 36% when compared to conventional 2D TSE dark blood sequences. While overall SNR was 8.1% lower, comparable CNR between the vessel wall and the lumen (dark blood) was achieved in all trials. See Figure 1.

Conclusions: This PSIF acquisition combines the SSFP spin echo and asymmetric sampling methods to achieve dark blood T_2-weighted vascular images. This study suggests that asymmetric PSIF can provide dark blood vascular wall images and effective visualization of the carotid artery wall with a 36% scan time reduction relative to TSE. The PSIF sequence provides comparable CNR between the vascular wall and lumen, but less signal intensity, when compared to currently

Copyright © Marcel Dekker, Inc. All rights reserved.

ORDER REPRINTS

used TSE methods. Asymmetric PSIF and other new sequences offer great promise in rapid dark blood T_2-weighted imaging of the carotid artery wall.

493. Cardiac CINE Imaging with ''Dixon'' Fat–Water Separation and Steady-State Free Precession

Scott B. Reeder, M.D., Ph.D., Michael Markl, Ph.D., Jeffrey C. Hellinger, M.D., Robert J. Herfkens, M.D., Norbert J. Pelc, Sc.D. *Department of Radiology, Stanford University Medical Center, Stanford, CA, USA*.

Introduction: SSFP is a rapid imaging technique with high SNR and excellent blood–myocardial contrast, and has gained widespread use for cardiac imaging. SSFP is limited by the fact that water and fat both appear bright and are difficult to distinguish, possibly obscuring underlying pathology such as pericardial disease, fatty infiltration with ARVD, or fatty myocardial tumors. Current fat supression techniques used with SSFP are relatively sensitive to field heterogeneities (Scheffler et al., 2001), as are alternative fat-suppression techniques such as spatial–spectral pulses (Meyer et al., 1990).

Typical ''Dixon'' water–fat decomposition techniques are insensitive to field heterogeneities, however, short TRs are necessary to prevent image degradation resulting from field heterogeneities, as well as ''freeze'' cardiac motion—these factors limit TE increments to small values not used with typical ''Dixon'' techniques (Glover et al., 1991).

To address these challenges, water and fat CINE movies were decomposed with a recently described iterative least-squares algorithm (Reeder et al., 2003) that facilitates multi-coil acquisition of data sets with arbitrary (short) TE spacing and allows fat–water separation with CINE cardiac SSFP imaging acquired with short TRs.

Methods: Image acquisition was performed on a 1.5T CV/i scanner (GEMS, Milwaukee, WI) with a retrospectively ECG-gated CINE SSFP sequence that sequentially obtains sets of CINE images at 3–4 echo times. A phased-array torso coil was used. Imaging parameters were: TE = 0.8, 1.7, 2.6 ms; TR = 4.7–5.0 ms; BW = ±125 kHz; FOV = 32 cm; slice = 8 mm; Nx = 224 (partial-echo); Ny = 128; views per segment = 12–16, temporal resolution = Nseg*TR = 60–80 ms, 20 CINE phases, and breath-hold time was 21–27 heartbeats. One heartbeat was discarded before each echo increment to ensure magnetization was in steady-state. Images were obtained in eight patients. Prior to imaging, informed consent was obtained and the study was approved by our IRB. Product automated shim routines were used for all imaging. Fat–water decomposition using the linear least-squares algorithm was performed off-line.

Results: Examples of water/fat/source images are shown in Figures 1–3. Excellent fat–water separation was obtained in all studies. Distinction between epicardial fat and pericardial fluid was well demonstrated, as were intra-atrial lipomatous changes (Figure 1). Delayed hyper-enhancement in the left

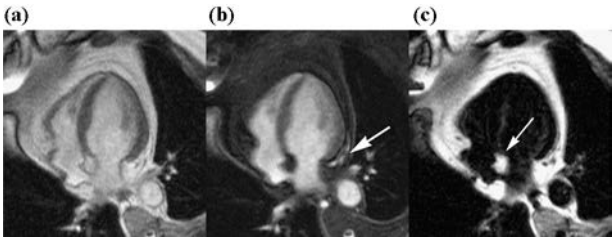

Figure 1. One (of 20) source (a), water (b), and fat (c) images showing intra-atrial lipomatous changes (thin arrow) best visualized in the fat image. Excellent conspicuity of coronary vessels is seen in the AV groove (thick arrow) in the water image.

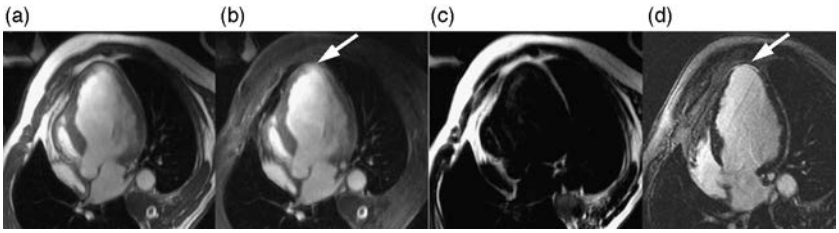

Figure 2. One (of twenty) source (a), water (b), and fat (c) images obtained 15 min after intravenous injection of Gd-DTPA. Delayed hyper-enhancement (arrow) from prior myocardial infarction is seen in the LV apex, and better appreciated in the water image. An inversion recovery SPGR image is shown for comparison (d).

Copyright © Marcel Dekker, Inc. All rights reserved.

ORDER REPRINTS

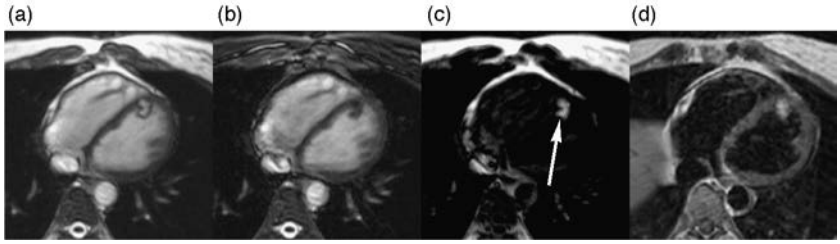

Figure 3. One (of 20) source (a), water (c), and fat (c) images obtained from a patient with a pathologically proven lipoma. A T1-weighted spin-echo image is shown for comparison (d).

ventricular apex of a patient with a known myocardial infarction is well demonstrated, with increased conspicuity in the calculated water images (Figure 2). A pathologically proven left ventricular septal lipoma is shown in Figure 3.

Conclusions: Multi-coil ''Dixon'' techniques using an iterative least-squares fitting algorithm can be combined with SSFP cardiac CINE imaging to obtain water and fat movies with excellent fat–water separation. This facilitates improved visualization of water and fat structures within and around the heart while retaining the high CNR of SSFP imaging, and has potential for clinical applications that require uniform fat–water separation, such as coronary artery imaging, ARVD, and pericardial disease.

REFERENCES

Glover, et al. (1991). *Magn. Reson. Med.* Apr 18(2):371–383.

Meyer, et al. (1990). *Magn. Reson. Med.* Aug 15(2):287–304.

Reeder, et al. (2003). *Magn. Reson. Med. in press.*

Scheffler, et al. (2001). *Magn. Reson. Med.* Jun 45(6):1075–1080.

494. Dual-Inversion Bright-Blood Coronary MRA: Arterial Spin Labeling Without the Need for Subtraction

Matthias Stuber,[1] Harikrishna Tandri, M.D.,[2] Henning Steen,[2] Elmar Spuentrup.[3] [1]*Radiology, Johns Hopkins University, Baltimore, MD, USA*, [2]*Cardiology, Johns Hopkins University, Baltimore, MD, USA*, [3]*Radiology, RWTH Aachen, Aachen, Germany*.

Introduction: Motion suppression and contrast enhancement between the coronary lumen blood-pool and the surrounding tissue are most important determinants in contemporary coronary magnetic resonance angiography (MRA). Black-blood contrast has been generated using dual-inversion pre-pulses and a bright-blood visualization has been obtained using magnetization transfer pre-pulses, T2Prep, extracellular and intravascular T1-lowering contrast agents, or arterial spin labeling. While arterial spin labeling enables an exclusive and selective 3D visualization of the coronary artery lumen blood-pool with high contrast-to-noise ratio (CNR), disadvantages include an increase in scanning time (factor of 2), the need for subtraction, and thus an enhanced sensitivity to misregistration.

Purpose: The development of an accelerated, more robust coronary arterial spin labeling technique without the need for subtraction.

Methods: Concept—Coronary arterial spin labeling without the need for subtraction (Figure 1) has been

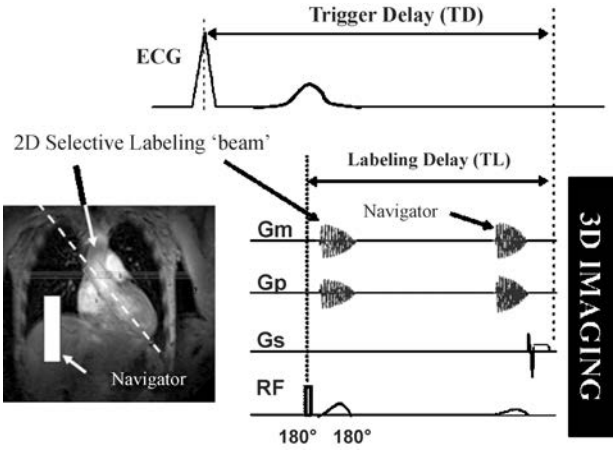

Figure 1. Localization of cylindrical aortic labeling pulse (left) and imaging sequence (right) used for non-subtractive free-breathing coronary arterial spin labeling. The labeling delay TL allows for simultaneous signal-nulling of the myocardium and inflow of the re-invented blood-magnetization into the coronary arteries. (*View this art in color at www.dekker.com.*)

Copyright © Marcel Dekker, Inc. All rights reserved.

ORDER REPRINTS

developed using a non-selective inversion of the magnetization that is immediately followed by a cylindrical re-inversion of the magnetization in the blood-pool of the ascending aorta.

A time delay (TL, Figure 1) between the non-selective inversion and the imaging part of the sequence simultaneously allows for signal-nulling of the myocardium and in-flow of the re-inverted, fully restored (labeled) aortic blood-pool magnetization into the coronary arteries, where imaging is performed. Therefore, it is expected that a high signal intensity is obtained from the blood flowing into the coronary arteries while the signal from the myocardium should be nulled. Implementation—The technique was implemented on a commercial 1.5T Philips Intera system. A non-selective inversion pulse was combined with a 2D selective aortic re-inversion of the blood-pool magnetization (Figure 1). For the 2D selective cylindrical radiofrequeny (RF) pulse oriented along the ascending aorta, a 180 Deg excitation angle, 12 cycles in k-space, and an individually adjusted diameter of the cylindrical excitation was used. The TL was calculated using the heart-rate dependent Fleckenstein formula (Fleckenstein et al., 1991) in which a T1 of 850 ms was used for signal-nulling of the myocardium (TL = 300..400 ms). This dual-inversion pre-pulse scheme was combined with a real-time navigator for respiratory motion suppression (5 mm gating window), a fat saturation pre-pulse, and a 3D volume-targeted radial SSFP imaging sequence (360 mm FOV, 512 matrix, 75% angular coverage, 12 3 mm slices, 16 profiles per RR interval, TR/TE = 7.2/3.6 ms (acquisition window = 115 ms), Alpha = 120 Deg). The trigger delay (TD) was individually adjusted to collect the image data in a diastolic period of minimal myocardial motion.

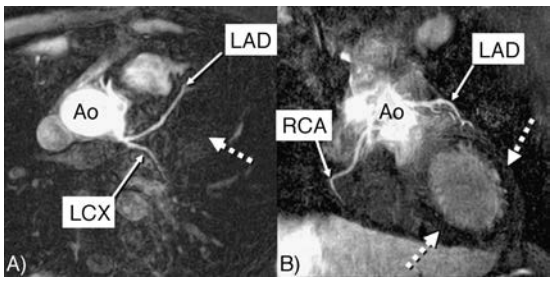

Figure 2. Images acquired with non-subtractive coronary arterial spin labeling in conjunction with a real-time navigator for respiratory motion correction and a 3D radial SSFP imaging sequence. Left coronary circumflex = LCX, aorta = Ao, left anterior descending = LAD, right coronary artery = RCA.

Results: In Figure 2, two images acquired using coronary arterial spin labeling without subtraction are displayed. In Figure 2A, the ascending aorta (Ao), the left coronary circumflex (LCX) and the left anterior descending (LAD) including a more distal branch display with high visual contrast.

The myocardium is effectively suppressed (dashed arrow, Figure 2A) while some residual signal is seen in the region of the right ventricular outflow tract and the anterior chest. Similar results can be observed in Figure 2B, where the right coronary artery (RCA) and the LAD appear signal enhanced. Again, the myocardium appears signal-suppressed (dashed arrow), while an enhanced signal can also be seen in the region of the great cardiac vessels and the liver. Scanning time per 3D data set is 6–7 min.

Discussion and Conclusions: The proposed method provides a new bright-blood endogenous contrast enhancement mechanism for coronary MRA, and the signal from the myocardium can very effectively be suppressed. However, despite the very high visual contrast between the coronary lumen blood-pool and the surrounding tissue, signal-enhancement from tissue with short T1 is still observed.When compared to earlier spin labeling approaches, no subtraction is needed, susceptibility to mis-registration and subsequent subtraction artifacts is removed, and scanning time is abbreviated by a factor of 2.

REFERENCE

Fleckenstein, et al. (1991). *Radiology* 179(2):499–504.

495. Rectilinear Self-Gated Cardiac Cine Imaging

Mark E. Crowe, B.E.,[1] Andrew C. Larson, M.S.,[2] Qiang Zhang, Ph.D.,[3] Orlando P. Simonetti, Ph.D.[3] [1]*Biomedical Engineering and Radiology, Northwestern University, Chicago, IL, USA*, [2]*Laboratory of Cardiac Energetics, NHLBI, National Institutes of Health, Bethesda, MD, USA*, [3]*Siemens Medical Solutions, Chicago, IL, USA*.

Introduction: ECG and pulse-oximetry based gating require additional patient preparation time, are susceptible to RF and magnetic interference, and are ineffective in a significant percentage of patients. So-called ''wireless'' or ''self-gating'' techniques have been described using either interleaved central k-space lines (Spraggins, 1990), or projection reconstruction

Copyright © Marcel Dekker, Inc. All rights reserved.

ORDER REPRINTS

(Larson et al., 2004) to obtain MR signals synchronous with the cardiac cycle. The interleaved, central line method results in a doubling of the acquisition time, while radial streak artifacts are encountered with the projection reconstruction method. In this work, a new self-gating technique is presented to overcome these limitations.

Purpose: Demonstrate the feasibility of self-gated cardiac cine imaging using a conventional rectilinear TrueFISP sequence, and to compare the image quality of these self-gated cine images with those obtained using ECG and pulse oximetry gating.

Methods: The sequence—This technique is a modified TrueFISP cine sequence that acquires a second echo after the readout and phase gradients have rewound. Only a slight shift of the slice select gradient is required to form this second echo that is used as the gating signal. The TR increases slightly but remains short, preserving the advantages of the TrueFISP sequence. The peak amplitude of the second echo varies in proportion to the average signal in the image, which changes during the cardiac cycle. A low-pass filter with a 3 Hz cut-off is applied to the echo-peak information to remove high frequency noise and a peak-detection algorithm determines the trigger positions. Experimental Setup—Short and long axis cine images were retrospectively reconstructed from 8 healthy volunteers using self-gating, ECG gating, and pulse oximetry gating. Imaging was performed using a Siemens 1.5T Sonata (Malvern, PA) with a 4-channel body array coil. Breath-held acquisitions were performed using the following parameters: 255*340 matrix, 135 phase-encoding lines, 16 phases, 3.42 ms TR, 5 mm slice thickness, and a 965 Hz/pixel bandwidth. Left ventricular volume and mass were measured using the Siemens software package Argus.

In an effort to quantitatively evaluate the gating effectiveness and image quality of the self-gating method, contours were generated on the end-diastolic and end-systolic phases of all short axis images. The ejection fraction (EF), myocardial mass, end-diastolic volume (EDV), end-systolic volume (ESV), and stoke volume (SV) measurements for self-gating, ECG gating, and pulse oximetry gating were compared. For this comparison, the ECG gated ventricular measurements were assumed to be the 'gold standard.'

Results: An example of a filtered echo-peak signal and the resulting trigger positions is illustrated by Figure 1A. High quality images were obtained in all volunteers using all three gating methods. The end-diastolic and end-systolic images from the middle short axis slice of a volunteer for self-gating, ECG gating, and pulse oximetry gating are shown in Figure 1B. The

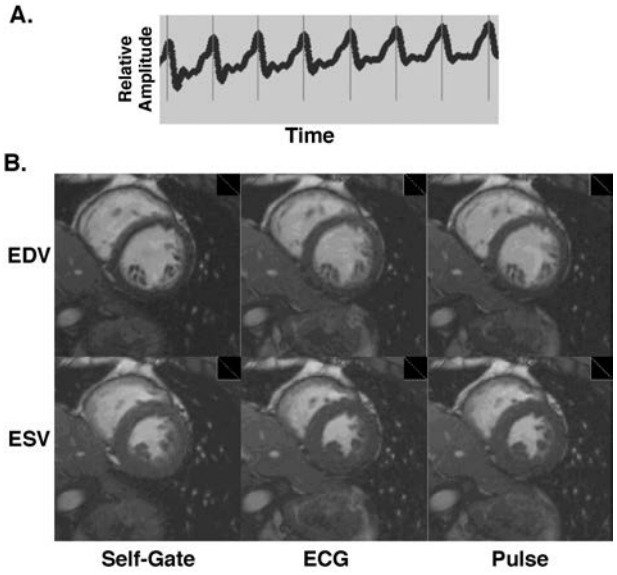

Figure 1. A. A filtered echo-peak gating signal with the determined trigger positions (vertical lines) and B. ED and ES images from a middle short axis slice obtained using three gating techniques. (*View this art in color at www.dekker.com.*)

self-gated and pulse oximetry gated LV function parameters had the following average errors when compared to ECG gating: EF (4.59±4.57% vs. −0.30±5.01%), myocardial mass (−1.05±7.99% vs. 1.18±2.98%), EDV (−4.75±3.78% vs. −0.39±4.02%), ESV (−9.94±5.29% vs. 0.51±8.86%), and SV (−0.27±7.35% vs. −0.75±4.07%).

Conclusions: Initial results suggest that the proposed self-gating method is an effective technique for obtaining cardiac cine images retrospectively. This self-gating method has the potential to be an alternative to ECG-based and pulse oximetry-based gating.

REFERENCES

Larson, et al. (2004). *Magn. Reson. Med.in press.*
Spraggins (1990). *Magn. Reson. Imaging* 8(6):675–681.

496. First-Pass Perfusion Imaging of the Lower Limb

Jin Hyung Lee, Bob S. Hu, M.D., Dwight Nishimura, Ph.D. *Electrical Engineering, Stanford University, Stanford, CA, USA.*

Copyright © Marcel Dekker, Inc. All rights reserved.

ORDER REPRINTS

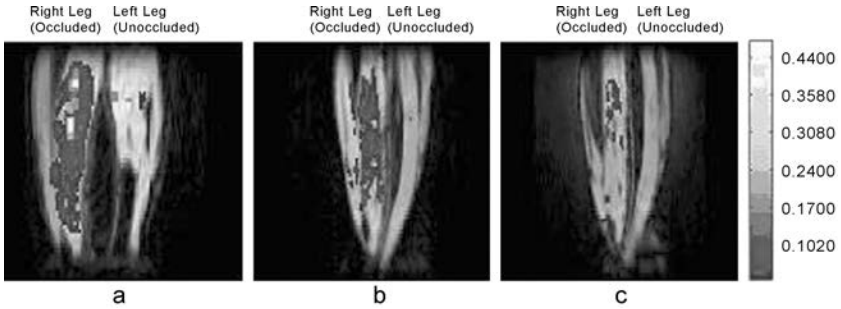

Figure 1. Color map of the perfusion parameter for (a) a normal vounteer (b) a patient with ABI of 0.615 and (c) the same patient after 6 months when the ABI was 0 and X-ray angiography indicated that the patient has severe PVD. (*View this art in color at www.dekker.com.*)

Introduction: Due to promising new interventional techniques such as gene or stem cell therapy, there is increased need for accurate measurement of perfusion deficits and post-therapy improvements. First-pass perfusion imaging using bolus tracking is a validated potentially quantifiable technique (Isner et al., 1998; Wilke, 1997), but requires sufficient volumetric coverage with high temporal resolution. In this study, first-pass perfusion of the lower limb is assessed using a variable-density (Tsai et al., 2000) stack-of-spirals trajectory (Irarrazabal et al., 1995) to obtain full volumetric coverage with high temporal resolution. To verify this technique, normal volunteers and patients with peripheral vascular disease (PVD) (ankle-brachial index (ABI)<0.9) were scanned.

Purpose: The purpose of this study is to assess regional perfusion of the lower limb using variable-density stack-of-spirals scanning.

Methods: A variable-density stack-of-spirals trajectory with a spoiled gradient-echo acquisition was implemented. Using this fast imaging technique, a $27\times27\times28$ cm^3 FOV was covered with $2.5\times2.5\times8$ mm^3 spatial resolution and 2.8 s temporal resolution. Spectral–spatial excitation pulses (Meyer et al., 1990) were used to suppress fat.

The study was performed by scanning the infra-popliteal region of both legs repeatedly to obtain temporal information over a large volme. The protocol involved occluding the ischemic leg by inflating a blood pressure cuff to above the subjects systolic blood pressure level. Then, 20 sec into the scan, 10 cc of Magnevist was injected in the arm over 3 sec. Approximately 50–80 seconds after the injection, the cuff was deflated. Occlusion of one leg was performed to demonstrate the differential perfusion of the ischemic vs. normal leg. The release of the occlusion gives a hyperemic response which is potentially a better, more sensitive measure of ischemia.

Results: Nine patients known to have PVD with ABI less than 0.9 were scanned. Three of the patients came in for a follow-up scan after approximately 6 months.

Figure 1 shows an oblique slice in the z direction from one of the seventy volumetric data sets for a normal volunteer (Figure 1a) and a patient with PVD (Figure 1b,c). The color overlay represents the slope of the signal intensity rise for each pixel in percentage relative to the pre-contrast signal intensity. Color was overlayed on pixels with slope higher than 0.04%/sec. The maximum slope was 0.47%/sec. The images were filtered with a low-pass filter before calculating the slope to reduce noise in the signal intensity curve. The slope of the signal intensity rise was estimated by taking the maximum value of the difference between signals that are 5 temporal samples apart. It can be clearly seen in the occluded leg (right leg) that the normal volunteer generally has higher slope. Figure 1b and c, taken 6 months apart, show that the method successfully evaluates the progression of the disease. The unoccluded leg has no color overlayed since the slope is generally much bigger in the occluded leg due to the hyperemic response.

Conclusions: First-pass perfusion imaging using the proposed technique demonstrates promise in diagnosing and monitoring the disease progression in patients with PVD.

REFERENCES

Irarrazabal, P., et al. (1995). *MRM* 33:656–662.
Isner, J. M., et al. (1998). *J. Vasc. Surg.* 28:964.
Meyer, C., et al. (1990). *MRM* 15:287–304.

Copyright © Marcel Dekker, Inc. All rights reserved.

ORDER REPRINTS

Tsai, C.-M., et al. (2000). *MRM* 43:452–458.
Wilke, N. (1997). *MRM* 29:485.

497. Improved Resolution in First Pass Perfusion Studies

Ching-Hon Luk,[1] Yiu-Cho Chung,[2] Michael Jerosch-Herold,[3] Orlando Simonetti,[4] Chi-Ming Wong.[1]
[1]*Sir Run Run Shaw Heart Center, St. Teresa's Hospital, Kowloon, Hong Kong Special Administrative Region of China*, [2]*Cardiovascular MR R&D, Siemens Medical Solutions USA, Inc., Chicago, IL, USA*, [3]*University of Minnesota, Minneapolis, MN, USA*, [4]*Cardiovascular MR R&D, Siemens Medical Solutions USA, Inc., Chicago, IL, USA*.

Introduction: First pass perfusion imaging is useful for myocardial ischemia detection (Wilke et al., 1997). Current fast imaging techniques only improve spatial coverage of the heart. Here, we propose to use parallel imaging to increase spatial resolution of imaging slices and demonstrate its ability to detect small perfusion defects in IHD (ischemic heart disease) patients. We believe that improved spatial resolution of first pass perfusion images would improve myocardial ischemia detection.

Purpose: Design saturation recovery turboFLASH (SR-TFL) for first pass perfusion imaging that gives 3–4 slices per heart beat with voxel size of about 1.8 mm × 2.7 mm × 8 mm, depending on patient heart rate.

Methods: SR-TFL is used with GRAPPA (Griswold et al., 2002) (acceleration factor = 2). ~8 addi-8 additional lines were collected for coil sensitivity profiles. SNR loss associated with parallel imaging and improved resolution was compensated by choosing readout bandwith (~440–530 Hz/pixel, heart rate dependent) and contrast dosage (0.07 mmol/kg of Gd-DTPA) carefully. Other sequence parameters are: flip angle ~10–15 deg, TR/TE ~2.6 ms/1.2 ms, TI ~ 75–85 ms. Matrix size ~95 ~192, FOV ~260 mm × 370 mm, 135–160 ms per slice (heart rate and bandwidth dependent). The sequence ran on a MAGNETOM Sonata (Siemens, Erlangen, Germany).

The technique was tested on 6 patients suspected to have IHD before having PTCA/PTCS. MR imaging started with heart chamber localization. Scout images were used to plan the three short axis slices and (optional) 4-chamber slice for perfusion imaging. First pass perfusion imaging was performed with patient at stress (using adenosine). After ~10 minutes whereby cardiac cines were acquired, perfusion imaging was repeated at rest. An additional 0.03 mmol/kg of Gd-DTPA was immediately injected and infarct imaging was performed after another 10 minutes wait. In some patients, perfusion study at rest was done before the stress study.

Results: X-ray angiograms revealed coronary artery stenosis for all patients found to have myocardial perfusion defects. Figure 1 shows how higher inplane resolution may help depict small myocardial perfusion defect in a typical set of first pass perfusion images. In (a), a small perfusion defect was visible at rest, whose size increases (meaning there is ischemic myocardium nearby the region) during adenosine stress in (b). The delayed enhancement image showed that the small hypoperfused area at rest was an infarct (c).

Conclusions: This study demonstrated how parallel imaging may help improve spatial resolution of perfusion images. Improved resolution helps depict subendocardial perfusion defect and reduces truncation artifacts common in first pass perfusion images. It complements efforts to improve spatial coverage of the heart using EPI (Ding et al., 1998), Compared to an EPI sequence with TR = 5.8 ms and ETL = 4, the current technique is slightly faster—it collects about 4 lines in 5.2 ms (acceleration factor = 2, TR = 2.6 ms), with ~10% overhead for reference line collection. However, the EPI technique has two limitations for high resolution perfusion imaging: the high bandwith limits the number of readout datapoints and hence image resolution (to 128 × 128 matrix), and T2* effect blurs any resolution improvement achieved by reducing image FOV. TrueFISP based parallel imaging techniques give higher SNR than turboFLASH but they are more susceptible to artifacts. It is expected that the improved resolution would help distinguish artifacts

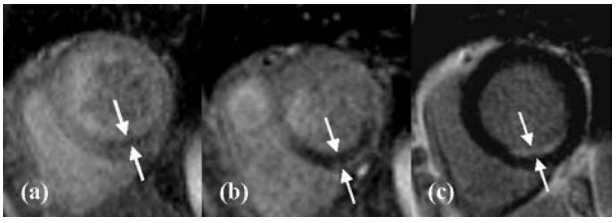

Figure 1. Images from a perfusion study using the sequence. (a) perfusion image at rest shows a tiny hypoperfusion region. (b) hypoperfusion area increased under adenosine stress. (c) delayed enhancement image shows that the hypoperfusion region at rest was a subendocardial infarct.

Copyright © Marcel Dekker, Inc. All rights reserved.

ORDER REPRINTS

from ischemic regions and hence improve the accuracy of the technique in detecting IHD.

Acknowledgment: Dr. Jennifer Kwok for patient referral.

REFERENCES

Ding, S., et al. (1998). *MRM* 39(4):514–519.
Griswold, M. A., et al. (2002). *MRM* 47(6):1202–1210.
Wilke, et al. (1997). *Radiology* 204(2):373–384.

498. CINE First Pass MR Myocardial Perfusion Imaging: Preliminary Observations

James W. Goldfarb, Ph.D., Yi Wang, D.Sc., Nathaniel Reichek, M.D. *Research and Education, St Francis Hospital, Roslyn, NY, USA.*

Introduction: Myocardial perfusion imaging typically provides a time sequence of images at several slice locations spanning the left ventricle during a bolus infusion of a gadolinium contrast agent. Typically, several slices are acquired at different phases of the cardiac cycle. We hypothesized that contrast agent concentration changes, as wells as physiological effects, which occur at different phases of the cardiac cycle will cause measurable signal intensity changes.

These variations in signal intensity as a result of the function of the heart might cause artifacts or provide diagnostic information. Signal intensity changes could be a result of myocardial blood volume changes, inflow of fresh spins or dephasing due to flow.

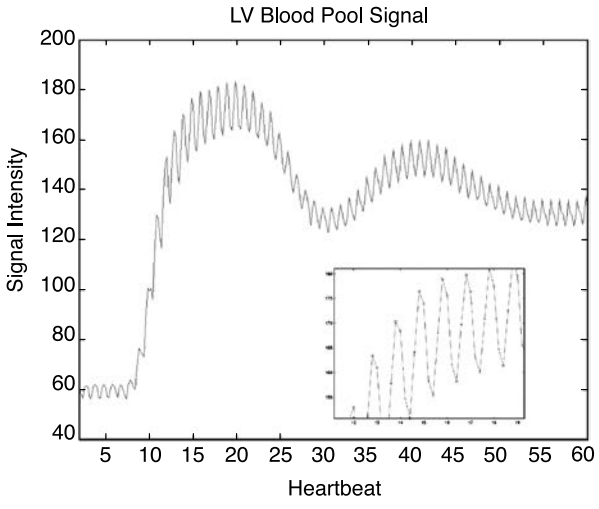

Figure 1. (*View this art in color at www.dekker.com.*)

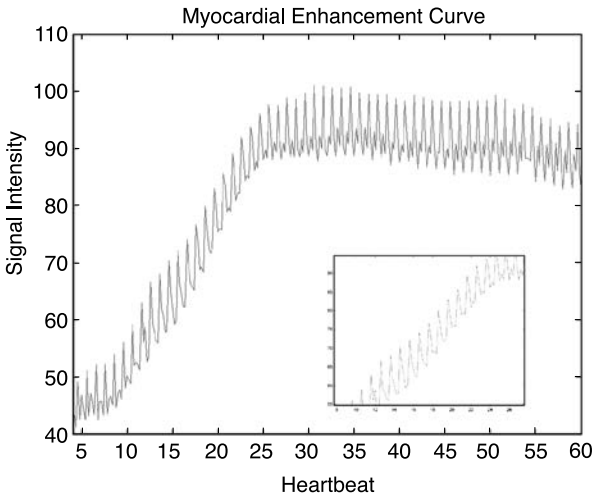

Figure 2. (*View this art in color at www.dekker.com.*)

Purpose: To quantify the magnitude and verify the periodicity of signal changes related to the cardiac cycle in MR myocardial perfusion imaging.

Methods: Eight subjects (age: mean = 46 years; range = 34–51) participated in the study. Imaging was performed using a 1.5T clinical scanner (Magnetom Sonata). Two sequences capable of measuring resting myocardial perfusion during bolus injection were used: 1) a 2D saturation recovery True-FISP sequence (TR = 2.9, TE = 1.3, FA = 50, TI = 90, BW = 960 Hz/pixel, voxel size = $3.5 \times 1.9 \times 8.0$ mm^3) and 2) 2D real-time FLASH sequence was used (TR = 2.0, TE = 1.3, FA = 25, BW = 1560 Hz/pixel, voxel size = $4.2 \times 3.1 \times 10.0$ mm^3). 0.1 mmol/kg of gadodiamide (Omniscan) was injected at 2 ml/s followed by a 15 ml saline flush. Region-of-interest analysis was performed in the resulting images. Regions of the left ventricular blood pool and myocardium were hand drawn. Mean signal intensities were calculated and variations during the cardiac cycle were analyzed.

Results: In each case, both LV blood pool signals (Figure 1) and myocardial signals (Figure 2) were periodic with the cardiac cycle. Figures 1 and 2 are representative examples of the multi-phase saturation recovery True-FISP acquisition. Region-of-interest analysis of single phase images showed smooth curves without oscillations consistent with our experience using mutli-slice acquisitions. The mean peak-to-peak signal variations for the saturation recovery True-FISP sequence was14%. The realtime FLASH sequence had mean peak-to-peak variations of 31%.

Copyright © Marcel Dekker, Inc. All rights reserved.

ORDER REPRINTS

Conclusions: Signal intensities in images obtained during bolus infusion of the myocardium are dependent on the phase of the cardiac cycle. Quantitative methods and models should take this into account. These signal changes may be due to inflow of blood (perfusion) and/or changes in myocardial blood volume and could contain diagnostic information.

499. Multi-View Active Appearance Models for Automatic Detection of Endo- and Epicardial Contours in Long-Axis and Short-Axis Cardiac MR Views

Boudewijn P. F. Lelieveldt, Ph.D.,[1] Rob J. van der Geest, M.Sc.,[1] Theodorus A. M. Kaandorp, M.D.,[2] Hildo J. Lamb, Ph.D,[2] Johan H. C. Reiber, Ph.D.,[1] Milan Sonka, Ph.D.[3] [1]*Division of Image Processing, Leiden University Medical Center, Leiden, Netherlands*, [2]*Department of Radiology, Leiden University Medical Center, Leiden, Netherlands*, [3]*Department of Electrical and Computer Engineering, the University of Iowa, Iowa City, IA, USA*.

Introduction: In a cardiac MR patient examination, typically multiple acquisitions are acquired following fixed imaging protocols, where images may depict different geometrical or functional cardiac features. For instance, the short-axis, long-axis, perfusion, rest-stress and delayed enhancement images provide complementary information about different aspects of geometry and function of the same heart. To quantify cardiac function and morphology from such image sets, a (preferably automatic) segmentation of the heart is required. However, typically, automatic segmentation methods focus on one subpart of a patient examination. Segmentation is achieved for one view at a time, and the different parts of a patient examination are treated separately. As a result, a sub-optimal segmentation result is achieved, because not all the available information is used, and additional shape information of the same organ may be present in different views.

Purpose: The goal of this work was to develop and validate a segmentation method that exploits existing shape- and intensity redundancies and correlations between different parts of a cardiac patient examination. Potentially, this increases robustness, and enforces segmentation consistency between views, therefore yielding a better segmentation.

Methods: In previous work, it has been shown that so-called Active Appearance Models (AAMs) are suitable for automatic detection of endo- and epicardial contours in short-axis cardiac MR studies. An AAM consists of two components: a statistical model of the shape of the heart, which is combined with a statistical model of the image appearance of the heart in a set of example cardiac MR images. An AAM can be applied to fully automated contour detection in MR images by minimizing the difference between the model and the image, where the model is constrained to ''statistically plausible'' LV appearances, yielding the locations of the ENDO and EPI contours.

So far, AAM's have been applied to single 2D, 2D+time and 3D cardiac MR studies. In this work, we have developed the Multi-View AAM to simultaneously model multiple views from one patient examination, while preserving the shape correlations between the different views. Model training and matching are performed on multiple 2D views simultaneously, thus combining information from all views to yield a segmentation result.

The Multi-View AAM was tested on the ED two chamber view, the ED four chamber view and the ED mid-ventricular short-axis slice from 29 patients. Endo- and epicardial contours were drawn manually by an expert observer in all views. Validation and training was performed using a leave-one-subject-out approach. The initial position for the model matching was manually set by indicating the apex and base in the long-axis views, and the LV midpoint in the short-axis views.

Results: For 27 out of 29 patients, the endo- and epicardial contours were detected correctly, whereas in 2 cases, partial failure was observed, where the model drifted away from the LV boundaries in one of the three views. Examples of automatically detected contours in the cardiac MR views are given in

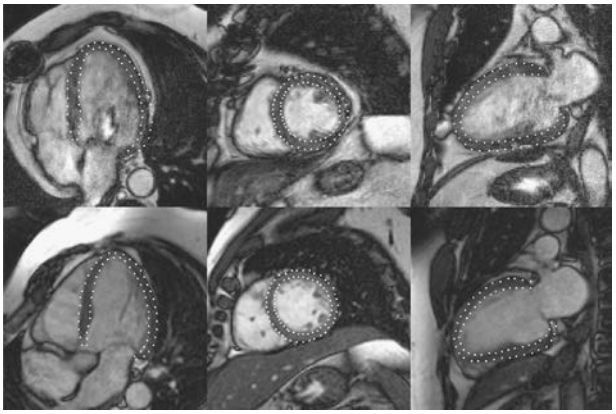

Figure 1.

Copyright © Marcel Dekker, Inc. All rights reserved.

ORDER REPRINTS

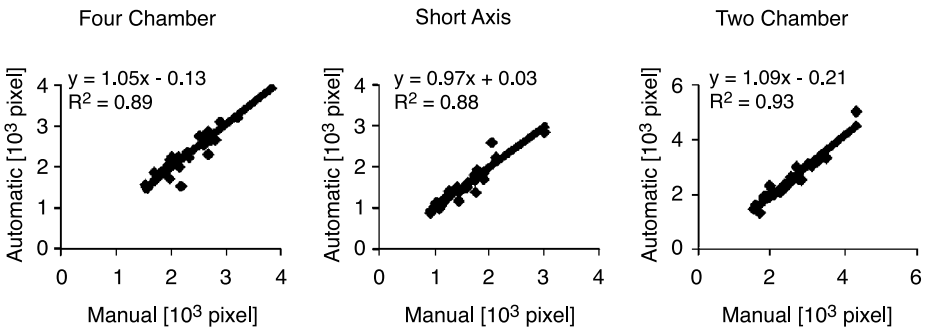

Figure 2.

Figure 1. For the contours from successful matches (87 out of 89 images in total, 98 %), area correlations between manually and automatically detected contours are given in Figure 2. Area calculations, which serve as a basis for LV volume estimates, did not differ statistically significantly between manual and automatic analysis ($p>0.7$ for all views). Average border positioning errors amounted 1.5 ± 0.7 pixels (comparable to errors reported for other AAM methods), and within clinically acceptable margins.

*Conclusions:*The presented Multi-View AAM demonstrated to be a robust contour detection method for ENDO and EPI contours in combined long-axis and short-axis cardiac MR pairs, and may potentially reduce analysis time for cardiac MR examinations to a minimum.

500. Interleaved Spiral Phase Velocity Mapping of Coronary Artery Blood Flow: Correction for Through-Plane Motion Using Selective Fat-Only Excitation

Jennifer Keegan, Ph.D.,[1] Peter Gatehouse, Ph.D.,[1] Guang-Zhong Yang, Ph.D.,[2] David Firmin, Ph.D.[1]
[1]*Cardiovascular Magnetic Resonance Unit, Royal Brompton and Harefield NHS Trust, London, United Kingdom*, [2]*Department of Computing, Imperial College of Science Technology and Medicine, London, United Kingdom.*

Introduction: Interleaved spiral phase velocity mapping has recently been used to acquire high temporal resolution velocity maps in both left (lca) and more mobile right (rca) coronary arteries (Keegan et al., 2003). However, whereas the flow velocities in the lca may be corrected for the through-plane motion of the vessel by subtracting the velocity of an area of adjacent myocardium, the right ventricular wall is too thin to allow such a correction for the rca.

Purpose: The purpose of this work is to develop a method of through-plane motion correction that is applicable to both left and right arteries by selectively exciting and velocity mapping the surrounding epicardial fat.

Methods: As preciously described, navigator gated velocity mapping of coronary blood flow (TE = 6.1 ms, TR = 22 ms) may be achieved using a water-excitation pulse, a 10.1 ms spiral readout gradient and a 2.2 ms bi-polar velocity encoding gradient which alternates on consecutive cardiac cycles and results in velocity maps with a phase sensitivity to flow of ±25 cm/s (Keegan et al., 2003). Two methods of through-plane correction were investigated. In the first, a separate velocity mapping acquisition was performed using the same imaging parameters but with fat-excitation, rather than water-excitation, of the imaging slice. In the second method, water-excitation and fat-excitation were interleaved throughout the cardiac cycle, reducing the temporal resolution to 44 ms, but allowing the acquisition to be completed without extending the imaging duration. Studies were performed in 10 right and 5 left coronary arteries and velocity through the cardiac cycle was plotted for both separate and combined acquisitions 1) without correction and 2) with correction. Paired t-tests were used to compare the before and after correction mean diastolic and mean systolic velocities derived from the separate water-excitation and fat-excitation acquisitions with those derived from the shorter duration but poorer temporal resolution combined fat-excitation/water-excitation acquisition.

Results: Figure 1 shows the mean (±SD) velocities measured in the 5 left and 10 right coronary arteries both before (a) and after (b) correction for through-plane motion, the data being derived from the separate

Copyright © Marcel Dekker, Inc. All rights reserved.

ORDER REPRINTS

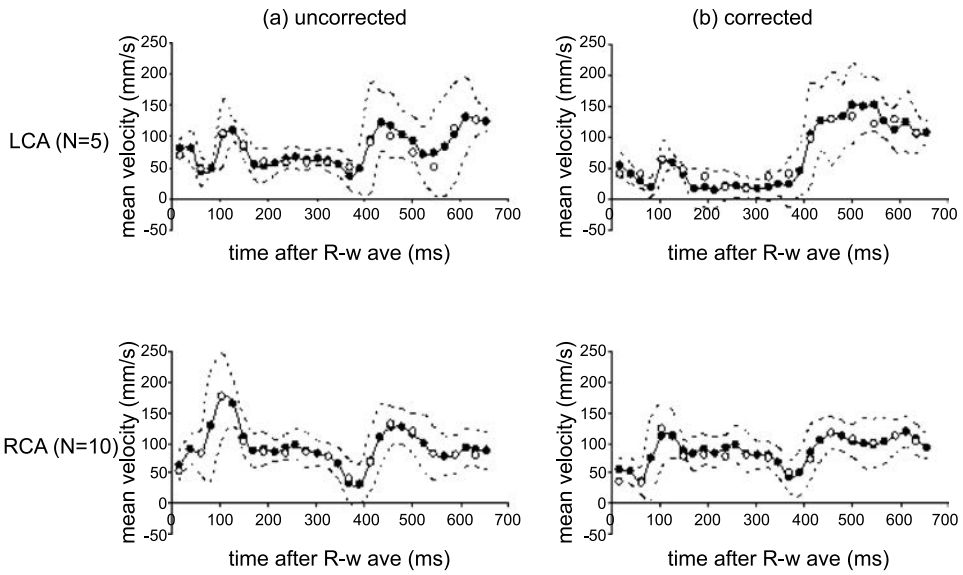

Figure 1. Mean (±SD) flow velocities in 5 left (top) and 10 right (bottom) coronary arteries before (a) and after (b) correction for through-plane motion of the vessel. (Solid circles = data derived from separate water-excitation and fat-excitation acquisitions, open circles = data derived from interleaved water-excitation/fat-excitation acquisition).

water-excitation and fat-excitation acquisitions (solid circles). The mean velocities derived from the combined water-excitation/fat-excitation acquistion are superimposed (open circles) and can be seen to follow the separate acquisition data closely. As expected, for the left arteries, the through-plane correction removes the systolic flow component, leading to strongly predominant diastolic flow. For the rca, the through-plane motion correction reduces and broadens the systolic flow velocity peak, resulting in the biphasic profile expected from Doppler Flowire studies. The mean diastolic/mean systolic velocity ratio was 1.06 (±0.28) before correction and 1.30 (±0.21) after correction ($p<0.01$). For the both left and right arteries, their were no significant differences in the mean diastolic and mean systolic velocities both before and after correction when comparing the data derived from the separate water-excitation and fat-excitation acquisitions with that derived from the combined water-excitation/fat-excitation acquisition. However, for the right coronary arteries, the poorer temporal resolution resulted in the uncorrected peak systolic velocity being significantly underestimated with the combined water-excitation/fat excitation acquisition (219 mm/s vs. 185 mm/s, $p<0.01$).

Conclusion: Selective excitation of the surrounding epicardial fat enables through-plane correction of both left and right coronary artery flow velocities. Although there were no significant differences in the mean systolic and mean diastolic velocities derived from the separate water-excitation and fat-excitation acquisitions compared to those derived from the combined fat-excitation/water-excitation acquisition, the poorer temporal resolution of the latter (44 ms) results in the blunting of rapidly changing flow profiles such as those found in the rca in early systole.

REFERENCE

Keegan, et al. (2003). *Proc. ISMRM*. Toronto.

501. Self-Gating in Pediatric Cardiac MRI

Tiffanie R. Johnson, M.D.,[1] Orlando Simonetti, Ph.D.,[2] Andrew Larson, Ph.D.,[2] Mark A. Fogel, M.D.[3]
[1]*Pediatric Cardiology, Riley Hospital for Children, Indiana University, IN, Indiana, USA*, [2]*Siemens Medical Solutions, Malvern, PA, USA*, [3]*Cardiology, Children's Hospital of Philadelphia, Philadelphia, PA, USA*.

Introduction: The established method of obtaining cardiac magnetic resonance (MR) images utilizes the electrocardiogram (ECG) to synchronize image data acquisition. In about 5% of cases, a reliable ECG

Copyright © Marcel Dekker, Inc. All rights reserved.

ORDER REPRINTS

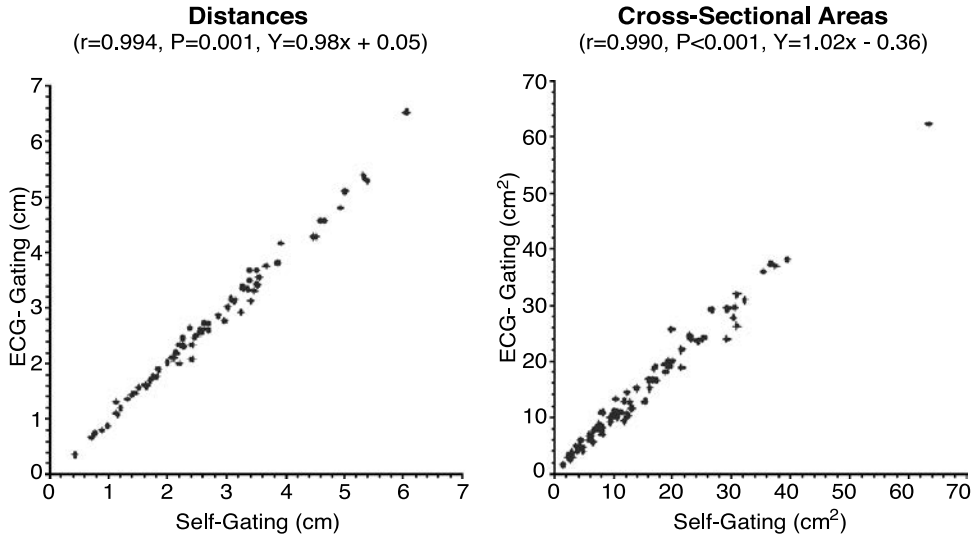

Figure 1. (*View this art in color at www.dekker.com.*)

signal cannot be obtained. The ability to perform cardiac MR without the ECG would make the modality more robust.

Purpose and Methods: A new method of using motion-induced changes in the image data to retrospectively synchronize the data to the cardiac cycle has been developed. The purpose of this study was to determine if this ''self-gating'' method of cine MR can be substituted for the ECG. We performed cardiac MR with this new sequence on 20 pts (1.2 to 20.2 years) with various forms of congenital heart disease. Pts referred for routine cardiac MR had additional imaging with the self-gating technique. Examples of diagnoses included the Fontan operation, pulmonary stenosis/regurgitation, Tetralogy of Fallot, pulmonary atresia with intact ventricular septum, and Rastelli operation. Shortening fraction, fractional area change, and blood vessel diameter in both ECG and self-gated techniques were measured. Statistical analysis was performed using paired t-test, Pearson correlation, and regression analysis.

Results: All self-gated acquisitions were successful. For all linear and area measurements performed (n = 218), there was no significant difference between the ECG-gated and self-gated images (P = 0.507, Power = 99%), and correlation between the two was excellent (r = 0.995). No statistically significant difference in measurements performed between the ECG-gated and self-gated images could be identified (Power = 99%) (see Figure 1).

Conclusion: Cardiac MR in congenital heart disease can be successfully performed without the use of the ECG. The new self-gating technique provides accurate information, makes the modality more robust, and is a technical advance in the field.

502. Integrated Real-Time Cardiac Imaging Environment

Andres Carrillo,[1] Ajit Shankaranarayanan,[1] Jane W. Johnson,[1] Juan M. Santos,[2] Michael M. McConnel,[3] Phillip C. Yang,[3] Jean H. Brittain,[1] Bob S. Hu.[4] [1]*ASL West, GE Medical Systems, Menlo Park, CA, USA*, [2]*Electrical Engineering, Stanford University, Stanford, CA, USA*, [3]*Cardiology, Stanford University, Stanford, CA, USA*, [4]*Cardiology, Palo Alto Medical Foundation, Palo Alto, CA, USA*.

Introduction: Magnetic resonance imaging has improved the traditional evaluation of ventricular function and has enabled novel non-invasive methods for evaluating coronary artery disease, valvular function, and myocardial viability. However, no systematic effort has been made to integrate these important tools into a single dynamic environment that reduces the examination time to the actual imaging time. Our real-time imaging environment significantly reduces the examination time while allowing for the flexible interactivity frequently needed in the course of a comprehensive cardiac examination.

Following the flexible architecture proposed by Santos et al. (2002), we have developed a novel dynamic real-time cardiac imaging environment to provide a comprehensive *suite* of cardiac applications

Copyright © Marcel Dekker, Inc. All rights reserved.

ORDER REPRINTS

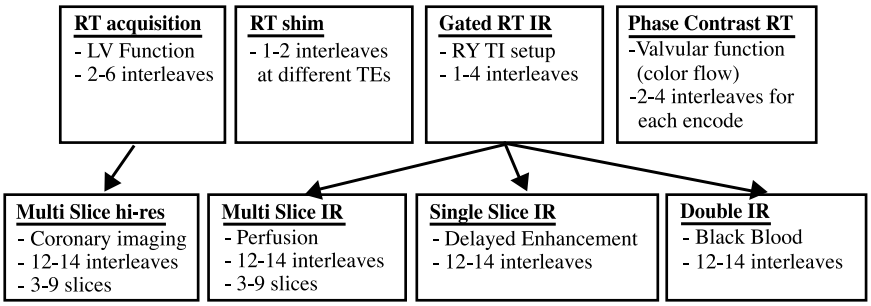

Figure 1. Available imaging modes in the integrated real-time cardiac suite. Each box corresponds to a particular imaging mode. The target clinical application and the unique imaging parameters are shown for each mode. The top row shows the real-time modes. The bottom row shows the high-resolution modes. Arrows illustrate some of the transitions between real-time and high-resolution gated modes.

within a single ''switch-on-the-fly'' user interface. The ability to perform real-time adjustment of slice location and sequence parameters increases the flexibility and efficiency in performing a complete cardiac evaluation.

Methods: Our cardiac real-time imaging environment is implemented on a GE 1.5 Signa Twinspeed system (GE Medical Systems, Milwaukee, WI) that includes EXCITE technology running optimized sliding-window, gridding reconstruction software (Shankaranarayanan et al., 2003).

Figure 1 illustrates the different modes of operation available in our cardiac suite. The current implementation utilizes a spiral acquisition. However, the infrastructure can be easily combined with other imaging approaches. The imaging parameters common to all modes include a 13 ms spectral–spatial excitation pulse, 16 ms readout, 5 mm slice thickness, 30#176; flip angle and 20 cm fov. Transitions between modes are initiated by a single button push from the user interface and are executed in less than 500 ms. Contextual information including slice location, prescan parameters, and shim values is automatically shared between the different modes. Images from different modes are saved into different display buffers. Each buffer is accessible separately during image review and has customized image analysis tools.

Results: Figure 2 shows images acquired during the cardiac evaluation of a healthy volunteer completed using the integrated real-time cardiac imaging environment. During the evaluation images were acquired for (A) high-resolution, bright-blood coronaries and (B) short axis with nulled myocardium for delayed enhancement. Phase contrast and perfusion images were also acquired.

Discussion and Conclusion: Cardiac magnetic resonance imaging is a clinically useful tool for a broad range of cardiac pathology. However, there are limitations that hinder the widespread clinical applicability of these techniques, including the inability to perform dynamic adjustments of contrast preparation, local shims, flip angles and other parameters, as well as the impossibility of performing final adjustments in the location of the scan before the gated acquisitions are initiated. Our real-time cardiac environment eliminates most of these limitations. In addition, scan time limitations often do not allow for the complete examination of cardiac function, valvular function, myocardial characterization, and coronary artery imaging. The improvement in the workflow and the efficiency achieved with our real-time cardiac environment brings us effectively to the goal of equating examination time with imaging time.

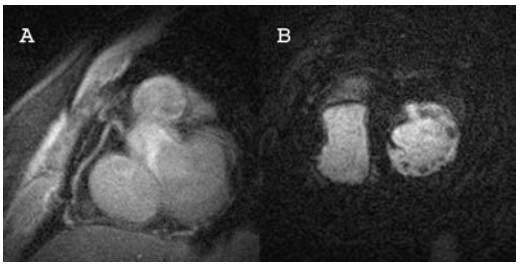

Figure 2. Images acquired during a study using the integrated real-time cardiac environment. Each image was acquired with an optimal set of shim values adjusted in real-time for its specific location. Image (A) shows a right coronary artery, and (B) shows a short axis delayed enhancement image after real-time adjustment of the inversion time. Fortunately for this healthy volunteer, no scar was detected.

REFERENCES

Santos, et al. (2002). *ISMRM*738.
Shankaranarayanan, et al. (2003). *SCMR*294–296.

Copyright © Marcel Dekker, Inc. All rights reserved.

MARCEL DEKKER, INC.
270 Madison Avenue, New York, New York 10016

ORDER REPRINTS

503. Non-Contrast-Enhanced Peripheral Angiography Using Balanced SSFP with Improved Arterial–Venous Separation at 3T

Jean H. Brittain,[1] Ann Shimakawa,[1] Graham A. Wright,[2] Brian A. Hargreaves,[3] Phil Yang,[4] Michael McConnell,[4] Bob Hu.[5] [1]*ASL-West, GE Medical Systems, Menlo Park, CA, USA*, [2]*Sunnybrook and Women's College Health Sciences Center, Toronto, ON, Canada*, [3]*Department of Electrical Engineering, Stanford University, Stanford, CA, USA*, [4]*Department of Medicine, Stanford University, Stanford, CA, USA*, [5]*Department of Cardiology, Palo Alto Medical Foundation, Palo Alto, CA, USA*.

Introduction: The short time window between arterial and venous enhancement limits the spatial resolution of contrast-enhanced angiograms below the knee. Even with restricted acquisition duration, arterial conspicuity is often limited by the superposition of enhancing deep veins (Bilecen et al., 2003). Recently, non-contrast-enhanced approaches have been explored using balanced SSFP acquisitions to acquire high-resolution angiograms (Brittain et al., 2003; Hargreaves et al., 2003; Lu et al., 2003). To separate arteries from veins, these techniques rely on T_2 differences between arterial and venous blood (Thulborn et al., 1982). The Luz–Meiboom model predicts that the difference in R_2 relaxation rate ($1/T_2$) between arterial and venous blood ($R_{2,venous} - R_{2,arterial}$) is proportional to the square of field strength (Luz et al., 1963). Hence, imaging at higher fields should improve arterial–venous separation. In this work, we present simulation and volunteer data showing approximately a three-fold improvement in arterial-to-venous-blood CNR at 3T compared to 1.5T.

Methods: The signal resulting from a balanced SSFP sequence with fat suppression (Scheffler et al., 2001) was simulated using measured T_1 and T_2 values. The simulations assumed identical coil performance at 1.5T and 3T and neglected in-flow effects. Imaging flip angles were selected to maximize arterial-blood-to-muscle contrast.

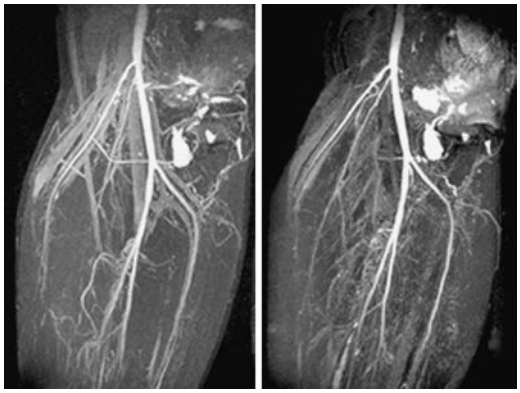

Figure 1. Coronal MIPs of a patient with claudication acquired at 1.5T (left) and 3T (right). Note the appearance of the deep veins in the 1.5-T image that are suppressed in the 3-T result.

Experiments were performed on a 1.5T-Signa TwinSpeed and a 3T-Signa VH/i scanner (GE Medical Systems, Milwaukee, WI). A balanced SSFP sequence with fat suppression was used with the following parameters at 3T: TE/TR = 2.2/4.7 ms, BW = ±100 kHz, Matrix = $256 \times 180 \times 128$ zero padded to $512 \times 512 \times 256$, FOV = $24 \times 16.8 \times 12.8$ cm, flip = 50°, fat-selective inversion every 32 TR, scan time = 3.2 min. Images at 1.5T used the same parameters with the following exceptions: TE/TR = 1.9/4.1 ms, flip = 60°, scan time = 3 min. A transmit-receive extremity coil (Medical Advances, Milwaukee, WI) was used at 1.5T. A prototype transmit-receive extremity coil with similar geometry was used at 3T. Volunteer images were acquired following informed consent.

Results: Table 1 lists the simulation-predicted and experimentally-measured improvement ratios of SNR and CNR at 3T vs. 1.5T. We imaged 2 patient volunteers with claudication and 2 healthy volunteers at 1.5T and 3T. As shown in Table 1, the average improvements in SNR and CNR at 3T vs. 1.5T closely matched predicted values. However, as shown by the range listed in Table 1, improvements by individual

Table 1.

	Predicted	Measured	
		Mean	Range
Ratio of Arterial-Blood SNR at 3T vs. 1.5T	1.5	1.5	1.3–2.0
Ratio of Arterial-Blood-to-Muscle CNR at 3T vs. 1.5T	1.4	1.4	1.2–1.7
Ratio of Arterial-to-Venous-Blood CNR at 3T vs. 1.5T	3.1	3.1	1.7–5.2

Copyright © Marcel Dekker, Inc. All rights reserved.

ORDER REPRINTS

varied by up to 71%. Such variations are expected due to individual differences in tissue and blood relaxation rates including those due to variations in hematocrit level and venous oxygen saturation.

Figure 1 illustrates coronal maximum intensity projections (MIPs) of non-contrast-enhanced angiograms of the popliteal trifurcation of a patient with claudication. As predicted, venous structures are less conspicuous at 3T compared to 1.5T. The excellent acquired spatial resolution of approximately 0.9 mm^3 allows visualization even of small vessels.

Conclusions: Balanced SSFP with fat-suppression and an optimized imaging protocol generates non-contrast-enhanced angiograms with high SNR, CNR, and spatial resolution. Imaging at 3T improves SNR and CNR compared to 1.5T.

REFERENCES

Bilecen, D., et al. (2003). *Proc. 11th ISMRM*. 85.
Brittain, J., et al. (2003). *11th ISMRM*. 1710.
Hargreaves, B. (2003). *11th ISMRM*. 548.
Lu, et al. (2003). *Proc. 11th ISMRM*. 320.
Luz, Z., et al. (1963). *J. Chem. Phys.* 39:366.
Scheffler, K., et al. (2001). *MRM* 45:1075.
Thulborn, K., et al. (1982). *Biochim. Biophys. Acta* 714:265.

504. Real-Time Optimization for Myocardial Delayed Enhancement Imaging

Ajit Shankaranarayanan,[1] Andres Carrillo,[1] Bob Hu,[2] Mike McConnell,[3] Jane Johnson,[1] Jean Brittain,[1] Phil Yang.[3] [1]*ASL West, GE Medical Systems, Menlo Park, CA, USA*, [2]*Palo Alto Medical Foundation, Palo Alto, CA, USA*, [3]*Stanford University, Palo Alto, CA, USA.*

Introduction: Myocardial delayed enhancement (MDE) imaging (Kim et al., 1999) has been used extensively for characterizing myocardial viability, differentiating scar from non-infarcted myocardium. A key issue for the success of current MDE techniques is the determination of the optimal inversion time (TI) for maximal contrast between these tissue types. The optimal TI to null viable myocardium varies with contrast dose and timing, as well as between patients. The traditional approach of repeating acquisitions until an adequate TI is found is inefficient. Preliminary work has been reported using real-time adjustment strategies or phase preservation techniques (Glockner et al., 2003; Kellman et al., 2002). However, these approaches continue to suffer from poor sequence integration and potential reduced CNR considerations. To address these limitations, we have developed a tool that enables real-time adjustment of TI plus rapid switching to a gated, high-resolution MDE acquisition.

Method: The new high-resolution MDE tool was implemented on a GE 1.5T Signa Twinspeed system (GE Medical Systems, Milwaukee, WI) with a high performance gradient system achieving a maximum gradient strength of 40 mT/m and maximum slew rate of 150 mT/m/msec. The configuration included EXCITE technology with vector array processors running optimized sliding-window, gridding reconstruction software (Shankaranarayanan et al., 2003) and a Linux host for high display rates.

Figure 1 shows the workflow of this new tool. It has four modes of operation: a real-time interactive localization mode used to navigate to the slice of interest, a real-time shimming tool (Carrillo et al., 2003) used to optimize the center frequency and shim for the localized volume of interest, a low-resolution gated real time delayed enhancement tool used to optimize the TI, and a high-resolution gated delayed enhancement tool used to acquire diagnostic MDE images in a breath hold.

The user can change between these imaging modes with a single button push. Contextual information

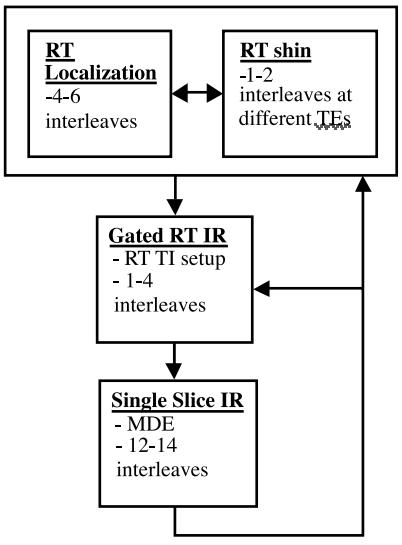

Figure 1. Schematic showing the workflow of the real time MDE tool. (*View this art in color at www.dekker.com.*)

Copyright © Marcel Dekker, Inc. All rights reserved.

ORDER REPRINTS

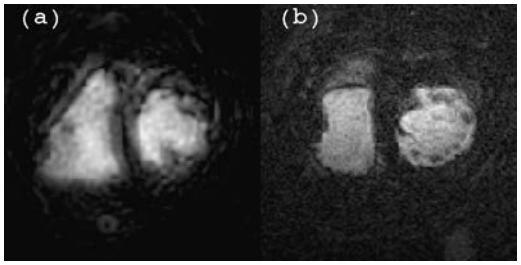

Figure 2. Comparison images of a healthy volunteer (no scar expected) from (a) gated real time MDE sequence and (b) the high resolution gated breath held MDE acquisition. As expected, the degree of myocardium suppression is comparable.

including slice location and orientation and ''prescan'' parameters is automatically shared. The timing of the two delayed enhancement modes was designed to ensure consistent image contrast between the two modes for a given TI. Typically, the low-resolution mode was utilized during free breathing to optimize the TI using a slider on the real-time user interface. The current implementation uses a spiral acquisition. However, the infrastructure can be utilized with any acquisition strategy. Default parameters for all acquisitions included 5 mm slice thickness, 20 cm FOV and 30° flip angle.

Results: Figure 2 illustrates short axis MDE images of a healthy volunteer (no scar expected). Note the similar myocardial suppression in the gated real time image and the high resolution gated breath held image.Since the tuning of the TI was accomplished from the real-time user-interface, no additional breath-holds were required.

Discussion and Conclusion: Myocardial delayed enhancement studies require high-resolution images with the inversion time optimized to null myocardial signal. We have developed a technique that allows the fine-tuning of the TI in real time and an immediate switch to high resolution gated imaging. This integrated tool eliminates unnecessary breath-holds and increases exam efficiency.

REFERENCES

Carrillo, A., et al. (2003). *SCMR* 417.
Glockner, J. F., et al. (2003). *SMRM* 1574.
Kellman, P., et al. (2002). *Magn. Reson. Med.* 372–383.
Kim, R. J., et al. (1999). *Circulation* 100:1992–2002.
Shankaranarayanan, A., et al. (2003). *ISMRM* 1072.

505. A New Approach for Rapid Assessment of the Cardiac Rest Period for Coronary MRA

Cosima Jahnke, M.D.,[1] Ingo Paetsch, M.D.,[1] Kay Nehrke, Ph.D.,[2] Bernhard Schnackenburg, Ph.D.,[1] Axel Bornstedt, Ph.D.,[1] Rolf Gebker, M.D.,[1] Eckart Fleck, M.D.,[1] Eike Nagel, M.D.[1] [1]*Cardiology, German Heart Institute Berlin, Berlin, Germany*, [2]*Philips Research Laboratories, Hamburg, Germany*.

Background: Effective suppression of cardiac motion is crucial in coronary MRA. We evaluated a new approach for rapid and automatic detection of the cardiac rest period in comparison to the conventional visual assessment of the left and right coronary artery rest periods.

Methods: 57 consecutive routine cardiac patients were examined (Philips Intera 1.5T system). First, visual determination of the duration and starting point of the rest periods of the left and right coronary artery was done using a cine-bFFE scan with a transversal slice orientation (retrospective gating, 40 phases/cardiac cycle). The rest period was defined as the duration of the coronary artery moving = 25% of its cross-sectional area. Then a new, automatic approach was applied which allows the detection of the cardiac rest period from a graph (Figure 1) displaying the cross-correlation of consecutive cine images. The position of the shim volume was used to define a correlation kernel. The cardiac rest period calculation is based on the plateau phase defined by the two highest adjacent data points with neighbouring data

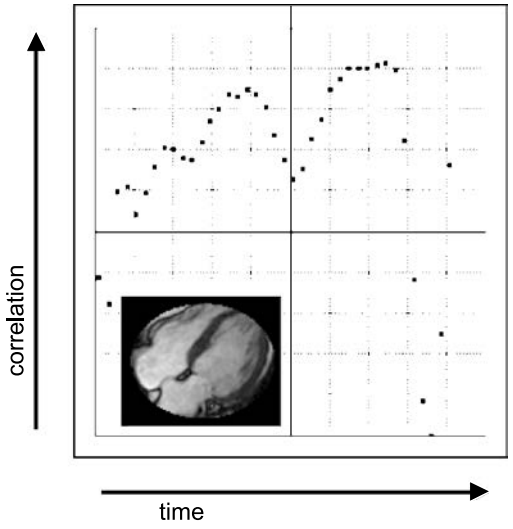

Figure 1.

Copyright © Marcel Dekker, Inc. All rights reserved.

ORDER REPRINTS

Table 1.

	Visual LCA	Visual RCA	Intersection (LCA/RCA)	Automatic cardiac rest period
Rest period duration [ms]	157±68	120±50	110±50	102±40*
Correlation to cardiac rest period	0.83*	0.83*	0.88*	
Starting point [ms]	519±152	539±163	545±161	554±168
Correlation to cardiac rest period	0.97*	0.98*	0.98*	

*$p<0.01$.

points showing <5% deviation. The correlation between the automatically detected cardiac rest periods and the visually evaluated coronary rest period was assessed for each single vessel as well as for the intersection of the rest periods.

Results: An excellent correlation between the automatically and visually determined starting points for the cardiac rest period and the coronary artery rest period was found. In addition the intersection of the left and right coronary artery rest periods demonstrated a high correlation with the cardiac rest period (Table 1). The automatically detected cardiac rest period was significantly shorter in comparison to the visually assessed left and right coronary artery rest period.

Conclusions: Comparing the cross-correlation between consecutive cine images allows automatic detection of the cardiac rest period. The automatic approach facilitates the assessment of the cardiac acquisition window without the need for user interaction and is a promising tool when aiming at single scan imaging of the complete coronary tree.

506. Volume–Time Curve (VT_c) Quantitation of Left Ventricular Functional Metrics Using 3D MRI

Brandon M. Mikolich, M.D.,[1] Vikas K. Rathi, M.D.,[2] Hakki Bolukoglu, M.D.,[2] June Yamrozik,[2] Ronald B. Williams,[2] Diane A. Vido,[2] Maria Jaksec,[2] Mark Doyle, Ph.D.,[2] Robert W. W. Biederman, M.D.[2]
[1]*Drexel University, Philadelphia, PA, USA*, [2]*Allegheny General Hospital, Pittsburgh, PA, USA*.

Introduction: Classic estimations of ventricular function employ volume–time curves (VTc) and provide left ventricular metrics beyond ejection fraction. Typically, VTc's are utilized most often by nuclear imaging (MUGA). However, neither spatial or temporal resolution, nor the precision of such imaging, is near optimal, limiting their application and sophistication, yet such imaging is frequently employed.

Hypothesis: Given MRI's high spatial resolution, inherent 3D volume precision and with optimized temporal resolution, we hypothesized that application of MRI may offer added insight to VTc examinations of the cardiac cycle.

Methods: Contiguous, semi-automated endocardial and epicardial LV contours were mapped throughout the entire cardiac cycle (including atrial systole) derived from FIESTA (GE CV/i) with high temporal spatial resolution (20±5 ms) in 16 subjects. Eight patients had severe aortic stenosis (mean age: 68±11) undergoing valve replacement (AVR) at pre (Pre) and 6 months (Post) AVR, while eight age-matched normals served as controls (mean age: 60±9). Left ventricular VTc's were constructed and, through interactive programming (MATLAB), unique systolic volumetric-time parameters were derived, including: peak negative $-dv/dt$ and $-d^2v/dt^2$ (first and second derivative of instantaneous LV volume decline; velocity and acceleration, respectively), peak ejection rate (PER) and time to PER (PER_t). As well, diastolic metrics were derived: peak positive $+dv/dt$ and $+d^2v/dt^2$ (first and second derivative of instantaneous LV volume increase; velocity and acceleration, respectively), peak filling rate (PFR), and time to PFR (PFR_t). Linear regression equations defining the active decay and rise of LV volume change were also generated.

Results: VTc's can be performed by MRI with high temporal and spatial resolution, providing novel indices of volume changes, such as first and second derivatives of volume change over time; velocity and acceleration of LV *volume* change, respectively (see Table 1). Specifically, LV systolic indices improve modestly after AVR as compared to similar indices of diastole, which demonstrate marked improvement commensurate with regression of hypertrophy following AVR, largely in the direction of age matched normals.

Conclusion: Whereas all systolic indices of VTc ($-dv/dt$, $-d^2v/dt^2$, PER and PER_t) remained fairly stable following AVR, the indices of diastolic fiunction

Copyright © Marcel Dekker, Inc. All rights reserved.

ORDER REPRINTS

Table 1. Volume–time curve (VTc).

Indices	AS-Pre	AS-Post	Controls
LVmass (g)	157.79±0.338*	141.16±33.8**	94.9±21.39***
−dv/dt (ml/msec)	−0.773±0.338	−0.543±0.171**	−0.393±0.15***
dv/dt (ml/msec)	0.487±0.23*	0.584±0.17**	0.297±0.09***
$-d^2v/dt^2$ (ml/msec)	−0.271±0.22	−0.531±0.34**	−0.243±0.11***
d^2vol/dt^2 (ml/msec)	0.360±0.3	0.499±0.23	0.286±0.06***
Systolic slope	−0.305±0.07	−0.355±0.09**	−0.043±0.03***
Diastolic slope	0.139±.03*	0.2±.08**	0.06±.04***
Peak ejection rate	496.4±133.23	476.9±97.73**	352.2±87.41***
Peak flow rate	383.9±154.18*	462.4±91.91**	221.1±104.66***

For all marked with asterisks p = <0.05; *dx* = derivative; vol = volume; t = time.
(By ANOVA comparison.)
*Pre vs. post.
**Pre vs. control.
***Post vs. control.

(+*dv*/*d*t, $+d^2v/dt^2$, PFR but not PFR_t) substantially improved in conjunction with a regression in LVmass. As well, the diastolic but not systolic slope of the regression equation improved. Taken together, this may suggest that the collagen matrix, heavily modulatable by matrix metalloproteinases and not under direct influence of mRNA unlike hypertrophy, may regress slightly faster than hypertrophy at six months. The utility of highly refined interrogations using 3D MRI time–volume approach merits further considerations.

507. Very Fast and Highly Automated Method for Myocardial Motion. Analysis with Phase Contrast Magnetic Resonance Imaging

Erik Bergvall, M.Sc.,[1] Peter Cain, M.D., Ph.D.,[2] Gunnar Sparr, Ph.D.,[1] Hakan Arheden, M.D., Ph.D.[2]
[1]*Center for Mathematical Sciences, University of Lund, Lund, Sweden*, [2]*Department of Clinical Physiology, University of Lund, Lund, Sweden*.

Introduction: Visual assessment of cardiac function is user dependent and requires extensive training in order to become adequately competent. Quantification of left ventricular function using pre-saturation grid tagging (GRID) is limited by lower resolution and is difficult to post-process. As an alternative, phase contrast MR can provide instantaneous velocity maps of the myocardium with high resolution. Motion is calculated by integrating velocity fields with respect to time. Previous integration attempts have required lengthy post-processing and user interaction. We present an optimal Fourier-based integrator (FOUR) combined with a segmentation algorithm based on particle traces which allows very fast myocardial deformation analysis.

Purpose: To develop a fast post-processing algorithm of phase contrast MR images for the purpose of quantitative measurements of myocardial deformation and examine the feasibility and accuracy of in-plane motion analysis.

Methods: Assuming the myocardial motion to be periodic, the mathematical tool of Fourier-methods can be used in the analysis. Using an iterative solution scheme, convergence is fast and the computational cost is low. Segmentation of images is performed by analysis of calculated particle traces which is feasible as particles in blood and myocardium have different motion patterns. Four image planes (3 pts) were acquired using in-plane phase contrast imaging (Philips Intera, GE Signa). Image parameters: 1.5T, 32 frames/heart beat, venc 0.2 m/s. Voxel size: 1.5 mm in-plane, 4–10 mm slice thickness. Processing time (PC, 2.6

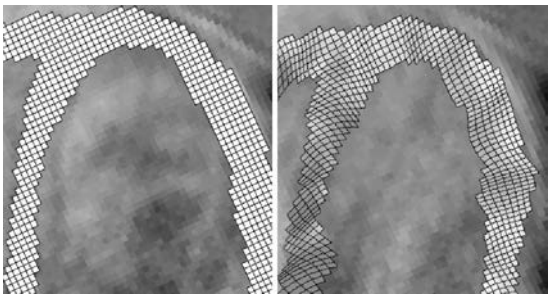

Figure 1. (*View this art in color at www.dekker.com.*)

Copyright © Marcel Dekker, Inc. All rights reserved.

ORDER REPRINTS

GHzm 1 GB ram, running MATLAB) was compared to the previously described 'forward–backward' (FB) integration method. A sequence of GRID images was acquired with equal voxel size for validation purposes. GRID tags were manually traced over the heart cycle.

Results: Blood and lung was separated from tissue by the segmentation algorithm, leaving only few, easily removable artefacts. Processing time was greatly reduced with FOUR technique (16 sec vs. 81 min) for FOUR and FB, respectively. The mean relative error of FOUR, as compared with manually traced GRID tags sequences was 8.8±3.1% of total path length, corresponding to a subvoxel variation. Figure 1 shows myocardial deformation in a long-axis slice (end diastole left, end systole right), visualized by deforming an initially square grid, imitating GRID. Resolution of FOUR tags is increased a factor 5 compared to GRID tags.

Conclusions: Fourier based tracking of myocardial motion with segmentation allows very fast quantitative assessment of myocardial motion and deformation which may be feasible in the clinical setting due to the very short post-processing time. Motion analysis based on phase contrast measurements allows automated quantitation of myocardial deformation as opposed to GRID, where post-processing is difficult and time consuming.

508. A Novel Non-Invasive Method of Measuring Pulmonary Vascular Resistance Using Phase Contrast MR

Vivek Muthurangu, M.B.Ch.B. (hons),[1] David Atkinson, Ph.D.,[1] Maxime Sermesant, Ph.D.,[1] Andrew Taylor, M.D.,[1] Marc Eric Miquel, Ph.D.,[1] Robert Tulloh, D.M.,[2] Derek Hill, Ph.D.,[1] Reza Razavi, M.B.B.S.[1] [1]*Division of Imaging, King's College London, London, United Kingdom*, [2]*Paediatric Cardiology, Guys Hospital, London, United Kingdom.*

Introduction: Pulmonary hypertension is assessed at cardiac catheterization by measurement of pulmonary vascular resistance (PVR). However, there are risks attached to cardiac catheterization and therefore a non-invasive method of PVR quantification would be useful. Doppler echocardiography has been used to accurately assess systolic and diastolic pressure. Unfortunately, it has been difficult to accurately measure mean pulmonary artery pressure and mean pulmonary artery flow using this technique, preventing the calculation of PVR. Phase contrast magnetic resonance (MR) has been shown to provide accurate quantification of blood flow. We use MR flow data as an input to a simple windkessel model, allowing the non-invasive quantification of PVR.

Purpose: To demonstrate the feasibility of this potentially non-invasive method of PVR quantification.

Methods: 10 patients underwent cardiac catheterization, in an MR interventional suite (1·5T Intera I/T MRI scanner, Philips, The Netherlands) with x-ray back-up (BV Pulsera cardiac x-ray unit, Philips, Best, The Netherlands). Invasive pressure and MR flow was acquired at baseline (condition 1) and at 20 ppm nitric oxide (condition 2) allowing calculation of PVR.

A series of pressure curves were calculated using MR flow data inputted into a 2 element windkessel model with a range of PVR's and vascular compliances. Using an error minimization protocol we were able to find the PVR that produces a pressure curve with systolic and diastolic values closest to the actual pressures. All data is expressed as median (interquartile range) unless otherwise specified. Correlation coefficients, linear regression and Bland Altman analysis were used to compare the actual PVR and the modelled PVR.

Results: At condition 1, the median actual PVR was 7.56 WU.m^2 (3.23–12.1 WU.m^2) and the modelled PVR was 7.32 WU.m^2 (3.41–11.4 WU.m^2) which represents a difference of 3.1% between the 2 methods. At condition 2, the median actual PVR was 6.54 WU.m^2 (2.73–8.93 WU.m^2) and the modelled PVR was 6.07 WU.m^2 (2.35–8.07 WU.m^2) which represents a difference of 7.2% between the 2 methods. The percentage change in the actual median PVR in response to nitric oxide was 13.5% and the percentage change using the modelled PVR was 17.1%.

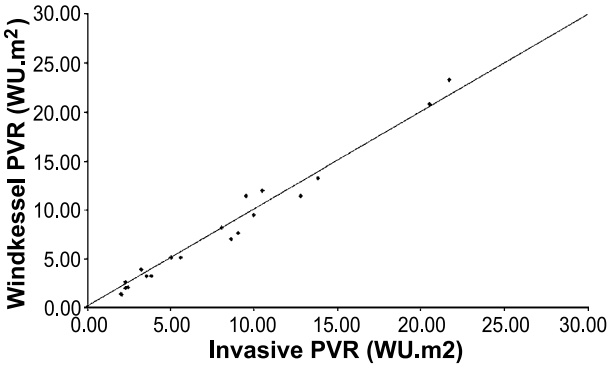

The correlation coefficient between the actual PVR and the modelled PVR using all the data sets was 0.99 ($p<0.001$), the linear regression between the 2 methods revealed a gradient of 1.04 and an intercept of −0.47 WU.m^2. Bland Altman analysis using all data

Copyright © Marcel Dekker, Inc. All rights reserved.

ORDER REPRINTS

sets revealed a bias of 0.12 WU.m^2, an upper limit of agreement of 2.04 WU.m^2 and a lower level of agreement of −1.8 WU.m^2.

Conclusion: We have demonstrated the feasibility of using a 2 element windkessel model and MR flow data to quantify PVR. This will hopefully form the basis of a wholly non-invasive method of PVR quantification. Currently PVR is quantified at cardiac catheterisation using invasive pressure and flow measurements. We have previously demonstrated the feasibility of combining invasive pressure measurements of MR flow data to accurately invasively calculate PVR. Invasive catheterisation, however, is associated with significant morbidity and mortality, due to vascular damage, x-ray radiation exposure, and general anaesthetic. Therefore an accurate non invasive method would be useful, particularly in paediatric practice. Our model requires MR flow data and systolic and diastolic pressures (which can be accurately assessed using Doppler echocardiography) and correlate well with invasively calculated PVR. Furthermore new velocity mapping techniques will hopefully allow accurate quantification of regurgitant jet velocity, allowing all required input data to be acquired using MR. This should make MR a useful tool in the assessment of pulmonary hypertension.

509. Cardiovascular Magnet Resonance Assessment of Human Myocarditis; IR Gradient Echo Compared to T1 Turbo Spin Echo Imaging Protocols

Stefan Hager, M.D.,[1] Martina Mangin, M.D.,[1] Anja Wagner, M.D.,[2] Heiko Mahrholdt, M.D.,[1] Udo Sechtem, M.D.[1] [1]*Cardiology, Robert Bosch Medical Center, Stuttgart, Germany*, [2]*Cardiology, Duke Cardiovascular MR Center and Robert Bosch Medical Center, Durham, NC, USA and Stuttgart, Germany*.

Introduction: Active myocarditis can occasionally lead to sudden death in young adults and 10% of all patients may develop chronic dilated CMP. Contrast CMR using T1 turbo spin echo (T1 TSE) pulse sequences is well established for the evaluation of myocarditis. However, new IR gradient echo (IR GRE) CMR techniques increasing image contrast up to 500% and reduce breathing artifacts. Thus, such pulse sequences may provide better sensitivity for the detection of myocardial damage in the setting of myocarditis compared to the established T1 TSE protocol.

Methods: We compared contrast CMR using new IR GRE techniques to the standard T1 TSE protocol established by Friedrich et al. (1998) in patients presenting with known (n = 4) or suspected myocarditis (n = 14). All T1 TSE images were evaluated by calculating relative enhancement according to Friedrich et al. IR GRE images were read in the AHA/ACC recommended 17-segment model. Each segment was divided in 4 quartiles (epicardial, mid-epi, mid-endo and endocardial) and each quartile was individually graded as enhanced or not enhanced by consensus of two experienced readers.

Results: In the four patients with known myocarditis (confirmed by biopsy) IR GRE CMR depicted epicardial signal enhancement in all four patients, whereas T1 TSE detected increased epicardial signal in only one patient. In the 14 patients presenting with clinically suspected myocarditis IR GRE revealed signal enhancement in seven patients compared to four patients who were diagnosed to have myocarditis based on signal enhancement on T1 TSE images. Thus, IR GRE imaging detected myocarditis in more patients than T1 TSE (11/18 vs. 5/18 $p = 0.036$). T1 TSE imaging did not diagnose myocarditis in any case that was ruled negative by IR GRE. Areas of enhancement IR GRE images were most frequently located in the subepicardial part of the LV lateral wall. In contrast, enhancement on T1 TSE imaging was more transmurally distributed.

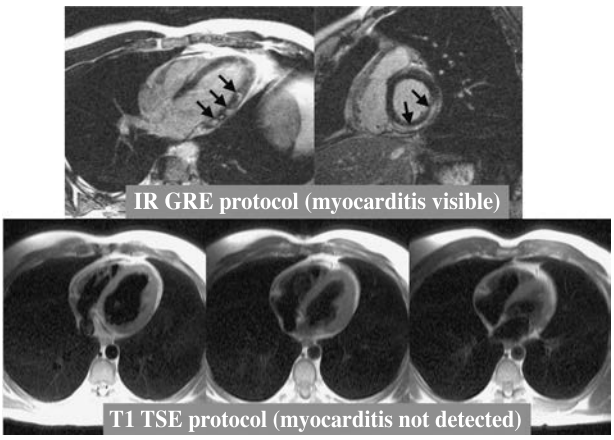

Conclusions: Contrast CMR imaging is capable of detecting myocarditis in vivo. IR GRE imaging may provide a higher sensitivity for the detection of myocarditis compared to T1 TSE imaging. The area of signal enhancement differs between IR GRE and T1 TSE protocols.

REFERENCE

Friedrich, et al. (1998). *Circulation* 97:1802–1809.

Copyright © Marcel Dekker, Inc. All rights reserved.

ORDER REPRINTS

510. Novel Hybrid Breath-Hold/Free Breathing Navigator Echo Technique: Applications for Quantitative Myocardial Perfusion and Angiogenesis Imaging

Jeffrey Goldman, M.D.,[1] Niels Oesingman,[2] Emil Cohen,[1] Neesha Patel, M.D.,[1] Simone Hoffer, M.D.[1]
[1]*Radiology, Mount Sinai, New York, NY, USA*, [2]*Radiology, Siemens Medical Systems, Ehrlangen, Germany*.

Introduction: Quantitative analysis of contrast enhanced myocardial perfusion for over a breath-hold is difficult due to respiratory motion. More delayed contrast enhanced tracer kinetic information has been shown to be important in imaging of angiogenesis, collateral coronary circulation and myocardial vaibility information. It would be beneficial to be able to image myocardial enhancement over a longer period of time. The dilemna of acquiring data using navigator echoes to the diaphragm, is that during the maximal temporal resolution, if data is acquired at end expiration, is one data set per respiratory cycle. We hypothesized that inorder to obtain tracer kinetic information for over a breath-hold we would like to acquire the first pass myocardial perfusion data at a high temporal resolution during a breath-hold and that the remainder of the contrast washout part of the curve could be acquired at lower temporal resolution during free breathing. Inorder to measure contrast uptake and washout kinetics for longer than a single breath-hold we have developed a technique which images continuously during a breath-hold and then acquires data at end-expiration during free breathing using a navigator echo technique.

Purpose: The purpose of our study was to evaluate our ability to measure contrast enhancement kinetics over a seqment of LV myocardium for up to 5 minutes using a hybrid breath-hold /free breathing technique navigator echo technique.

Methods: Five normal volunteers underwent contrast enhanced myocardial perfusion MRI on a 1.5T Siemens Sonata MRI. Single slice short axis perfusion imaging was performed using a saturation recovery turbloflash sequence. Imaging was acquired during a 21 second breath-hold and then during free breathing for 5 minutes with images being acquired during each respiratory cycle at end expiration. A data analysis tool was developed which converted data acquired during free breathing to a SI/time curve.

Results: Displacement of the LV free wall during normal free breathing was 11.3 mm and 7 mm in the superior to inferior (S–I) direction and anterior to posterior (A–P) direction respectively. Using the hybrid breath-hold/free breathing technique, displacement of the LV free wall was 2.5 mm and 1.7 mm in the S–I and A–P direction respectively. The LV was divided into 6 sectors. ROI's were placed within the myocardium in each sector in each patient in order to obtain contrast uptake and washout curves. In each sector of each patient an ROI was able to be place and remain within the wall of the myocardium without extending into the ventricular cavity. The average time from injection to peak contrast uptake was 19 seconds. The average time to plateau or visual downsloping of the curve was 25 seconds. This was judged as the minimal data necessary to calculate time to peak and to fit a SI/time curve for myocardial enhancement in healthy controls.

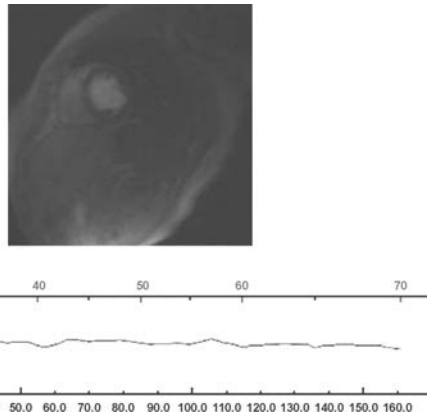

Conclusion: To our knowledge this is the first description of tracer kinetic measurement myocardial enhancement kinetics for up to 5 minutes. Our novel hybrid breath-hold/free breathing navigator echo technique allows for collection of the washout portion of the myocardial enhancement curve during free breathing and may be extended over longer acquisition times. This technique may help in the quantitative evaluation of myocardial viability and angiogenesis. The technique should also prove useful in evaluation of myocardial first pass perfusion in patients who have difficulty maintaining a breath-hold. Other applications for the hybrid breath-hold free breathing technique may include coronary artery imaging.

511. The Feasibility of High Resolution SSFP Coronary MRA Using Self-Calibrating Parallel Acquisition at 3T

Jaeseok Park, Debiao Li. *Department of Biomedical Engineering and Radiology, Northwestern University, Chicago, IL, USA*.

Copyright © Marcel Dekker, Inc. All rights reserved.

ORDER REPRINTS

Introduction: High resolution coronary MRA has been limited to acceleration due to signal-to-noise ratio (SNR). The SNR limitation may be resolved by the transition to the higher static magnetic field strength of 3T. The significant gain of SNR at 3T can be exploited the most by SSFP and a self-calibrating GRAPPA (GeneRalized Auto-calibrating Partially Parallel Acquisition) method allowing the reduction in imaging time and the increase in spatial resolution.

Purpose: The purpose of this work is to investigate the feasibility of high resolution coronary MRA at 3T using SSFP and improved GRAPPA.

Methods: Coronary artery imaging using ECG triggered, breath-hold, segmented 3D SSFP was performed on a 3T Siemens Trio system (Erlangen, Germany) (Deshpande et al., 2001). Images of the left anterior descending coronary artery (LAD)were acquired in a healthy volunteer. The imaging parameters were: TR/TE/flip angle = 3.7 ms/1.6 ms/65°, FOV = 252×350 mm^2, data acquisition matrix = 259×512, number of lines/heartbeat = 37, imaging time = 38 sec, number of partitions = 6 (interpolated to 12), slice thickness = 3 mm (interpolated to 1.5 mm). Eight coils were used at anterior and posterior positions. Fully sampled data was acquired, and then subsampled for an acceleration factor of 2.

Improving GRAPPA: The central k-space was sampled at Nyquist rate, while the outer k-space above a certain cutoff-spatial frequency (COSF) was reduced by outer reduction factor (ORF). To avoid high-energy aliasing artifact, the Nyquist sampled region was increased with higher ORF. This may result in blurring, since high spatial frequency lines are sampled less. To compensate for this, the ORF was alternated between 2 and 4. The total acceleration factor is two.

The coil weights were computed using all auto calibration signal (ACS) lines (Griswold et al., 2002). It may yield inaccurate reconstruction of high spatial frequency lines due to the dissimilarity between low and high spatial frequency regions. In this work, the ACS lines in the upper or lower region of central k-space are used for the coil weights to reconstruct the missing lines above or below the COSF, respectively.

Five sliding blocks over all coils are employed to yield multiple reconstructions for a missing line. The missing line is reconstructed by a weighted average (Griswold et al., 2002). In this work, all coil k-spaces are segmented along the frequency encoding direction. The improved GRAPPA reconstruction is performed segment by segment.

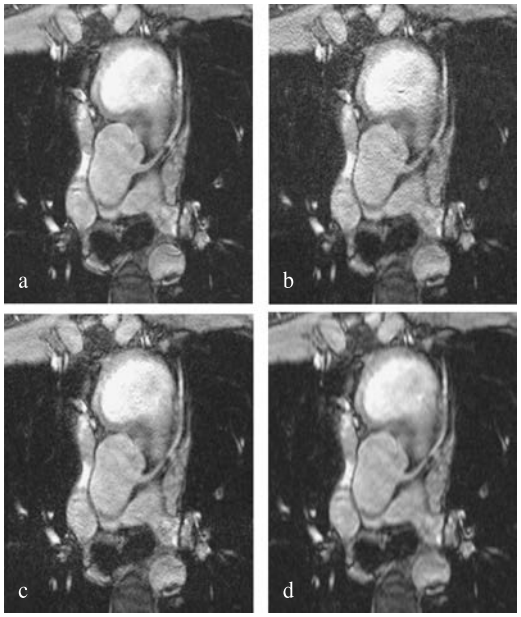

Figure 1. LAD images reconstructed using: a) fully sampled data, b) original GRAPPA with ORF of 4, c) improved GRAPPA with ORF of 2 and 4, d) 50% low frequency lines and zero padding.

Results: Figure 1 shows the LAD images reconstructed using: a) the full reference, b) original GRAPPA with ORF of 4, c) improved GRAPPA with ORF of 2 and 4, and d) 50% low frequency lines and zero padding. The improved GRAPPA significantly reduces the artifacts shown in the original GRAPPA. In the same imaging time, the improved GRAPPA image presents higher vessel sharpness than the 50% zero-padded image. The SNR of the full reference is 38.9, and that of the improved GRAPPA image is 29.1.

Conclusions: The LAD was successfully visualized with SSFP at 3T using the improved self-calibrating GRAPPA. The significant signal gain at 3T was exploited very well by using SSFP and increasing the high-energy Nyquist sampled region in the central k-space. The improved GRAPPA scheme is promising for high resolution coronary MRA at 3T, showing sufficiently high SNR and CNR.

REFERENCES

Deshpande, et al. (2001). *MRM* 46:494–502.
Griswold, et al. (2002). *MRM* 47:1202–1210

Copyright © Marcel Dekker, Inc. All rights reserved.

Marcel Dekker, Inc.
270 Madison Avenue, New York, New York 10016

ORDER REPRINTS

512. Enhanced Signal-to-Noise Ratio in DENSE MRI by Combining Stimulated Echoes

Daniel Kim,[1] Frederick H. Epstein,[2] Wesley D. Gilson,[2] Leon Axel.[1] [1]*Radiology, New York University, New York, NY, USA*, [2]*Radiology, University of Virginia, Charlottesville, VA, USA.*

Introduction: Displacement-encoding with stimulated echoes (DENSE) (Aletras et al., 2001) and harmonic phase imaging (HARP) (Osman et al., 1999) are MRI techniques for assessing intramyocardial function without the need for explicit tag detection. However, DENSE and HARP produce relatively low signal-to-noise ratio (SNR) because of the 50% signal loss inherent to stimulated echoes or bandpass filtering only one of the acquired echoes, respectively.

Purpose: In this study we describe a new technique to enhance the SNR in DENSE MRI (ESDENSE), by acquiring both echoes and combining them during image reconstruction.

Methods: In Figure 1, the magnitude, phase, and the corresponding k-space images are shown in order to illustrate how the two stimulated echoes are acquired and combined during image reconstruction. The two stimulated echoes of a CSPAMM data set (Figure 1A–C) can be combined during image reconstruction, by dividing the k-space at $k_x = 0$ (Figure 1C) to produce two sub-sampled and shifted data sets (Figure 1D–I), and by suitably averaging the two resulting phase-reconstructed image sets (Figure 1E,H). In order to achieve equivalent spatial and temporal resolution and scan time as cine DENSE, ESDENSE must use a higher value of displacement-encoding strength (k_e) and over-sample the readout points by a factor of two, at the cost of increasing the receiver bandwidth.

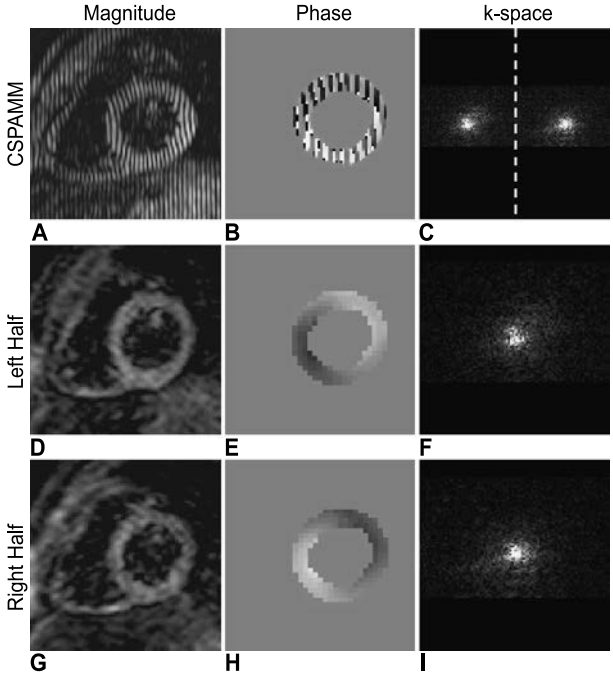

Figure 1. The magnitude, phase, and the corresponding k-space images are shown in order to illustrate how the two stimulated echoes are acquired and combined during image reconstruction. The two stimulated echoes of a CSPAMM data set (A–C) can be combined by parsing the k-space at kx = 0 (C) to produce two sub-sampled and shifted data sets (D–I) and suitably averaging the two resulting phase-reconstructed image sets (E,H).

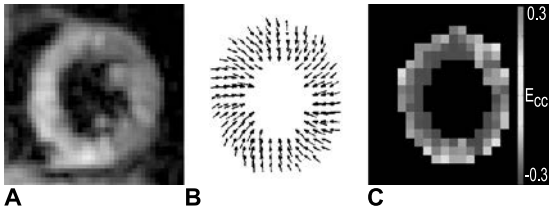

Figure 2. Examples of magnitude-reconstructed (A), displacement (B), and Ecc (C) images of a basal slice from one volunteer at end systole. Both the displacement and Ecc maps illustrate a transmural increase in contractile function from the subepicardium to subendocardium. (*View this art in color at www.dekker.com.*)

The ESDENSE sequence was implemented on a 1.5T scanner (Sonata, Siemens). Short-axis imaging was performed in 5 healthy volunteers (3 slices) using ESDENSE and cine DENSE. Imaging parameters for ESDENSE included: field of view = 340×340 mm^2, acquisition matrix = 192×60, slice thickness = 8 mm, TR = 13.4 ms, flip angle = 15°, bandwidth = 1370 Hz/pixel, echo train length = 10, phase-encoding lines per cardiac phase per cardiac cycle = 30, breath-hold duration = 19 cardiac cycles, and temporal resolution = 40.2 ms. Displacement was encoded in the frequency-encoding direction with 90° RF pulses and a gradient pulse that achieved $k_e = 0.14$ cycles/mm. Displacement was also encoded in the orthogonal direction by swapping the frequency-encoding and phase-encoding axes. Cine DENSE used the same imaging parameters except matrix = 96×60, bandwidth = 1240 Hz/pixel and $k_e = 0.08$ cycles/mm.

The CSPAMM raw data matrix of 192×60 was parsed at $k_x = 0$ (Figure 1C) into two 96×60 matrices as shown in Figure 1F,I. After background phase correction, image sets were sign-adjusted (Figure 1E,H) and averaged. The resulting phase image was then used to compute displacement and strain as previously described (Kim et al., 2003). For each of two encoding

Copyright © Marcel Dekker, Inc. All rights reserved.

ORDER REPRINTS

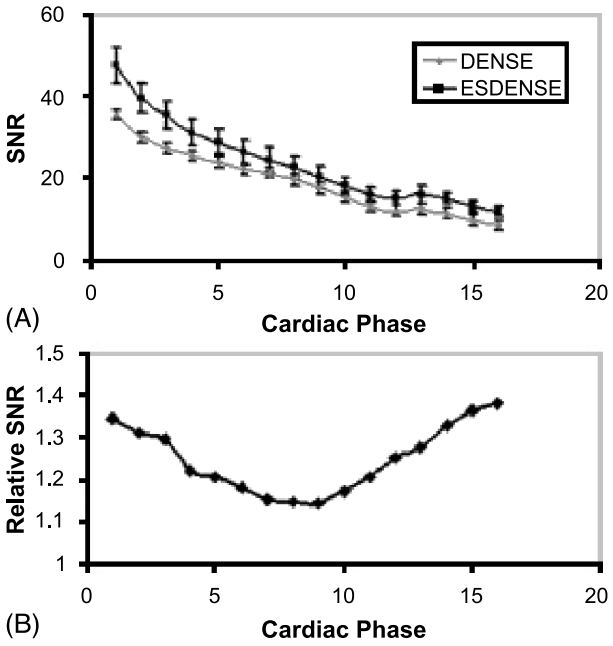

Figure 3. Plots of SNR and relative SNR as a function of cardiac phase. (A) SNR of ESDENSE vs. SNR of cine DENSE. (B) Relative SNR.

directions, the composite magnitude images were constructed as the sum of two sub-sampled magnitude images (Figure 1D,G).

For magnitude images, the SNR was measured over multiple cardiac phases. Relative SNR was calculated as the ratio of $SNR_{ESDENSE}$ and SNR_{DENSE}. Circumferential strain (E_{cc}) was computed for multiple cardiac phases.

Results: In Figure 2, a magnitude image, a vector displacement map, and a E_{cc} map of a basal slice from one volunteer at end systole are shown. ESDENSE produced significantly higher SNR than cine DENSE throughout the cardiac cycle (Figure 3A), from early systole (47.7 ± 2.6 vs. 35.4 ± 4.4; $p<0.01$) to late diastole (11.9 ± 1.2 vs. 8.6 ± 1.3; $p<0.01$). Relative SNR was on the order of 1.34 at early systole and late diastole and showed a uniphasic response with a minimum value of 1.15 at end systole (Figure 3B). Given that ESDENSE used a higher value of k_e than cine DENSE, this uniphasic response as a function of cardiac phase is consistent with previously reported motion-induced signal loss in cardiac STEAM techniques (Fischer et al., 1995).

Conclusions: A new technique was developed to enhance the SNR in DENSE MRI. Future work may include imaging at higher field strengths and with dedicated cardiac coils for further improvements.

REFERENCES

Aletras, A. H., et al. (2001). *MRM* 46:523–534.
Fischer, S. E., et al. (1995). *MRM* 34:80–91.
Kim, D., et al. (2003). *Radiology*in press.
Osman, N. F., et al. (1999). *MRM* 42:1048–1060.

513. Ultra-short Breathhold 3D Coronary Artery Angiography Employing Steady-State Free Precession and Parallel Imaging

Thoralf Niendorf,[1] Manojkumar Saranathan,[1] Anila Lingamneni,[2] Thomas K. Foo,[3] Neil M. Rofsky.[4]
[1]*Applied Science Laboratory, GE Medical Systems, Boston, MA, USA*, [2]*GE Medical Systems, Waukesha, WI, USA*, [3]*Applied Science Laboratory, GE Medical Systems, Boston, MA, USA*, [4]*Beth Israel Deaconess Medical Center, Harvard Medical School, Boston, MA, USA*.

Introduction: Coronary artery magnetic resonance angiography (CMRA) has been proven to be of clinical value for the detection of coronary artery disease but remains technically challenging due to cardiac and respiratory motion (Bunce et al., 2003; Kim et al., 2001).

Purpose: This study is aimed at the development of volume acquisition strategies that offer 1) very short breath-hold times of 10–15 seconds and 2) short acquisition windows, with the goal (a) to minimize the impact of cardiac and respiratory motion and (b) to improve patient compliance. For this purpose an ECG gated 3D SSFP technique was combined with sensitivity encoded parallel imaging.

Methods: CMRA was performed in 15 volunteers using a 1.5T EXCITE whole body system (GE Medical Systems, Waukesha, WI, USA) using 8-element cardiac phased array coils (GE Medical Systems, Waukesha, WI, USA; GORE, Newark, DL, USA). A gradient echo sequence was used to determine coil sensitivity maps. A 3D SSFP sequence was implemented with an interpolated spatial resolution of $(0.6 \times 0.6 \times 0.5)$ mm^3. An acceleration factor of 2–4 was applied for parallel imaging using two different acquisition schemes:

(i) 1 R–R interval approach: Data acquisition is completed in a single heartbeat for each slice partition. For 12 slice partitions, the total scan time is 12 R–R intervals instead of 24 used in the

Copyright © Marcel Dekker, Inc. All rights reserved.

ORDER REPRINTS

non-accelerated version, resulting in ultra short breath-hold periods.

(ii) 2 R–R interval approach: Data acquisition for each slice partition is distributed over 2 consecutive cardiac cycles. The acquisition window length is reduced by the acceleration factor for each R–R interval. This shortens the acquisition window so that it fits into the middiastolic cardiac rest period even for high heart rates. The total scan time corresponds to 24 R–R intervals and is not prolonged compared to the non-accelerated case.

The accelerated acquisition strategies were compared with a conventional, non-accelerated approach, which employed variable sampling in time (VAST) segmentation (Foo et al., 2002). No contrast media were administered.

Results: High signal-to-noise ratio (SNR≈30) was obtained for both acquisition strategies when using an acceleration factor of 2. With the 1R–R interval strategy, image quality (vessel definition) was substantially improved compared to the conventional approach (Figure 1a,b). The 1 R–R interval scheme halves the breath-hold time (10 sec for a heart rate of 60 bpm) leading to a reduction in the blurring artifacts (Figure 1b), which are associated with the diaphragmatic drift encountered during prolonged breath-holds. No extra cardiac motion related blurring was introduced since the acquisition window length was identical to that used in the non-accelerated approach due to the decimation of phase encoding steps. At high heart rates the application of the 2 R–R interval scheme eliminated the need to shift the acquisition window towards systole in order to complete the acquisition before the next QRS complex occurs. The shortening of the acquisition window fosters the reduction of cardiac motion artifacts compared to the non-accelerated approach (Figure 2), especially for the right coronary artery because of its more extreme extent of displacement.

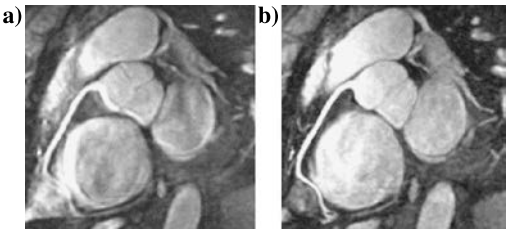

Figure 1. RCA images (MIP) derived from a healthy volunteer using the conventional sampling scheme leading to a breath-hold time of 25 sec (left) and the 1 R–R interval parallel imaging approach resulting in a breath-hold time of only 12 sec (right). The heart rate was 55 bpm. Note the substantial improvement in delineation of the RCA at the region of genu achieved with the 1 R–R interval parallel imaging approach (b).

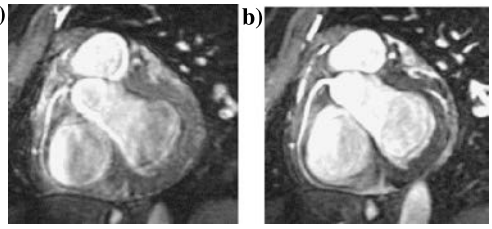

Figure 2. Comparison of RCA images (MIP, slice thickness = 3 mm) obtained from a healthy volunteer exhibiting a heart rate = 80 bpm and a mid-diastolic cardiac rest period of 90 ms. For the left image the VAST sampling scheme was applied, while the 2 R–R interval approach was used for the right image.

Conclusions: It has been demonstrated that the proposed 3D acquisition strategies result in coronary artery images of high quality. The 1 R–R interval approach is especially applicable at low heart rates, leading to short breath-hold times, which improve image quality and patient comfort. The 2 R–R interval approach is tailored for high heart rates. The application of 3D SSFP combined with parallel imaging permits to image the major coronary artery distributions in 2–3–4 breath-holds. The substantial scan time reduction compared to free-breathing techniques offers the potential to integrate CMRA into a comprehensive cardiac examination for the detection of ischemic or congenital heart disease.

REFERENCES

Bunce, N. H., et al. (2003). *Radiology* 227:201–208.
Foo, T., et al. (2002). *Proc. ISMRM* 1642.
Kim, W. Y., et al. (2001). *N. Engl. J. Med.* 345:1863–1869.

514. The Impact of High Field (3 Tesla) Imaging on Myocardial Tagging by MRI

Uma Valeti,[1] Donald D. Potter, M.D.,[2] Philip A. Araoz, M.D.,[3] Kiaran P. McGee, Ph.D.,[3] James F. Glockner, M.D.,[3] Timothy F. Christian, M.D.[1] [1]*Cardiology, Mayo Clinic, Rochester, MN, USA*, [2]*Surgery, Mayo Clinic,*

Copyright © Marcel Dekker, Inc. All rights reserved.

ORDER REPRINTS

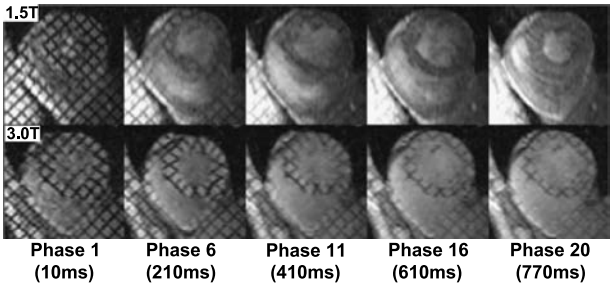

Figure 1.

Rochester, MN, USA, [3]*Radiology, Mayo Clinic, Rochester, MN, USA*.

Introduction: MRI can measure multiphase myocardial strain at high resolution but such algorithms are heavily dependent on the contrast between the tag lines and the myocardium (TMC). Clinical strain measurements have been limited by the short persistence of tag lines during the cardiac cycle from T1 recovery.

Purpose: To determine whether imaging at 3T can improve and prolong the TMC compared to images acquired at 1.5T.

Methods: 13 normal volunteers were scanned at 1.5T (GE signa, CV/i) and 3T (GE VH/i) with field specific surface coils. A gradient echo sequence with modulated magnetization was used for tagging during a multislice 20 phase cine acquisition. TMC was determined by the ratio of mean signal intensity (SI) of tagline to mean SI of myocardium (1.0 = no contrast). Matched apical, mid, basal short-axis and long-axis slices were analyzed.

Results: There was no change in heart rate between exams (65±11 for both) The average TMC over the cardiac cycle was superior (lower ratio) at 3T compared to 1.5T for all slices (0.60±0.15 vs. 0.74±0.17, $p<0.0001$). This difference remained significant at cycle initiation (0.36±0.06 vs. 0.43±0.10, $p=0.03$), endsystole (0.60±0.05 vs. 0.74±0.07, $p<0.0001$) and end R–R interval (0.76±0.08 vs. 0.91±0.06, $p<0.0001$). Tags at 1.5T had <25% contrast relative to the myocardium by phase 8 whereas that threshold was not reached till phase 19 at 3T (Figure 1).

Conclusions: Imaging at 3T significantly improves and prolongs TMC with excellent visualization throughout the cardiac cycle. This is likely due to the higher myocardial SI at 3T. This technique may produce improved strain analysis through the entire cardiac cycle by better enabling tag detection algorithms.

515. Intracoronary Injection of Bone Marrow Cells Labelled with Supraparamagnetic Iron Oxide Particles. In-vivo and ex-vivo Imaging Results

Robert J. M. van Geuns, M.D.,[1] Ewoud J. van den Bos, M.D.,[1] Zhuoli Zhang, Ph.D.,[2] Amber Moelker,[1] Piotr A. Wielopolski, Ph.D.[2] [1]*Cardiology, Erasmus MC, Rotterdam, Netherlands*, [2]*Radiology, Erasmus MC, Rotterdam, Netherlands*.

Introduction: Cellular transplants of myoblasts or bone marrow cells are a potential treatment for myocardial dysfunction. Close monitoring is crucial during development of this therapy. Labelling of myoblasts with FDA approved superparamagnetic iron oxide particles has been used for visualisation of local myocardial injections. Intracoronary injection of cell transplants could improve the delivery and distribution of the cells to the infarct area and may be preferable to local injections. Visualisation of these distributed cells requires a high-resolution imaging.

Purpose: To evaluate the possibilities to track intracoronary injected iron oxide labeled cells.

Methods: Pig bone marrow cells were labeled with superparamagnetic iron oxide particals by uptake of iron oxide incorporated into cationic transfection liposomes. The iron oxide–liposome complexes were made as follows: 30 µl of Lipofectamine 2000 (Gibco) was diluted in 0.5 ml of Opti-MEM reduced serum medium (Gibco). Separately, iron oxide was diluted in a concentration of 100 µg total iron, in 0.5 ml of Opti-MEM. After 5 minutes the suspensions were combined and gently mixed by pipetting. After 20 minutes the complexes containing the iron oxide–liposome complex were added drop wise to the dishes.

In seven Pigs (weight 20–25 kg) a myocardial infarct was created by a balloon occlusion of the left circumflex coronary artery of 2 hours followed by reperfusion. After 1 week MRI imaging was performed on a GE 1.5T Signa CVi scanner (General Electric Medical Systems, Milwaukee, USA) with the standard clinical imaging gradient set (40 mT/m and SR150) and a small phased array torso coil with cine FIESTA, delayed contrast enhanced inversion recovery GE sequence and a T2* weighted gradient echo sequence. Shortly after MRI imaging the labeled bone marrow cells where injected in the circumflex coronary artery in one pig, in two pigs non-labeled cells were injected. In the remaining four pigs only medium was injected. After four weeks the imaging protocol was repeated.

After the last imaging session, the pig was taken to the animal facility and prior to excising its heart, a 0.1

Copyright © Marcel Dekker, Inc. All rights reserved.

ORDER REPRINTS

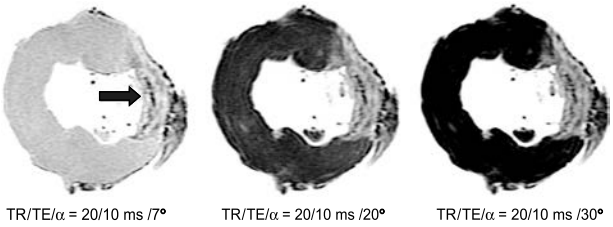

Figure 1. (*View this art in color at www.dekker.com.*)

mmol/kg of Gd-DTPA was again injected and the animal was sacrificed. The heart was extracted from the chest and immediately placed in a special container with frozen walls (approximately 1 cm thick) with cold saline doped with Gd-DTPA to enhance image contrast. A set of 3D SPGR sequences were performed on the excised heart with three different flip angles (10°, 20° and 30°, proton density for cell tracking to heavy T1-weighting to visualize the infarcted region) covering the entire heart.

Results: Contrast enhanced IR-GE imaging demonstrated the infarct area clearly. A central dark zone was detected in all pigs at baseline. T2* weighted imaging at 1 week after the infarct demonstrated low signal intensities in the infarct area in all seven pigs which were still present on the in-vivo images at 4 weeks. At microscopy only five of the seven pigs demonstrated haemosiderine deposits in the infarct regions which could explain the low signal intensity spots in the T2* weighted images. In the other two pigs only collagen structures where recognized during microscopy. In the single pig injected with labelled bone marrow cells, in-vivo and ex-vivo T2* imaging demonstrated spots of signal loss without haemorrhage at microscopy but which corresponds with iron particles (Figure 1). Unfortunately these images where comparable with the images of the non-labeled cell and medium injections.

Conclusions: High-resolution in-vivo and ex-vivo T2* weighted images of myocardial infarction demonstrate large amounts of low signal intensity spots where small amounts of iron oxide labelled cells can not be recognized.

516. MnDPDP Myocardial Uptake as a Metabolic Marker of Viability. An MRI Study in Patients with Chronic Myocardial Infarction

Massimo Lombardi, M.D., Brunella Favilli, Ms.C. *MRI Laboratory, CNR, Clinical Physiology Institute, Pisa, Italy*.

Introduction: in animal studies MnDPDP has been shown to evaluate myocardial viability in SE T1 images. However, due to the low sensitivity of these images an unacceptable high dosage of MnDPDP is required to achieve this goal.

Purposes: of the present study were: 1) to evaluate MnDPDP myocardial uptake in human beings using a inversion prepared GRE sequence; 2) to follow the pharmacokinetic behaviour of MnDPDP within the myocardium.

Methods: MnDPDP was intravenously injected (0.01 mmol/Kg) in 6 patients with previous (>24 weeks) transmural myocardial infarction as assessed by clinical history, ECG and Echocardiographic findings. MRI studies were performed using a 1.5T scanner (CVi, GE, Milwaukee, USA) equipped with 40 mT gradients and a 4 channels phased array surface coil. MR images in three short axis of the heart (positioned at 25, 50 and 75% of longitudinal left ventricle axis) were obtained using an ECG gated, inversion prepared GRE sequence (TE 3.2 a TR depending from heart rate, slice thickness of 10 mm). Inversion Time was individually optimised using a real time approach. Images were obtained at baseline, 30 min, 240 min, 1440 min after MnDPDP injection. An external reference (animal muscle tissue) was used to normalize signal intensity measured within myocardial profile on each image. Echocardiography was used to define myocardial segments as normal when a normal contractility pattern was detected while the presence of akinesia in two contiguous segments was considered a marker of necrosis. A 12 segmentation model was adopted both for echocardiography and MR images.

Results: 23 out of a total of 72 segments were classified as necrotic. After MnDPDP injection, signal increment resulted: 122%, 248% and 309% in normal tissue vs. 88%, 198%, 208% in necrotic tissue at 30 min ($p = 0.04$), 240 min ($p = 0.01$) and 1440 min ($p = 0.02$) respectively. The most significant increment was detected at 240 min ($p = 0.01$). Inversion time raged between 230 and 300 msec.

Conclusions: MnDPDP uptake resulted significantly different between normal and necrotic tissue. In this study a progressive uptake of MnDPDP was detected during the 24 hours of monitoring. A clear significant difference between baseline and contrast enhanced values was evident since 240 min after contrast administration.

Copyright © Marcel Dekker, Inc. All rights reserved.

ORDER REPRINTS

517. Time-Resolved Volume Rendering for Diagnosis and Evaluation of Dynamic Cardiac Disorders

Marijn E. Brummer, Ph.D.,[1] W. James Parks, M.D.,[2] Grégory Quillard, M.S.,[1] Marie-Laure Piednoir, B.S.,[3] Cécile Marboeuf, M.S.,[4] Charles B. Kitchen, B.S.,[1] Denver Sallee, III, M.D.,[2] Kirk R. Kanter, M.D.,[2] Melinda Dobbs, R.N.[2] [1]*Radiology, Emory University, Atlanta, GA, USA*, [2]*Children's Heart Center, Children's Healthcare of Atlanta, Atlanta, GA, USA*, [3]*Electrical Engineering, Georgia Institute of Technology, Atlanta, GA, USA*, [4]*Supelec, Rennes, France*.

Introduction: Animated cyclic ciné display of time-resolved cardiac MRI is common practice for evaluation of ventricular function and other dynamic parameters in the heart.Volume rendering methods have not been widely used for dynamic display. Performance constraints in hardware and software for volume rendering, as well as limitations in attainable 3-D resolution in cine MRI formed important obstacles. Recent advances in hardware-accelerated volume rendering technology, along with the recent introduction of high-signal, high-speed, steady-state free precession (SSFP) methods for cine acquisition, provide reason to reconsider the use of dynamic volume rendering in cardiac MRI.

Purpose: The purpose of this study is to evaluate dynamic volume rendering as a display technology for certain classes of pediatric heart disorders. The focus of this investigation centered on congenital heart disorders involving right and left ventricular outflow tract obstructions, for which complete characterization involves assessment of the dynamics of structure and blood flow.

Methods: Multi-slice SSFP ciné image stacks were acquired at one or more stack orientations using the FIESTA protocol on a GE Signa TwinSpeed 1.5T imager for evaluation of LVOT and RVOT disorders in pediatric patients, with as typical scan parameters: 8–18 slices spaced 6–11 mm contiguously to cover anatomy of interest, with TR = 3.2 ms, TE = 1.4 ms, and 45 degree flip angle. DICOM images were transferred to a SGI Fuel workstation which has integrated acceleration hardware for volume rendering. Visualizations were performed by a modified version of the ''HeartViz'' software, developed in-house for advanced CMRI viewing. Dynamic volume rendering functionality was implemented using extensions of OpenInventor software (Template Graphics, San Diego, CA) by timed cycling though volume models of each cardiac phase. Volume cropping and image segmentation were performed semi-automatically using intensity thresholding methods, augmented by morphological image processing and manual region editing.

Evaluation of 13 patients following right ventricular outflow tract obstruction (RVOTO) repair was augmented with volume rendering visualization; Tetralogy of Fallot (TOF) (n = 8), TOF with pulmonary atresia (n = 1), TOF with absent pulmonary valve syndrome (n = 1), pulmonary atresia with intact septum (n = 1), valvular pulmonary stenosis (n = 2). BSA = 0.69–2.18 m2, median = 1.37 m2, mean = 1.30 m2, Age Range = 5–39 yr, mean age 20 yr.

Results: We were able to visualize residual RVOTO and residual tissue in the RVOT spared at repair. Patency of the outflow tract, regurgitation and thickened valve leaflets, used in surgical repair, could be seen as well. Gross evaluation of ventricular function and paradoxic septal motion were also illustrated as was significant pulmonary or aortic regurgitation. Branch pulmonary artery obstruction was also shown when present as was aortic root and branch pulmonary artery dilatation.

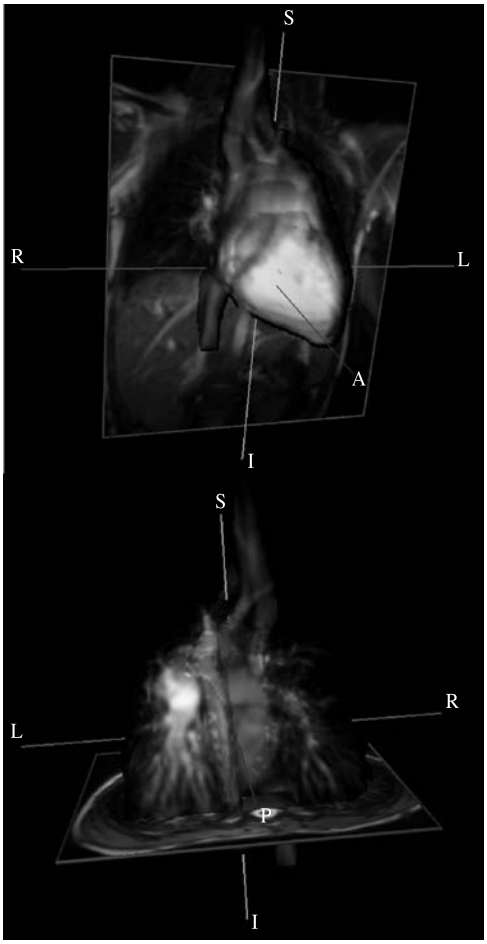

Conclusions: Initial experience with use of time-resolved volume rendering of bright-blood SSFP appears to be helpful in observing dynamic processes

Copyright © Marcel Dekker, Inc. All rights reserved.

ORDER REPRINTS

that are not fully visualized in slice views. Improved visualization of valvular motion and of ventricular and septal dynamics was obtained. Current bright-blood SSFP acquisitions with thin slices appear to provide adequate volume data for visualization of obstructive heart disease post repair.

518. A Comparison of Hybrid EPI with FLASH for Stress Myocardial Perfusion Cardiovascular Magnetic Resonance

Andrew G. Elkington, M.R.C.P., Timothy M. Cannell, Peter D. Gatehouse, Ph.D., Sanjay K. Prasad, M.D. M.R.C.P., David N. Firmin, Ph.D., Dudley J. Pennell, M.D. F.R.C.P. *CMR Unit, Royal Brompton and Harefield NHS Trust, London, United Kingdom.*

Introduction: The optimal sequence and technique for myocardial perfusion cardiovascular magnetic resonance (CMR) are still being determined. The majority of perfusion CMR work has been with FLASH sequences. A hybrid EPI sequence offers potential advantages, including improved contrast to noise ratio (CNR), spatial and temporal resolution.

Aim: To compare hybrid EPI with FLASH stress myocardial perfusion CMR in patients with coronary artery disease.

Methods: 15 patients with known coronary artery disease were studied (Siemens Sonata, 1.5T). The study was approved by the local ethics committee, and each subject gave written, informed consent. On seperate days, each subject underwent perfusion CMR studies by hybrid EPI (FoV read 340–400 mm, FoV phase 75–87.5%, base resolution 128–160, phase resolution 75–100%, flip angle 30°, EPI factor 4, saturation recovery time to centre of k space 60–100 ms,image time 110–196 ms, slice thickness 8 mm) and FLASH (FoV read 340–400 mm, FoV phase 68.8%, base resolution 128, phase resolution 94%, flip angle 8°, saturation recovery time to centre of k space 90 ms, image time 173 ms, slice thickness 8 mm). FoV was varied to avoid wrap-around into the myocardium. A rest and stress (adenosine 140 micrograms/kg/min infused for 4 minutes) study was performed in each subject, with both sequences (Magnevist, 0.1 mmol/kg for each bolus injected at 7 ml/s, 10 ml normal saline flush using Medrad power injector). For each study at least 3 short axis (SA) slices were acquired each cardiac cycle. A region of interest (ROI) was drawn in each wall of the myocardium (anterior, lateral, inferior and septum) of a mid-ventricular SA slice at rest and stress by a blinded researcher. The CNR in each region was calculated by dividing the signal increase from baseline to peak in the myocardium by the temporal standard deviation (SD) of the signal in the myocardium pre-contrast enhancement.

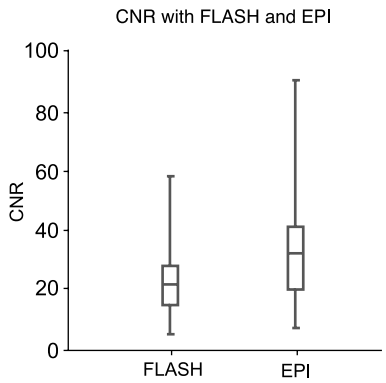

Figure 1. The box plot indicates the 25th and 75th percentile. The whiskers indicates the maximum and minimum. The line in box plot indicates the median. The mean value for FLASH was 23 and the mean value for EPI was 33 ($P<0.001$). (*View this art in color at www.dekker.com.*)

Results and Discussion: The myocardial CNR was significantly higher using the hybrid EPI sequence ($P<0.001$). The mean CNR was 67% greater with hybrid EPI than with FLASH. Furthermore, the spatio-temporal resolution was superior with the hybrid EPI sequence. For similiar spatial resolution (EPI 2.7×3.6 mm to 3.1×4.1 mm adapted to patient size; FLASH 2.7×2.9 mm to 3.1×3.3 mm) the hybrid EPI had superior temporal resolution (110 ms for each image acquired) to that with FLASH (173 ms for each image acquired). Alternatively, when the sequences had similiar temporal resolution (EPI 196 ms; FLASH 173 ms) the hybrid EPI had superior spatial resolution (EPI 2.1×2.1 mm to 2.5×2.5 mm; FLASH 2.7×2.9 mm to 3.1×3.3 mm). The saturation recovery times of the sequences varied with image duration, but this did not contribute to the higher CNR of the hybrid EPI (Figure 1).

Conclusion: Hybrid EPI has superior CNR and spatio-temporal resolution to FLASH for use in myocardial perfusion CMR.

519. Stereotactic Real-Time Guidance for Anatomic Radiofrequency Ablation Using Three-Dimensional MRI

Timm Dickfeld, Hugh Calkins, Menekhem Zviman, Glenn Meininger, Ariel Roguin, Krystl Frank, Ron Berger, Henry Halperin, Stephen Solomon. *Johns Hopkins University, Baltimore, MD, USA.*

Copyright © Marcel Dekker, Inc. All rights reserved.

ORDER REPRINTS

Background: Targets for radiofrequency ablation (RFA) of atrial fibrillation, atrial flutter, and non-idiopathic ventricular tachycardia (VT) are increasingly being selected based on anatomic considerations. Because fluoroscopy provides only limited information about the relationship between catheter positions and cardiac structures, and is associated with radiation risk, other approaches to mapping may be beneficial.

Methods: To evaluate true anatomical catheter guidance, three dimensional (3D) Magnetic Resonance (MR) images were superimposed on an electromagnetic catheter positioning system using fiducial markers. This allowed the dynamic display of the catheter position on previously acquired MRI in real time. Position error during catheter navigation was determined in a phantom model and during left and right heart catheterization of domestic swine (n = 7). To assess the reproducibility of RFA repeated ablations were performed at the same anatomic site in the RA (n = 8). Straight three point lines were created in the RV and LV to assess the ability to facilitate complex ablation procedures (n = 6).

Results: Display of the catheter position in real-time on the MRI allowed targeted catheter navigation without the use of fluoroscopy. In vitro-accuracy and precision were (mean ± SEM) 1.11 ± 0.06 mm and 0.30 ± 0.07 mm and in vivo-accuracy and precision were 2.74 ± 0.52 mm and 1.97 ± 0.44 mm, respectively. Average distance of the repeated RA ablations was 3.92 ± 0.5 mm. The ventricular three point lesions deviated 1.70 ± 0.24 mm from a straight line and point distance differed by 2.25 ± 0.63 mm from the pathological specimen.

Conclusion: Real-time display of the catheter position on 3D-MRI allows accurate and precise RFA guided by the true anatomy. This may facilitate anatomically based ablation procedures in e.g. atrial fibrillation or non-idiopathic VT and decrease radiation times.

520. Monoexponential Fit of Washout in Myocardial Perfusion Curve After Myocardial Infarction. Correlation with the Transmural Extent of the Delayed Hyperenhancement

Alexandre Comte, M.Sc.,[1] Alain Lalande, Ph.D.,[1] Alexandre Cochet, M.D.,[1] Claude Touzery, Ph.D.,[1] Paul M. Walker, Ph.D.,[1] Yves Cottin, M.D.,[2] Jean Eric Wolf, M.D.,[2] François Brunotte, M.D.[1] [1]*Laboratoire de Biophysique, Faculté de Médecine, Dijon, France*, [2]*Service de Cardiologie II, CHU de Dijon, Dijon, France*.

Introduction: Magnetic resonance first-pass imaging of a bolus of contrast agent is well adapted to distinguish normal and hypoperfused areas of the myocardium. In most cases, the signal intensity–time curves in user defined regions of interest are studied. Several parameters can be extracted from these curves. Widely used indices are the maximum signal intensity and the curve up-slope. By contrast the washout has not been extensively studied.

Purpose: The purpose of this study was to analyse the relationship between the washout of the first-pass MR perfusion curves and the delayed contrast-enhancement. Curves were obtained in patients studied early after a reperfused myocardial infarction. The acquisition time was approximatively 8 minutes, allowing a satisfactory monoexponential fit of the washout. Since delayed hyperenhancement probably reflects modifications of the tracer kinetic, the aim of the present study was to analyse the relationship between the washout and the delayed hyperenhancement.

Methods: Nine patients were included. All had a recent myocardial infarction less than 10 days before the MRI examination. Myocardial function was studied in three short-axis slices by FLASH 2D cine-MRI. Perfusion curves were obtained in the same three short-axis slices using a multi-slice inversion recovery turbo-FLASH sequence during the intra-venous bolus injection of Gd-DTPA. The images were acquired every two cardiac cycles, providing a perfusion acquisition time of about 8 minutes. In each slice, the myocardium was divided into eight segments. Finally, 216 curves were obtained. Each curve was a set of 60 points. In normally perfused segments, curves depict a rapid upslope reaching a peak followed by a decline (washout). Usually, the washout covers a time of about 5 minutes which is long enough to permit an accurate fit of the washout. For normal curves with a well-defined first-pass peak, the washout was fitted from this peak to the end of the acquisition. In some cases, the peak was poorly visible and even in case of severe hypoperfusion, may be undetectable. In that case, the fit is started at the same time as for curves acquired in normally perfused myocardial segments of the same patient. The washout of each curve was fitted to the function $f(t) = a*\exp(-\lambda t)$. The subsequent studies used only the parameter λ.

For each myocardial segment, the transmural extent of infarction was visually assessed using a score ranging from 0 to 4.

The wall thickening of each segment was calculated from manually tracings of endocardial and epicardial contours at diastole and systole in cine-MR images and expressed in millimetres.

The mean value of λ was calculated in each of the 5 groups defined by the transmural score. These groups were compared using an ANOVA. Additionally, a

Copyright © Marcel Dekker, Inc. All rights reserved.

ORDER REPRINTS

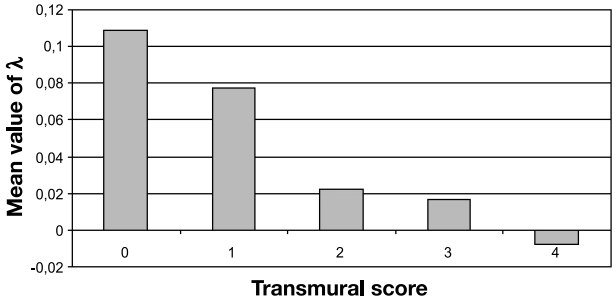

Figure 1. Mean value of λ versus the transmural score of delayed hyperenhancement. (*View this art in color at www.dekker.com.*)

linear regression between the parameter ? and the wall thickening was performed.

Results: The mean value of λ differed significantly ($p<10^{-9}$) according to the transmural extent of the delayed hyperenhancement (see Figure 1). The parameter λ correlated also significantly ($p<10^{-3}$) with the wall thickening.

Conclusions: Washout of myocardial perfusion curves appears to be correlated to the transmural extent of the myocardial infarction and to the wall thickening. The parameter ? is easy to calculate and does not rely on visual analysis. Moreover, the present approach is independent on the maximum intensity of the curve and the risk of error due to a possible local heterogeneity of the phased-array coil is minimized. This approach permits to quantitatively assess the severity of the myocardial infarction. Further studies are needed to determine the value of this approach in myocardial viability assessment.

521. Steady-State Free Precession CINE MR: Influence of Different Reconstruction Algorithms on Image Quality

Kai-Uwe Waltering,[1] Peter Hunold,[1] Oliver Bruder,[2] Thomas Schlosser,[1] Markus Jochims,[2] Jörg Barkhausen.[1] [1]*Radiology, University Hospital Essen, Essen, Germany*, [2]*Cardiology, Elisabeth Hospital Essen, Essen, Germany*.

Introduction: Steady state free precession (SSFP) Cine MRI provides images with high spatial and temporal resolution and must be considered as the standard of reference for the assessment of ventricular volumes and ejection fraction. To compensate for cardiac motion two different techniques are currently available: prospective ECG-triggering and retrospective ECG-gating.

Purpose: The aim of this study was to assess the image quality of a recently developed triggered–retrogated (Tretro) data acquisition scheme combining the advantages of both modalities in comparison to the standard prospective triggering technique.

Methods: 81 patients (60 male, 21 female, mean age 61.9±36.1 years) referred to cardiac MRI were included into this study. 10 patients were suffering from atrial fibrillation, 9 patients had frequent extrasystoles and 62 patients had sinus rhythm. All examinations were performed on a 1.5 T scanner (Magnetom Sonata, Siemens). In all patients long axis Cine-loops were measured three times with a SSFP sequence (TR 2.8 ms, TE 1.4 ms, FA = 60°, pixel size 1.9 mm × 1.7 mm, temporal resolution 43 ms) using different reconstruction algorithms in random order: 1) prospective triggering, 2) the triggered–retrogated (Tretro) and 3) a modified triggered–retrogated sequence which allows for arrhythmia rejection (Tretro-mod). Image quality was assessed based on a 5-point Likert scale ranging from 1 = excellent, 2 = good, 3 = equivocal, 4 = poor to 5 = non-diagnostic. Additionally signal to noise (SNR) and contrast to noise (CNR) measurements were performed.

Results: The average acquisition time of all studies was 10.0±2.1 s for standard SSFP sequences, 10.9±6.2 s for Tretro and longest 11.5±4.7 s for Tretro-mod sequences. The mean image quality score of all patients showed no significant differences (standard SSFP 2.6±0.9; Tretro 2.4±0.9; Tretro-mod 2.3±0.8; $p<0.05$). However, in case of arrhythmia the mean image quality score was significantly higher for the modified Tretro sequence 2.8±0.8 versus 3.2±0.9 for Tretro and 3.7±0.9 for the standard sequence ($p<0.05$). SNR and CNR measurements showed no significant differences ($p<0.01$). Figure 1 shows a 4-chamber view in a patient with arrhythmia performed using prospectively triggering (a), Tretro- (b) and the modified Tretro sequence (c). The Tretro sequence with arrhythmia rejection (c) shows the best image quality.

Conclusions: The recently developed Tretro-SSFP imaging technique combining prospective triggering

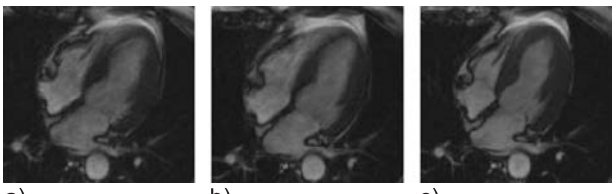

Figure 1.

Copyright © Marcel Dekker, Inc. All rights reserved.

ORDER REPRINTS

and retrospective gating offers important advantages compared to prospectively triggered sequences. In patients with sinus rhythm the acquisition window has not be adapted to the patients heart rate prior to imaging. Due to the retrospective gating the sequences covers the entire cardiac cycle, including the late diastole, typically missed by prospective triggering. Artifacts and blurring caused by arrhythmia can be reduced, resulting in better image quality in patients with atrial fibrillation and frequent extrasystoles. In conclusion the triggered–retrogated SSFP Cine MRI technique improves the workflow and image quality especially in patients with extrasystoles or arrhythmia.

522. Automatic Planning of Short-Axis MRI Acquisition: Prospective Validation Study

Mikhail Danilouchkine, Ph.D., Jos Westenberg, Ph.D., Hildo Lamb, Ph.D., Johan Reiber, Ph.D., Boudwijn Lelieveldt, Ph.D. *Radiology, Leiden University Medical Center, Leiden, Netherlands.*

Introduction: The complexity of cardiac MRI planning requires the use of well-defined acquisition protocols and solid understanding of the intrinsically complicated human heart anatomy. Conventionally a series of preliminary acquisitions (i.e. scout, two and four-chamber views) are obtained to devise the optimal imaging planes for the short-axis acquisitions. Manual cardiac planning still remains a challenging job even for experienced operators.

To ease the work of operators we developed a novel system for fully automatic planning of short-axis cardiac acquisitions. Our approach is based upon the three-dimensional geometric model of human thoracic cavity. This model comprises a number of analytical templates of the thoracic organs combined together into a tree-like structure. The latter preserves the realistic topology of the human thoracic cavity.

This model is used to automatically devise the spatial orientation of the short-axis imaging planes. Once the boundaries of the organs included in the model are extracted and aligned with the model, the short-axis imaging planes can be deduced.

Purpose: In this prospective validation study we evaluated the clinical feasibility of automatic planning of short-axis MRI acquisitions.

Method: Twelve healthy volunteers underwent cardiac MRI on a Philips 1.5T Intera MRI system. Four series of left ventricular short-axis slices were acquired using the Balanced-FFE protocol during breath-holding. Manual planning of the short-axis acquisition were done twice by one observer and once by another observer. The forth series was prospectively devised in an automatic manner. The scout images were transported to a remote workstation via the DICOM protocol and were analyzed by our software package. The proposed orientations and angulations were manually entered on the operators' console of the MRI scanner. The automatically devised short-axis stack was projected onto two- and four-chamber views and visually assessed by two independent observers. The angular deviations of the imaging planes in the last three series with respect to the first one numerically augments the observer's visual evaluation (Figure 1).

Endocardial and epicardial contours were manually outlined in all four series for end-systolic and end-diastolic phases using MASS (MR analytical software,

Table 1. Mean and standard deviation of the left ventricular axis angular deviation.

	Inter-observer	Intra-observer	Manual vs. auto
Angular deviation	2.67 ± 1.49	4.06 ± 1.79	10.50 ± 5.45

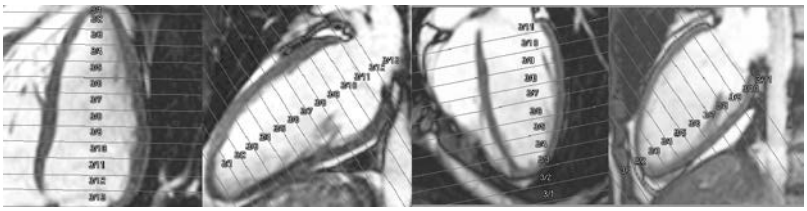

Figure 1. Projection of automatically planned short-axis imaging planes onto 2- and 4- chamber views for successful planning (left) and slightly angulated stack (right). (*View this art in color at www.dekker.com.*)

Copyright © Marcel Dekker, Inc. All rights reserved.

ORDER REPRINTS

Table 2. Pearson's correlation coefficients for different quantitative parameters.

	Inter-observer	Intra-observer	Manual vs. auto
LV EDV	0.99	0.99	0.97
LV ESV	0.96	0.97	0.93
EF	0.92	0.96	0.92
LVM ED	0.95	0.96	0.92
LVM ES	0.97	0.93	0.96

MEDIS, Leiden). The quantitative parameters left ventricular end-diastolic (LV EDV) and end-systolic (LV ESV) volumes, ejection fraction (EJ), left ventricular mass at end-diastolic (LV EDM) and end-systolic (LV ESM) phases were also computed by MASS software. To assess the clinical feasibility of the automatic planning we regarded the quantitative parameters obtained for the first series as a golden standard. The parameters from the other series were compared to the golden standard and the Pearson's correlation coefficients were derived.

Results: Approximately in half of the cases the observers agreed that the automatically planned short-axis acquisitions required no manual corrections. In the rest of the cases the proposed orientation of the imaging planes was slightly angulated with respect to the left ventricular axis results in a larger degree of angular deviation from the left ventricular axis (Table 1). Table 2 shows a high degree of correlation between the quantitative parameters (>90%). Pearson's coefficients revealed no statistically significant differences between these parameters (p-value 0.01 for the hypothesis supporting the absence of correlation).

Conclusions: The presented study demonstrates that the automatic planning of short-axis cardiac acquisition can be used in the clinical practice. Although the automatically devised acquisitions tend to be slightly angulated with respect to the left ventricular axis, this does not affect the quantitative assessment of the cardiac functions.

523. Estimation of Myocardial Stiffness from Tagged MRI Using Finite Element Modeling: Validation of Methods and Apparatus

Kevin F. Augenstein, B.E.,[1] Brett R. Cowan, Mb.C.Hb.,[2] Ian J. LeGrice, Ph.D.,[3] Poul M. F. Nielsen, Ph.D.,[1] Alistair A. Young, Ph.D.[4] [1]*Bioengineering Institute, University of Auckland, Auckland, New Zealand*, [2]*Department of Medicine, University of Auckland, Auckland, New Zealand*, [3]*Department of Physiology, University of Auckland, Auckland, New Zealand*, [4]*Department of Anatomy with Radiology, University of Auckland, Auckland, New Zealand*.

Introduction: The stiffness or compliance of soft tissue organ components can substantially influence their function, and alterations to tissue material properties are often indicative of disease processes. One major area of interest is diastolic dysfunction of the heart, which is commonly observed in heart failure patients and may occur before measurable evidence of systolic dysfunction. In order to non-invasively estimate material properties of the heart in vivo, we must first determine the extent to which material properties can be estimated in the case where precise knowledge of the applied boundary conditions is available.

Purpose: Firstly, to validate a method for the estimation of myocardial material properties from tagged MR images, using controlled inflation of a silicon gel phantom. Secondly, to demonstrate the utility of the experimental apparatus to perform controlled inflation experiments on isolated arrested hearts.

Methods: Actuator and Recording Apparatus—A reciprocating pump was built to inflate the heart cyclically with physiological saline. The piston was driven via lead screw by a stepper motor and driver, controlled by a microprocessor, allowing generation of near-arbitrary pulse sequences and movement profiles. A diaphragm pressure transducer recorded the pressure in the ventricle, using a fluid filled catheter. Imaging—A potassium arrested isolated pig heart was tested, together with a silicon gel (Sylgard 527, Dow Corning) deformable phantom cast in the shape of a cylindrical annulus. MR imaging was performed using a standard 1.5 Tesla clinical MRI scanner (Vision, Siemens). Tagged cine images were acquired in short and long axis orientations to calculate 3D deformation. Phase contrast flow images were acquired at the level of the mitral inlet to calculate stroke volume. Diffusion tensor imaging was performed to characterize heart tissue microstructure. Finite Elasticity and the Finite Element Method—The motions and stresses within a deformable object can be found using the finite element (FE) method to solve the equations of motion arising from the theory of finite elasticity. The equations of motion were solved subject to the applied boundary conditions (internal pressure and fixed attachments) using the Galerkin FE method. A sequential quadratic programming optimization technique was used to estimate the

Copyright © Marcel Dekker, Inc. All rights reserved.

ORDER REPRINTS

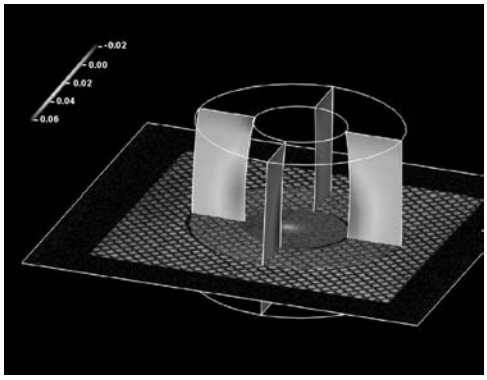

Figure 1. Cylindrical annulus tagged image and FE model. Color map shows circumferential strain. (*View this art in color at www.dekker.com.*)

constitutive parameters from the MR tagged data. The basic estimation algorithm was:

1. Determine the undeformed geometry, and initialise the material parameters.
2. Use the FE model with measured boundary conditions to solve the finite elasticity problem and predict deformed geometry and stress.
3. Compare model deformation with 3D deformation reconstructed from the images.
4. If the error is too large, adjust material parameters and repeat steps 2–3.

Results: A neo-Hookean material was used to model the silicone gel. An independant rotational shear test determined the material parameter to be 8.71 ± 0.06 kPa.

FE parameter estimation required seven iterations to converge and took approximately 2 hours to run on an IBM Regatta using eight Power4 processors. The resulting spatially varying parameters averaged 8.80±0.86 kPa. Figure 1 shows the FE model in relation to the SPAMM tagged images, together with the resulting circumferential strain.

The isolated arrested heart was imaged while undergoing an inflation/deflation cycle of period 1.2 s in which the piston was controlled in a parabolic motion profile with a stoke volume of 16 ml. The resulting pressure–volume relationship showed a non-linear compliance and hysteresis due viscoelastic effects, which are both characteristic of isolated heart experiments.

Conclusion: The apparatus and method developed in this study was capable of accurate estimation of regionally varying material parameters under controlled cyclical deformation conditions. Independent material tests showed that the material parameters estimated were accurate and precise.

524. Accelerated Non-contrast Enhanced 3D Whole Body MRA of the Aorta Using Cardiac Gated SSFP

Thoralf Niendorf,[1] Charles McKenzie,[2] Clint Hamilton,[2] Ivan Pedrosa,[2] Norman Farrar,[2] Harvey Cline,[3] Dennis R. Zuck,[4] James W. Monroe,[4] Neil M. Rofsky.[2]
[1]*Applied Science Laboratory, GE Medical Systems, Boston, MA, USA*, [2]*Beth Israel Deaconess Medical Center, Harvard Medical School, Boston, MA, USA*, [3]*GE Global Research Center, Niskuyana, NY, USA*, [4]*W.L. GORE & Associates Inc., Newark, DE, USA*.

Introduction: MR angiography (MRA) of the large vessels is a common clinical cardiovascular MR application. The conventional first pass approach is based on contrast enhancement using contrast media (Prince et al., 1993). The comparatively short time intervals associated with contrast agents passage require rapid imaging techniques for continuous bolus tracking or appropriate timing for bolus chasing. Common clinical concerns raised by the traditional approach are the 1) dependence on contrast agents and 2) image artifacts associated with cardiac and vessel motion. A non-accelerated 2D gated SSFP evaluation has shown efficacy for dissection and aneurysm of the thoracic aorta, but does not have the reformatting versatility of a 3D sequence.

Purpose: This study examines the clinical feasibility of cardiac gated, breath-hold MRA of the aorta using a non-contrast enhanced, flow independent 3D steady state free precession (SSFP) technique. For this purpose an ECG gated 3D FIESTA technique was implemented. Sensitivity encoded parallel imaging was applied to overcome scan time constraints. A novel coil array, comprised of 10 elements, was employed in order to achieve whole body coverage from the aortic arch down to the bifurcation without the need to reposition the coil or the patient.

Methods: Volunteer studies (N = 8) were conducted on a 1.5 T TwinSpeed system (GE Medical Systems, Waukesha, WI, USA). A 10-element phased array coil (GORE, Newark, DL, USA) was used for large FOV coverage. For parallel imaging coil sensitivity maps were determined using a gradient echo sequence. A prospectively ECG-gated 3D FIESTA sequence was

Copyright © Marcel Dekker, Inc. All rights reserved.

ORDER REPRINTS

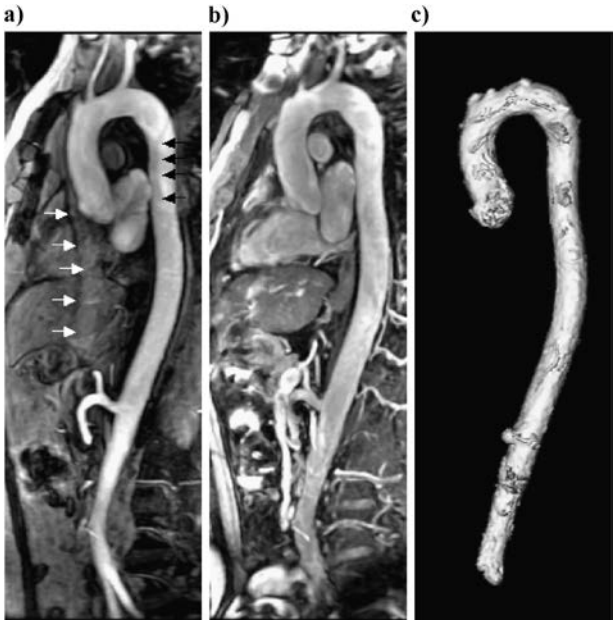

Figure 1. MR angiograms (a,b: maximum intensity projection, c: volume rendering) of the aorta covering an 48 cm FOV along the superior–inferior direction. A standard contrast enhanced gradient echo technique revealed cardiac and aortic motion artefacts as highlighted by the arrows in the left hand image. These artefacts were eliminated by using an ECG-gated non-contrast enhanced 3DFIESTA sequence as shown in the middle image. The right hand image depicts a volume rendered image derived from the 3DFIESTA data set.

developed. Fat saturation was used to enhance the dynamic range. For parallel imaging a net acceleration factor of 2 was applied. An in-plane FOV of (48×48) cm^2 was used to cover a region enclosing the aortic arch and the bifurcation. A 3D multi-oblique volume consisting of 40 slice partitions was prescribed. For each slice partition data acquisition was completed in a single heartbeat leading to a breathhold duration, which is clinically acceptable. The data acquisition window was placed into the mid-diastolic cardiac rest period to minimize the impact of cardiac and aortic motion. No contrast media were administered when using the 3D-FIESTA sequence. For comparison a conventional contrast enhanced 3D gradient echo sequence ($c = 0.2$ mmol/kg body weight) was applied. Surface coil intensity correction was performed.

Results: Large FOV images of the aorta were obtained for both the conventional approach and the new fat saturated, ECG-gated 3D FIESTA technique. The intrinsic contrast and flow independent characteristics of the 3D FIESTA technique yielded angiograms of the aorta with high spatial resolution as illustrated in Figure 1b. For comparison Figure 1a depicts the MRA derived from a contrast enhanced gradient echo acquisition. Cardiac and aortic motion related image artifacts, which occurred in the contrast enhanced non-gated gradient echo images (Figure 1a) are suppressed in the cardiac gated 3D FIESTA images (Figure 1b). While a dependence on appropriate timing of contrast delivery is eliminated, the 3D SSFP technique yields non-selective bright-blood images.

Conclusions: The feasibility of breath-hold, non-contrast, whole body MRA of the aorta using a 3D SSFP technique has been proven in a volunteer study. Motion artefacts are substantially reduced via cardiac gating without exceeding scan time requirements for breath-hold acquisitions. The 3D SSFP preserves versatile reconstruction options while eliminating a reliance on contrast media. The latter has practical, economic and safety implications. In summary, the initial results indicate that 3D FIESTA may provide benefits for clinical whole body aortic MRA applications. We anticipate extending the applications development to patient studies for the detection of aortic pathologies.

REFERENCES

Pereles, F. S., et al. (2002). *Radiology* 223(1):270–274.
Prince, M., et al. (1993). *J. Magn. Reson. Imaging* 3:877–881.

525. Anatomical versus Electrical Axis of the Left Ventricle as Studied by MRI and Standard 12-Lead ECG

Henrik Engblom,[1] Erik Hedstrom,[1] Galen S. Wagner, M.D.,[2] Olle Pahlm, M.D., Ph.D.,[1] Hakan Arheden, M.D, Ph.D.[1] [1]*Clinical Physiology, Lund University Hospital, Lund, Sweden*, [2]*Duke University Medical Center, Durham, NC, USA*.

Background: The traditional assumption has been that there is fairly close relationship between the spatial direction of the anatomical left ventricular long axis (LVLA) and the electrical axis of the heart (the mean QRS axis). Previous studies have shown such a relationship based on post-mortem and plane chest x-ray studies to describe the LVLA spatial direction. MRI enables image acquisition in any arbitrary plane, hence it is possible to make an accurate description of the

Copyright © Marcel Dekker, Inc. All rights reserved.

ORDER REPRINTS

heart orientation in vivo based on direct visualization of cardiac landmarks.

Purpose: Our aim was to test the accuracy of MRI to describe spatial directions and to test the hypothesis that there is a relationship between LVLA spatial direction described by MRI and mean QRS axis in the frontal and transverse plane that could be used to correct ECG for orientation of the heart.

Methods: Sixty-three healthy individuals (31 males, 32 females; age, 21–82 years) with no history of cardiac disease, no ECG abnormalities and blood pressure <140/90 were studied. All subjects had a MR examination and a 12-lead ECG recorded. The LVLA spatial direction was determined by a vector from the center of the mitral ostium through the LV apex in end-diastole using three-dimensional coordinates. The resulting vector was then projected in the frontal and transverse plane for comparison with the mean QRS axis in corresponding planes. The mean QRS vector was determined by identification of the transitional lead in the frontal (limb leads) and transverse (precordial leads) plane, respectively. To validate angle measurements with MRI a LV phantom, freely adjustable in all planes, was used.

Results: In the frontal plane the LVLA spatial direction and the mean QRS axis measured 37±10° (16–57°) and 36±32° (−30–90°), respectively. The findings in the horizontal plane were 46±7° (29–58°) and −32±19° (−75–15°), respectively. The correlation between LVLA spatial direction and mean QRS axis was r = 0.35 (p<0.01) and r = 0.19 (p = NS) in the frontal and horizontal plane, respectively (Figure 1a,b). In the phantom study phantom LV spatial direction by MRI showed a mean error of 0±1° versus the true phantom direction in the frontal and horizontal planes, and the maximum error was 3° (Figure 1c).

Conclusions: MRI can be used for accurate determination of three-dimensional spatial directions of vectors defined on two-dimensional MR images. In contrast with previous studies (Dougherty, 1970; Hyman et al., 1948) the findings in the present study show only a weak correlation between anatomical LV spatial direction and mean QRS axis in the frontal plane, and no correlation in the horizontal plane. Thus, the LV spatial direction cannot be used to correct mean QRS axis derived from the standard 12-lead ECG.

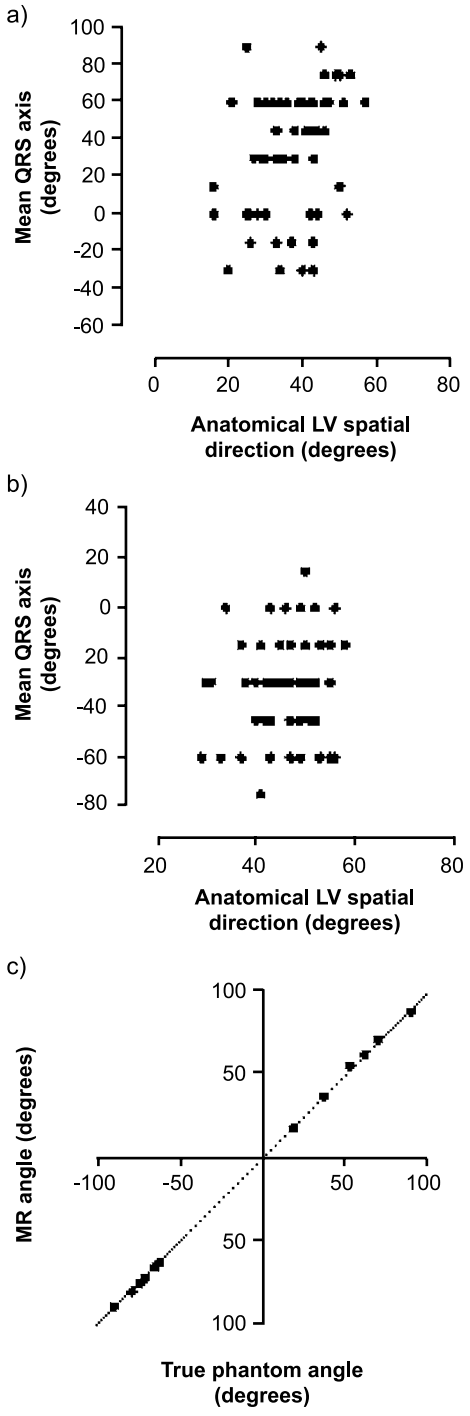

Figure 1.

REFERENCES

Dougherty, J. D. (1970). The relation of the frontal QRS axis to the anatomic position of the heart. *J. Electrocardiol.* 3:267–284.

Hyman, A., Failey, R., Ashman, R. (1948). Can the longitudinal anatomical axis of the ventricles be estimated from the electrocardiogram? *Am. Heart J.* 36:906–910.

Copyright © Marcel Dekker, Inc. All rights reserved.

ORDER REPRINTS

526. A Novel Method for Viability Assessment by Cinematographic and Late Contrast Enhanced Magnetic Resonance Imaging

Gao Gang, Thomas Martin, Paul Cockshott, John Foster, Alex Elliott, Henry Dargie, Bjoern Groenning. *Cardiology Department, GCMRU, Glasgow, United Kingdom.*

Introduction: At present a myocardial viability score is produced by visual evaluation of wall motion abnormalities from cinematographic (CINE) magnetic resonance (MR) images in combination with presence or absence of late hyper enhancement (LE) on contrast enhanced MR (ceMR) images. We set out to develop and validate image processing techniques capable of reducing the observer dependence and improving accuracy in the diagnosis of viable myocardium.

Purpose: Currently, ceMRI and cine MRI data are collected separately, and subsequently compared each other to derive a viability score. This approach may face co-registration problem due to image misalign between the two sets of breath-hold images. We propose an algorithm which integrates the LE information into CINE images. We believe such CINE-ceMR images would be convenient for visual or automated assessment of myocardial viability.

Methods: 15 patients with chest pain who were both troponin I and LE positive were recruited. MR was performed at a median (range) of 69 (16–120) hrs on a Siemens Sonata 1.5T system using a phased array chest coil. LV dimensions were evaluated by CINE trueFISP breath-hold sequence. ceMR was performed 10 minutes after injection of 0.2 mmol/kg gadolinium-DTPA using a breath hold segmented turboFLASH inversion–recovery sequence. Cardiac motion was extracted from the CINE images by registering a selected reference image with the other images covering the cardiac cycle. A set of 2D arrays are obtained, which specify for each pixel in the reference image, the location of its corresponding point in the other CINE images. Using the 2D arrays, it is possible to animate the LE image in a process known as ''warping'' creating a warped CINE-LE image. Data were manually extracted from both original and warped images using in-house off line software.

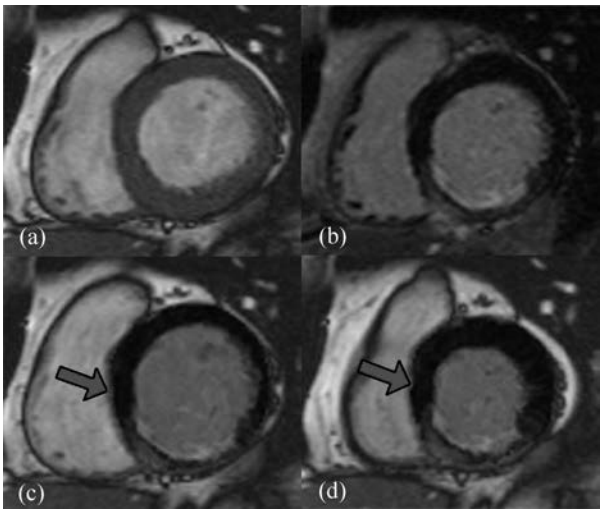

Figure 1. (a) The selected reference image; (b) Original late enhanced image; (c) Warped diastole late enhanced image; (d) Warped systole late enhanced image; The arrows show a myocardial area which moves abnormally but has not been contrast enhanced. With the help of a cine image with late enhancement, this area is efficiently located.

Results: From the 15 patients a total of 45 short axis (SA) slices were obtained (for each patient, a basal, a mid and an apical slice were selected). Mean (SD) LV end diastolic volume (EDV) in each of the slices was measured by planimetry (original/ warped) = 20.6/21.35 ml, $p = 0.35$. LV end systolic volume (ESV) = 12.92/12.23 ml, $p = 0.33$. Mean (SD) wall thickening was calculated in each of the 720 segments from original and warped diastolic and systolic images as the distance from the centre of the LV cavity to the endocardial border in diastole and systole (original/ warped): 3.53/2.83 mm, $p = 0.09$. Mean (SD) LE area of each segment (original/warped) = 14.50/14.30 ml, $p = 0.48$ (Figure 1).

Conclusions: A novel method for LV viability assessment using combined CINE and ceMR images has been developed. We have shown that there are no significant differences in LVEDV, LVESV, LE volume and LV wall thickening between the original CINE and ceMR images and the warped ceMR-CINE images. The method therefore appears to be promising as an improved viability assessment tool.

527. Gadolinium-DTPA may Decrease the Size of Susceptibility Artifacts in BOLD-MRI of the Human Heart

Andreas Kumar, M.D., Rainer Dietz, M.D., Matthias G. Friedrich, M.D. *Cardiology, Humboldt University Berlin, Charite Franz-Volhard-Klinik, Berlin, Germany.*

Introduction: BOLD-MRI of the heart is feasible and is reported to be useful in detecting myocardial ischemia. However, susceptibility artifacts usually seriously

Copyright © Marcel Dekker, Inc. All rights reserved.

ORDER REPRINTS

impair BOLD image quality. A recent study on BOLD venography suggested the reduction of susceptibility artifacts by the use of a T1 shortening contrast agent.

Purpose: We investigated the influence of Gadolinium-DTPA (Gd-DTPA) on overall BOLD image quality and reduction of susceptibility artifacts in cardiac MR imaging.

Methods: 16 patients (3 females, mean age 59±11) with chronic inferior myocardial infarcts underwent cardiac MRI in a 1.5 T clinical scanner (GE Medical Systems, CV/*i*, Milwaukee, USA). An echoplanar readout gradient echo sequence (TR 1 R–R interval, TE 16–18 msec, flip angle 20°) was applied in three short axis views (slice thickness 15 mm, spacing 5 mm) at breath-hold. The same sequence was repeated three minutes after administration of 0.2 mmol/kg Gadolinium-DTPA. Images were evaluated for BOLD overall image quality (1 = good, 2 = fair, 3 = non-diagnostic), presence of susceptibility artifacts (1 = none, 2 = some, 3 = severe, 4 = non-diagnostic), influence of Gadolinium-DTPA on spatial extent of susceptibility artifacts by visual assessment (increased, equal or decreased spatial extent after application of contrast) and number of evaluable segments in a 12-segment model.

Results: Overall image quality (pre-Gd 1.9±0.5 vs. post-Gd 2.1±0.4), presence of susceptibility artifacts by the above scoring system (pre-Gd 2.4± 0.6 vs. post-Gd 2.6±0.5) and number of evaluable segments (pre-Gd 8±2 vs. post-Gd 7±2) did not differ significantly before and after the application of contrast. However, after Gd-DTPA artefact extension was more likely to decrease (6 patients, 38%) or was unchanged (7 patients, 44%) than to increase (3 patients, 19%).

Conclusion: In BOLD-MRI, the administration of Gd-DTPA does not reduce the number of susceptibility artifacts, but may reduce their spatial extent. Further studies are required to analyze this effect and its clinical impact.

528. Real Time Coronary MR Angiography at 3T

Patricia K. Nguyen, Krishna S. Nayak, Charles H. Cunningham, Juan M. Santos, John M. Pauly, Bob S. Hu, Michael V. McConnell, Phillip Yang. *Cardiology, Stanford, Stanford, CA, USA*.

Introduction: Previous studies have demonstrated the clinical utility of real-time cardiac MR in evaluating cardiac function, visualizing cardiac flow, and localizing scan planes without the need for cardiac-gating or breath-holding. Real-time coronary imaging at 1.5 T, however, has been limited by SNR. High field imaging at 3T may improve SNR to achieve the necessary spatial and temporal resolution for coronary artery assessment. Susceptibility to off-resonance effects and RF inhomogeneity, however,must be addressed. We, therefore, developed an optimized 3 T real-time spiral coronary imaging sequence.

Methods: Scanning was performed on a GE Signa 3T VH/i system capable of 40 mT/m amplitude and 150 T/m/s slew rate with receivers supporting 4 us sampling (±125 kHz). Five inch-surface coils were used for signal reception. A custom-designed communication and real-time reconstruction and display framework were used to control the scanner and view images in real time. A spectral–spatial RF pulse that excites thin 3 mm slices with sharp slice profile was designed for the MRCA application. Thin slices were achieved using a 1-3-3-1 1.2 ms sublobe envelope with 4 G/cm amplitude and 4.8 ms total duration. The pulse sequence achieves 1.24 mm resolution over a 20 cm FOV with 4.7 mm slice thickness, every 180 ms (12 interleaves, 15 ms TR, 8.192 ms readouts). Images were reconstructed on 256 × 256 matrix and displayed at 16–24 frames/second using a sliding window. Thirteen subjects (8 men, 5 women) were recruited consecutively.

All MRCA images were evaluated by an observer who is experienced in MRCA. The coronary segments were identified according to the AHA classification system. Image quality of each coronary segment was judged using a grading scale based on the extent of the contiguity of the vessel border and the amount of artifact present in the segment (1 = excellent, 90–100% contiguity with minimal artifact; 2 = good quality, 75–90% contiguity with minimum to mild artifact; 3 = fair quality, 51–74% contiguity with minimum to moderate artifact; and 4 = non-diagnostic quality, <50% contiguity).

Results: All patients completed the scan without complications in less than 20 minutes. A total of 117 coronary segments were analyzed. Of the total segments, 85% of the segments were seen. The mean percentage of segments visualized for each coronary were 100 % pRCA, 100% mRCA, 77% dRCA, 100%% LM, 100% pLAD, 100% mLAD, 77% dLAD LCx. Good to excellent image quality was seen in 77% of segments. Non-diagnostic image quality was seen in 14% of segments. These segments were mostly located in the distal LAD. The mean image quality of each coronary segment are: pRCA 1.15+0.36, mRCA 1.15+0.36, dRCA 2+1.24, LM 1.23+0.57, pLAD

Copyright © Marcel Dekker, Inc. All rights reserved.

ORDER REPRINTS

1.23 +0.42, mLAD 1.38+1.49, dLAD 2.31+1.20, pLCX 2.15+0.77, dLCX 3.69+0.82. Susceptibility artifacts were not present in the real time images.

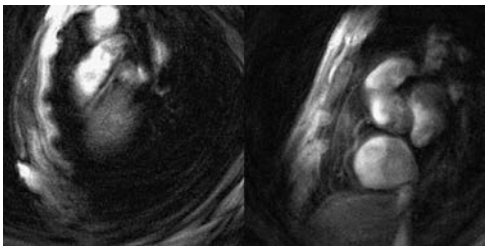

Conclusion: We have demonstrated real time coronary imaging at 3T with good spatial and temporal resolution. Complete coronary evaluation can be achieved in less than 20 minutes without cardiac-gating or breath-holding. Coronary images have good-to-excellent image quality with good anatomic coverage. Real-time coronary artery imaging is feasible at 3T. Further studies are needed to determine its clinical utility in the evaluation of patients with coronary artery disease.

529. Factors Influencing the Arterial Input Function in Myocardial Perfusion Cardiovascular Magnetic Resonance

Andrew G. Elkington, M.R.C.P.,[1] Taigang He, Ph.D.,[1] Peter D. Gatehouse, Ph.D.,[1] Sanjay K. Prasad, M.D. M.R.C.P.,[1] Mohammed Khan,[2] David N. Firmin, Ph.D.,[1] Dudley J. Pennell, M.D. F.R.C.P.[1] [1]*CMR Unit, Royal Brompton and Harefield NHS Trust, London, United Kingdom*, [2]*Health Service Research Unit, Royal Brompton and Harefield NHS Trust, London, United Kingdom.*

Introduction: For quantitative myocardial perfusion cardiovascular magnetic resonance (CMR) using deconvolution, the optimal characteristics of the arterial input function (AIF) include sharpness and high peak gadolinium concentration. Greater understanding of the influences upon the AIF would allow its optimisation for improved quantitative perfusion CMR.

Purpose: To determine the effects of injection rate and cardiac function upon the AIF.

Methods: Patients undergoing a CE-CMR study (Siemens Sonata, 1.5T) for late enhancement assessment had gadolinium (Magnevist) injected at 3, 5 or 7 ml/s using a Medrad power injector in the right antecubittal fossa (0.1 mmol/kg followed by 10 mls normal saline flush). In each cardiac cycle during the first pass a series of saturation-recovery FLASH low-resolution images (TE 0.35 ms, TR 1.06 ms, matrix 64×48) with exponentially increasing saturation delay times were acquired. The sequence used a 5° flip angle and non-selective saturation to avoid fresh inflow effects. The short 50 ms FLASH sequence and a centric-out phase-encoding order enabled acquisition with short saturation-recovery delays. The calculation of shortest T1 during peak gadolinium concentration in the ascending aorta was performed by fitting mean ROI magnitude against saturation delay times. The duration of the AIF was also determined from these curves.

Results: The T1 at the peak concentration of the bolus in the ascending aorta shortened as the injection rate increased from 3 to 7 ml/s ($P<0.01$, $n=15$). The duration of the AIF shortened as the injection rate increased from 3 to 7 ml/s ($P=0.046$, $n=15$). No

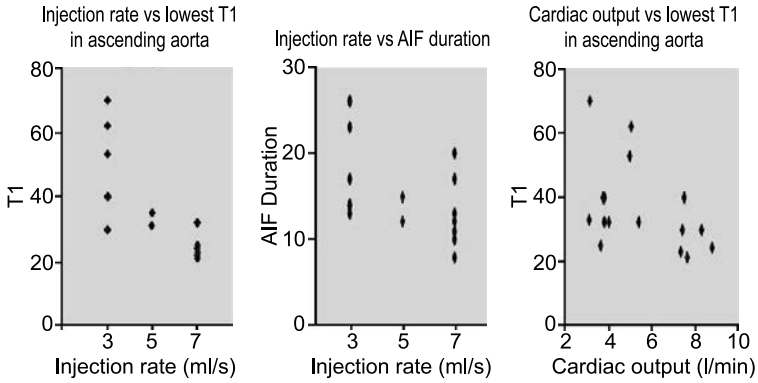

Figure 1. Influences upon the AIF. (*View this art in color at www.dekker.com.*)

Copyright © Marcel Dekker, Inc. All rights reserved.

ORDER REPRINTS

significant relationship between T1 values and LV function, RV function or heart rate was found in this initial study. The variability of the T1 between different patients was found to be much reduced at 7 ml/s (Figure 1).

Conclusions: An injection rate of 7 ml/s gives a consistently superior AIF compared with the AIF found at 3 ml/s. Poor cardiac output adversely affects the AIF. This technique for measuring short T1 values will be used to investigate other potential influences upon the AIF, including site of injection, breath hold, volume of normal saline flush and type of gadolinium.

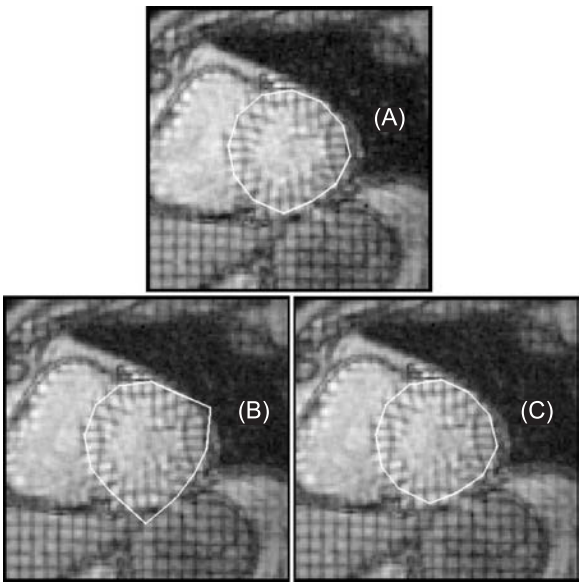

Figure 1.

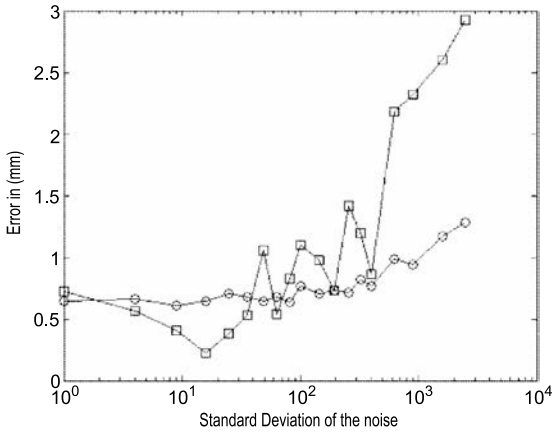

Figure 2. Error of HARP (squares) and modified HARP (circles) technique versus noise value.

530. Robust Motion Tracking of Tagged MR Images Using Combined Harmonic Phase (HARP) and Active Contour Model

Ayman M. Khalifa,[1] Nael F. Osman.[2] [1]*Biomedical Engineering Departement, Helwan University, Cairo, Egypt*, [2]*Johns Hopkins University, Baltimore, MD, USA*.

Introduction: HARP is an image processing technique used for rapid analysis of tagged cardiac magnetic resonance imaging (Osman et al., 1999). The technique filters specific peaks in the k-space of the tagged images to produce phase images, called harmonic phase (HARP) images. Using the fact that the phase of any material point does not change with time, HARP can track the motion of any point through a cine of tagged images. In order to calculate the circomferential and radial strain, a circular mesh is manually built at a specifi timeframe and all the points are then tracked using the HARP technique. Because of regional fading of tags, too rapid motion, or through plane motion, the tracking of some indivisual points on the mesh could fail, resulting in miscalcuation of regional function. In order to reduce this error, we propose a method for correcting the mistracked points by using *active contour methods*.

Purpose: We propose combining HARP imaging with Active Contour Model (ACM) techniques to correct the mistracked points automatically.

Methods: The development of active contour models, or snakes, results from the work of Kass et al. (1988). The active contour model is defined by an energy function. The energy function to be minimized is a weighted combination of internal and external forces. The internal forces emanate from the shape of the snake, while the external forces come from the image and/or from higher-level image understanding process. In our work, the external forces is computed from the HARP images as a funciton of the difference between the harmonic phase value at a specific point in the initial time frame and the phase of the tracked point at any other time frame. The mis-tracked points would be corrected by the internal force.

We tested and compared the new algorithm to conventional HARP using computer experiment. In this experiment, we used an example of tagged MR images in which HARP worked without an error. Using HARP a circular mesh was tracked through the time frames and considered to be the reference mesh A white Gaussian noise was then added to these tagged images and the two algorithms (HARP and modifed HARP) were used for

Copyright © Marcel Dekker, Inc. All rights reserved.

ORDER REPRINTS

tracking the mesh. The root-mean-square (rms) of the difference between the resulting meshes and the reference mesh. The standard deviation of the noise was increased gradually from 0 to 2500 and for each level the rms of the resulting meshes was computed.

Results: Figure 1(A) shows an example of an initial contour drawn manually on the initial time frame. Figure 1(B) shows the contour after tracking using convetional HARP at the following time frame with two mistracked points. Figure 1(C) shows the same contour after tracking using the modified HARP technique.

Figure 2 shows the resulting rms difference. As can be seen in the plots, the modified HARP tachnique is more robust to the increase in noise than the conventional HARP method. This shows that the technique is more robust to the fading of tags or lower-quality tagged MR images.

Conclusion: Combining HARP and ACM techniques have demonstrated to be robust against the fading of the tagged MR images. This results in more accurate calculation of regional strain by reducing the number of mistracked points.

REFERENCES

Kass, M., et al. (1988). Snake: active contour models. *Int. J. Comput. Vis.* 1(4):321–331.

Osman, N. F., et al. (1999). Cardiac motion tracking using CINE harmonic phase (HARP) magnetic resonance imaging. *MRM* 42:1048–1060.

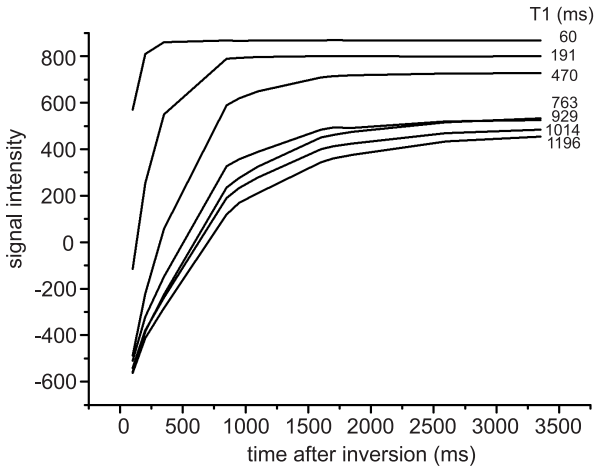

Figure 1.

531. A New Pulse Sequence Scheme for Myocardial T1 Measurements

Daniel R. Messroghli, M.D.,[1] Aleksandra Radjenovic,[1] Sebastian Kozerke, Ph.D.,[2] David M. Higgins,[1] Tim Jones, M.Sc.,[1] Mohan U. Sivananthan, M.D.,[1] John P. Ridgway, Ph.D.[1] [1]*Cardiac MRI Unit, Leeds General Infirmary, Leeds, United Kingdom*, [2]*Institute of Biomedical Engineering, University of Zurich, Zurich, Switzerland*.

Introduction: Standard techniques for measurement and mapping of longitudinal relaxation time T1 are not suitable for cardiac applications in a clinical setting on 1.5 Tesla MR scanners because they do not account for cardiac motion, they are too time-consuming, or both. The approach developed by Look and Locker (LL) has been shown to be highly efficient in non-cardiac applications.

Purpose: To introduce a Modified LL Inversion Recovery scheme (MOLLI) which is designed to provide high-resolution myocardial T1 measurements within one breath-hold.

Methods: Two major modifications were introduced into a conventional LL pulse sequence: 1) ECG triggering and 2) merging of multiple LL experiments into one image set. For each study, three inversion recovery LL experiments were performed with inversion times of 100, 200, and 350 ms. Signal recovery was allowed for >4 s between LL experiments. Single images were acquired in <200 ms with a measured voxel size of $1.58 \times 2.28 \times 8$ mm. 7 Gadolinium-doped gel phantoms were studied while different heart rates were simulated (over-all acquisition time: 14 to 23 s). T1 values were calculated from a 3-parameter Levenberg–Marquardt fit. Pixel-wise T1 mapping was performed using a customized software program.

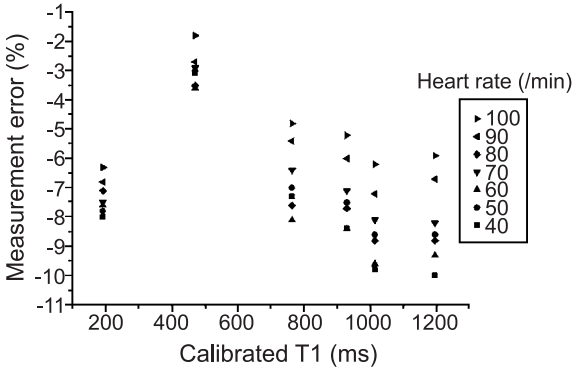

Figure 2.

Copyright © Marcel Dekker, Inc. All rights reserved.

ORDER REPRINTS

Results: The mean measurement error with MOLLI for 7 T1 values ranging from 60 to 1200 ms at heart rates from 40 to 100/ min was $-8.6 \pm 4.9\%$, with highest error for T1 = 60 ms. Figure 1 shows signal intensity curves from merged image sets for 7 phantoms at a heart rate of 80/ min. Figure 2 gives the percentage T1 estimation error at different heart rates. Using a simple empirically derived algorithm correcting for heart rate and T1, estimation error could be further reduced to $-1.5 \pm 1.5\%$ for the full range of T1 and heart rate.

Conclusions: he proposed MOLLI scheme produces highly accurate T1 estimates in vitro and potentially allows high-resolution data acquisition for myocardial T1 mapping within one breath-hold.

532. Radial Self-Gated Cine MRI: Initial Clinical Experience

Orlando P. Simonetti, Ph.D.,[1] Richard D. White, M.D.,[2] Max Choi,[3] Andrew C. Larson, M.S.,[4] Mark Crowe,[3] John Salanitri, M.D.,[5] Arthur Stillman, M.D., Ph.D.,[2] F. Scott Pereles, M.D.[5] [1]*Siemens Medical Solutions, Chicago, IL, USA*, [2]*Radiology, Cleveland Clinic Foundation, Cleveland, OH, USA*, [3]*Biomedical Engineering, Northwestern University, Chicago, IL, USA*, [4]*Nhlbi, NIH, Bethesda, MD, USA*, [5]*Radiology, Northwestern University, Chicago, IL, USA*.

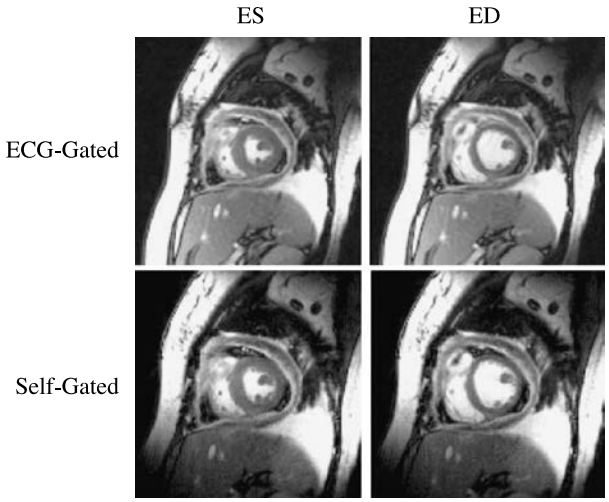

Figure 1. Cine images acquired at End-Systole (left) and End-Diastole (right) using ECG-gating (top) and self-gating (bottom).

Introduction: Cine MRI is dependent on an adequate ECG signal for synchronization of data acquisition with the cardiac cycle. In a significant number of cases, a reliable ECG signal cannot be obtained from the patient within the magnet bore. A newly developed self-gated cine sequence acquires data with radial k-space filling and derives a cardiac trigger signal from changes in the amplitude of the MR signal, rather than from an external physiological signal. In normal volunteers, this self-gated cine sequence has been shown to generate images equivalent to conventional ECG gating (Larson et al., 2004).

Purpose: The purpose of this study was to demonstrate the clinical feasibility of the self-gated cine sequence in a series of patients referred for clinical cardiac MRI exams.

Methods: Using a radial k-space sampling scheme in which every sampled line passes through the center of k-space, cardiac timing data was extracted directly from changes in the amplitude of the echo peak. A low-pass filter (3 Hz cut-off) removed high frequency noise and a simple peak-detection algorithm provided the trigger signal used for retrospective reconstruction. Using this strategy, self-gated cine imaging was performed in multiple cardiac views on 20 patients using 1.5T Siemens Sonata MR systems at two major medical centers. Clinical indications for cardiac MR included assessment of myocardial viability (n = 8), pericardial disease (n = 3), valvular disease (n = 2), aortic aneurysm (n = 3), exclusion of right ventricular dysplasia (n = 2), left ventricular outflow obstruction (n = 1), and right atrial thrombus (n = 1). Conventional cine images utilizing retrospective ECG triggering were obtained in identical views. All acquisitions were performed during breath-holding. Typical parameters for the self-gated sequence were 340 mm^2 FOV, 7 mm slice, 192×192 matrix, 3.6 msec TR, and 55° flip-angle while acquiring 16 ines/segment during each of 12, one second acquisition windows.

A single-slice ejection fraction (EF) was calculated for each cine series obtained in every patient. Linear regression analysis was used to determine the correlation between the EF results calculated from the self-gated sequence with those calculated from the ecg-gated images.

Results: In 18 out of 20 patients, self-gated images satisfactorily demonstrated areas of normal and abnormal myocardial wall motion and valve anatomy. Example self-gated and ECG-gated images from one patient with constrictive pericarditis are shown in Figure 1. In two patients, some motional blurring was noted in the self-gated images which was not present in the ECG gated cine scans. The R^2 value for the

Copyright © Marcel Dekker, Inc. All rights reserved.

ORDER REPRINTS

correlation between the self-gated and ECG-gated values of EF was 0.9866, and the slope was found to be 0.9863. The mean and standard deviation of the percentage difference between the self-gated and ECG-gated values of EF was 2.9622% ± 5.9496%, indicating a close agreement between the two measurements.

Conclusions: It has been demonstrated in a small population of clinical patients that self-gated radial cine MRI can be successfuly used to image the heart without the need for ECG synchronization.

REFERENCE

Larson, A., et al. (2004). *Magn. Reson. Med.* in press.

533. Qualitative Mapping of Human Myocardial Perfusion Using Breath-Hold Arterial Spin Labeling TrueFISP MRI

Raymond Huang, Jing An, M.S., Qun Chen, Ph.D. *Department of Radiology, New York University School of Medicine, New York, NY, USA.*

Introduction: Arterial spin labeling (ASL) perfusion MRI, i.e. the use of magnetically labeled flowing blood as an endogenous contrast agent for the measurement of regional blood flow, offers the advantages of high spatial resolution and does not require contrast injections (Detre et al., 1992; Edelman et al., 1994; Kim, 1995; Kwong et al., 1995). While this technique is widely used for quantitative measurements of cerebral blood flow, its application in measuring human myocardial perfusion has been limited by technical difficulties (Poncelet et al., 1999; Wacker and Bauer, 2003). Our current work shows that the combination of a segmented high-SNR TrueFISP imaging sequence with the ASL technique may help overcome these difficulties, and thus provide a potentially useful tool for the non-invasive imaging of myocardial perfusion.

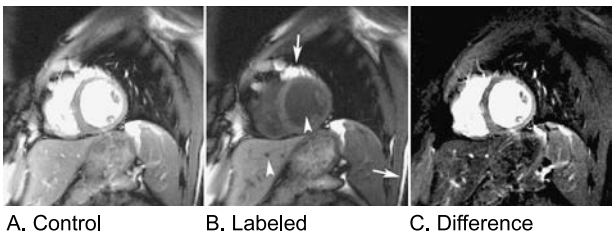

Figure 1. A)–B) Control and labeled images demonstrating the FAIR technique. Flowing blood was suppressed (arrow heads) whereas the signal intensity of stationary tissue (e.g. fat) remains unchanged (arrows). C) The difference map provides qualitative information related to regional blood flow.

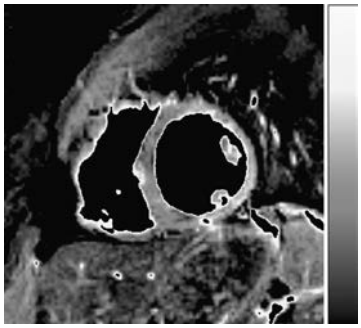

Figure 2. Color display of myocardial blood flow. (*View this art in color at www.dekker.com.*)

Purpose: To demonstrate the feasibility of a breath-hold TrueFISP ASL imaging method for the qualitative assessment of myocardial perfusion.

Methods: Five healthy volunteers were studied on a 1.5T clinical scanner (Magnetom Sonata, Siemens, AG). Phased array coils were used for these experiments. FAIR technique was used for spin labeling (Kim, 1995; Kwong et al., 1995). Briefly, two images at the same slice location were acquired during one single breath-hold (16–20 heart beats) using segmented approach, one with the application of a slice selective inversion pulse (control) and the other with a slice nonselective pulse (label). A qualitative flow map was generated by subtracting one image from the other. Cardiac triggering was used and images were obtained 600–700 ms after the inversion pulses to take advantage of high coronary blood flow during diastole. Segmented TrueFISP sequence, because of its high SNR, was used for image acquisition. Imaging parameters were: TR/TE = 3.0 ms/1.5 ms, section thickness = 10–12 mm, matrix size = 128–192 × 128–192, and field of view = 30–35 cm.

Results: Examples of a control and a labeled image are shown in Figure 1A and B. Notice that the signal intensity of the flowing blood in the ventricles and blood vessels is suppressed by the slice nonselective pulse (arrow heads, Figure 1B), whereas the signal intensity of fat remains bright (arrows). A qualitative blood flow map, calculated from the difference between control and labeled images, is displayed in Figure 1C. Note the high signal intensity in the LV and RV, as well as in the blood vessels in this map. As a comparison, signal difference in fat tissue is near zero at the background noise level. To better visualize

Copyright © Marcel Dekker, Inc. All rights reserved.

ORDER REPRINTS

myocardial perfusion, the map was magnified to show only the heart, and was displayed in a color range with an offset that levels out the bright signal intensity of the LV and RV (Figure 2). Higher signal intensity in the LV wall and in the papillary muscles is observed, as compared to the surrounding tissues.

Conclusion: We have shown that it is feasible to qualitatively map human myocardial blood flow using a breath-hold TrueFISP ASL technique. To quantify myocardial perfusion, however, more theoretical work and slice profile improvement of the slice selective pulse are necessary. Furthermore, studies in patients with coronary artery disease are needed to determine the potential of this technique for detecting myocardial perfusion defects.

REFERENCES

Detre, J. A., Leigh, J. S., Williams, D. S., et al. (1992). *MRM* 23:37–45.

Edelman, R. R., Siewert, B., et al. (1994). *Radiology* 192:513–520.

Kim, S. G. (1995). *MRM* 34:293–301.

Kwong, K. K., Chesler, D. A., et al. (1995). *MRM* 34:878–887.

Poncelet, B. P., Koelling, T. M., et al. (1999). *MRM* 41:510–519.

Wacker, C. M., Bauer, W. R. (2003). *Herz* 28:74–81.

534. Method for Multi-slice Quantitative Measurement of Myocardial Perfusion

Hammond G. Reynolds,[1] Raymond Kwong,[2] Thomas K. Foo.[3] [1]*Applied Science Lab, GE Medical Systems, Framingham, MA, USA*, [2]*Cardiology, Brigham an Women's Hospital, Boston, MA, USA*, [3]*Applied Science Lab, GE Medical Systems, Balitmore, MD, USA*.

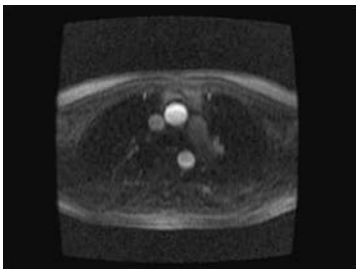

Figure 1.

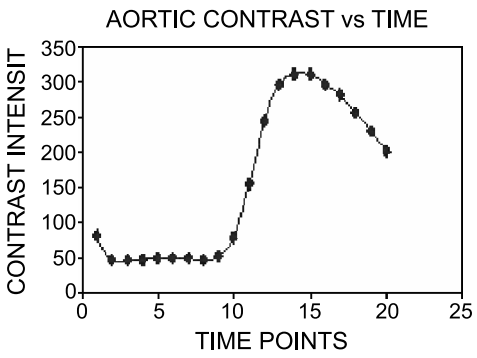

Figure 2. (*View this art in color at www.dekker.com.*)

Introduction: Current techniques of myocardial perfusion quantification using MR require the measurement of the input function or the concentration of the contrast media in the blood pool. The notched perfusion acquisition of Slavin et al. (2001) meets the requirements of being able to provide good spatial coverage of the myocardium and high image S/N through the use of longer actual TI times (Bertschinger et al., 2001) after the application of a saturation-recovery preparation rf pulse. However, the proposed method seeks to maintain the spatial coverage advantage of the notched saturation but yet allow the acquisition of a measurement slice for a linear measurement of signal intensity vs. concentration in the blood pool.

Methods: In the notched perfusion sequence, a saturation recovery rf pulse (SR1) is followed immediately by the acquisition sequence of slice 1 (SL1). A saturation recovery rf pulse and slice acquisition occurs after SL1 for each slice in the scan. Each saturation pulse rf pulse is effective everywhere except for the immediate slice being acquired. The spins in SL2 will have experienced the effect of SR1 with an actual TI time equivalent to the time needed to play out the preparation segment, SR1 and the image acquisition segment, SL1. Similarly, SR2 is effective everywhere except over the slice location SL2 and prepares the magnetization for readout at a later TI time at SL3. The TI time for SL1 is the result of the last saturation rf pulse from the previous R–R interval and may be inconsistent due to variations in heart rate. Unsaturated blood from the notched pulse can flow into any imaged slice and mix with saturated blood leaving the blood pool signal indeterminate and somewhat independent of contrast media concentration.

In the proposed approach, the first notched preparation pulse is replaced by a non-selective rf pulse SR1′. In addition, SL1 is modified to have half the

Copyright © Marcel Dekker, Inc. All rights reserved.

ORDER REPRINTS

spatial resolution of the other imaging sequences. The acquisition and TI times for slice 1 are now SL1′ = SL1/2 and TI1′ = SL1/2 respectively. The non-selective saturation recovery pulse, SR1′, is effective for slice 1 and also the next slice (SL2) in the series. SL1′ can now be placed at any orientation or plane independently of the other slice locations. This allows the user to prescribe a slice along the pulmonary vein or aortic outflow tract for a better measurement of the contrast media concentration (input function).

Results: Figure 1 shows an image from the first ''calibration slice'' of a series of 20 time course images. With a reduced spatial resolution of 128×64 pixel, the first pass of a 0.05 mmol/kg of gadolinium in the aortic outflow tract in clearly noted. Figure 2 shows the measurement of the signal intensity in the aorta over the time course of the acquisition. This demonstrates the ability to obtain input contrast concentration data from a low spatial resolution acquisition.

Conclusion: We have demonstrated a hybrid acquisition sequence that allows the simultaneous acquisition of the input function of the contrast bolus and multi-slice perfusion data in the heart.

REFERENCES

Bertschinger, K. M., Nanz, D., Buechi, M., Luescher, T. F., Marincek, B., von Schulthess, G. K., Schwitter, J. (2001). Magnetic resonance myocardial first-pass perfusion imaging: parameter optimization for signal response and cardiac coverage. *J. Magn. Reson. Imaging* 14:556–562.

A poster by Elkington et al. (SCMR 2003, #244) alluded to a dual resolution technique described by Gatehouse, et al. However, a medline search did not turn up any published journal articles.

Slavin, G. S., Wolff, S. D., Gupta, S., Foo, T. K. F. (2001). First-pass myocardial perfusion MRI with interleaved notched saturation: feasibility study. *Radiology* 219:258–263.

535. Quantitative High-Resolution MRI of an Atherosclerotic Rabbit Model with a Whole Body 1.5 Tesla MRI System

Henning Steen, M.D.,[1] Joao A. C. Lima, M.D.,[1] Subroto Chatterjee, M.D.,[2] Rene Rodriguez, M.D.,[3] Hugo A. Katus, M.D.,[4] Matthias Stuber, Ph.D.[5]
[1]*Cardiology, Johns Hopkins Hospital, Baltimore, MD, USA*, [2]*Pediatrics, Johns Hopkins Hospital, Baltimore, MD, USA*, [3]*Pathology, Johns Hopkins Hospital, Baltimore, MD, USA*, [4]*Cardiology, Universitätsklinikum, Klinik III, Heidelberg, Germany*, [5]*Radiology, Johns Hopkins Hospital, Baltimore, MD, USA*.

Introduction: MRI is a promising non-invasive technique for the characterization of atherosclerosis. However, limited signal-to-noise ratio SNR poses major technical challenges for high-resolution visualization of the vessel walls. We established a methodology that allows for high-resolution MRI black-blood aortic vessel wall imaging and quantitative characterisation in a rabbit model. We developed a black-blood MRI sequence with a spatial resolution of 0.25 mm on a commercially available 1.5T scanner. Secondly, we adopted a previously described coronary analysis software tool for objective quantification of vessel wall thickness, -sharpness, SNR and contrast-to-noise ratio (CNR) between vessel wall and lumen (Etienne, 2002). Finally, the high-resolution MR imaging sequence and the quantitative analysis tool were used to study different atherosclerotic stages in the vessel wall of Watanabe rabbits pre and post contrast.

Methods: Aortic vessel wall imaging pre and post contrast was investigated in 9 Watanabe rabbits (Group I: 3 normals, Group II: 6 high cholesterol fed for 2 months). Imaging was performed on a commercial 1.5T Gyroscan ACS-NT whole body MR system (Philips Medical Systems, Best, The Netherlands,

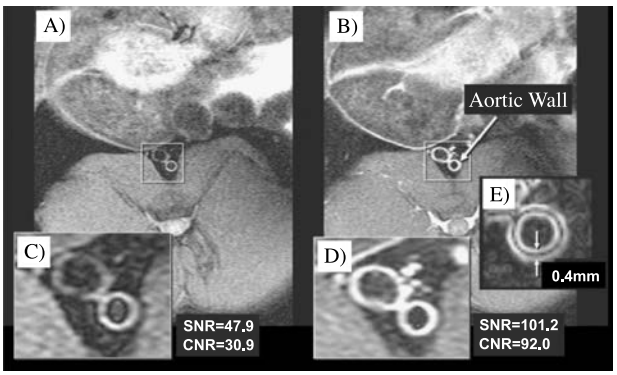

Figure 1. Delayed hyperenhancement in an atherosclerotic (Watanabe) rabbit model. A) Pre-contrast with magnified version in C) B) & D) (magnified version) display the same delayed hyperenhancement section 15 min post Gd injection with a substantially increased vessel-wall SNR and CNR. The vessel wall thickness as measured with the 'Soap-Bubble' analysis software (E) is 0.4 mm. (*View this art in color at www.dekker.com.*)

Copyright © Marcel Dekker, Inc. All rights reserved.

ORDER REPRINTS

23 mT/m, 220 ms rise time), vector ECG triggering, and a two element phased array coil (diameter = 10 cm). Pre-contrast, we acquired 3 adjacent 20 mm thick 3D volumes perpendicular to the subrenal aorta using a dual-inversion fat suppressed 3D black-blood fast spin-echo imaging sequence (TI = 400 ms, TR = 3RR intervals, TE = 10.5 ms, ETL = 18, interecho spacing = 10.5 ms, acquisition window = 190 ms per RR interval, FOV = 76 mm, matrix = 304, in-plane spatial resolution = 0.250 mm, slice thickness = 2 mm, NSA = 2) with phase encoding during each echo train in Z direction. Subsequently, Gadolinium (Magnevist, 0.1 mmol/l) was administered and 5 min post injection, black-blood vessel wall imaging was repeated at the same locations while TI was adjusted to ~300 ms. For an objective quantitative analysis, SNR, CNR, vessel wall thickness and 'sharpness' (=first-order derivative at the vessel border) of the subrenal aortic vessel wall were analyzed semi-automatically pre- and post contrast ('Soap-Bubble' tool. All statistical comparisons were made using a two-tailed paired Student's t-test.

Results: High black blood image quality of the aortic vessel wall could consistently be obtained (Figure 1) in all animals. Average scan time per 3D volume was 11 min. In Group I, SNR increased 30% post contrast (47.1±13.1 to 61.1±19.4) and CNR 70 % (32±9.2 to 55±18.3). Vessel sharpness increased by 55% from 0.46±0.07 to 0.72±0.28 while the vessel wall thickness did not change significantly (from 0.38±0.04 mm to 0.41±0.08 mm. In Group II the SNR increased from 42±23.4 to 124.9±30.7 (297%), CNR from 32.2±18.3 to 102.8±27.5 (318%) and the vessel sharpness from 0.57±0.13 to 0.89±0.24 (58%), (all $p<0.05$). In Group II, a tendency for an increased vessel wall thickness was found when compared to Group I. No significant change in vessel wall thickness post contrast was observed in Group II (0.43±0.03 mm to 0.45±0.04 mm).

Discussion and Conclusions: High quality aortic vessel wall images can be routinely obtained pre and post contrast in an atherosclerotic rabbit model. The dramatic increase of SNR, CNR and vessel sharpness in Group II could be explained by the lipophilic character of Magnevist being avidly absorbed into the cholesterol loaded vessel wall. The increased SNR post contrast could potentially be invested for a further enhanced spatial resolution for improved plaque characterization. The 'Soap bubble' analysis software is well-suited for an objective and quantitative characterization of the atherosclerotic vessel wall. Combination of a 3D high-resolution black-blood imaging sequence pre and post contrast with a quantitative analysis software provides a valuable methodology for the objective assessment and quantification of atherosclerotic vessel wall disease.

REFERENCE

Etienne, A. (2002). *Magn. Reson. Med.*Oct 48(4):658–666.

536. Flow-Gated MRI Using Radial Acquisitions

Richard Thompson, Elliot McVeigh. *Laboratory of Cardiac Energetics, National Institutes of Health, Bethesda, MD, USA*.

Introduction: Phase contrast experiments, for imaging blood and tissue velocity, are typically segmented into many cardiac cycles in order to obtain sufficient spatial and temporal resolution and thus require a gating signal to combine data from multiple cardiac cycles. The surface electrode ECG is the gating waveform of choice for cardiovascular MRI, although alternative gating methods are required for fetal cardiac imaging, due to the unavailability of fetal ECG signals, and for cases of ECG contamination via the strong magnetic fields within the MR scanner. This study demonstrates the feasibility of using imaging data from flow-encoded MRI experiments to derive times for cardiac gating.

Purpose: We validate gating times measured using imaging data from phase contrast experiments by comparison with ECG gating times.

Methods: A standard segmented retrospectively-gated phase contrast imaging protocol was used for all experiments in this study. Prior to retrospective reconstruction, real-time flow-weighted images were generated using only the lines from each segment of k-space (4 to 8 lines). Real-time image content was simplified by using complex-difference reconstruction to retain signal from moving spins while eliminating stationary tissue. A radial acquisition scheme was used to reconstruct images from vastly under-sampled k-space data without severe loss of spatial resolution or field of view. The projection angles within each segment were interleaved evenly around 180 degrees with an offset for each new segment. A flow-gating waveform was measured from a desired ROI from the real-time images, from which gating times were derived using a template matching method to correlate the cyclic patterns of flow to a reference pattern. The

Copyright © Marcel Dekker, Inc. All rights reserved.

ORDER REPRINTS

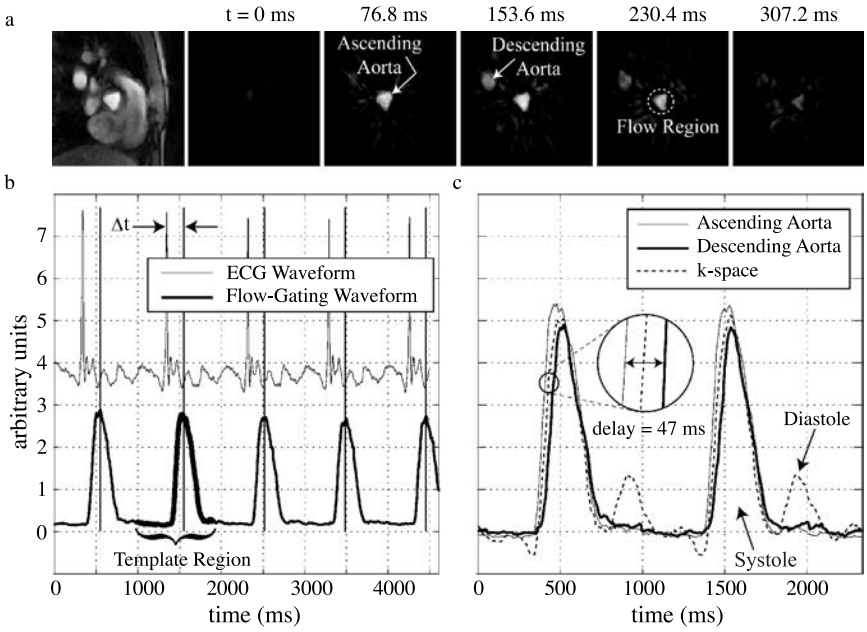

Figure 1. a) A series of real-time complex-difference images acquired from the level of the aortic valve plane from a normal volunteer show the flow-weighting in both the ascending and descending aorta for several time frames across systole. A magnitude image is shown on the left. A flow-gating waveform, measured from the ascending aorta shown in a), is plotted in b. A portion of the flow-gating waveform used as a template to derive the times of the gating impulses is highlighted. The corresponding gating times are indicated in b) by the vertical lines. The ECG waveform recorded throughout the phase contrast experiment is also plotted in b). Three different flow-gating waveforms measured from this same experiment are shown in c). Two image space measurements, from the ascending and descending aorta, are compared with a k-space measurement.

flow-derived gating times were then used for conventional retrospective reconstruction of the data. Breathhold flow-gated phase contrast experiments were performed on five normal volunteers with prescriptions that targeted the ascending aorta, the pulmonary and renal arteries and a three-chamber view orientation. All MR measurements were performed using a Siemens 1.5 T Sonata scanner (Siemens Medical Systems, Erlangen, Germany). Imaging parameters: FOV = 360 mm, 176 readout points, 64 to 88 projections, 4 to 8 views per segment, 5 mm slice, BW = 88 kHz, flip angle = 20 degrees, Venc = 80 to 160 cm/s and TE/TR = 2.8 ms/4.6 ms. Real-time images were updated with every new projection angle (sliding window) for an effective sampling interval of $2*TR = 9.2$ ms. Raw ECG signals were recorded with a sampling rate of 400 Hz during all experiments for timing comparison with the flow-derived gating times.

Results: Figure 1 displays a typical series of real-time complex difference images, a corresponding flow-gating waveform and the calculated gating times. Flow-gating waveforms measured from within the ascending aorta and descending aorta are compared with an unlocalized (k-space-derived) waveform. Table 1 displays the mean standard deviations between the timing of the ECG gating and flow-derived gating times for each of the four regions studied for all five volunteers. Flow derived gating signals were successfully measured for all flow regions studied in all volunteers.

Conclusions: Phase contrast experiments with radial k-space sampling patterns can be used to reconstruct images both in real-time and with conventional gating and segmentation, using the real-time information to derive the gating times for retrospective reconstruction. The real-time complex-difference data

Table 1. Standard deviation of the difference between ECG and flow-derived gating times.

	Aorta	Pulmonary artery	LV chamber	Renal artery
Image space (n=5)	4.2±1.5 ms	5.1±1.9 ms	10.9±2.5 ms	11.6±10.2 ms
k-space (n=5)	4.5±1.7 ms	5.0±0.9 ms	9.5±3.6 ms	12.5±11.5 ms

Copyright © Marcel Dekker, Inc. All rights reserved.

ORDER REPRINTS

was successfully processed to generate gating times using both raw k-space or image space information for all slice prescriptions in all volunteers. The standard deviation of the difference between ECG and flow-derived gating times is adequately small (5 to 12 ms) to give rise to negligible differences between ECG and flow-gated phase contrast images.

537. Auto-calibrated Spiral TSENSE for Cardiac Imaging

Reza Nezafat, Peter Kellman, J. Andrew Derbyshire, Ellliot R. McVeigh. *Laboratory of Cardiac Energetics, National Heart, Lung and Blood Institute, NIH, Bethesda, MD, USA*.

Introduction: Cardiac imaging with both high spatial and temporal resolution using spiral sampling of k-space is challenging. Multi-shot, segmentd spiral imaging is superior to single shot imaging for cardiac cine application since the latter suffers from motion artifacts and T_2* decay. Parallel imaging, exploiting the sensitivity of the coils, can be used to reduce the number of interleaves acquired for reconstruction of a full FOV image. Coil sensitivity calculation is one of the crucial steps in parallel imaging. Here we demonstrate an auto-calibrated acquisition scheme for calculation of the coil sensitivity maps based on TSENSE (Kellman et al., 2001). High spatial and temporal resolution cardiac cine imaging is demonstrated with reduced breath-hold duration.

Purpose: To demonstrate auto-calibrating spiral TSENSE for cardiac imaging.

Methods: The required number of interleaves for fully sampled spiral imaging was reduced using Sensitivity Encoding (SENSE) reconstruction (Pruessmann et al., 2001). Here, the TSENSE (Kellman et al., 2001) method, in which the sensitivity map for each coil is calculated adaptively from the imaging data without the need for a seperate calibration scan, was generalized to spiral imaging. An acquisition alternating between the even and odd spiral interleaves in consecutive cardiac phases was used to image a single short axis slice through the complete cardiac cycle. A low temporal resolution complex reference image without artifact was reconstructed for each coil. This was accomplished by temporal integration of the k-space data for all cardiac phases, producing a full k-space dataset, followed by re-gridding using a Kaiser–Bessel kernel and Fourier reconstruction. Image reconstruction was carried out using an iterative conjugate gradient SENSE reconstruction method (Pruessmann et al., 2001), with the speed up improvement suggested by Wajer et al. (2001). All images were reconstructed off-line using Matlab (The Mathworks, Natick, MA).

Images were acquired on a GE Signa Excite 1.5T MR imaging system (GE, Waukesha, WI) and an 8-channel cardiac phased array coil (Nova Medical, Wakefield, MA). A cardiac gated, breath-held, segmented cine spiral pulse sequence was developed to acquire the even and odd interleaves on alternate phases of the cardiac cycle. Two low resolution, ungated single-shot images with different echo times were acquired at the beginning of the cardiac scan for off-resonance map calculation and correction using the linear field map for subsequent cardiac phases (Irarrazabal et al., 1994).

Normal volunteers were imaged with informed consent as approved by the NHLBI IRB. The spiral

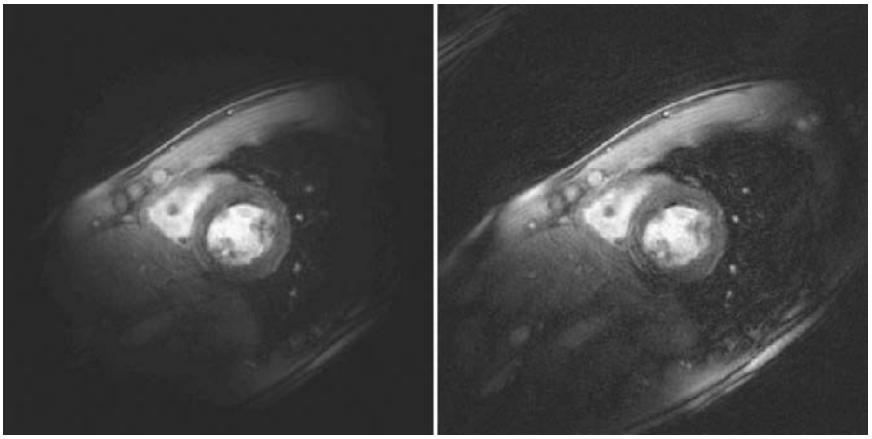

Figure 1. Short axis cardiac image using full k-space spiral acquisition (left) and R=2 spiral TSENSE (right).

Copyright © Marcel Dekker, Inc. All rights reserved.

ORDER REPRINTS

sequence consisted of 32 interleaves with 1024 acquisition points in each interleave. The field of view of 34 cm was prescribed producing a nominal resolution of 1.3×1.3 mm. Flip angle/slice thickness/TR/BW of 30°/8 mm/22 ms/$\pm$125 kHz were used for data acquisition. A single interleave per segment was used to achieve a high temporal resolution and reduce motion blurring. Parallel imaging with acceleration rate $R = 2$ was used to reduce the breath-hold duration from 32 to 16 heartbeats.

Results: Figure 1 shows an example short axis view of the heart comparing full k-space acquisition (left) and rate 2 undersampled reconstruction using TSENSE (right).

Conclusions: Spiral imaging using TSENSE acquisition has been demonstrated for single slice short axis heart imaging. Adaptive sensitivity map estimates were constructed from the data based on the TSENSE method. Accelerated acquisition was used to reduce the breath-hold duration, with a reduction in SNR due to reduced acquisition time and g-factor. Higher acceleration factors should be possible at the expense of increased SNR penalty.

REFERENCES

Irarrazabal, P., et al. (1994). *Magn. Reson. Med.* 35(2):278–282.

Kellman, P., et al. (2001). *Magn. Reson. Med.* 45(5):846–852.

Pruessmann, K. P., et al. (2001). *Magn. Reson. Med.* 46(4):638–6351.

Wajer, F. T. A. W., et al. (2001). *ISMRM 9th Annual Meeting*. 767.

538. POCSENSINNG with Accelerated Iterations for Sensitivity Encoding with Non-uniformly Sampled K-Space Data

Hisamoto Moriguchi, M.D., M.S.E., Jeffrey L. Duerk, Ph.D. *Radiology, University Hospitals of Cleveland, Cleveland, OH, USA*.

Introduction: Spiral MRI offers short acquisition time and reduced sensitivity to flow artifacts. As such, it

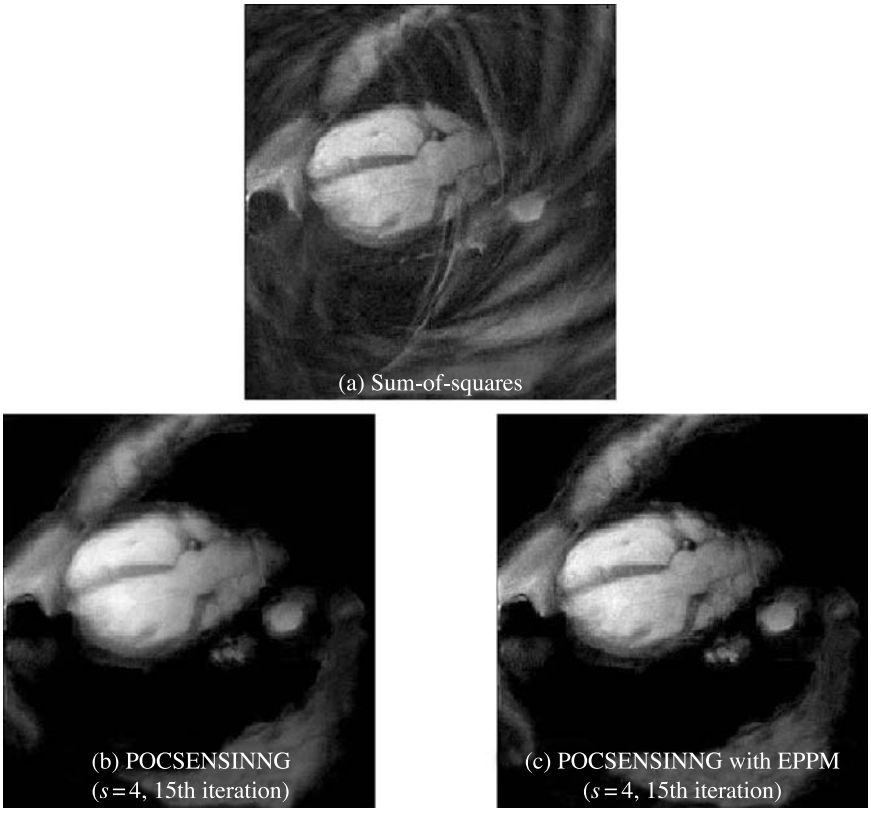

Figure 1.

Copyright © Marcel Dekker, Inc. All rights reserved.

ORDER REPRINTS

has been used for numerous cardiac imaging applications. However, further reduction of acquisition time would be desirable since time reductions help to reduce both cardiac and respiratory motion artifacts. Although parallel imaging techniques have also been proposed as methods to reduce the acquisition time, image reconstruction is usually computationally intensive when k-space data are sampled on a non-uniform grid. POCSENSINNG has recently been proposed as an efficient reconstruction algorithm for sensitivity encoding using non-uniformly sampled k-space trajectories thereby allowing the advantages of these methods to be combined (Moriguchi et al., 2003a). It is an extension of POCSENSE, a method used with rectilinear acquisitions (Kholmovski et al., 2002) that permits non-uniform sampling schemes through the INNG algorithms (Moriguchi et al., 2003b). POCSENSINNG avoids complicated gridding procedures thereby significantly improving the computational efficiency. However, relatively high computational demands are still required when the number of receiver channels, n, is large because 2n Fast Fourier Transforms need to be performed on large rescaled matrices at each iteration. It has also recently been shown that the number of iterations for POCSENSE can be significantly reduced by modifying a relaxation parameter (Samsonov et al., 2003). This method takes advantage of the previously proposed extrapolated parallel projection method (EPPM) (Combettes, 1997). In this study, we show that EPPM is also effective at improving the convergence and computational efficiency of POCSENSINNG.

Purpose: To compare image quality and the number of iterations required for the POCSENSINNG with EPPM and those required for the original POCSENSINNG.

Methods: In the newly proposed algorithm, a relaxation parameter is changed at each iteration in POCSENSINNG. Specifically, the updated image g(p) after p-th iteration is expressed as:

$$g(p) = g(p-1) + r(p-1) \times (g'(p) - g(p-1)) \quad (1)$$

where $g'(p)$ is the reconstructed image after 1 iteration from $g(p-1)$ using the normal procedures of the POCSENSINNG and $r(p-1)$ is a relaxation parameter. $r(p-1)$ is set to 1 in the original POCSENSINNG algorithm. In the new algorithm, $r(p-1)$ is determined based on the extrapolation coefficient, as described by Combettes (1997) and Samsonov et al. (2003).

Both POCSENSINNG and that with EPPM were applied to in-vivo cardiac data acquired using spiral trajectories for comparison. Data acquisitions were performed with a 1.5-Tesla Siemens Sonata scanner (Siemens Medical Solutions, Erlangen, Germany) using a four-element phased array torso/body surface coil. Nine spiral interleaves were used with an FOV of 320 × 320 mm. The reduction factor was 2. A slice thickness of 7 mm, and TE/TR = 6.6/40.0 ms. Three spiral interleaves were successively acquired for one cardiac cycle.

In the image reconstruction, a scaling factor s was set to 4. Off-resonance correction was performed using BRORC (Moriguchi et al., 2003c) on both images.

Results: Figure 1 shows the reconstructed images (a: Sum-of-squares method; b: POCSENSINNG after 15 iterations; c: POCSENSINNG with EPPM after 15 iterations). The aliasing artifacts in image (a) are effectively reduced in both images (b) and (c). However, high frequency components are not well reproduced in (b) when compared with (c). Approximately 30 iterations were required for the original POCSENSINNG algorithm to reconstruct an image comparable to (c).

Conclusions: The number of iterations required for POCSENSINNG can be effectively reduced when it is combined with EPPM with no degradation in image quality. The newly proposed method is quite useful in practice to reduce computational burden of POCSENSINNG. Therefore, this method has significant potential for real-time cardiac applications.

REFERENCES

Combettes, P. L. (1997). *IEEE Trans. Image Process.* 6:493–506.
Kholmovski, E. G., et al. (2002). *Proc. ISMRM*. 194.
Moriguchi, H., et al. (2003a). *Proc. ISMRM*. Late-breaking MR abstract.
Moriguchi, H., et al. (2003b). *Proc ISMRM*. 1066.
Moriguchi, H., et al. (2003c). *MRM* 50:643–648.
Samsonov, A. A., et al. (2003). *Proc. ISMRM*. 2343.

539. Correlation between Diaphragm and Coronary Artery Motion: Findings from ECG Triggered Realtime Imaging

Yi Wang, D.Sc., Bin Luo, James W. Goldfarb, Ph.D., Nathaniel Reichek, M.D. *Cardiac Research, St. Francis Hospital, SUNY Stony Brook, Roslyn, NY, USA*.

Introduction: Breath-hold coronary MRA is an excellent technique to minimize respiratory motion of the heart, but has limited spatial resolution. Navigator echo techniques have also been used to obtain high-

Copyright © Marcel Dekker, Inc. All rights reserved.

ORDER REPRINTS

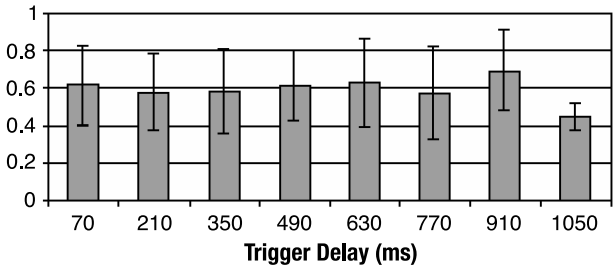

Figure 1. Mean and standard deviation of the scale factors at various cardiac phases. (*View this art in color at www.dekker.com.*)

resolution coronary images by compensating for respiratory motion of the heart using measurements of diaphragmatic position. The navigator approach is based on the assumption that the respiratory motion-induced coronary craniocaudal displacement is the primary displacement to be monitored and is proportional to displacement of diaphragm with a scale factor that is uniform across individuals (Wang et al., 1995). We performed a real-time free breathing study to determine the movement of the proximal left main coronary artery relative to the dome of the right diaphragm to investigate the inter-subject variability and effects of cardiac cycle phase.

Methods: Twenty volunteers (ages: 20 to 79 mean 60, 5 females) were consented and enrolled with IRB approval. After scout imaging located the proximal left main coronary artery, a 2D ECG-triggered TrueFISP sequence was used to acquire coronal images of left main and diaphragm over 50 heartbeat with a 1.5 T Siemens Sonata scanner (Siemens Medical Solutions, Malvern, PA) and a CP body array flex coil. TR/TE/FA = 2.9 ms/1.3 ms/50°, data matrix 144×192, and voxel spatial resolution $3.5 \times 1.9 \times 10$ mm^3. Between 4–8 images (140 ms/image) per cardiac cycle were acquired dependent on cycle length.

MATLAB (Mathworks, Natick, MA) software was used for data processing. A seed point was chosen for diaphragm and coronary respectively. An edge detection algorithm based on image intensity gradient was used to follow the craniocaudal movement of both diaphragm and coronary. Displacement of both diaphragm and coronary artery relative to their own reference point were extracted and a scale factor was calculated based on the displacement and averaged over 50 heartbeats for each cardiac phase.

Results: Images showed good contrast between coronary and surrounding fat, as well as between diaphragm and lung. The standard deviation (STD) over cardiac phase for each subject was small (Mean and STD over STDs from 20 subjects: 0.089 ± 0.048). Figure 1 shows the mean scale factor for each cardiac phase for 50 cardiac cycles in each of 20 subjects with standard deviation at each cardiac phase among 20 subjects displayed.

Conclusions:

1. The respiratory induced displacement of the left main coronary artery correlates well with diaphragmatic motion;
2. For any given volunteer, there is no significant variation in coronary motion relative to diaphragmatic motion within the cardiac cycle;
3. There is a substantial disparity among different subjects, suggesting that prior free breathing scans to establish a scale factor may be desirable prior to navigator coronary imaging.

REFERENCES

Wang, Y., Grimm, R. C., Rossman, P. J., Debbins, J. P., Riederer, S. J., Ehman, R. L. (1995). 3D Coronary MR angiography in multiple breath-holds using a respiratory feedback monitor. *Magn Reson Med.* Jul 34(1):11–16.

540. Comparison of Flow Independent Radial and Cartesian Imaging Techniques for Coronary MRA

Cosima Jahnke, M.D., Ingo Paetsch, M.D., Bernhard Schnackenburg, Ph.D., Axel Bornstedt, Ph.D., Rolf Gebker, M.D., Eckart Fleck, M.D., Eike Nagel, M.D. *Cardiology, German Heart Institute Berlin, Berlin, Germany.*

Background: Coronary magnetic resonance angiography (MRA) has traditionally been performed using a Cartesian k-space data acquisition scheme. On the other hand, radial k-space sampling is known to be less sensitive to motion artefacts. Thus, potential improvements may be achieved with radial k-space data acquisition using flow independent steady state free precession techniques (bTFE). Consequently, we directly compared bTFE coronary MRA using Cartesian and radial k-space data acquisition.

Methods: 30 consecutive patients with suspected coronary artery disease underwent free-breathing, navigator-gated MRA of the left or right coronary artery using bTFE (TR/TE/flip angle: 4.5 ms/2.3 ms/

Copyright © Marcel Dekker, Inc. All rights reserved.

ORDER REPRINTS

Table 1.

	Diagnostic accuracy (%)	Visual score (low=1, high=4)	Visible vessel length (mm)	Visible side branches	Vessel diameter (mm)	Vessel sharpness (%)
bTFE Cartesian	88.3	3.1±0.9	112±28	4.0±1.8	3.2±0.4	49.0±5.1
bTFE Radial	83.6	2.9±1.0	109±31	2.9±1.4*	2.7±0.5*	59.9±6.7*

*$p<0.05$.

90°; Philips Intera CV 1.5T) twice, once with Cartesian and again with radial k-space data acquisition. The following quantitative parameters were determined: visual score, visible vessel length, number of visible side branches, average vessel diameter, vessel sharpness. Diagnostic accuracy was determined in comparison to invasive x-ray angiography.

Results: Radial bTFE resulted in a significant increase in vessel sharpness but a decrease in visible side branches and vessel diameter compared to Cartesian bTFE (see Table 1). There were no differences regarding the diagnostic accuracy, the visual score and the visible vessel length (Fig. 1).

Conclusions: Coronary MRA with radial k-space sampling appears to be on a par with Cartesian approach regarding diagnostic accuracy of stenosis detection in an unselected patient population. Nevertheless with current implementations radial is inferior to Cartesian data acquisition regarding the visualization of side branches despite better vessel sharpness.

541. Fast Extended-Coverage Parallel Dark Blood Imaging of Vessel Walls

Venkatesh Mani, Ph.D., Vitalii V. Itskovich, Ph.D., Juan Gilberto S. Aguinaldo, M.D., Zahi A. Fayad, Ph.D.
Mount Sinai School of Medicine, New York, NY, USA.

Introduction: Dark blood (DB) magnetic resonance (MR) imaging is a non-invasive technique for assessment of atherosclerotic plaque in humans. Conventional MR DB sequences are limited to imaging 1–3 slices in one acquisition and thus requires long experiment time.

Purpose: The purpose of this study was to develop a new fast extended-coverage parallel DB MR sequence for vessel wall imaging was developed.

Methods: A 1.5T clinical MR system was used to create and test new multi-slice double inversion recovery (DIR) MR imaging method on 5 healthy subjects and 5 patients with history of atherosclerosis. Simultaneous breath-hold imaging (less than 30 seconds) of multiple DB slices (16–20) were achieved by shortening inversion time of blood using repeated DIR modules in one heart cycle, acquiring several slices (3–5) following each DIR module and utilizing parallel imaging with Generalized auto-calibrating partially parallel acquisitions (GRAPPA).

Results: Examples of 16 slice DB aortic images from a 57-year-old patient are shown in Figure 1. Compared to conventional MR single slice DB method, the new fast-extended coverage technique had higher signal to noise ratio per unit time per slice (17.8±3.5 for new method vs. 8.0±1.0 for conventional sequence, $p<0.05$) and comparable contrast to noise ratio (flow suppression) (16.3±4.9 vs. 21.4±3.3, p = ns). Average acquisition times for the new sequence protocols ranged from 25 (16 slices) to 34 (20 slices) seconds, as compared to equivalent conventional sequence protocols that ranged from 400 to 680 seconds.

Conclusions: The new fast extended coverage DB MR method enabled breath hold acquisition of multiple

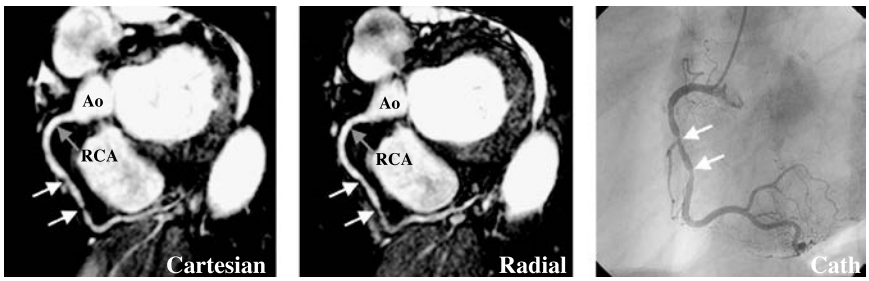

Figure 1.

Copyright © Marcel Dekker, Inc. All rights reserved.

ORDER REPRINTS

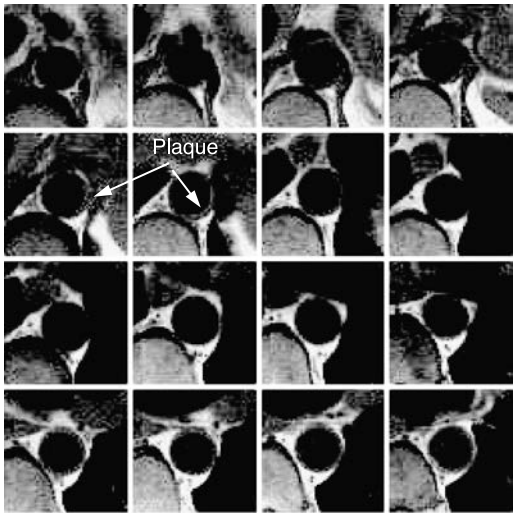

Figure 1.

slices of the vessel wall, reduced imaging artifacts, thereby improving image quality.

542. Visual Estimation of the Global Myocardial Extent of Hyperenhancement on Delayed Contrast-Enhanced MRI

Alain LALANDE, Ph.D.,[1] Alexandre Comte, M.Sc.,[1] Alexandre Cochet, M.D.,[1] Paul M. Walker, Ph.D.,[1] Yves Cottin, M.D.,[2] Jean Eric Wolf, M.D.,[2] François Brunotte, M.D.[1] [1]*Laboratoire de Biophysique, Faculté de Médecine, Dijon, France*, [2]*Service de Cardiologie II, CHU de Dijon, Dijon, France*.

Introduction: MRI with paramagnetic contrast agent allows the assessment of the extent of myocardial tissue injury after infarction. Visual scoring has been widely used to define the transmural extent of the myocardial infarction. No attempt has been made to use visual scores in order to assess the percentage of infarction on the entire myocardium.

Purpose: The purpose of this study was to conceive a rapid visual evaluation method of the extent of transmural infarction from delayed contrast-enhanced MRI. For regional analysis, the myocardium was divided into 17 segments (Cerqueira et al., 2002). In each segment the transmural extent of the hyperenhancement was scored. The sum of the local scores defines a parameter of the extent of the hyperenhancement on the whole left ventricle. The global score was compared with planimetric evaluation of the hyperenhancement.

Methods: The study population comprised 34 patients (27 men, 7 women, mean age: 54 years, range 25 to 80 years) with a recent myocardial infarction. Magnetic resonance imaging was performed on a 1.5 T Siemens Magnetom Vision. ECG-gated T1-weighted images were obtained ten minutes after intravenous injection of a bolus of 0.1 mmol/kg gadolinium contrast agent. Images were acquired during breath-hold. The entire left ventricle was scanned with short-axis slices of 8 mm thickness and 7 mm gap.

The myocardium was divided into 17 segments. The basal and the mid-cavity regions were segmented into 6 segments, the apical region was segmented into 4 segments, and there is one segment for the apex (Cerqueira et al., 2002). This latter segment was determined from long-axis slices. To characterise each segment, the late hyperenhancement was evaluated by 2 observers according to the following scheme: 0: no hyperenhancement, 1: 1% to 25% of the segment with hyper signal, 2: 26% to 50% of the segment with hyper signal, 3: 51% to 75% of the segment with hyper signal, 4: 76% to 100% of the segment with hyper signal. The global score was defined as the sum of the scores on each segment. The global score was expressed as a percentage of the maximum possible score (i.e. 68).

Secondly, on each image, the myocardium and the hyperenhancement area (if present) were manually drawn. The left myocardium and the hyperenhancement volumes were calculated as the sum of the surfaces determined on each slice multiplied by the distance between two slices. The volume of hyperenhancement was expressed as a percentage of the left ventricle myocardial volume.

The two aforementioned methods were performed by two experienced observers. The percentage of hyperenhanced myocardium obtained with visual interpretation and manual tracing were compared.

Results: For the visual global score, there are good intra and inter observer correlations ($r = 0.98$ and $r = 0.98$, respectively). For the planimetry, there are good intra and inter observer correlations ($r = 0.98$ and $r = 0.97$, respectively). For the estimation of the extent of hyperenhancement, there is a good correlation between the visual scoring and the manual tracing of hyperenhanced myocardium ($r = 0.92$; $y = 1.1 \times - 0.06$; $SEE = 5.5$).

Conclusions: Currently, late contrast-enhancement MRI is widely used to study the myocardial impairment on a regional basis. No attempt has been made to derive a more global parameter which could

Copyright © Marcel Dekker, Inc. All rights reserved.

ORDER REPRINTS

be applied to the whole myocardium. In our study, we have shown that a visual approach based on a 17 segment model can be used to evaluate the global myocardial extent of the hyperenhancement with similar results to planimetry.

REFERENCE

Cerqueira, M. D., et al. (2002). *Circulation* 105:539–542.

543. High Resolution 3D Breath-Hold SSFP Coronary MRA Using Self-Calibrating Parallel Acquisition

Jaeseok Park,[1] Richard McCarthy,[2] Debiao Li.[1]
[1]*Department of Biomedical Engineering and Radiology, Northwestern University, Chicago, IL, USA*, [2]*Radiology, Northwestern University, Chicago, IL, USA*.

Introduction: Breath-hold imaging time constraints have limited the spatial resolution of coronary MRA. Three-dimensional (3D) SSFP technique increased SNR, making parallel imaging feasible. Self-calibrating GRAPPA (GeneRalized Auto-calibrating Partially Parallel Acquisition) was recently proposed to allow a significant reduction in imaging time or an increase in the spatial resolution.

Purpose: The purpose of this work is to optimize GRAPPA and to do both qualitative and quantitative comparisons between the conventional and accelerated images under the same imaging time.

Methods: Coronary artery imaging using ECG triggered, breath-hold, segmented 3D SSFP was performed on a 1.5T Siemens Sonata (Erlangen, Germany) (Deshpande et al., 2001). LAD (Left Anterior Descending) or RCA (Right Coronary Artery) data were acquired in seven healthy volunteers. The imaging parameters were: TR/TE/flip angle = (3.4–3.7) ms/(1.3–1.5) ms/70°, FOV = (200–225) × (340–380) mm^2, data acquisition matrix = 124 × 512, number of lines/heartbeat = 31, total imaging time = 18–20 sec, number of partitions = 6 (interpolated to 12), slice thickness = 3 mm (interpolated to 1.5 mm). Eight coils were used at anterior and posterior positions. Each volunteer was scanned twice by conventional sampling and accelerated sampling with a factor of 2 under the same imaging time.

Optimizing GRAPPA: Sixteen phase encoding liens in the central k-space were sampled at the Nyquist rate, while the outer k-space is undersampled by outer reduction factor (ORF) of 2. The coil weights are extracted using the auto calbration signal (ACS) lines in the central k-space (Griswold et al., 2002). Five different sliding blocks over all coils are employed to yield multiple reconstructions for a missing line. The missing line is reconstructed by a weighted average based on goodness of fitness for ACS lines (Griswold et al., 2002). In this work, each coil k-space is segmented along the frequency encoding direction. The GRAPPA (Griswold et al., 2002) is performed segment by segment.

Image Quality Analysis: Two images with GRAPPA and without GRAPPA were presented to two of the authors, and then visually graded according to the delineation of vessel. Scoring was on a 4-point scale: 1) poor (markedly blurred); 2) good (moderately blurred); 3) very good (mildly blurred); 4) excellent (sharply defined).

Image quality was evaluated quantitatively by measuring SNR, vessel sharpness, and vessel diameter (Steen et al., 2001). A two-tailed t-test with a P value of 0.05 was used.

Results: The images reconstructed by GRAPPA with accelerated sampling showed higher visual rating than those by conventional sampling as shown in Table 1. Mean SNR was decreased 36% by accelerated sampling, while the sharpness of vessel was increased 24 %. The accelerated sampling did not reduce the diameter of vessel. Figure 1 shows two RCA images between conventional and GRAPPA reconstruction.

Conclusions: Coronary arteries have been successfully demonstrated with higher sharpness using the self-calibrating GRAPPA under the same imaging time despite SNR loss. The vessel was also better delineated with GRAPPA. This technique is promising for high

Table 1. Comparison of images reconstructed by conventional and accelerated sampling.

	Visual rating	Mean SNR	Sharpness (1/mm)	Diameter (mm)
No GRAPPA	2.9±0.53	12±1.9	0.79±0.077	2.7±0.57
GRAPPA	3.7±0.47*	7.7±1.2*	0.98±0.11*	2.5±0.48

*P<0.05, indicating significant differences.

Copyright © Marcel Dekker, Inc. All rights reserved.

ORDER REPRINTS

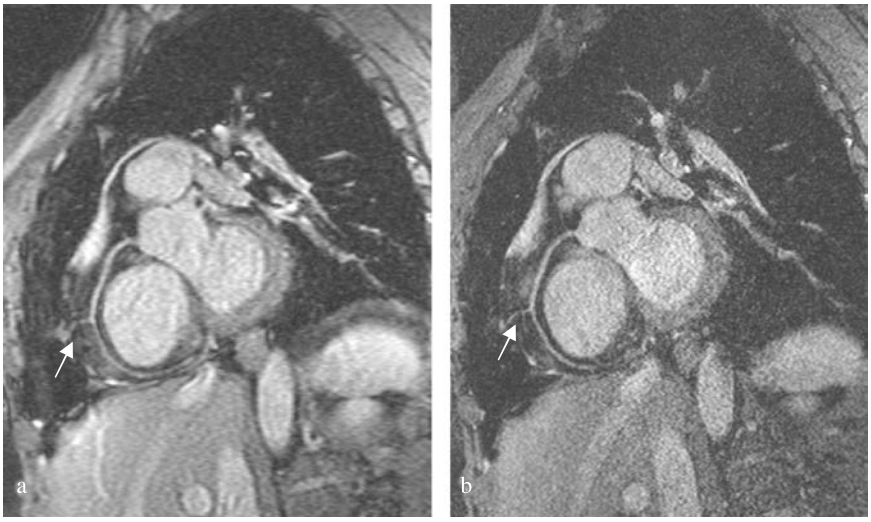

Figure 1. RCA images reconstructed by: (a) conventional sampling and (b) accelerated sampling with GRAPPA. Note the better delineation and higher sharpness of vessel. Vessel branch (arrow) is clearly delineated with GRAPPA.

resolution coronary MRA. Higher acceleration may be feasible at 3T due to significant signal gain.

REFERENCES

Deshpande, et al. (2001). *MRM* 46:494–502.
Griswold, et al. (2002). *MRM* 47:1202–1210.
Steen, et al. (2001). *JMRI* 13:301–307.

544. Cine MRI of Myocardial Mass at End-Diastole and End-Systole

Cory Swingen, Ph.D., Xiaoen Wang, M.D., Michael Jerosch-Herold, Ph.D. *Radiology, University of Minnesota, Minneapolis, MN, USA*.

Introduction: The evaluation of cardiac mass is an important indicator for the prognosis and diagnosis of various forms of congenital and acquired heart disease. Accurate and reproducible values of myocardial mass are also an important marker for the quantitative evaluation of pharmacological responses through serial assessments of the left ventricle (LV). Many studies in human volunteers and patients have suggested there is a significant difference between the myocardial mass at end-diastole (ED) and end-systole (ES). This has raised the hypothesis that the myocardial tissue is compressible, however other studies have indicated that LV mass is preserved throughout systole and diastole.

Purpose: The aim of this study was to examine the difference in the myocardial mass between end-diastole

Figure 1. Set of TrueFISP slices using the 3D analysis protocol with co-registered long- and short-axis images (3 of 6 short-axis images shown for clarity) with the calculated 3D model of the LV (epicardial surface in yellow, endocardial surface in red).

Copyright © Marcel Dekker, Inc. All rights reserved.

ORDER REPRINTS

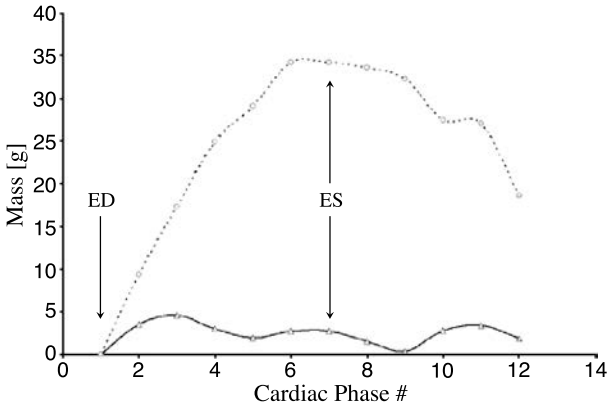

Figure 2. Example showing the variation in LV mass throughout the cardiac cycle in 2 subjects. The subject analyzed using the 3D method is shown by the solid line while the subject analyzed with the 2D technique is shown with a dashed line. All mass values offset by the ED mass.

and end-systole using a steady-state precession gradient-echo cine sequence and two different analysis techniques—a widely utilized 2D analysis technique involving only short-axis images and a newly developed robust 3D method incorporating both long- and short-axis views of the LV.

Methods: 44 human subjects were scanned in a 1.5-T clinical scanner. Contiguous short-axis slices were acquired from base to apex during repeated breath-holds in a group of 20 subjects for a 2D retrospective analysis. The remaining subjects were prospectively imaged using the same pulse sequence with view sharing of the phase encodings, to acquire 2 slices per breath-hold. In this fashion, 2 long-axis images were acquired followed by 4–6 short-axis images in 24 subjects suitable for a newly developed 3D analysis method (Figures 1 and 2).

Results: No significant variance in the myocardial mass was found (mean difference = 0.1% ± 9.1%, $p = 0.8764$) between end-diastole (ED) and end-systole (ES) using the 3D approach while the 2D technique yielded significantly larger values for the LV mass at ES than ED (mean difference = 14.7% ± 16.8%, $p < 0.0001$) (Table 1).

Conclusions: Our findings support the notion that myocardial mass is incompressible and any discrepancies between muscle mass at ED and ES during analysis can be attributed to acquisition and analysis procedure. A 3D analysis as proposed offers distinct advantages for avoiding problems characteristic to 2D analysis due to slice misregistration and systolic motion.

545. The Visual Assessment of LVEF and Wall Motion Abnormalities by CVMRI: Comparison with 16-Slice Multidetector Computed Tomography (MDCT-16)

Erasmo De La Pena-Almaguer,[1] Ramiro Flores-Ramirez, M.D.,[2] Jose R. Azpiri-Lopez, M.D., FSCAI,[2] Felipe Gonzalez-Camid, M.D.,[2] Rafael Zamarripa-Morales, RT-MRI,[1] Enrique Ponce de Leon-Martinez, M.D.,[2] Javier Loera-Torres, RN(ICU),[2] Jose L. Assad-Morell, M.D., FACC.[2] [1]*Cardiovascular Imaging, Christus-Muguerza Medical Center, Monterrey, Nuevo Leon, Mexico*, [2]*Cardiovascular Medicine, Christus-Muguerza Medical Center, Monterrey, Nuevo Leon, Mexico*.

Introduction: The evaluation of left ventricular ejection fraction (LVEF), and segmental wall motion abnormalities (WMA) using a semi-quantitative (i.e. visual) approach has been shown to be adequate with methods such as echocardiography, contrast and radioisotopic ventriculography. Due to its high temporal resolution, Multislice CT obtains anatomical information of the coronary tree along with LV function parameters, however,the value of this additional information is still unclear when assessing ischemic heart disease.

Purpose: To compare the performance of MDCT-16 in the evaluation of LVEF and WMA as compared with MRI, using cine MRI (SSFP) as the standard of reference.

Methods: MRI—Fifteen Patients were scanned in a 1.5 T magnet optimized for cardiovascular applications. Using a gated steady state fast precession sequence (SSFP, 10 mm slice thickness, Flip Angle 45, FOV 36 cm., NEX 1, Frequency 256, phase 128, Partial FOV

Table 1. LV mass parameters (mean ± SD) with 95% confidence intervals.

Technique	ED mass (g)	ES mass (g)	*p*-Value
3D ($n=24$)	124.03 ± 27.45 (112.43–135.63)	124.18 ± 27.88 (112.40–135.96)	0.87
2D ($n=20$)	129.01 ± 27.45 (111.57–146.42)	150.46 ± 47.29 (128.32–172.59)	<0.0001

Copyright © Marcel Dekker, Inc. All rights reserved.

ORDER REPRINTS

0.75, 16 VPS), 3 short axis (SAX) and two and four chamber views (2–4CHV) cines were obtained. LVEF was obtained from 6 to 8 SAX. MDCT-16—Patients were scanned with a GE Lightspeed-16 scanner with the following settings: Prospective gating, Cardiac burst, gantry rotation 0.5 sec., gantry tilt 0, Slice thickness 1.25 mm, 1.25 mm interval, speed 6.0, pitch 0.3:1., SFOV Large, Kv 120, mA 380. After 80 cc of IV contrast, the volume of interest was acquired and 6 to 8 slices of the left ventricle were reconstructed off-line as in MRI. LV was divided into a 17 segments validated model and wall motion scored with 1 = normal, 2 = hypokinetic, 3 = akynetic and 4 = diskynetic. Wall motion score index (WMSI) was calculated by adding the score of each segment and dividing it by the number of segments assessed. Both studies were analyzed by 2 independent blinded observers with an inter and intra-observer correlations for both of $\geq 94\%$. Comparisons were analyzed using a paired Student ''t'' test and correlations using linear regression, and differences considered significant if $p \geq 0.05$.

Results: There was good correlation in the measurement of LVEF by CT and MRI ($r = 0.79$, $p < 0.0001$), but LVEF was significantly lower by CT ($48 \pm 15\%$ vs. $54 \pm 20\%$, $p = 0.03$). Segmental wall motion was similar when assessed by both techniques; however there was a trend for a lower score in the inferoseptal (1.13 ± 0.35 vs. 1.46 ± 0.74, $p = 0.09$), anteroapical (1.53 ± 0.91 vs. 1.93 ± 1.22, $p = 0.08$) and septal–apical (1.13 ± 0.35 vs. 1.60 ± 1.05, $p = 0.06$) segments with CT than with MRI, respectively. There was no difference in WMSI among studies (MRI 1.42 ± 0.59, CT 1.44 ± 0.47).

Conclusions: This findings suggest that apical wall motion may be overestimated by CT. LVEF when visually assessed by CT is lower than that measured by the more precise MRI method. Although, there is a good correlation between techniques, this finding may prove important if sequential LV function studies for a single patient are needed and can have profound impact when assessing patients with ischemic heart disease affecting the apical region.

546. Three-Dimensional MR Technique for the Imaging of Myocardial-Delayed Hyperenhancement: A Comparison with Two-Dimensional Technique

Servet Tatli, M.D.,[1] Kelly H. Zou, Ph.D.,[1] Mark Fruitman, M.D.,[1] Hammond Glenn Reynolds, Ph.D.,[2] Thomas K. Foo, Ph.D.,[2] Raymond Kwong, M.D.,[3] E Kent Yucel, M.D.[1] [1]*Radiology, Brigham and Women's Hospital, Harvard Medical School, Boston, MA, USA*, [2]*Applied Science Laboratory, GE Medical Systems, Milwaukee, WI, USA*, [3]*Cardiology, Brigham and Women's Hospital, Harvard Medical School, Boston, MA, USA*.

Introduction: In coronary artery disease, the distinction of viable and non-viable myocardium is important to guide management of the patient. Delayed hyperenhancement (MDE) of the infarcted tissue with Gd-DTPA has been emerging as a practical and powerful technique to detect myocardial infarction. The standard application uses a two-dimensional (2D) technique, which is post Gd-DTPA, cardiac-gated, breath-hold, T1-weighted sequence with an inversion recovery prepulse. Many end-expiratory breath-holds, variation in inversion time of myocardium during the study and low signal-to-noise ratio are shortcomings of the 2D technique. Recently, three-dimensional (3D) technique was also applied to MDE imaging. Shorter total acquisition time, fewer total breath-holds and higher signal-to-noise ratio are theoretical advantages of the 3D over the 2D technique.

Purpose: The purpose of this study is to compare the 2D and 3D techniques in the detection of myocardial infarction and in the grading transmural extent.

Methods: Twelve patients with clinically proven myocardial infarction were included prospectively. Short axis images were obtained for all patients with 2D and 3D techniques using cardiac-gated, breath-hold, T1-weighted sequence with an inversion recovery pulse following Gd-DTPA at 0.2 mmol/kg. Representative slices from the base, mid and apical levels of the heart were randomized. Two readers (R1 and R2) divided the slices according to the 16-segment modal, identified the areas of hyperenhancement, and graded transmural extent. Signal intensity of most intense portion of the hyperenhanced myocardium, normal myocardium, blood pool and noise were also measured. Contrast-to-noise, signal-to-noise, and signal intensity ratios (CNR, SNR and SIR, respectively) were derived for each technique and were compared using Student's t-test. Intra and inter-observer agreement were measured by percent agreement.

Results: All infarcts visualized on the 2D scans were demonstrated by 3D images. The mean total imaging time was 14 minutes for 2D versus 24 seconds for 3D. The whole heart can be imaged in one breath-hold with the 3D compared to 15 breath-holds in 2D. From 2D to 3D, statistical significant difference were

Copyright © Marcel Dekker, Inc. All rights reserved.

ORDER REPRINTS

found in the mean CNR (11.65 versus 56.59; $p = 0.002$), SNR (18.03 versus 76.90; $p = 0.001$) and SIR (3.6 versus 6.36; $p = 0.05$). Intra-observer agreement between 2D and 3D were R1: 74% and R2: 90%. Inter-observer agreements between the readers were 2D:77% and 3D:79%.

Conclusions: Images with 3D technique have less noise, and more signal. Mean CNR, SNR and SIR are significantly increased in 3D technique compared to conventional 2D technique.

547. Real-Time Cardiac MRI at 3T and 1.5T: SNR and CNR Comparison

Krishna S. Nayak,[1] Charles H. Cunningham, Ph.D.,[2] Juan M. Santos,[2] John M. Pauly, Ph.D.[2] [1]*Electrical Engineering, University of Southern California, Los Angeles, CA, USA*, [2]*Electrical Engineering, Stanford University, Palo Alto, CA, USA*.

Introduction: Real-time cardiac and coronary MRI at 1.5T is relatively signal starved, and the 3T platform has become attractive for its immediate factor of two increase in magnetization. Cardiac imaging at 3T is, however, both subtly and significantly different from imaging at 1.5T because of increased susceptibility artifacts, differences in tissue relaxation, and RF homogeneity issues.

Purpose: The purpose of this work was to implement real-time cardiac MRI sequences on 3T and 1.5T platforms, to evaluate SNR efficiency and CNR at both field strengths, and to make critical observations about image quality.

Methods: Spiral gradient echo real-time sequences were implemented on 3T and 1.5T GE Signa scanners. A body coil was used for RF transmission and 5-inch surface coil was used for reception in all studies. The pulse sequences consisted of spectral–spatial excitations followed by a spiral readouts and gradient spoilers. At 1.5T, a 7 ms excitation and 16 ms readouts resulted in a 28 ms TR. Four interleaves were used to form images every 112 ms. At 3T, the readouts were shortened to 8 ms to maintain comparable off-resonance artifacts, and the excitation was shortened to 3.6 ms, taking advantage of the doubled fat–water frequency difference at 3T. The TR was 15 ms, and eight interleaves were used to form images every 120 ms. Both protocols achieve 1.5 mm in-plane resolution over a 20 cm FOV, with a 5.52 mm calibrated and measured slice thickness. The excitation achieved 32 dB of lipid suppression. Complete images were reconstructed and displayed at 24 frames/s using a sliding window.

Table 1. SNR and CNR measurements at 3T and 1.5T.

	3T	1.5T
MID SYSTOLE		
SNR_{blood}	42.7 ± 4.5	27.3 ± 0.2
LATE DIASTOLE		
SNR_{blood}	57.6 ± 1.3	22.1 ± 1.1
$SNR_{myocardium}$	24.7 ± 3.6	12.5 ± 2.5
CNR	33 ± 4.8	9.6 ± 1.6

Blood signal level was computed from single timeframes from mid-systole, by averaging the pixels in a region of interest in the left ventricle. The choice of mid-systole was intended to give signal from blood under similar conditions as in real-time coronary artery imaging, i.e. in-flow enhancement and full oxygenation. Blood-myocardium contrast was computed from single times frames from late-diastole as the difference between average LV blood signal and average septal myocardium signal in regions of interest. In all cases, noise levels were computed by taking the standard deviation in images acquired with identical slice orientations, but with the RF pulse turned off.

Results: Nine healthy volunteers were scanned at 3T, three of which were also scanned at 1.5T. Sample short-axis images from one subject at both field strengths and sample real-time coronary artery images from two other subjects are shown in the attached figure. Measurements of SNR and CNR at 3T and 1.5T are summarized in the attached Table 1.

Real-time imaging at 3T showed a 53% improvement in blood SNR efficiency, and a 249% improvement in blood-myocardium CNR. The pure SNR improvement may be attributed to increased magnetization. The greater CNR improvement is likely also the result of better saturation of the myocardium during continuous imaging, due to the shorter TR and longer myocardium T1 at 3T.

One noted difference is that sensitivity of 5-inch surface receive coils varies with field strength and body size. In general, the coil falloff is faster at higher field which reduces signal from the lateral wall at 3T. The shortened readouts at 3T mitigate the increase in susceptibility off-resonance, and no additional artifacts were observed. The new 3.6 ms spectral–spatial excitation produced excellent fat suppression which can be seen in the real-time coronary images (Fig. 1).

Conclusions: We have demonstrated robust real-time cardiac imaging at 3T using a commercial, whole body system. An estimated 53% increase in SNR efficiency (compared with 1.5 Tesla) is achieved, with reasonable management of susceptibility effects and excellent fat suppression. Real-time cardiac imaging at

Copyright © Marcel Dekker, Inc. All rights reserved.

ORDER REPRINTS

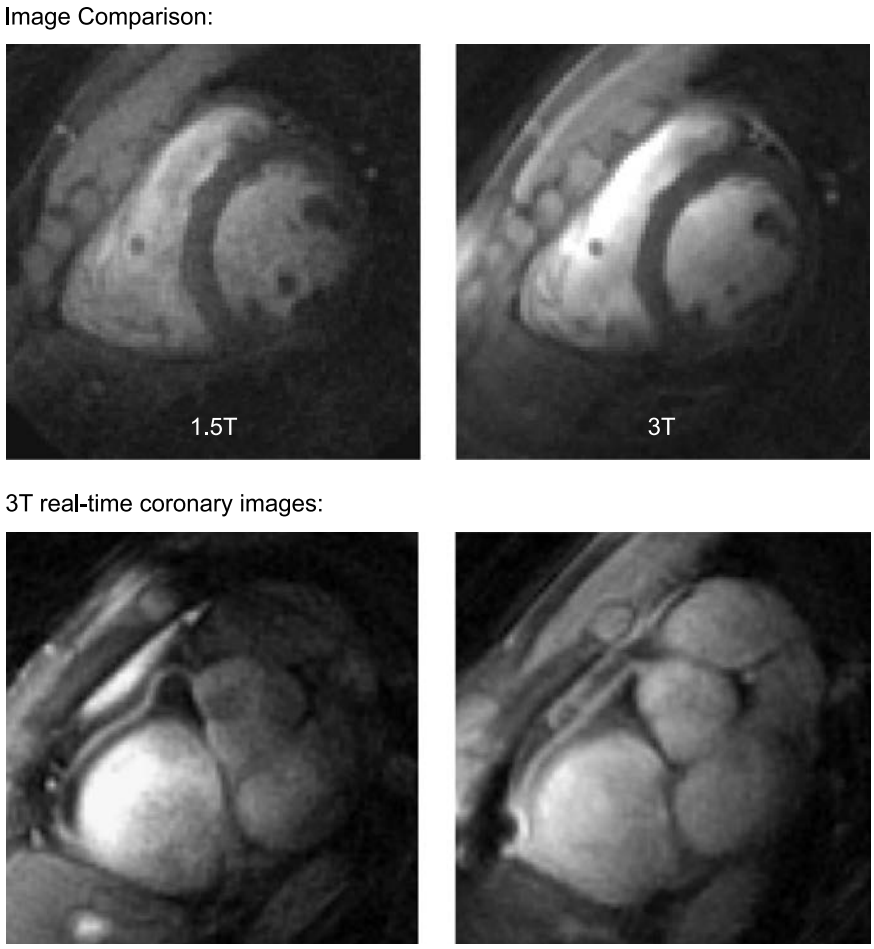

Figure 1.

3T is feasible, and is advantageous due to the increased SNR and increased blood-myocardium contrast.

548. Respiratory Motion of the Heart: Translation, Rigid Body, Affine, or More?

Shechter Guy,[1] Cengizhan Ozturk, M.D., Ph.D.,[1] Jon R. Resar, M.D.,[2] Elliot R. McVeigh, Ph.D.[1] [1]*NHLBI, NIH, DHHS, Bethesda, MD, USA*, [2]*Johns Hopkins University, Baltimore, MD, USA*.

Introduction: Three dimensional MR coronary imaging requires scan times longer than possible breath-hold durations. Respiratory motion compensation can be used to increase scan efficiency, reduce exam duration, and improve image quality. Previous studies of respiratory motion of the heart using MRI have been limited by the use of breath-holding, the use of 2D imaging for real-time acquisitions, or data averaging over multiple breathing and cardiac cycles for 3D free breathing studies (Danias, 1999; Manke, 2002; McLeish, 2002; Wang, 1995).

Purpose: To characterize the motion and deformation modes of the coronaries during spontaneous tidal breathing. X-ray imaging provides the high temporal and spatial resolution images necessary for this study. The motion is analyzed in the context of three 3D MR motion correction techniques: 1) translation; 2) rigid body (translation+rotation); and 3) affine (rigid body+shear+scale).

Methods: Biplane x-ray coronary angiograms were obtained in nine patients. We captured natural respiratory motion by not giving patients any breathing instructions. A three dimensional+time model of the coronary arteries was generated from the cine-angiograms using stereo reconstruction and automatic motion tracking techniques (Shechter, 2003).

Diastasis images nearest to end-inspiration (EI) and end-expiration (EE) were identified in each

Copyright © Marcel Dekker, Inc. All rights reserved.

ORDER REPRINTS

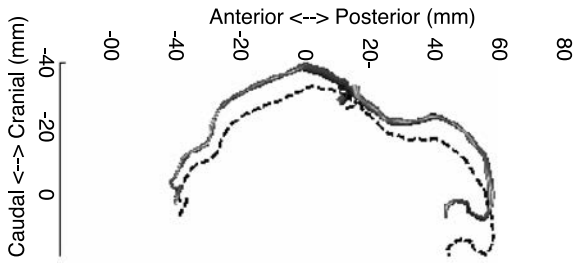

Figure 1. Position of the left coronary tree at EE (solid model) and EI (dotted lines) for patient P2. (*View this art in color at www.dekker.com.*)

dataset. Displacement of the diaphragm as seen in the images provided a measure of respiratory phase. To quantify the magnitude of the respiratory motion, a 3D RMS distance (e_{3D}) was computed between the EI and EE coronary models for each patient.

The two trees were registered to each other using each of the 3D motion models and residual errors (e_T, e_R, e_A) were computed. The residual errors are the e_{3D} between the two coronary models after optimal registration.

Results: The left coronary tree was studied in nine patients. The mean length of the reconstructed left coronary tree was 26±6 cm. The selected images spanned 56–99% (mean = 82%) of the respiratory cycle. The maximum difference in cardiac phase between an EE–EI image pair was 2.2% (22 ms for a heart rate of 60 beats/minute). This suggests that the motion we measured is not due to the cardiac contraction (Figure 1).

The mean e_{3D} was 6.1±1.8 mm (range = 3.8–9.7 mm). 3D translation accounted for 66±19% of the motion (range = 33–83%); the rigid body transformation for 81±15% (range = 46–93%) of the motion; and the affine deformation for 86±14% (range = 51–94%) of the motion (Table 1).

Table 1. Results for the left coronary tree.

Patient	Percent of respiratory cycle (%)	e_{3D} (mm)	e_T (mm)	e_R (mm)	e_A (mm)
P1	78	4.7	0.8	0.7	0.4
P2	56	6.2	4.1	1.9	1.4
P3	63	5.7	3.6	3.1	2.8
P4	84	7.7	3.1	1.0	0.6
P5	80	3.8	1.1	0.4	0.3
P6	93	9.7	1.7	1.1	0.7
P7	90	4.6	1.3	1.0	0.6
P8	97	6.9	1.2	0.5	0.4
P9	99	5.2	1.2	0.6	0.4

The majority of the tidal respiratory motion can be explained by a 3D translation. However, correcting the translation alone reduced $e_{3D} \leq 1$ mm in only 1/9 patients. Using a rigid body transformation, $e_{3D} \leq 1$ mm in 6/9 patients. Affine correction provided $e_{3D} \leq 1$ mm in 7/9 patients.

The respiratory motion of the left coronary tree in two patients demonstrated significant local deformations, such that none of the tested motion models was able to reduce $e_{3D} \leq 1$ mm.

Conclusions: Tidal respiratory motion of the coronary arteries was measured from x-ray angiograms. In 6 of 9 patients, a rigid body transformation was sufficient for explaining the motion of the coronary tree (3D RMS error ≤ 1 mm) over a significant portion (mean = 82%) of the tidal respiratory cycle. The more complex affine deformation model adds one more patient to this group.

REFERENCES

Danias, P. (1999). *AJR* 172:1061–1065.
Manke, D. (2002). *JMRI* 15:661–671.
McLeish, K. (2002). *IEEE TMI* 21(9):1142–1150.
Shechter, G. (2003). *IEEE TMI* 22(4):493–503.
Wang, Y. (1995). *MRM* 33(5):713–719.

549. Validation of a Single Breath Hold Three-Dimensional Projection Reconstruction Steady-State Free Precession Magnetic Resonance Imaging Method for Cardiac Function Evaluation

Daniel B. Ennis, B.S.,[1] Mushabbar Syed, M.D.,[2] Pratik Rohatgi,[2] Elliot R. McVeigh, Ph.D.,[2] Andrew E. Arai, M.D.,[2] Dana C. Peters, Ph.D.[2] [1]*Biomedical Engineering, John Hopkins Univeristy, Baltimore, MD, USA*, [2]*National Heart, Lung, and Blood Institute, National Institutes of Health, Bethesda, MD, USA*.

Introduction: Steady-state free precession (SSFP) imaging has emerged as the clinical magnetic resonance (MR) standard for characterizing cardiac function. Most techniques use two-dimensional (2D) Cartesian encoding and require repeated breathholds for full cardiac coverage, resulting in ~7–12 minute exam

Copyright © Marcel Dekker, Inc. All rights reserved.

ORDER REPRINTS

Table 1.

	FOV	Slice thickness	Acquisition matrix	Temporal resolution	Breathhold
3D PR SSFP	32 cm	8–10 mm	$192 \times 32 \times 12$–14	60–70 ms	24 heartbeats
2D SSFP	32 cm	8 mm, skip 3 mm	192×160	40–50 ms	12 heartbeats

time. In order to reduce the total time a three-dimensional (3D) projection reconstruction steady-state free precession magnetic resonance imaging technique (3D PR SSFP) was developed and validated.

Purpose: The purpose of this project was to validate single breathhold 3D PR SSFP as a suitable alternative to standard multi-breathhold 2D SSFP techniques for characterizing left ventricular end systolic volume (LVESV), end diastolic volume (LVEDV), ejection fraction (LVEF), and myocardial mass (LVMM).

Methods: Informed consent was obtained from ten healthy normal volunteers. Subjects were imaged using a 3D PR SSFP (Peters et al., 2002) cardiac imaging technique, with 45° flip angle, ±125 kHz bandwidth, TR/TE = 3.4/1.5 ms, zero-filling, and UNFOLD (Madore et al., 1999). Projections were acquired for in-plane resolution, and phase-encodings were used to resolve the slice dimension. Only one 24 heartbeat breathhold was required to obtain entire LV coverage. 2D SSFP was also used to evaluate LV function. Each 2D slice required a 12 heartbeat breathhold, resulting in a total exam time of 7–12 minutes. All MR imaging was performed using a GE Excite 1.5T Signa scanner and a four element cardiac phased-array coil, with ECG gating. The imaging parameters are given in Table 1. To compare the 3D PR SSFP technique to the 2D SSFP technique LV epicardial and endocardial contours were drawn by a trained observer using custom computer software and reviewed by a cardiologist. ED and ES contours were used to quantify LVESV, LVEDV, LVEF, and LVESM. A P-value of <0.05 was considered significant.

Results: 3D PR SSFP generally produced good quality cine MRI with acceptable, albeit noticeable, radial artifacts that did not preclude qualitative or quantitative analysis. Qualitatively the 2D SSFP technique yielded images with greater contrast and reduced artifact. There was a tendency toward reduced contrast between blood and myocardium near the apex and between myocardium and lung.

3D PR SSFP vs. 2D SSFP: Measurements of LVESV, LVEDV, LVEF, and LVESM by 3D PR SSFP and 2D SSFP were statistically similar (P>0.17, P>0.10, P>0.62, P>0.09 respectively) (Table 2). The correlation coefficient between 3D and 2D measures of LV volumes (end diastolic and end systolic) was R = 0.99 and the bias was +4.4 mL (3D–2D). The correlation coefficient between 3D and 2D measures of LV end systolic mass was R = 0.98 and the bias was +4.1 g (3D–2D).

Inter-Observer Variability: There were significant inter-observer differences for the 3D PR SSFP measurements (Table 3). There was a bias for one observer to under estimate LVEDV by 11 mL (6.6%), over estimate LVESM by 7.8 grams (7.5%), and under estimate EF by 2.9%. There were no clinically significant differences between observers' 2D SSFP measurements.

Conclusions: The 3D PR SSFP imaging technique is a promising alternative to the clinical 2D SSFP technique for quantifying cardiac function. Although there were some statistically significant inter-observer differences for the 3D PR SSFP measurements, the magnitude of these errors is relatively small compared with the ranges encountered clinically. 3D PR SSFP measures of LVESV, LVEDV, LVEF, and LVESM did not prove to be statistically different from the 2D SSFP technique. To our knowledge, this is the first reported validation of a single breath-hold 3D cardiac function evaluation technique.

Table 2. Summary of 3D PR SSFP and 2D SSFP functional measures.

	3D PR SSFP	2D SSFP	P-value
LVESV (mL)	64±13	61±14	0.17
LVEDV (mL)	172±40	166±36	0.10
LVEF (%)	62± 3	63± 4	0.62
LVESM (g)	102±33	98±31	0.09

Table 3. Summary of inter-observer differences measurements from 3D PR SSFP.

	Observer #1	Observer #2	P-value
LVESV (mL)	64±13	64±13	0.912
LVEDV (mL)	172±40	161±35	0.004
LVEF (%)	62±3	59±5	0.045
LVESM (g)	102±33	110±31	0.005

Copyright © Marcel Dekker, Inc. All rights reserved.

ORDER REPRINTS

REFERENCES

Madore, B., Glover, G. H., Pelc, N. J. (1999). *Magn. Reson. Med.* 42:813–828.

Peters, D. C., Ennis, D. B., McVeigh, E. R. *ISMRM 2002*. Honolulu, Hawaii.

550. Rapid, Accurate Detection of Myocardial Infarcts Using Phase-Sensitive Inversion–Recovery: Comparison to Standard IR-Flash Methods

Edwin Wu, M.D.,[1] Daniel C. Lee, M.D.,[1] Orlando Simonetti, Ph.D.,[2] YiuCho Chung, Ph.D.,[2] Francis J. Klocke, M.D.,[1] Nirat Beohar, M.D.,[1] Robert O. Bonow, M.D.,[1] Thomas A. Holly, M.D.[1] [1]*Department of Medicine, Division of Cardiology, Northwestern University, Chicago, IL, USA*, [2]*Siemens Medical Systems, Chicago, IL, USA*.

Introduction: Prior studies have shown that the inversion–recovery gradient-echo pulse sequence can accurately delineate the extent and size of myocardial infarction. Careful adjustment of the inversion–time (TI) throughout the cardiac examination is paramount to obtain appropriate images due to the dynamic wash-in and wash-out of gadolinium contrast agent. A recently developed technique utilizes a phase-sensitive image reconstruction to visualize hyperenhanced (HE) myocardium independent of the operator experience.

Purpose: Demonstrate that the area of HE seen with the phase-sensitive image reconstruction technique correlates with traditional inversion–recovery technique.

Methods: Cardiac MRI studies were performed on 8 pigs that underwent experimental myocardial infarction by a 90 minute balloon occlusion of the proximal circumflex coronary artery. In addition, 20 patients also underwent a research cardiac MRI evaluation post MI.

Delayed contrast-enhanced images were obtained using a phase-sensitive, inversion–recovery, gradient-echo sequence (PSIR) acquired 10–15 minutes after IV administration of gadolinium (0.1 to 0.2 mmol/kg). Traditional inversion–recovery technique (IR-FLASH) was also acquired during the same breath hold. The TI was dynamically changed (250–350 ms) during the examination to appropriately ''null'' normal myocardium. Images were transferred to a desktop workstation, and HE areas in multiple short axis views encompassing the entire left ventricle were hand planimetered using NIH Image. Brightness and contrast were freely manipulated to provide the best contrast between nulled and HE myocardium.

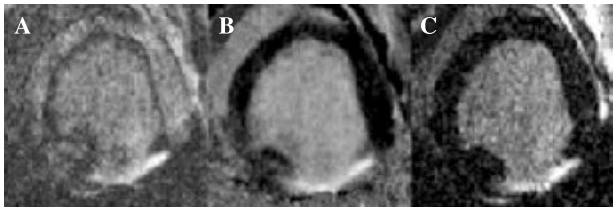

Figure 1. Three ceMRI short-axis images at the same image slice. IR-FLASH (A) with TI initially set incorrectly. PSIR (B) acquired during the same breath-hold with appropriate contrast between HE infarction and normal myocardium. (C) IR-FLASH image obtained with the TI set correctly.

Results: No studies were excluded due to poor image quality. In the 8 pigs studied, the amount of infarcted HE myocardium as measured by PSIR (mean, 11.8 ± 6.2 gm) correlated well with IR-FLASH (mean, 10.9 ± 6.1 gm) ($y = 1.0028x + 0.8926$, $R^2 = 0.9923$). The same correlation was true for the additional 20 human subjects ($y = 0.9294x + 1.1187$, $R^2 = 0.9233$). The mean HE by PSIR was 23.1 ± 14.6 gm and by IR-FLASH was 22.5 ± 14.2 gm ($p = NS$). When the TI was set incorrectly, PSIR imaging quality remained similar to the correctly acquired IR-FLASH (see Figure 1).

Conclusions: Contrast-enhanced MRI utilizing a phase-sensitive, inversion–recovery sequence is accurate in detecting areas of MI in both animal model and human subjects. Utilizing a technique that is insensitive to changes in TI allows for quicker and accurate image acquisitions.

551. Registration and Spatial Normalization of Cardiac MR Images Using HAMMER

Harold Litt, M.D-Ph.D., Dinggang Shen, Ph.D., Christos Davatzikos, Ph.D. *Department of Radiology, University of Pensylvania Medical Center, Philadelphia, PA, USA*.

Introduction: Studies of imaging findings associated with diseases may be aided by a process called spatial normalization. Resizing and registration of images so that structures have similar shape, size, and orientation to a predefined template allows data from subjects to be averaged to increase statistical power for analysis of differences between normal and pathologic states. In addition, the transformation map for a subject or group to the atlas is a descriptor of the variation from the

Copyright © Marcel Dekker, Inc. All rights reserved.

ORDER REPRINTS

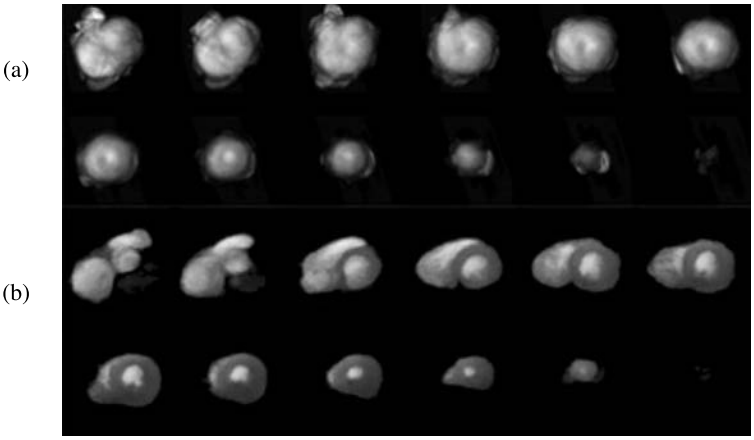

Figure 1. (a) Intensity-based registration Atlas. (b) HAMMER registration ATLAS.

atlas, allowing insights into structural or functional changes that are not visually apparent.

In neuroimaging, the Talairach atlas provides a standard template to which images are normalized prior to analysis (Talairach and Tournoux, 1998), however there is no agreed upon atlas for cardiac imaging. We have previously presented an atlas template for cardiac MR (Litt et al., 1999) calculated using an intensity-based registration algorithm (Woods et al., 1998). This is an automated process which operates on pixel intensities, without the need for manual methods such as contour tracing.

We have developed a new method for image registration without the problems of intensity based methods. Hierarchical Attribute Matching Mechanism for Elastic Registration (HAMMER) creates an attribute vector for each voxel in the data set that includes information about the voxel as well as elements that

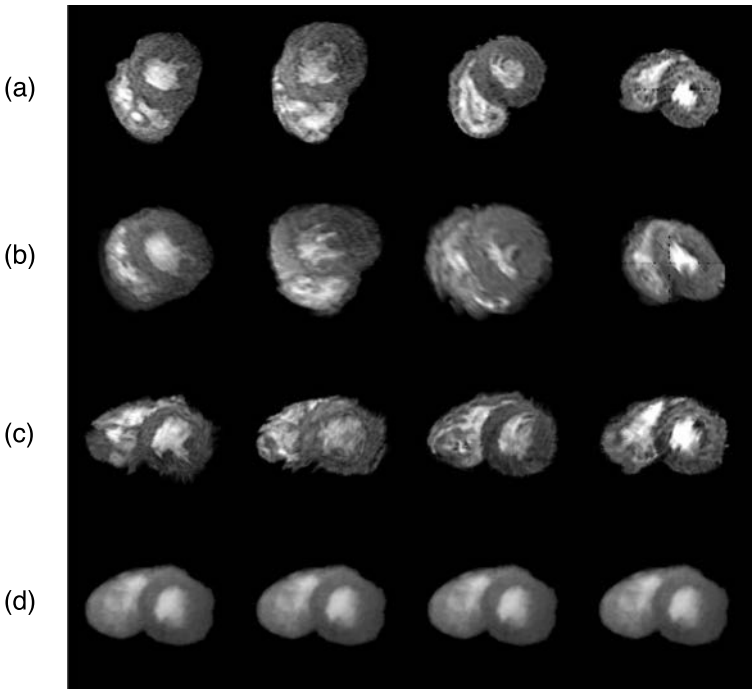

Figure 2. (a) Original data; (b) intensity-based registration; (c) HAMMER registration; (d) Atlas template.

Copyright © Marcel Dekker, Inc. All rights reserved.

ORDER REPRINTS

reflect the structure of the underlying anatomy (Shen and Davatzikos, 2002). The attribute vector, if rich enough, can distinguish between different parts of an image, e.g. most voxels within the myocardium look similar, but have different geometric relationships to the cardiac apex. This method has been applied to registration of MR imaging of brains and spinal lesions and prostate ultrasound images, displaying performance as good as human experts (Davatzikos et al., 2002; Shen and Davatzikos, 2003).

Purpose: To create an atlas template for cardiac MR imaging using the HAMMER method, and to compare the results with our previous template obtained using intensity-based registration.

Methods: Short axis cine GRASS images of the heart obtained at end-systole in 20 normal volunteers (mean age 39 years, range 21 to 79) were used. These were the same datasets used for the previous study. A linear transformation was applied first to minimize variability in orientation and overall size of the hearts. All subjects were then registered to a single subject using a version of the HAMMER algorithm adapted for lower resolution cardiac MR images. The atlas template was then created by averaging the 20 registered datasets.

Results: Figure 1(a) shows the atlas obtained by averaging the 20 subjects after HAMMER registration, demonstrating the superior performance of HAMMER compared to the atlas previously obtained using intensity based registration in Figure 1(b). Figure 2 compares registration results obtained with HAMMER versus intensity-based registration for selected subjects. Note the marked improvement in accuracy of the registration, even for subjects whose hearts differed in shape and orientation from the template.

Conclusions: Application of HAMMER resulted in markedly improved performance over the previous intensity-based registration for construction of a cardiac atlas template. Future work will include incorporation of higher resolution MR and CT datasets to improve the atlas, systematic analysis of the transformation maps for normal and abnormal hearts, and extension of HAMMER to 4-D datasets, which will allow generation of an atlas which represents the average structure *and* function of the heart.

REFERENCES

Davatzikos, C., Liu, D., Shen, D., Herskovits, E. H. (2002). *Radiology* Sep 224(3):919–926.

Litt, H. I., Axel, L., Blom, A. J. (1999). *Cardiovasc. Magn. Reson.* 1(4):370–371.

Shen, D., Davatzikos, C. (2002). *IEEE Trans. Med. Imaging* Nov 21(11):1421–1439.

Shen, D., Davatzikos, C. (2003). *NeuroImage* Jan 18(1):28–41.

Talairach, J., Tournoux, P. (1998). *Co-planar Stereotactic Atlas of the Human Brain*. Thieme: Stuttgart.

Woods, R. P., Grafton, S. T., Holmes, C. J., et al. (1998). *JCAT* 22:141–154.

552. Single Breath-Hold, 4 Dimensional, Fast Assessment of LV and RV Function Using Triggered, Real-Time, Steady-State Free Precession MRI in Heart Failure Patients: A Novel, Clinically Robust Protocol

Girish Narayan, M.D.,[1] Krishna Nayak, Ph.D.,[2] John Pauly, Ph.D.,[2] Bob Hu, M.D.[3] [1]*Cardiology, Stanford University, Stanford, CA, USA*, [2]*Electrical Engineering, Stanford University, Stanford, CA, USA*, [3]*Electrical Engineering and Cardiology, Stanford University and Palo Alto Medical Foundation, Palo Alto, CA, USA*.

Introduction: Accurate, reproducible quantitation of LV and RV volumes and function is important for the care of heart failure patients.However, existing techniques to perform this with MRI are not clinically robust in the heart failure population given the need for long acquisition times, requirement for multiple patient breath-holds, and sensitivity to arrhythmias. In addition, the need to obtain scout images, define scan planes, and use of multiple breath-holds render exisiting strategies susceptible to motion artifact and mis-registration.

Methods: We have developed a new real-time, spiral, steady state free precession (SSFP) strategy that achieves complete volumetric coverage of the RV and LV in a single breath-hold throughout the entire cardiac cycle. We compared this technique to the gold standard, multiple breath-hold, gated, segmented k-space strategy (FEISTA) in 20 patients with heart failure. In addition, we studied the inter-study variance of this technique using a single breath-hold versus multiple breath-holds.

Results: Image quality in all cases allowed excellent myocardial-blood border definition (see Figure 1: top, end-systole, bottom, end-diastole). The technique was highly concordant with the gold standard technique in the assessment of LVEDV ($r = 1.04$), LVESV ($r = 0.92$), RVESV ($r = 0.99$), RVEDV ($r = 1.16$), and

Copyright © Marcel Dekker, Inc. All rights reserved.

ORDER REPRINTS

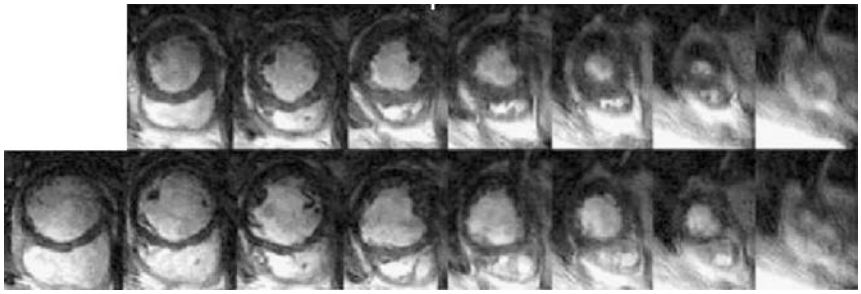

Figure 1.

LVMASS (1.19). In addition, data acquisition was only 9±2 seconds versus 312±41 seconds for the FIESTA technique. The inter-study variance of the real-time technique during free breathing was much larger than the single breath hold approach (mean of 17% vs. 8%).

Conclusions: Thus, real-time, spiral, single breath-hold SSFP allows *rapid and accurate* quantitation of RV and LV function in patients with heart failure. This technique provides a clinically robust, rapid modality to accurately assess cardiac function in heart failure patients using Cardiac MRI.

553. Two-Dimensional Delayed Enhancement Imaging with a Radial Acquisition

Dana C. Peters, Ph.D., Kraig V. Kissinger, Rene M. Botnar, Ph.D., Susan Yeon, M.D., Warren J. Manning, M.D. *Cardiology, Beth Israel Deaconess Medical Center, Boston, MA, USA*.

Introduction: Recently introduced cardiac magnetic resonance (CMR) delayed enhancement methods (Kim et al., 1999) for imaging infarct size provide accurate assessments of infarct morphology, as demonstrated by histology. These methods provide roughly $1-2\times1-2$ mm in-plane spatial resolution. To further increase spatial resolution requires increases in scan time (breath-hold length). Techniques exist for increasing resolution at constant speed, e.g. half-Fourier, SENSE, etc., but Cartesian undersampling is limited by fold-over artifacts. However, for radial acquisitions the undersampling artifact is less serious, and submillimeter resolutions have been obtained with undersampling factors of 3 or more (Peters et al., 2002a).

Purpose: We sought to study the feasibility of delayed enhancement imaging using a 2D radial acquisition, with the goal of achieving higher resolution images of infarction.

Methods: 2D delayed enhancement CMR was implemented with a radial acquisition. Imaging was performed roughly 20 minutes after injection of 0.1 mmol/kg gadolinium contrast agent in a swine model of ischemia/infarction. Imaging was performed on a Philips 1.5T Gyroscan ACS-NT (Philips Medical Systems, Best, NL) using a 5-element cardiac receiver coil. Scan parameters were: 2D Ecg-gated segmented gradient echo acquisition, FOV 20 cm, 96 Nr × 96 Np, TR/TE/θ = 3.8/1.2/15°, 2RR intervals between inversion pulses and a TI = 400 ms, 96 ms temporal window. 2D Cartesian images using delayed enhancement method were also obtained, with similar acquisition parameters.

Results: Figure 1 depicts a delayed enhancement image with a radial trajectory with a comparison image, both of equal spatial resolution. No infarct was observed. These initial images suggest that adequate myocardial suppression can be achieved as needed for delayed enhancement imaging General contrast between the myocardium and blood pool is similar for the two methods.

Conclusions: To our knowledge this is the first investigation of 2D delayed enhancement imaging with a radial acquisition, demonstrating its feasibility. Future work will focus on the use of higher readout resolution in conjunction with undersampling, to obtain

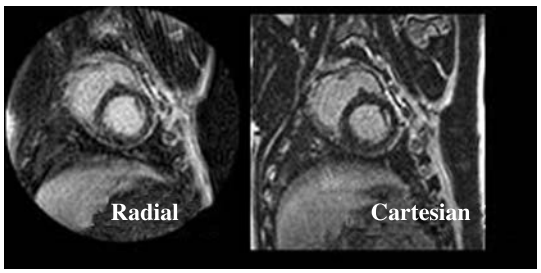

Figure 1.

Copyright © Marcel Dekker, Inc. All rights reserved.

ORDER REPRINTS

higher resolution images of infarcts, potentially valuable for providing new insights into the relation between infarct morphology and heart disease. Concern that the inversion pulses may provide less T1-weighting due to the radial k-space trajectory will be addressed by investigating k-space weighting methods. Additionally, the streak artifacts due to undersampling might be reduced by further suppression of signal from unwanted anatomy, or use of half-Fourier radials (Toropov et al., 2001).

REFERENCES

Kim, R. J., et al. (1999). *CIRC* 100:1992–2002.
Peters, D. C., et al. (2002a). *MRM* 43:91–101.
Peters, D. C., et al. (2002b). *MRM* 48:82–88.
Toropov, Y., et al. (2001). *ISMRM*, (1809).

554. Spatio-Temporal Guide Point Modelling for Fast Analysis of Four-Dimensional Cardiac Function

Brett R. Cowan, M.B.Ch.B.,[1] Thomas O'Donnell, Ph.D.,[2] Alistair A. Young, Ph.D.[3] [1]*Department of Medicine, University of Auckland, Auckland, New Zealand*, [2]*Siemens Corporate Research, Princeton, NJ, USA*, [3]*Department of Anatomy with Radiology, University of Auckland, Auckland, New Zealand.*

Introduction: Temporal characteristics of LV function are widely used in clinical practice for diagnosis, prognosis and evaluation of systolic and diastolic dysfunction. However, MRI studies typically result in large data sets containing hundreds of images, and correction of automated segmentation errors are often time consuming. A temporally coherent analysis method is required in which user interaction is real-time, efficient, intuitive and minimal.

Purpose: To extend a previously described method of interactive 3D modeling of LV function (Young et al., 2000) to a four-dimensional (space and time) analysis of LV motion. Information is incorporated from all slices and frames into a single coherent model of LV function, using a simple and intuitive user interface.

Methods: Fifteen patients with high risk for cardiovascular disease were scanned on a Siemens Sonata scanner. Prospectively gated true-FISP cine images were acquired with 6 equally spaced short axis slices from apex to base and 3 long axis slices at 60 degree increments about the central axis of the LV. Imaging parameters were TR/TE/flip/FOV = 18.5 ms/1.82 ms/70°/340 mm, slice thickness 6 mm, image matrix 256×208. There were 20–51 frames per slice depending on heart rate.

A mathematical model of the LV geometry for each frame was deformed under the influence of image-derived edge information and user-placed guide points. After each guide point edit, model parameters from all frames were fitted in time using Fourier basis functions with five harmonics. The time fit result was then used as the spatial prior for subsequent image processing and user editing. The system allowed user interrupts, so that the user was able to make several changes to the current frame before these changes were propagated to the surrounding frames.

A plot of volume and mass versus time was interactively updated to provide feedback to the user on the convergence of the modeling process. Convergence characteristics of mass and volume with respect to number of guide points and time taken were automatically logged for each case.

Results: Time-varying 3D LV function was quantified in 8±2 minutes on average per study (range 5–12 minutes), on a 3.0 GHz Pentium 4 PC. The models required 54±20 guide points per study (range 25–98), or ~2 guide points per frame. This compares favorably with previous methods (Young et al., 2000), which required ~6 min and 20–80 guide points to analyze just the two frames at end-diastole and end-systole. The time–volume graph could be updated interactively, giving the user instant feedback on the effect of each edit. A root mean squared (RMS) error was computed over all frames between the LV volume at each guide point edit and the final LV volume. The median RMS error over the 16 patients vs. number of guide points added is plotted in Figure 1.

Conclusion: Interactive real-time 4D guide point modeling provides fast analysis of cardiac function

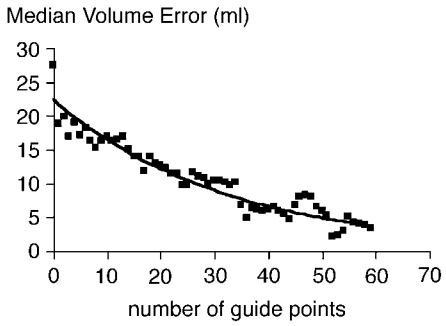

Figure 1. Median volume error per frame (RMS) vs. number of guide points added. Solid line shows the best fit exponential trend.

Copyright © Marcel Dekker, Inc. All rights reserved.

ORDER REPRINTS

throughout the cycle. Visual real-time feedback mass and volume vs. time allowed the user to determine how much effort is required for a desired accuracy.

REFERENCES

Young, M., et al. (2000). Left ventricular mass and volume: fast calculation with guide-point modeling on MR images. *Radiology* 216:597–602.

555. Rapid MR Determination of Cardiac Output by a Single Breath-Held Aortic Flow Quantification: Correlation with Standard Left Ventricular Contouring Technique

Mark Haupt, M.D.,[1] David Fieno, M.D., Ph.D.,[1] Samer Dibs, M.D.,[2] James Carr, M.D.,[1] Elizabeth Krupinski, Ph.D.,[3] Charles Fasanati, R.T.,[1] Nondas Leloudas, R.T.,[1] Frederick S. Pereles.[1] [1]*Radiology, Feinberg School of Medicine, Northwestern University, Chicago, IL, USA*, [2]*Cardiology, Feinberg School of Medicine, Northwestern University, Chicago, IL, USA*, [3]*Radiology, The University of Arizona, Tucson, AZ, USA*.

Introduction: The current accepted method for determining cardiac output with MR imaging uses post-image processing software to contour the left ventricle (LV) endocardial border in end-systolic and end-diastolic images from cine sequences. Despite new semi-automated software, this process is still time consuming and requires a great deal of subjectivity on behalf of the user.

Purpose: This study evaluates the use of the latest breath-held flow-quantification sequences across the aortic valve to determine cardiac output in comparison to LV contour methods.

Methods: Thirty normal volunteers (18 males, age 28 ± 11 years) underwent cardiac functional exams on a 1.5T Scanner (Siemens Sonata, Malvern, PA). Images for contour analysis were acquired in the short axis using a retrogated breath-held balanced gradient echo cine sequence. Parallel imaging (iPAT with GRAPPA) was implemented for faster acquisition times allowing two slices per breath-hold of 8–10 seconds. The volume of the left ventricle was captured in 6 mm slices with no gap from base to apex. Images for flow quantification analysis were acquired using a retrogated phase contrast velocity mapping sequence in a single slice across the aortic valve plane. Images from both protocols were loaded onto a 3D workstation with ARGUS image processing software (Siemens Leonardo, Malvern, PA). Volume analysis was performed on the short axis images to determine left ventricular end-diastolic and systolic volume, stroke volume, ejection fraction and cardiac output. Flow quantification analysis was performed on phase images acquired across the aortic valve. Results were compared using a Student's t-test.

Results: Cardiac output determined by aortic valve flow quantification analysis and contour analysis of short axis cine images were 5.43 ± 1.08 L/min and 5.81 ± 1.12 L/min respectively. The correlation between values across this study group was excellent ($r = 0.82$). There is a statistically significant difference between values ($p < 0.05$) with flow quantification consistently underestimating cardiac output by approximately 8%.

Conclusions: Due to very high agreement between techniques, retrogated flow-quantification analysis across the aortic valve may be a useful substitute for short axis cine contour analysis yielding significant time-savings. This may be especially relevant in cases of technically challenging patients who cannot tolerate the time needed to acquire sufficient cine images for conventional left ventricular contour analysis or whose LV borders are difficult to contour.

556. Magnetic Resonance Imaging For Third Trimester Fetal Cardiovascular Evaluation: Steady State Free Precession Versus Single Shot Fast Spin Echo Imaging

Khan M. Siddiqui, M.D.,[1] Cathleen A. Woomert, M.D.,[1] Frederick K. Emge, M.D.,[2] Rodney G. Shaffer, M.D.,[1] B. Dennis M. Go, M.D.[1] [1]*Radiology, Geisinger Medical Center, Danville, PA, USA*, [2]*Pediatric Cardiology, Geisinger Medical Center, Danville, PA, USA*.

Introduction: The benefit of magnetic resonance imaging (MRI) in the evaluation of non-cardiac fetal chest abnormalities has been described in a number of articles. A very few case reports have shown the ability of MRI in assessment of fetal cardiac masses. No literature on evaluation of fetal cardiovascular anatomy by MRI has been established to date. The main limitation for lack of adequate visualization of the fetal heart with MRI has been the lack of low enough temporal resolution of the current MRI imaging techniques. Newer techniques such as Single shot fast spin echo (SSFSE) and Steady state free precession (SSFP) imaging suggest some promise in evaluation of the fetal heart by MRI.

Copyright © Marcel Dekker, Inc. All rights reserved.

ORDER REPRINTS

Purpose: To assess feasibility and diagnostic accuracy of steady state free precession magnetic resonance imaging for the evaluation of fetal heart.

Methods: We retrospectively reviewed imaging studies of three patients who underwent pelvic magnetic resonance imaging for evaluation of the fetus. Due to advance maternal gestational age fetal echocardiography was limited in the evaluation of fetal heart. Informed consent was obtained from all patients. Single shot fast spin echo (SSFSE) and Steady state free precession (SSFP) imaging was performed in multiple planes for the evaluation of fetal chest. Accuracy of MRI sequences was assessed by comparison with postnatal echocardiographic and angiographic findings.

Results: SSFP imaging provided adequate image quality for evaluation of the fetal heart ($p<0.5$). Findings identified by SSFP images corresponded to majority of the postnatal echocardiographic or MRI findings. SSFSE sequences provided inadequate image quality for accurate evaluation of fetal anatomy when compared to postnatal echocardiographic or MRI findings. This was in part was due to lower temporal resolution of SSFSE sequences. of the three cases reviewed, one patient had normal cardiac anatomy and the other two had diagnosis of double inlet single ventricle and coarctation of aorta.

Conclusion: Fetal cardiac magnetic resonance imaging with steady state free precession provides adequate evaluation of fetal cardiac anatomy and can be used in conjunction with fetal echocardiography. This is especially true for evaluation of fetal heart at an advanced gestational age, where position of the fetus can make intracardiac evaluation limited by ultrasonography. Previously documented difficulty in imaging the fetal heart with MRI was due to inability to eliminate cardiac motion, which obscured the intracardiac detail. Short TR and lower views per segment during SSFP imaging overcome this limitation. Evaluation of wall motion and quantification of flow is still limited and with development of faster scanners and imaging sequences this would be possible in the near future.

557. High-Resolution Dynamic Ventricular Assessment in a Clinical Real-Time Environment

Andres Carrillo,[1] Ajit Shankaranarayanan,[1] Michael M. McConnell,[2] Phillip C. Yang,[2] Jean H. Brittain,[1] Bob S. Hu.[3] [1]*ASL West, GE Medical Systems, Menlo Park, CA, USA*, [2]*Cardiology, Stanford University, Stanford, CA, USA*, [3]*Cardiology, Palo Alto Medical Foundation, Palo Alto, CA, USA*.

Introduction: Ventricular assessment remains the single most important cardiac imaging application. Traditional evaluation of ventricular function has relied on repeated acquisitions using multiple breathholds for the necessary volumetric dataset. The resulting data frequently suffer from misregistration and are often corrupted in patients with arrhythmia. Furthermore, slice-selection is a laborious process that is known to highly influence the assessment of wall-motion (Mannaerts et al., 2002). Real-time acquisition techniques can acquire the requisite 4D dataset in as short as a single breathhold but suffer from lower resolution (Nayak, 2003). An ideal ventricular assessment strategy is to acquire selected high-resolution multiphase datasets with the selection of slice location facilitated by rapid switching from lower resolution real-time images.

We have developed a new dynamic real-time cardiac imaging environment that integrates new software and hardware changes to provide for a *suite* of cardiac applications all within a single ''switch-on-the-fly'' user interface (Santos et al., 2002). Within this environment we have developed and tested a gated high-resolution multi-phase imaging sequence that can acquire the necessary data sets in 3 to 5 heart beats.

Methods: Our new cardiac real-time imaging environment was implemented on a GE 1.5 Signa Twinspeed system (GE Medical Systems, Milwaukee, WI). The configuration included EXCITE technology running optimized sliding-window, gridding reconstruction software (Shankaranarayanan et al., 2003).

Our dynamic imaging environment provides modes of operation corresponding to the real-time interactive localization and the multiphase, high resolution gated acquisition. The real-time localization mode utilizes 3 spiral interleaves to achieve a 2.29 mm resolution over a 24 cm FOV. The high-resolution, gated multiphase mode consists of 5 spiral interleaves to achieve 1.58 mm resolution over the same FOV. The remaining default parameters for both acquisitions include a 13 ms spectral–spatial excitation pulse followed by a 16 ms spiral readout, a 6 mm slice thickness, and a 30° flip angle.

The user interface allows the real-time adjustment of slice thickness, flip angle, FOV and the shim values for a particular location. With the push of a single button, the acquisition instantaneously changes from real-time mode to gated, multiphase mode. Contextual information including prescan parameters and shim values is automatically shared between the two

Copyright © Marcel Dekker, Inc. All rights reserved.

ORDER REPRINTS

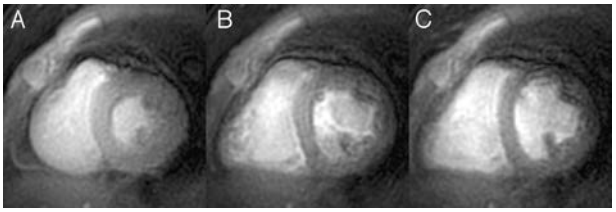

Figure 1. Selected images from a short axis multiphase acquisition. Image (A) shows a systolic phase, image (C) shows a diastolic phase and image (B) shows a phase between systole and diastole.

acquisitions. After the multiphase acquisition is complete, the system immediately returns to the continuous acquisition, reconstruction and display of real-time interactive images.

Results: Figure 1 shows selected images from a set of 17 phases acquired during a single 5 heart-beat breathhold. The temporal resolution of the multiphase dataset was 32 ms. The spatial resolution was 1.58 mm.

Discussion and Conclusion: The evaluation of cardiac morphology and function is one of the most important applications of cardiac imaging. The choice of slice location in cross-sectional imaging has long been known in echocardiography to significantly affect the interpretation of subtle wall motion. Real-time interactive imaging can provide accurate slice placement but can be limited by lower resolution. A real-time guided gated acquisition with a small number of interleaves overcomes both the slice positioning and resolution issues while minimizing the effects of cardiac arrhythmia. The method can be easily extended to examination of valvular morphology where careful slice selection and higher spatial and temporal resolution are even more essential.

Flexible inter-sequence switching in cardiac MR evaluation has enormous potential to improve the quality, accuracy and efficiency of cardiac magnetic resonance evaluation.

REFERENCES

Mannaerts, H. F., Kamp, O., van der Heide, J. A., Valocik, G., Visser, C. A. (2002). *JASE* 15:46.

Nayak, K. (2003). *Magn. Reson. Med.* Jan 49(1):188–192.

Santos, et al. (2002). *ISMRM*, 738.

Shankaranarayanan, et al. (2003). *SCMR*, 294–296.

558. Automatic Segmentation for Cardiac MR Image Sequence

Charnchai Pluempitiwiriyawej,[1] Yi-Jen Lin Wu,[2] Shinichi Kenno,[2] Chien Ho,[2] Jose M. F. Moura.[1]
[1]*Electrical & Computer Engineering, Carnegie Mellon University, Pittsburgh, PA, USA*, [2]*Pittsburgh NMR Center for Biomedical Research, Carnegie Mellon University, Pittsburgh, PA, USA*.

Introduction: To quantitatively analyze the heart's dynamic function, it is necessary to segment various parts of the heart chambers in a magnetic resonance (MR) image sequence. In clinical studies, segmentation task, particularly delineating the epicardium and the left and right ventricular endocardia, is often performed manually, which is very time consuming. To help expedite the process, an automatic image segmentation approach is desired.

Most current active contour methods for image segmentation are not fully automatic because, due to their purely edge-based nature, they are sensitive to noise and initialization. The initial contour must reside close enough to the true boundary for the contour to evolve. Moreover, turbulent blood flow in some images often causes faulty edges. Papillary muscles and other anatomy parts like chest wall pose additional challenges for segmentation because they have similar textures to the myocardium but should be segmented out.

Purpose: To develop and validate a new automatic cardiac MR image segmentation algorithm using active contour that is robust to noise and initialization and overcomes the problems with papillary muscles, chest wall, and turbulent blood flow.

Methods: We use energy minimization approach by searching for a contour that minimizes an energy functional, which consists of four terms: 1) model-matching term assuming statistical models (region-based); 2) gradient-image term utilizing edge-based information; 3) shape term controling the contour's global properties, we assume an ellipse shape; 4) contour-smoothing term regulating the contour's local properties. We implement our algorithm using the level set method.

The advantages of our new active contour algorithm are threefold. First, by assuming that the image consists of anatomy parts with different statistical models, our method can be applied to a large range of images, particularly when the contrast between distinct regions is difficult to distinguish by human eyes. These statistical models are aimed to resolve the similar textures between myocardium and chest wall. Second, our new active contour scheme utilizes both edge and

Copyright © Marcel Dekker, Inc. All rights reserved.

ORDER REPRINTS

region-based information. The region-based information provides forces on the contour front where the edge information is missing or when the contour front encounters spurious faulty edges. Therefore, our method is robust to noise and contour's initial condition. Furthermore, the balance between the region-based force and the edge-based force helps stabilizing the contour at the desired boundary. Third, the ellipse shape that we impose onto the contour helps overcoming the problem with the papillary muscles and turbulent blood flow in the image.

Results: Figure 1 shows the segmentation results obtained automatically by our new active contour algorithm on a set of 48 cardiac MR images. Figure 2 depicts the contours traced manually by an expert on the same set of images. There are three sets of contours, the boundaries of the left ventricle (LV), the right ventricle (RV), and the epicardium (EP).

We use the kappa statistic similarity measure described by Zijdenbos et al. (1994) to validate our new active contour scheme by comparing our results in Figure 1 against the one drawn manually by an expert in Figure 2, which is considered the ''gold standard.'' The average values of the similarity measures are 0.88 ± 0.06 for LV, 0.81 ± 0.09 for RV, and 0.95 ± 0.02 for EP. According to Zijdenbos et al. (1994), the similarity measure of more than 0.7 indicates a good agreement between the two comparing regions. Therefore, our new active contour algorithm yields excellent results.

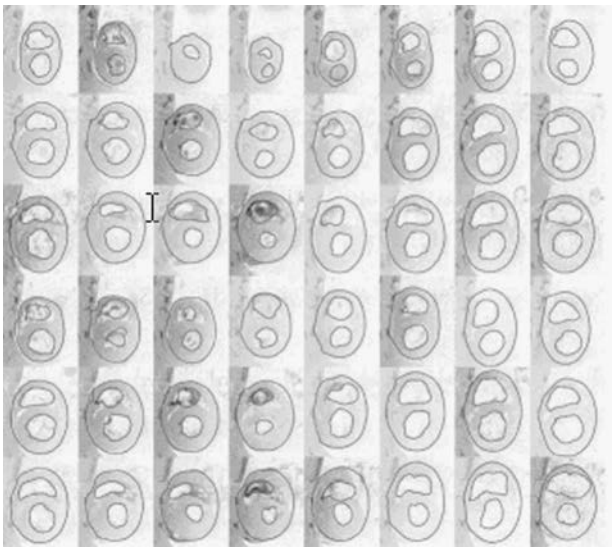

Figure 1. Contours obtained automatically by our new active contour algorithm. (*View this art in color at www.dekker.com.*)

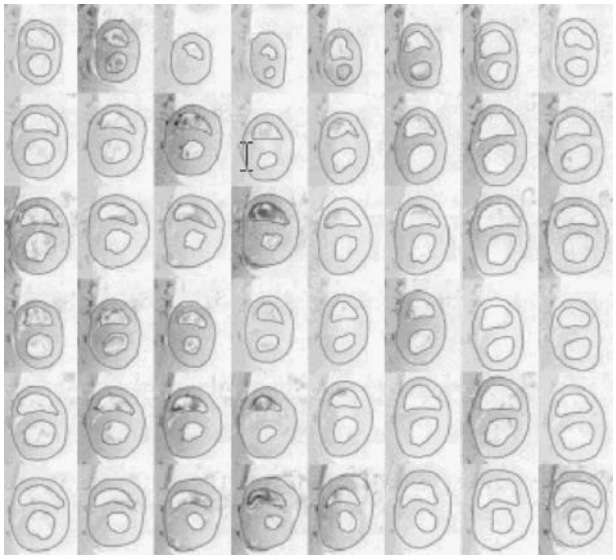

Figure 2. Contours traced manually by an expert. (*View this art in color at www.dekker.com.*)

Conclusions: We have designed a new active contour method that aims to overcome unique challenges arising in automating the segmentation of cardiac MR images. The algorithm was applied to a set of 48 cardiac images, obtaining excellent results when comparing them to the ones drawn manually.

REFERENCES

Zijdenbos, A. P., et al. (1994). *Morphometric Anaysis of White Matter Lesions in MR Images: Method and Validation.*

559. Relationship Between Global and Longitudinal Left Ventricular Function: A Cardiac Magnetic Resonance Study

Nikolay P. Nikitin,[1] Ramesh de Silva, M.B. Ch.B. MRCP,[1] Angela Lowe,[2] Elena Lukaschuk, M.Sc.,[1] John GF Cleland, M.D. FRCP FESC FACC.[1] [1]*Academic Unit of Cardiology, University of Hull, Hull, United Kingdom*, [2]*Lister Healthcare, Leeds, United Kingdom.*

Introduction: The analysis of longitudinal left ventricular (LV) function can help with the early diagnosis of cardiac dysfunction. There are several non-invasive

Copyright © Marcel Dekker, Inc. All rights reserved.

ORDER REPRINTS

techniques currently available for the analysis of LV long-axis function. Mitral annular displacement (MAD) can be measured using M-mode echocardiography and cardiac magnetic resonance (CMR), and mitral annular and segmental myocardial velocities can be assessed with tissue Doppler imaging. The important advantages of CMR over echocardiographic and Doppler techniques are that it is not dependent on the acoustic window and operator skills and provides more accurate and reproducible data. This study was designed to explore the relationship between global and longitudinal LV function as assessed by CMR.

Methods: The study population included 103 subjects (aged 70±7 yrs, ranged 30 to 90 years old) including 58 patients with LV systolic dysfunction (ejection fraction [EF]<45%), 16 patients with cardiac disease and preserved LV systolic function (EF>45%) and 29 normal subjects (EF>55%). The study subjects underwent CMR on a 1.5 Tesla scanner (Signa CV/i, GE Medical Systems) using ECG-triggered breath-hold FIESTA imaging. LV end-diastolic and end-systolic volumes and EF were calculated from a set of short-axis cine images with commercially available MRI-MASS software (MEDIS, Leiden, NL). MAD was measured at the lateral and septal sites in the horizontal long axis (4-chamber) view and at the anterior and inferior sites in the vertical long axis (2-chamber) view and averaged.

Results: The study subjects had a broad range of global LV systolic function (mean EF 42±18%, range from 13 to 78%) and longitudinal LV systolic function (mean MAD 9.3±3.8 mm, range from 2.2 to 19.0 mm). There was a significant correlation between EF and MAD ($r = 0.77$, $p < 0.0001$). Age and MAD were not related in the study group ($r = -0.15$, NS). When multiple regression was used, the addition of LV end-diastolic volume produced a significant increase in multiple R from 0.77 to 0.87 ($p < 0.0001$).

Conclusions: There is a close relation between global and longitudinal LV systolic function as demonstrated by CMR. LV end-diastolic volume is another important variable to consider in patients with LV systolic dysfunction. The role of age as a determinant of longitudinal LV function is diminished in the presence of LV systolic dysfunction caused by cardiac disease.

560. *i*23: A Novel Tool for Rapid Localization and Acquisition of High Resolution Breath-Held 3D MR Images of the Coronary Arteries

Manojkumar Saranathan, Marcela B. Montequin, Thomas K. F. Foo. *GE Medical Systems, Baltimore, MD, USA*.

Introduction: MR coronary artery imaging (CAI) is challenged by respiratory and cardiac motion and the tortuous course of the coronary arteries. Recently developed ultra-short breath-hold (BH) 3D FIESTA techniques (Foo et al., 2002) have shown great promise. However, localization of the coronary arteries, especially for visualization of distal sections, still remains a challenge. Conventional approaches have used either low spatial-high temporal resolution 2D spiral or EPI sequences to perform realtime CAI or used realtime imaging to acquire localizer planes for subsequent scanning with high spatial resolution 2D/3D sequences.

Purpose: We present here *i*23 (interactive to 3D), a novel tool that permits real time localization and acquisition using the **same** 3D sequence, eliminating any switching lags associated with current paradigms. We demonstrate that the use of high spatial-low temporal resolution localization provides the ability to quickly determine the appropriate scan planes for targeted volume 3D acquisitions of the different coronary artery distributions.

Methods: Five healthy volunteers were scanned on a 1.5 T GE CV*i* scanner under IRB-approved protocols after informed consent . CAI was performed using a fat suppressed 3D BH FIESTA acquisition employed a Variable Sampling in Time (VAST) segmentation scheme (Foo et al., 2002) to reduce scan time. For each slice partition, k-space data was acquired over 2 R–R intervals, resulting in a scan time of 24 heartbeats for 12 slice partitions. Scan parameters: 1.5 ms/4.8 ms TE/TR, 256×192 matrix, Half Fourier, 12 2.2 mm partitions. Imaging workflow—The scan was first started in a real time localization mode, which was performed free-breathing and by running the 3D sequence in a 2D FIESTA mode with a single 6 mm partition. After the scan planes of interest were localized and adjusted to visualize the maximum length of the coronary arteries, the volunteer was asked to breath-hold and 3D volumes were acquired, centered on each of the selected planes. The switching between the 2D and the 3D imaging modes was performed in real time. This permitted adjustments to the 3D scan plane after the start of BH to correct for possible discrepancies between the free breathing and the BH localizer planes if needed, prior to the 3D scan.

Results: The mean time for localization of each coronary artery distribution was under 50 seconds. This was measured from the start of the acquisition (from an axial, sagittal, or coronal scout) to the initiation of the

Copyright © Marcel Dekker, Inc. All rights reserved.

ORDER REPRINTS

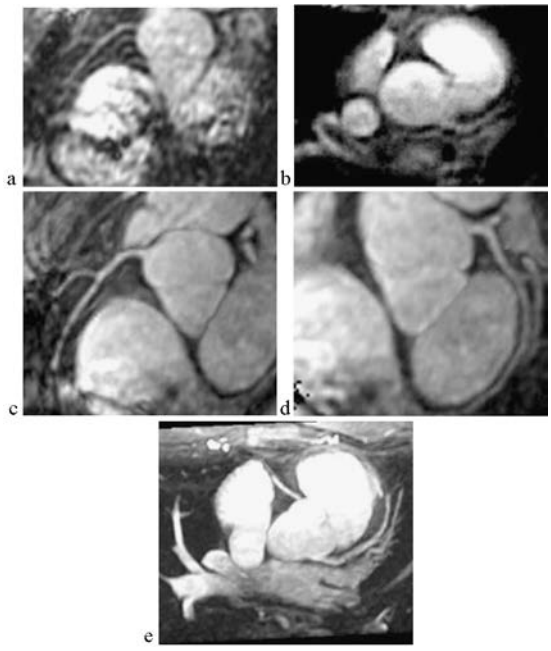

Figure 1. Realtime free-breathing images of the right and left coronary planes (a,b) and high resolution BH 3D FIESTA MIPs (c–e) obtained using volumes centered on these planes.

high resolution 3D BH scan. Figure 1 shows the right and left coronary imaging planes obtained using the localization mode (a–b) and MIPs of the corresponding 3D BH FIESTA volumes (c–e) obtained using these planes as a reference. Each 3D volume was acquired in a 24 heart-beat breath-hold. In this example, 9 cm of the left main/left anterior descending artery, 11 cm of the right coronary artery, and 12 cm of the left circumflex artery were visualized in the planar reformatted images.

Conclusions: We have developed a robust tool that permits rapid and accurate localization of coronary planes and high resolution CAI centered on these planes with no switching lags. This enables the acquisition of all three coronary distributions within 10 minutes, filling the current gap in the integrated cardiac examination. The tool also improves patient throughput by eliminating unnecessary breath-hold localizers and enabling the user to image the most optimal scanning plane, all from a single user interface. The same sequence can also be used to acquire 3D MDE and 3D CINE images.

REFERENCES

Foo, T. K. F., et al. (2002). *Proceedings, 12th ISMRM*. 1624.

561. Improved Left Ventricular Wall Analysis in Normals

Cory Swingen, Ph.D., Xiaoen Wang, M.D., Michael Jerosch-Herold, Ph.D. *Radiology, University of Minnesota, Minneapolis, MN, USA*.

Introduction: Cardiac MR studies in the short-axis have shown their importance for the accurate assessment of LV volumes, mass as well as regional parameters such as wall thickness and thickening. The major shortcoming of these local measurements is their confinement to a single 2D imaging plane and the assumption that the myocardial wall is always perpendicular to the acquisition plane containing contours of the endo- and epicardial borders. Improvements have been made to this technique, which estimate the curvature of the ventricle using proximal and distal slices.

Purpose: The goal of this study was to develop a new method for the quantitative measurement of myocardial wall thickness and regional function utilizing local LV shape information from a 3D model and evaluate the results from MR imaging data obtained from healthy volunteers.

Methods: A three-dimensional calculation algorithm was created to extract short-axis contours from a 3D model of the LV at the specified positions along the long-axis of the ventricle with 0% representing the apex and the base at 100%. The centerline method was applied to the short-axis contours to obtain an uncorrected measure of the wall thickness. The true, or corrected, values of wall thickness were calculated using the uncorrected values and a correction factor

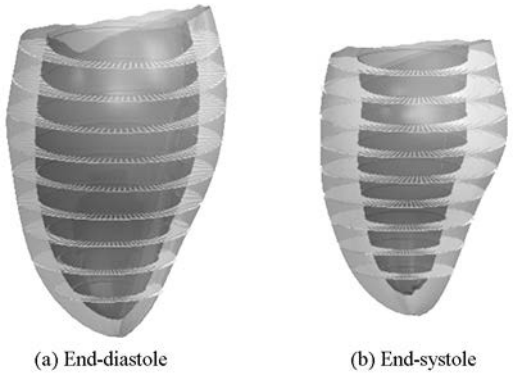

Figure 1. 3D models of the LV during diastole (left) and systole (right). At each phase, endo- and epicardial contours are extracted from the model at regular intervals (from base to apex) and the wall thickness measured using the centerline method. Thickness measurements are then corrected according to the regional curvature of the ventricle according to the 3D model. (*View this art in color at www.dekker.com.*)

Copyright © Marcel Dekker, Inc. All rights reserved.

ORDER REPRINTS

based on the local curvature of the ventricle-derived from the 3D model. Wall thickness was measured during end-diastole and end-systole and the wall thickening derived from these values. An evaluation of this technique was performed on an MR imaging study of 10 normal subjects (Figure 1).

Results: The new 3D method yielded smaller values for wall thickness at both ED and ES at the base and mid to apical portions of the LV. The uncorrected thickness measurements overestimated the wall thickness at the apex compared to the new method, 1.3 mm and 1.7 mm at ED and ES respectively. The uncorrected values were very similar to the corrected values at locations 60–80% of the base where the ventricular wall is nearly parallel to the long-axis. Thickening analysis revealed the average thickening in all subjects was the smallest at the base (35.89±21.64%) and the highest at the apex (81.34±27.17%) of the heart (Figure 2).

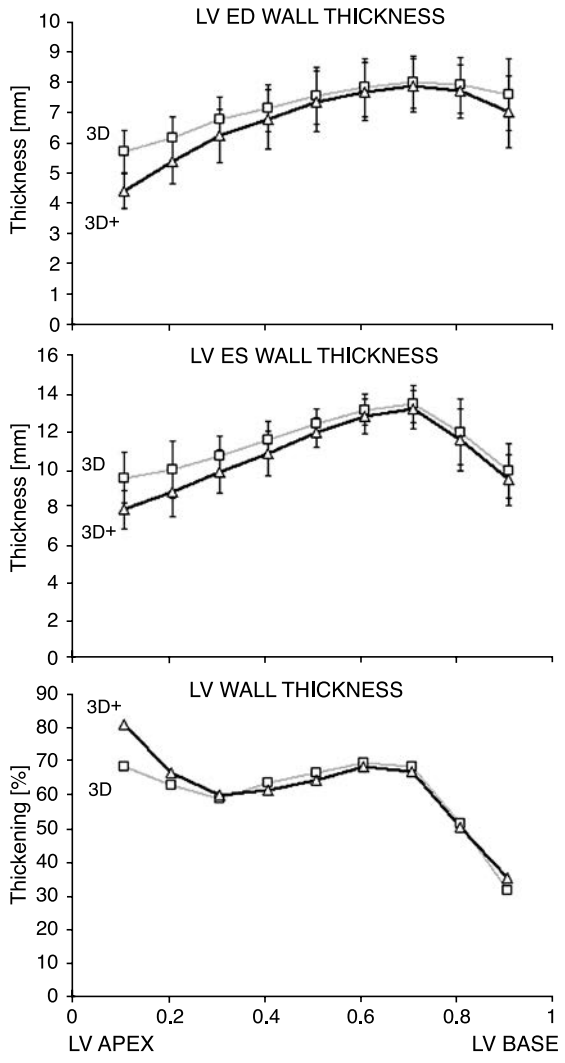

Figure 2. Wall thickness and thickening results averaged for 10 normal volunteers from apex to base (0–1). Wall Thickness measurements are very similar between the uncorrected (3D) and curvature corrected (3D+) where the ventricular wall is approximately parallel to the long-axis through the LV, while the corrected vaules are smaller than the uncorrected values towards the apex and very basal portions of the ventricle where there is typical curvature and tapering of the LV surface. (*View this art in color at www.dekker.com.*)

Conclusions: Cardiac wall thickness and thickening measurements from MR studies can be calculated with higher accuracy by a 3D approach ultilizing the shape of the ventricular surface, than with the standard 2D approach which relies on information within a single or a few short-axis imaging planes. This technique overcomes previous limitations associated with measurements strictly from 2D images including slice misregistration and accounting for systolic motion of the LV through the sole use of a 3D model.

562. Improved CMR Flow Measurements with High Spatial and Temporal Resolution in both Small and Great Vessels

Liesbeth P. Salm,[1] Joost Doornbos,[2] Hubert W. Vliegen,[1] Jeroen J. Bax,[1] Wouter Jukema,[1] Susan E. Langerak,[1] Ernst E. Van der Wall,[1] Albert De Roos,[2] Hildo J. Lamb.[2] [1]*Cardiology, Leiden University Medical Center, Leiden, Netherlands*, [2]*Radiology, Leiden University Medical Center, Leiden, Netherlands*.

Introduction: Cardiovascular magnetic resonance (CMR) has become a versatile tool in the evaluation of both ischemic and congenital heart disease. In order to measure flow velocity in both small vessels and great arteries we present an improved, high resolution, breathhold flow velocity sequence.

Purpose: To validate a high spatial and temporal resolution CMR flow velocity sequence to be used to measure flow velocity in both small vessels and great arteries.

Methods: A breathhold echo planar imaging (EPI) sequence was developed using a 1.5 Tesla Philips MR scanner (Gyroscan Intera Release 9) with the following parameters: FOV 150 mm, RFOV 40%, slice thickness 6 mm, EPI factor 5, TE/TR 7/13, flip angle 40°, retrospective cardiac triggering, 30 heart phases, 2 NSA, scan duration 20 sec, temporal resolution 33 ms, acquisition matrix 144×58, measured voxel size 1.04×1.06 mm, reconstructed to 0.29×0.29 mm. For

Copyright © Marcel Dekker, Inc. All rights reserved.

ORDER REPRINTS

validation a flow pump was used, creating pulsatile flow in tubes with 4 mm diameter. The pump was set to simulate a coronary artery flow pattern with stepwise increasing velocities. The new sequence was compared with a conventional, free-breathing gradient echo sequence previously validated at our institution, which had a scan duration of 5 minutes. The center velocity was measured and average, systolic and diastolic peak velocity (APV; SPV; DPV) were calculated by both methods. In 10 healthy volunteers volume flow and systolic peak flow (SPF) in the aorta was measured by both the new and conventional sequence.

Results: In vitro APV yielded an excellent correlation ($y = 1.06x - 2.6$; $r = 0.99$), as did SPV and DPV ($y = 1.05x - 2.1$; $r = 0.99$ and $y = 1.05x - 1.3$; $r = 0.99$, respectively). In Bland–Altman graphs 96% of measurements kept within 2 SD of the mean. In healthy volunteers aortic volume flow and SPF showed a good correlation between the new and the conventional sequence ($y = 1.2x + 152$; $r = 0.81$ and $y = 0.98x + 11$; $r = 0.92$, respectively). Both correlation and Bland–Altman showed a minor overestimation of volume flow measured by the new sequence.

Conclusion: The high resolution breathhold CMR flow velocity sequence showed good correlations with a conventional sequence. The new sequence provides a fast and accurate way to measure flow velocity in both small vessels, for instance coronary arteries, and great vessels.

563. Automated Detection of Regional Wall Motion Abnormalities from Magnetic Resonance Images

Enrico G. Caiani, Ph.D.,[1] Eran Toledo, Ph.D.,[2] Peter MacEneaney, M.D.,[2] Keith A. Collins, M.S.,[2] Roberto M. Lang, M.D.,[2] Victor Mor-Avi, Ph.D.[2] [1]*Biomedical Engineering, Politecnico di Milano, Milan, Italy*, [2]*Medicine/Cardiology, University of Chicago, Chicago, IL, USA*.

Background: Cardiac magnetic resonance (CMR) based diagnosis of regional left ventricular (LV) dysfunction relies on subjective and experience dependent visual interpretation of dynamic images. This interpretation is often performed by radiologists who do not have the specialized training and experience necessary for accurate diagnosis of regional wall motion abnormalities. Thus, the outcome of this methodology may vary widely between observers.

Aim: Our goal was to develop and test the feasibility of objective, automatic detection of regional wall motion abnormalities based on quantitative segmental analysis of semi-automatically defined LV endocardial boundaries.

Methods: Images were obtained using a 1.5T scanner (GE) using an EKG-gated steady state free precession (FIESTA) pulse sequence in 6 to 10 short axis slices in 10 consecutive cardiac patients (7 with wall motion abnormalities, and 3 with normal wall motion). Dynamic images were independently reviewed by two radiologists, who graded regional LV wall motion in each segment (6 segment model) in each slice as normal or abnormal. The inter-observer variability was calculated as percent of discordant segments. The same images were reviewed and graded by an expert cardiologist, whose grades were subsequently used as the ''gold standard'' for comparisons. In each slice, endocardial border was semi-automatically detected on end-systolic and end-diastolic frames and divided into 6 segments. For each segment, regional fractional area change (RFAC) in % of regional end diastolic area was calculated automatically and used as a quantitative index of regional systolic endocardial motion. Data were displayed in a color-coded ''bull's eye'' format. Segments where RFAC was below 50% were automatically classified as abnormal. The concordance rates with the ''gold standard'' expert grades were used to calculate the sensitivity, specificity and overall accuracy of the automated detection of regional wall motion abnormalities.

Results: The expert reader detected abnormal wall motion in 140/434 segments. The radiologists' gradings were discordant in 114/434 segments (26%), reflecting the high inter-observer variability of the non-expert readers. The calculation of RFAC was fully automated and required <1 sec per slice on a 2 GHz Pentium 4 personal computer. The ''bull's eye'' display of RFAC showed dark areas reflecting reduced RFAC in segments corresponding to abnormalities detected by the expert reviewer in most cases (Figure 1). The automated detection of wall motion abnormalities had sensitivity of 79%, specificity of 78% and accuracy of 78%.

Conclusions: Quantitative analysis of regional endocardial motion from CMR images is feasible and allows accurate detection of regional wall motion abnormalities. This fully automated, objective and experience-independent technique is free of inter-observer variability. While our approach is based on endocardial border detection only, it is not affected by possible errors associated with time-consuming epicardial detection. Since semi-automated border detection is available

Copyright © Marcel Dekker, Inc. All rights reserved.

ORDER REPRINTS

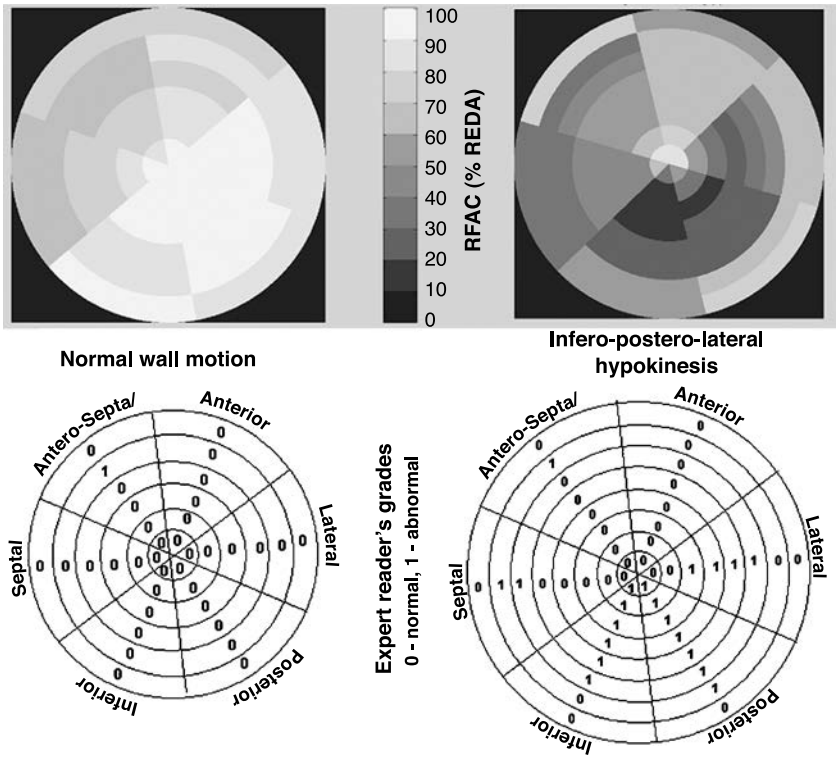

Figure 1.

in most commercial analysis software packages, this approach can be easily implemented into the existing tools and promises to become a clinically valuable addition in the diagnosis of ischemic heart disease.

564. Unsupervised Correction of Physiologically-Induced Slice-Offsets in 4D Cardiac MRI

Mikkel B. Stegmann,[1] Rasmus Larsen,[1] Henrik B. W. Larsson.[2] [1]*Informatics & Mathematical Modelling, Technical University of Denmark, Kgs. Lyngby, Denmark*, [2]*St. Olavs Hospital, Trondheim University, Trondheim, Norway*.

Introduction: Spatio-temporal cardiac MRI investigations are typically acquired using a breath-hold technique where each short-axis slice is recorded over a set of time phases during one single breath-hold. Subsequent slices use new breath-holds with potentially different inspiration levels. This causes slices in the apex-basal direction to be misaligned. Figure 1 (left) illustrates the problem.

Purpose: This work presents a rapid and unsupervised method correcting for respiratory noise in dynamic three-dimensional cardiac MRI. Statistical models of shape and appearance are employed to localise the left and right ventricle in a mid-apex-basal, short-axis slice. The segmented region is subsequently propagated through all slices in the apex-basal direction using a non-rigid registration process, thus providing an estimate of the inter-slice translation due to variation in inspiration. Qualitatively and quantitatively validation carried out on 13 subjects appear very promising.

Methods: The data material comprises 14 spatially corresponding, short-axis, end-diastolic, 2D slices (set A), and an independent set of 13 short-axis, dynamic volumes (set B), both acquired by a 1.0 Tesla Siemens Impact scanner with an ECG-triggered, FLASH sequence. Matrix = 256×256, field of view = 263×350 mm, slice thickness = 10 mm (2D slices) and 6 mm (volumes), phase time = 55 ms. Volume sizes were typically (x/y/z/phases) = $256 \times 256 \times 25 \times 11$ voxels.

Inter-slice variation in corresponding phases consists of two major components, 1) the spatial physiological changes, and 2) the movement of the heart and upper abdomen due to respiration. To estimate the

Copyright © Marcel Dekker, Inc. All rights reserved.

ORDER REPRINTS

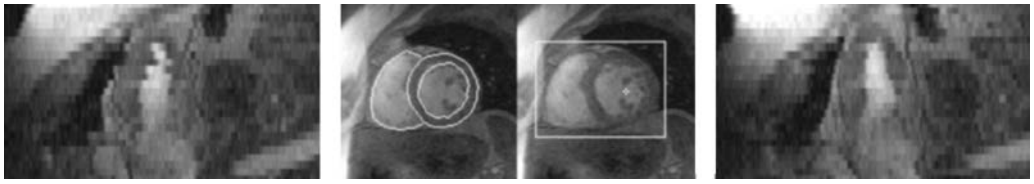

Figure 1. Left: 4D input image, Middle: Reference slice with LV-RV localisation and region of interest. Right: Corrected 4D image.

latter, the cardiac area is located using an active appearance model of the left and right ventricle (LV/RV) registered to the central 50% of all end-diastolic slices in each 4D cardiac MRI. The slice that provides the best model fit (in a least squares sense) denotes the reference slice, Figure 1 (middle). From this slice a region of interest and a reference point are propagated through every frame in the basal direction and subsequently in the apex direction. Propagation is carried out in a four-dimensional space composed of translation, scaling and rotation by iteratively applying parameter updates based on a gradient matrix precomputed from the previous slice. The initial reference point is the centre-of-gravity (COG) of the LV endocardial contour in the reference slice. The obtained reference points thus constitute estimates of the in-plane translation of the heart induced by inspiration. Finally, re-sampling all time phases of the 4D image by inverting the estimated translations carries out the correction.

Results: All 13 dynamic volumes in set B have been corrected using the above method showing a good qualitatively result. A typical result is shown in Figure 1 (right) during the end-systole. Quantitatively results are obtained by manually annotating each end-diastolic, endocardial contour, enabling comparison of COGs with and without correction. Since well-corrected volumes are assumed to have co-linear slice COGs, a performance measure is the mean distance, m, to the long-axis incident with the mean COG of all slices. The original scans had on average $m = 6.7 \pm 0.3$ mm compared to the rectified scans with $m = 4.2 \pm 0.2$ mm (mean, std.err.). Estimation and correction took less than 10 seconds per subject, on a standard PC.

Conclusions: This work weakly assume that respiration effects are purely in-plane translations, and the that LV is rotational symmetric. Although we recognise that these are not entirely met, the approximations are adequate to produce results of significantly higher fidelity compared to the raw noise-corrupted scans. This improvement leads to better anatomical understanding, increase in annotation accuracy, and more specific cardiac shape models. The latter having applications to unsupervised dynamic analyses, ejection fraction estimation, et cetera.

565. Open-Source Java Workstation for Calculation and Visualization of Time-Dependent Blood Flow across the Aortic Lumen

Stig F. Samnøy,[1] Erling Andersen,[1] Terje H. Larsen.[2]
[1]*Department of Clinical Engineering, Haukeland University Hospital, Bergen, Norway*, [2]*Department of Radiology, Haukeland University Hospital, Bergen, Norway*.

Purpose: MRI flow velocity mapping is considered to be a significant method for describing arterial blood flow. Volumetric velocity vector information is of particular value in assessing stenotic changes of cardiac valves and the vessels. Peak velocity, which may vary considerably at different sites within the vessel lumen, is frequently applied as a measure of the degree of

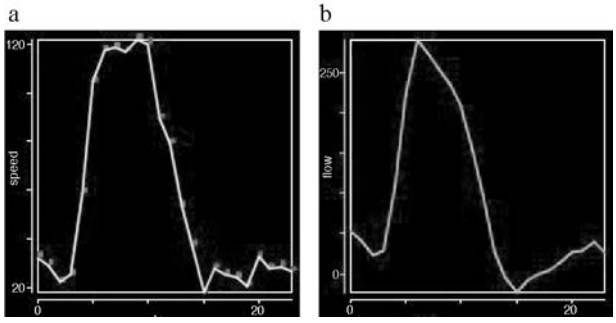

Figure 1. (a) Peak velocity within the vessel lumen throughout the cardiac cycle. (b) Flow in the vessel lumen throughtout the cardiac cycle. (*View this art in color at www.dekker.com.*)

Copyright © Marcel Dekker, Inc. All rights reserved.

ORDER REPRINTS

stenosis. This work has addressed these topics through an open-source Java based workstation.

Methods: A 1.5 T Siemens Magnetom Vision Plus was used for velocity measurements. The measurements were obtained from the ascending aorta. The acquisition method used was based on the phase shift velocity mapping technique, with flow sensitivity in three orthogonal directions. For each slice position three separate measurements were performed in order to obtain velocity vector information. In the main flow direction, the sequence applied was a 2D FLASH with velocity encoding range 2.5 m/s. Sequence parameters were TR = 24 ms, TE = 5 ms, Flip Angle = 30°, Slice Thickness = 6 mm, FOV = 300, Matrix = 128 × 256. In the transverse directions similar sequences were applied, with flow sensitivity in the readout direction, and velocity encoding range 0.75 m/s. For the second transverse direction the phase encoding and frequency encoding directions were swapped. Sequence parameters were TR = 25 ms, TE = 6 ms, Flip Angle = 30°, Slice Thickness = 6 mm, FOV = 300, Matrix = 128 × 256.

Results: The workstation is built using the Java programming language. For reading DICOM image files and visualizing the data, components from open-source projects dcm4che (http://sourceforge.net/projects/dcm4che) and VisAD (http://www.ssec.wisc.edu/~billh/visad.html) have been used, respectively.

The workstation presents time-dependent volumes of MRI data. Lumen can be selected semi-automatic for each slice. This is achieved by selecting the region of interest roughly in the first slice. Then the algorithm finds the region of interest in this and the next slices by region growing. The sensitivity of the region growing is user-defined. In addition the lumen can be selected manually.

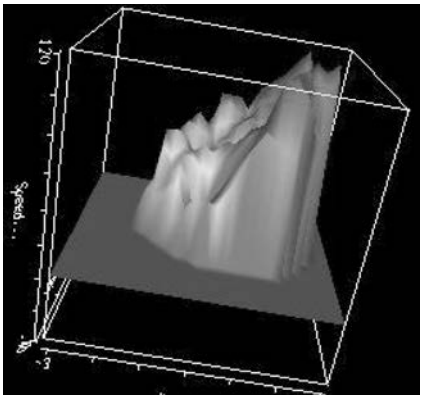

Figure 2. Distribution of velocity in a vessel cross section at a particular time during the cardiac cycle. (*View this art in color at www.dekker.com.*)

The velocity, acceleration and flow are calculated across the lumen throughout the cardiac cycle (see Figure 1). The workstation also estimates pumping power, the rate of energy expenditure required to drive the flow.

Derived data can be visualized in 2D, 3D and 4D (see Figure 2). It is also possible to study time variation in a pixel within the region of interest. This is important when considering local variations only.

Conclusions: The presentation of the peak velocities across the lumen throughout the cardiac cycle significantly reduces the possibility of missing the highest velocities in the vessel. Thus, this method improves the accuracy of the interpretation of stenosis when applying flow-weighted MRI.

566. The Inter-subject Variability of the Three-Dimensional Left Ventricular Axes

Thomas N. Martin, John Foster, Tracey Steedman, Alex Elliott, Henry Dargie, Bjoern Aaris Groenning. *Glasgow Cardiac Magnetic Resonance Unit, Glasgow, United Kingdom.*

Introduction: The interpretation of many diagnostic tools used in cardiology is based in part on the assumption that the three-dimensional (3D) cardiac anatomical axes are preserved. Magnetic resonance imaging (MRI) can provide a 3D alignment of the heart in the thorax.

Purpose: The aim of the study was to determine normal ranges and reproducibility of cardiac anatomical axes measurements using MRI.

Methods: 25 in-patients (13 men and 12 women, median (range) age = 54 (32–82) years, mean (SD) heart rate = 61 (9.3) bpm, with no history of cardiac disease and normal ECG were examined with MRI and after 28 days (n = 17). A Siemens Sonata 1.5T system with phased array chest coil was used. LV dimensions were evaluated by cinematographic (TrueFISP) breath-hold (expiration) sequence (slice = 8 mm, TR = 47.4 ms, TE = 1.58 ms, FA = 60°, FOV = 340 mm). The co-ordinates were calibrated using test phantoms. Two LV anatomical long-axes were defined using specific landmarks: From the middle of the mitral valve (vector 1) and from the spinal cord (vector 2) to the tip of the apex of the left ventricle, obtained from the 4-chamber long-axis view. The corresponding 3D anatomical frontal and horizontal axis vectors were derived using trigonometry.

Copyright © Marcel Dekker, Inc. All rights reserved.

ORDER REPRINTS

Results: Mean (range/ SD) anatomical frontal axis at baseline was 39 (16–66/14)° (vector 1) and 46 (24–71/13)° (vector 2); at 28 days 36 (15–49/9.6)° (vector 1) and 45 (23–66/11)° (vector 2): Mean (range/SD) anatomical horizontal axis at baseline was 50 (38–70/8.2)° (vector 1) and 58 (49–72/6.8)° (vector 2); at 28 days 51 (39–65 (7.1)° (vector 1) and 58 (47–69/6.5)° (vector 2). The reproducibility coefficients of the anatomical frontal and horizontal axis measurements were 16% and 8.7% (vector 1) and 14% and 7.9% (vector 2) (Bland–Altman limits of agreement (±2SD): (−13.3 to 1.35 to 10.4°) and (−9.69 to 0.83 to 8.03°) (vector 1) and (−12.5 to 0.02 to 12.5°) and (−8.8 to 0.34 to 9.46°) (vector 2)). Vector 1 and vector 2 in the baseline frontal ($r = 0.97$, $p = 0.0002$) and horizontal ($r = 0.85$, $p < 0.0001$) planes were highly correlated.

Conclusions: Reference values for cardiac anatomical frontal and horizontal axes have been provided. Frontal and horizontal 3D anatomical axes vary significantly between normal individuals suggesting that future adaptations may be beneficial for the improved diagnostic accuracy of these techniques. The applied MRI method is highly reproducible and may potentially serve as a new gold standard for measurement of cardiac axes.

567. Feasibility of an Automated Algorithm for Quantification of Infarct Size on Contrast Enhanced MRI

Theodorus A. M. Kaandorp, M.D.,[1] Joanne D. Schuijf,[2] Hildo J. Lamb, Ph.D.,[1] Rob J. van der Geest,[1] Albert de Roos, M.D.,[1] Jeroen J. Bax, M.D. Ph.D.[1] [1]*Radiollogy, Leiden University Medical Center, Leiden, Netherlands*, [2]*Cardiology, Leiden University Medical Center, Leiden, Netherlands.*

Introduction: Transmural extent of infarction may be an important determinant of functional recovery after revascularization. However, no studies have focused on precise quantification of the extent of scar tissue.

Purpose: The purpose of this study was to demonstrate the feasibility of an automated algorithm for quantification of transmurality and compare the findings with visual analysis, and to also relate the findings to the severity of contractile dysfunction.

Methods: Twenty-seven patients with chronic coronary artery disease underwent a resting cine MRI study to analyze regional and global LV function, followed by ce-MRI to determine infarct size. Transmural extent of infarction was determined both by visual and quantitative analysis and related to wall motion abnormalities.

Results: Regional wall motion was abnormal in 210 (56%) of the 387 segments and 209 (55%) segments revealed delayed enhancement. The extent of hyperenhancement paralleled the severity of contractile dysfunction ($P < 0.05$) and the likelihood of transmural hyperenhancement (>50% of LV wall thickness) was significantly higher in a- or dyskinetic segments than in mildly hypokinetic or normal segments (93% vs. 2%, $P < 0.05$). A good agreement was found between the visual and quantitative analysis, although quantification allowed more precise measurement of infarct size.

Conclusions: The transmural extent of infarction is related to the severity of resting wall motion abnormalities. Quantitative assessment of transmurality of infarction may increase accuracy and reproducibility of this technique.

568. Measurement of Cardiac Systolic Reserve Without Cardiac Gating

Petri Sipola,[1] Hannu Manninen,[1] Keijo Peuhkurinen.[2] [1]*Clinical Radiology, Kuopio University Hospital, Kuopio, Finland*, [2]*Department of Medicine, Division of Cardiology, Kuopio University Hospital, Kuopio, Finland.*

Introduction: A capability to increase cardiac systolic function under stress conditions predicts good prognosis in patients with idiopathic dilated cardiomyopathy. Measurement of systolic function in these patients is difficult due to cardiac arrhythmias.

Purpose: To evaluate whether cardiac systolic function can be measured independent of cardiag gating by MRI.

Methods: Aortic flow was measured in seven adult normal volunteers with regular sinus rhythm with ECG-gated velocity encoded cine MR imaging and with non-gated velocity encoded cine MR imaging with multiple acquisistions (non-gated MR imaging). In addition, aortic flow was measured at rest and under 15 ug/kg/min dobutamine stress in five patients with idiopathic dilated cardiomyopathy using non-gated imaging. All the patients had failed to undergone conventional ECG-gated aortic flow measurements.

Results: No statistically significant difference was seen between ECG-gated cardiac output and non-gated cardiac output measurements (5.3 ± 1.2 l/min vs. 5.3 ± 0.9 l/min; $p = 0.735$ and $r = 0.910$). Stadnard error of an estimate between measurements was 0.5 l/min. In

Copyright © Marcel Dekker, Inc. All rights reserved.

ORDER REPRINTS

patients with dilated cardiomyopathy, in non-gated MR imaging, the mean cardiac output at rest was 4.2±0.2 l/min, and during dobutamine stress 5.3±0.9 l/min.

Conclusions: :Non-gated velocity encoded cine MR imaging with multiple acquisitions is a robust method to measure cardiac output. Non-gated imaging can be used to evaluate cardiac systolic reserve in patients with IDCM.

569. A New Method for Cardiac MRI Analysis of Right Ventricular Function

Richard E. Slaughter, MBBS FRACR, Wendy E. Strugnell, BScApp, Robyn A. Riley, DipAppSc, Andrew Trotter, BScApp, George Javorsky, MBBS FRACP. *Cardiovascular MRI Research Centre, The Prince Charles Hospital, Brisbane, Australia.*

Introduction: Inherent difficulties exist in the current standard method of CMRI measurement of right ventricular (RV) volumes. This technique uses a series of short axis cine acquisitions prescribed from a 4 chamber acquisition with the first slice placed across the atrio-ventricular valve plane at end diastole and covering both ventricles through to the base. The use of this image data set for RV analysis assumes that the tricuspid valve lies in the same plane and position as the mitral valve. Our experience indicates that the use of this imaging plane makes analysis problematic as the tricuspid valve is not in-plane in the slice and the atrioventricular margin is difficult to distinguish. This leads to inaccuracies in measurements at the base of the RV and miscalculation of the RV volume.

Purpose: To develop a novel plane of imaging acquisition of the right ventricle to improve visualisation of the tricuspid and pulmonary valves thereby increasing the accuracy of RV analysis by CMRI.

Methods: We undertook a prospective study of 50 post cardiac transplant patients to evaluate the new technique. A series of short axis multi-slice cine acquisition FIESTA images were acquired using the current standard technique. From this data set, LV and RV stroke volumes were derived on an Advantage Windows workstation using planimetry of the endocardial and epicardial borders in end-systole and end-diastole. Our new technique involved obtaining a set of multi-slice cine acquisition FIESTA images in a plane perpendicular to a line from the centre of the pulmonary valve to the apex of the RV. Planimetry of the RV was then performed and a stroke volume calculated using the same method of analysis. Physiologically the left and right cardiac outputs are equal. RV stroke volumes obtained from both techniques were compared with LV stroke volumes.

Results: On the images acquired with the new technique, the tricuspid and pulmonary valves were more easily visualised leading to more accurate and reproducible planimetry of ventricular borders. RV stroke volumes calculated from the new method show better agreement with LV stroke volumes than with the current method. The new method is also less biased to underestimation of the true stroke volume.

Conclusions: RV function is assuming greater importance in clinical management of cardiac patients. Accurate reproducible quantification of RV function will expand treatment strategies and potentially assist in achieving the ultimate goal of improving patient management. This new method improves visualisation of the tricuspid and pulmonary valves and makes analysis easier and less prone to operator error. Serial RV assessments could be undertaken with greater confidence in diagnostic accuracy and reproducibility using this technique.

570. Sodium MRI of the Human Heart: Comparison Between ECG-Gated 2D Radial Projection and Gradient Echo Techniques

Sonia Nielles-Vallespin,[1] Michael Block,[2] Achim Bankamp,[2] Andre Bongers,[2] Christian Wacker,[2] Lothar R. Schad,[2] Wolfgang Bauer.[3] [1]*Medical Physics in Radiology (E0201), German Cancer Research Centre (DKFZ), Heidelberg, Germany*, [2]*Deutsches Krebsforschungszentrum (DKFZ), Heidelberg, Germany*, [3]*Department of Cardiology, Universität Würzburg, Würzburg, Germany.*

Introduction: Sodium MRI has the potential to differentiate between viable and non-viable myocardium [1,2]. In tissue, the sodium signal decays with two different T_2 relaxation times, a short component $T_{2f} = 0.7-5$ ms, and a long component $T_{2s} = 7-25$ ms [3,4]. Thus, to ensure the acquisition of the total sodium signal, techniques with short echo times TE are required. ECG-gated 3D radial projection techniques (RPT) allow for ultra-short TE of less than 0.5 ms [5]. However, their temporal resolution is limited by the amount of projections that need to be acquired. Conventional gradient echo (GRE) techniques, on the other hand, allow for time resolved imaging of the heart, but their longer TE prevents the accurate quantification of the total sodium content. In this work, a segmented

Copyright © Marcel Dekker, Inc. All rights reserved.

ORDER REPRINTS

ECG-gated 2D radial projection technique with a minimum TE of 0.6 ms that allows for time resolved ^{23}Na imaging of the heart is presented and compared to a standard segmented ECG-gated gradient-echo technique with a minimum TE of 3 ms.

Methods: To keep TE as short as possible in the 2D-RPT, a 512 μs sinc RF-pulse is used and the data is sampled immediately after the slice selection rewinder, during readout gradient ramp-up. The gradient echo sequence has a 1024 μs sync RF-pulse and asymmetric readout.

Measurements were performed in a 1.5T clinical scanner (1.5T Magnetom Symphony, Siemens Medical AG) using a ^{23}Na surface coil (Rapid Biomedical). Before acquisition of the ^{23}Na images, an ECG-triggered ^{1}H True-FISP sequence was used for slice positioning and anatomical localization of the ^{23}Na images. For both ^{23}Na ECG-triggered techniques, an acquisition window of 1000 μs was used to obtain 4 different cardiac phases. The field-of-view was FOV = 500 mm and the matrix size 128×128, divided in 3 segments. This resulted in a $30 \times \quad 4 \times 4$ mm^3 resolution for the GRE, while for the 2D RPT the final resolution after reconstruction was $30 \times 2 \times 2$ mm^3. With a bandwidth of 190 Hz per pixel, TR = 8 ms and 200 averages, the total scan time was 15 min.

Results: Figure 1 shows a comparison between the GRE and RPT ^{23}Na images corresponding to 4 different cardiac phases, together with the reference ^{1}H images. Right and left ventricles are visualized together with the myocardium. In both data sets it is possible to observe the contraction of the ventricles. The SNR in the ventricle is 10 for the gradient-echo sequence and 16 for the RPT. On the other hand, although theoretically the RPT images should show a higher resolution compared to the GRE images, this is not evident in the results. The reason for this is probably a blurring effect characteristic of the RPT that will need to be corrected with a more accurate reconstruction method.

Conclusions: A 2D RPT technique has been presented that can acquire time-resolved ^{23}Na images of the human heart in clinically acceptable measurement times. The 2D RPT is superior in SNR to the gradient-echo technique due to its shorter TE, while suffering from some blurring effects that need to be corrected for. Compared to the 3D RPT, the 2D RPT has the advantage of allowing for time resolved imaging of the heart. On the other hand, the TE of the 2D RPT is longer than that of the 3D RPT. However, it might still be short enough to allow for the measurement of the total sodium signal and, potentially, the quantification of the total sodium content in tissue. Future work aims at the improvement of the radial reconstruction method. Furthermore, the capability of the 2D and 3D radial techniques to measure the total sodium signal and to separate the two T_2 components will be evaluated to determine their diagnostic potential.

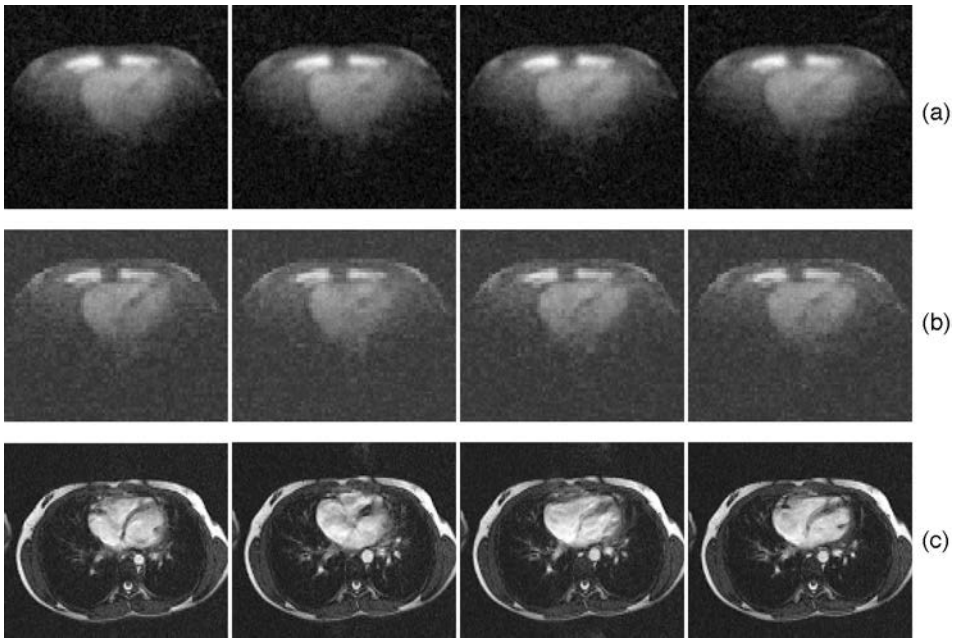

Figure 1.

Copyright © Marcel Dekker, Inc. All rights reserved.

MARCEL DEKKER, INC.
270 Madison Avenue, New York, New York 10016

Request Permission or Order Reprints Instantly!

Interested in copying and sharing this article? In most cases, U.S. Copyright Law requires that you get permission from the article's rightsholder before using copyrighted content.

All information and materials found in this article, including but not limited to text, trademarks, patents, logos, graphics and images (the "Materials"), are the copyrighted works and other forms of intellectual property of Marcel Dekker, Inc., or its licensors. All rights not expressly granted are reserved.

Get permission to lawfully reproduce and distribute the Materials or order reprints quickly and painlessly. Simply click on the "Request Permission/ Order Reprints" link below and follow the instructions. Visit the U.S. Copyright Office for information on Fair Use limitations of U.S. copyright law. Please refer to The Association of American Publishers' (AAP) website for guidelines on Fair Use in the Classroom.

The Materials are for your personal use only and cannot be reformatted, reposted, resold or distributed by electronic means or otherwise without permission from Marcel Dekker, Inc. Marcel Dekker, Inc. grants you the limited right to display the Materials only on your personal computer or personal wireless device, and to copy and download single copies of such Materials provided that any copyright, trademark or other notice appearing on such Materials is also retained by, displayed, copied or downloaded as part of the Materials and is not removed or obscured, and provided you do not edit, modify, alter or enhance the Materials. Please refer to our Website User Agreement for more details.

Request Permission/Order Reprints

Reprints of this article can also be ordered at

http://www.dekker.com/servlet/product/DOI/101081JCMR120028320